Testing of a Reinforced Concrete Core Wall for Tsunami Vertical Evacuation Shelter Structures in a Wave Flume

Christopher Niles Pyke

A thesis
Submitted in partial fulfillment of the
Requirements for the degree of:

Master of Science in Civil Engineering

University of Washington

2020

Committee:
Dawn Lehman, Chair
Charles Roeder
Michael Motley

Program Authorized to Offer Degree:
Civil and Environmental Engineering

University of Washington

Abstract:

Testing of a Reinforced Concrete Core Wall for Tsunami Vertical Evacuation Shelter Structures in a Wave Flume

Christopher Pyke

Chair of the Supervisory Committee:
Professor Dawn Lehman
Department of Civil and Environmental Engineering

Communities in the coastal northwest of the United States realize the threat of tsunamis. An important implementation to prevent loss of life during a tsunami is the construction of vertical evacuation shelters (VES). These shelters can be stand-alone towers or integrated into a building. For buildings, structural walls are the most common lateral force resisting system for VES structures. However, there have been few realistic tests of these systems in wave-flume facilities. This research investigates the fluid-structure interaction between a concrete core wall and an incoming tsunami wave using a large-scale wave-flume facility with an emphasis on advancements in test setup and instrumentation.

The research project was phased. The first task was to determine the core wall dimensions by designing a prototype to meet the ASCE 7-16 demands; the structure was sited in Seaside, Oregon to build on prior research on tsunami demands. The design philosophy was to first design the building to remain elastic under the maximum credible earthquake demands and then design for the tsunami loading including the amplification factors required for VES structures. The resulting wall was 23 ft. by 16 ft. with a thickness of 30 inches.

The second phase of the research utilized a 1:6 scale core-wall specimen. The specimen included the core wall with plan dimensions of 46 in. by 46 in. and a wall thickness of 5 in. The specimen

also included a pile foundation founded on a base slab. A soil box was placed around the piles and aggregate was used to simulate an idealized boundary condition on the piles with three conditions of the soil box: full, half full or empty. The full structure (wall, slab and piles) was supported by vertical and horizontal load cells to measure axial, shear and moment reactions. The load cells were supported by a specialized reaction frame that was attached to the base of the flume. Additional instrumentation was placed to measure strains in the piles and pressure along the face of the wall. This set of instrumentation permitted redundant measurements of the forces. The forces from the different methods of measuring force on the structure were then compared against each other and showed agreement between the different techniques. The measurements were also compared to an OpenFOAM simulation. The simulated and measured results were similar, validating the numerical model.

TABLE OF CONTENTS

TABLE OF FIGURES:

TABLE OF TABLES:

Chapter 1. INTRODUCTION

This thesis presents work completed between the summer of 2018 and the spring of 2020.

1.1 MOTIVATION

Communities in along the northwest coast of the United States have realized the threat that tsunamis pose to their residents and infrastructure. One way to prevent the loss of life during these disasters is the construction of vertical evacuation shelters (VES). VESs create an artificial high ground that residents can flee to in the event of a tsunami. These structures can take the form of an open stand-alone tower or can be integrated into a building. To date on such structure has been constructed in along the northwest coast with several others in the planning or construction phases. When integrated into a building the structures typically rely on large stiff reinforced concrete core walls as the lateral force resisting systems. To date there has been limited wave flume testing on realistic models of this structural system. This research was done to fill that void and provide a suite of results on a realistic structure that can be used to validate numerical modeling of such structures.

1.2 OBJECTIVES

The primary objectives of this research were:

- To complete a full scale building design utilizing reinforced concrete core walls as its lateral force resisting system.
- To take the full-scale building and scale it down to the largest size that could be tested given the limitations of the testing facility.
- To design a test setup that could accurately measure the axial, shear, and moment reactions of the specimen.
- To investigate how changing soil levels around the foundation of the core wall change the load transfer mechanisms for the test specimen.
- To provide a suite of results that can be used to validate numerical models and help to better understand the fluid-structure-soil interaction that occurs during tsunami inundation.

1.3 APPROACH

To meet the objectives of the project the following research approach was taken. First a review of existing literature was completed to investigate how previous researchers have set up wave flume experiments and measured forces on their specimens. Then a full scale structure was designed to resist tsunami loads given in in accordance with ASCE 7-16. The structure was designed to remain elastic during a maximum credible earthquake event that would precede a tsunami. The lateral force resisting system for the structure was a reinforced concrete core wall system. After loading on the structure was evaluated the core walls were sized to resist the design loads. The largest core wall was then taken and scaled down to a 1:6 scale in order to design a test specimen that would fit within the limits of the test facility. After the size of the specimen to be tested was determined a test setup was developed that utilized a series of vertical and horizontal uniaxial load cells connected to the structure with swivels to reduce interference between the different load cells. The load cells were attached to a custom stiff reaction frame that could be secured to the base of the flume. Multiple series of waves were then run on the specimen to obtain the desired results. Two different wave heights were examined, a 1.4m wave and a 1.45m wave.

1.4 THESIS OUTLINE

The succeeding chapters in this document take the following form. Chapter 2 discusses prior wave flume experiments related to tsunami wave-structure interaction with an emphasis on how the experiments were set up and the quality of results. Chapter 3 provides a background on existing vertical evacuation structures. It then discusses the full scale building design including the site selection, load evaluation for both tsunami and earthquake loading, and geometry iterations conducted. Chapter 4 details the experimental program including the design and construction of the test specimen, the instrumentation used during testing, validation testing that was done to ensure the setup worked properly before running any waves, and a summary of the different wave conditions run during the testing. Chapter 5 provides the results of the testing for all instruments. Chapter 6 then makes comparisons between the different methods of measuring force. It concludes by making comparisons between the experimental testing and an OpenFOAM simulation of the experiment, as well as comparisons to the anticipated force on the scaled structure using provisions

from ASCE 7-16. Chapter 7 provides a summary of important points and final conclusions for this research.

Chapter 2. LITERATURE REVIEW

This chapter presents a review of prior wave-flume experiments. For each paper, the test specimen and setup, instrumentation for measuring loads, and load cases are examined. Relevant takeaways that were applied to this research are listed in the takeaways section for each paper. There is an emphasis on understanding the advantages and disadvantages of the test setup. The evaluation of the setups was used to develop a test specimen and setup with realistic boundary conditions that could accurately simulate a structure subjected to a tsunami-like wave and measure the reaction forces in all directions.

Four unique test setups were examined and a diagram of them can be seen in Figure 2-1. That first setup (labeled (A) in Figure 2-1) consisted of a cantilever structure supported a the bottom with a multi-axis load cell to measure reactions and pressure sensors on the face of the test specimen to measure demands. The second setup (labeled (B) in Figure 2-1) consisted of a wall specimen supported by single axis load cells oriented in the direction of loading to measure reactions. The specimen was also instrumented with pressure sensors to measure demands. The third setup (labeled (C) in Figure 2-1) was an elevated structure supported from above by a reaction frame. Between the reaction frame and the specimen load cells were placed in the three primary directions to measure reactions. Pressure sensors were also used in this setup to measure demands. The final test setup (labeled (D) in Figure 2-1) consisted of a test specimen placed atop a series of uniaxial load cells. Table 2-1 lists the papers presented in this chapter in the order they appear.

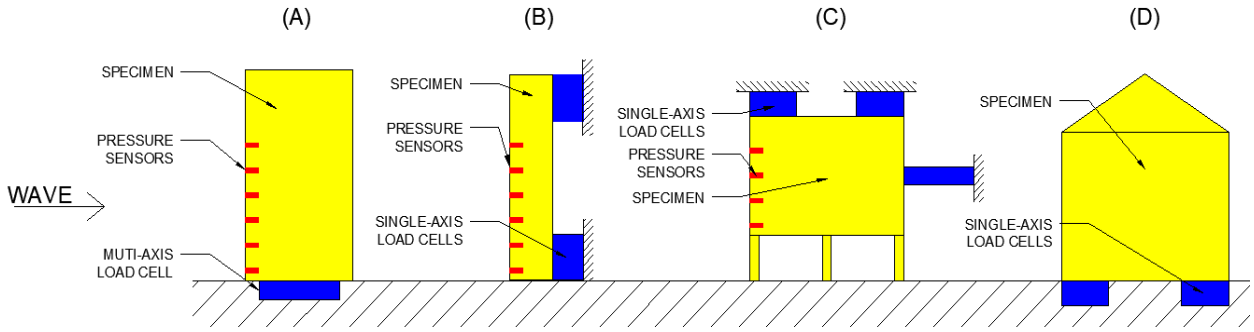

Figure 2-1: Test Setup Types Examined

Table 2-1: List of Papers Reviewed

Paper Title	Author	Year	Location	Type of Specimen	Setup Type
Experimental investigation of tsunami bore impact force and pressure on a square prism	Shafiei, Melville, Shamseldin	2016	The University of Auckland	Acrylic square prism	A
Experimental Modeling of Extreme Hydrodynamic Forces on Structural Models	Al-Faesly, Palermo, Nistor and Cornett	2012	University of Ottowa	Acrylic rectangular and cylindrical prisms	A
Breaking wave impact force on a vertical and inclined slender pile—theoretical and large-scale model investigations	Wienke and Oumeraci	2005	Germany, Leichtweiß Institut fur Wasserbau	Steel cylindrical pile	A
Evaluation of Tsunami Loads on Wood-Frame Walls at Full Scale	Linton, Gupta, Cox, van de Lindt, Oshnack and Clauson	2013	Oregon State University	full scale wood framed wall	B
Experimental and Numerical Validation of Three-Dimensional Tsunami Wave Pressures and Forces on an Elevated Structure	Gills	2018	Oregon State University	scale model elevated steel structure	C
Behavior of a One-Sixth Scale Wood-Framed Residential Structure under Wave Loading	Wilson, Gupta, van de Lindt, Clauson, and Garcia	2009	Oregon State University	1:6 scale wood framed structure	D

2.1 SHAFIEI, MELVILLE, SHAMSELDIN (2016) EXPERIMENTAL INVESTIGATION OF TSUNAMI BORE IMPACT FORCE AND PRESSURE ON A SQUARE PRISM

Shafiei, et al. (2016) conducted a research program at the University of Auckland to investigate tsunami bore interaction with an inland structure. Tests were conducted by releasing a small tsunami bore at a rectangular prism. Specifically, they sought to quantify the force from a tsunami bore on a structure at different orientations.

2.1.1 *Test Specimen and Setup*

The test specimen was a 300 x 300 x 600 mm square-prism constructed out of 5 mm thick acrylic sheets. As the structure was constructed out of sheets of acrylic glued together it was more representative of a shape than a realistic structure. The structure was secured to a six axis load cell and the load cell was connected to the flume floor to provide a fixed boundary condition at the

base of the structure. The load cell was recessed in a cavity below the floor of the flume as to avoid interfering with flow around the base of the structure. Orientations of the structure were changed by rotating the specimen on top of the load cell while leaving the x-axis of the load cell oriented in the direction of flow to measure the total base shear on the structure in different orientations. Small holes were cut into one face of the specimen to provide attachment points for pressure sensors. Figure 2-2 shows the test specimen, load cell and installed pressure sensors.

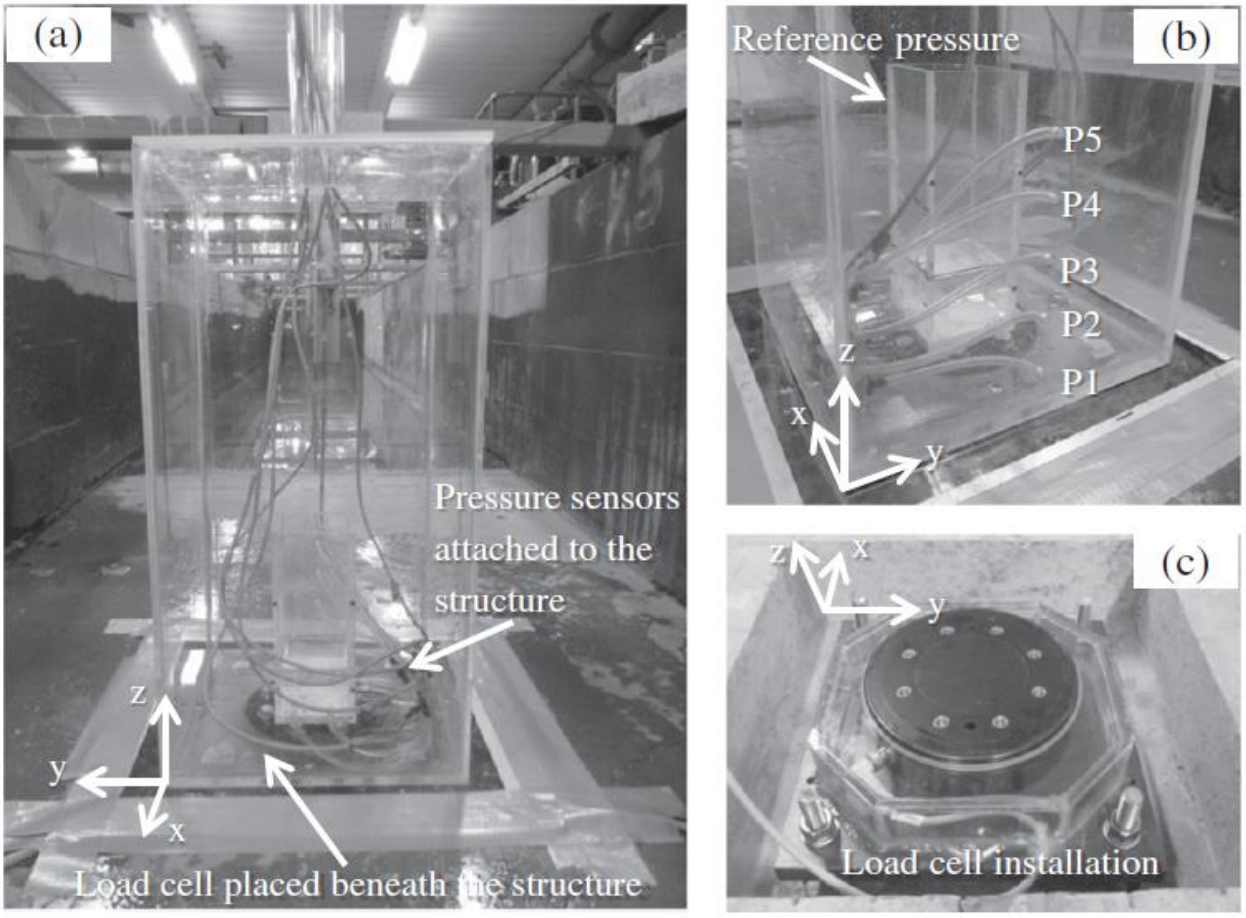

Figure 2-2: Shafiei, et al. (2016) Test Specimen

2.1.2 *Instrumentation*

The structure was instrumented with five pressure sensors placed vertically along the centerline of the front face. The pressure sensors ranged in elevation from 32 mm above the flume floor to 200 mm above the flume floor. The structure was also instrumented with a six-axis load to measure reaction forces and moments at the base of the structure. Wave heights and velocities were also

measured using wave gauges. Velocities and wave heights were then used as inputs to design equations to predict the total force on the structure and compare to the measured load from the load cell.

2.1.3 *Loading*

Loading for this test was varied by changing the tsunami bore height and the orientation of the structure to the tsunami bore. Primary test parameters were the height and corresponding velocity of the tsunami bore, as well as the orientation of the structure. Table 2-2 presents the different bore heights tested and Figure 2-3 shows the different structure orientations examined, the black dots in this figure indicate where pressure sensors were located relative to the flow direction. In the table WL stands for the height of the water impounded behind the gate in the flume, GO is the height the gate was lifted to allow the release of water, h_b is the height of the wave bore and u_b is the velocity of the wave bore. Each bore height test case and structure orientation combination was tested five times to ensure repeatability of results, this resulted in a total of 180 tests.

Table 2-2: Different Bore Heights and Velocities Tested

Case	WL (mm)	GO (mm)	h_b (mm)	u_b (m/s)
Case 1	400	200	140	1.98
Case 2	400	300	150	2.08
Case 3	500	200	160	2.14
Case 4	500	300	170	2.2
Case 5	600	200	190	2.33
Case 6	600	300	210	2.45

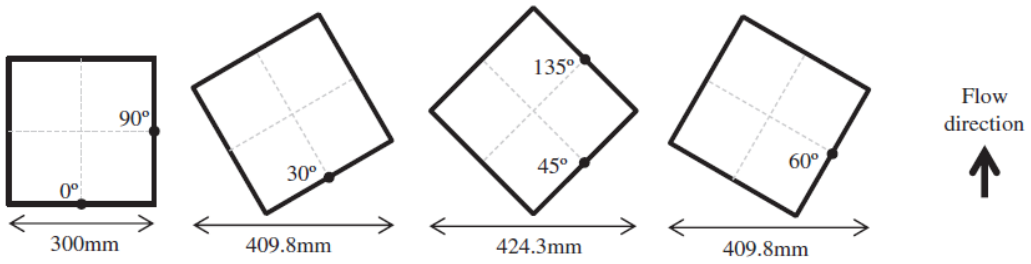

Figure 2-3: Structure Orientations during Testing

2.1.4 *Takeaways*

Pressure distributions were compared for different bore heights in the 0° orientation. It was found that after the structure becomes inundated that the distribution of pressures is similar to that of a

hydrostatic pressure distribution. It was found that for the 0° orientation the average measured force from the load cell could be accurately estimated from summing the hydrostatic and hydrodynamic forces on the specimen. It could also be accurately estimated by integrating the pressures over the front face of the specimen making the assumption that the centerline pressures were constant over the face of the structure. For this relatively small structure compared to others examined five pressure sensors were adequate for estimating the total force on the structure by integrating the pressures.

Shafiei, et al. (2016) showed that a six axis load cell worked well to measure the forces at the base of the structure. They also showed that integrating pressures over the face of a test specimen can accurately predict the total force on the structure. The test specimen was rather light compared to others examined here and bore heights were rather small. For a large scale experiment a much larger and more expensive load cell would likely be needed and more pressure sensors may be needed.

2.2 Al-Faesly, Palermo, Nistor and Cornett (2012) Experimental Modeling of Extreme Hydrodynamic Forces on Structural Models

Al-Faesly, et al. (2012) conducted a series of tests to investigate impact of extreme hydrodynamic forces on acrylic test specimens caused by a turbulent hydraulic bore representative of a tsunami wave. Primary test parameters investigated were: specimen shape (square or circular), bore depth time history, the initial flume bed condition (dry vs wet), and the effect of offshore walls to mitigate hydraulic bore forces. Base shear forces in the direction of flow were recorded for two different structural models and then compared to predicted base shear forces from literature.

2.2.1 *Test Specimen and Setup*

Testing was conducted in a high discharge flume where a large body of water was impounded behind a sluice gate and a winch was used to rapidly remove the gate resulting in a dam break type broken bore wave propagating down the length of the flume. Test specimens were placed in the flume at a distance that allowed the bore to fully develop before hitting the test specimen. Two different models were investigated, a square prism and a cylindrical specimen.

The specimens, shown in Figure 2-4, were constructed out of Acrylic glass sheets with an internal stainless steel frame to secure the specimens to a 6 degree of freedom load cell at the base. The specimens were 1m tall. The rectangular specimen had plan dimensions of 305 mm x 305 mm; the circular specimen had an outside diameter of 305 mm. As the specimens were constructed out of acrylic sheets with an internal steel frame to assist the transferring of loads to the load cell at the base they were more representative of the rough geometry and shape of a scaled down structure, however not representative of the force transfer mechanisms that would take place in a real structure.

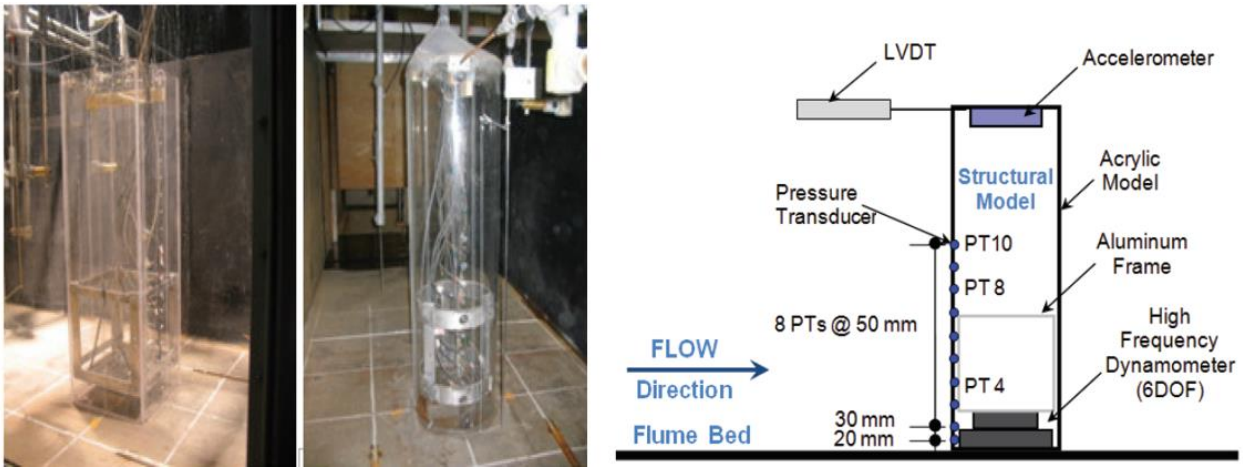

Figure 2-4: Al-Faesly, et al. (2012) Structural Model

2.2.2 *Instrumentation*

The structure was instrumented to measure loads by using a six axis load cell fixed to the bottom of the structure and the flume floor. This allowed for the measurement of forces and moments at the base of the structure. In addition to the load cell test specimens were instrumented with wave gauges, pressure transducers, an accelerometer and an LVDT. Wave gauges were attached to the structure to measure the bore depth around it. A line of pressure sensors wave placed along the centerline of the front face of the specimen. Additionally an accelerometer and LVDT were placed at the top of the structure to quantify displacements and accelerations on the specimen.

2.2.3 *Loading*

Loading was varied for this test by changing the level of water impounded behind the gate that was lifted to create the tsunami bore. Loading was also varied by changing the flume bed condition between a dry bed and a flume bed that had a small amount of standing water.

2.2.4 *Takeaways*

Relevant results found were that the dry bed condition produce higher tsunami bore impulse forces while both conditions exhibited about the same level of steady state hydrodynamic force for the same wave height as shown by Figure 2-5. Figure 2-5 (a) and (b) show the pressures and forces respectively for the dry bed conditions while Figure 2-5 (c) and (d) show the pressures and forces respectively for the wet bed conditions.

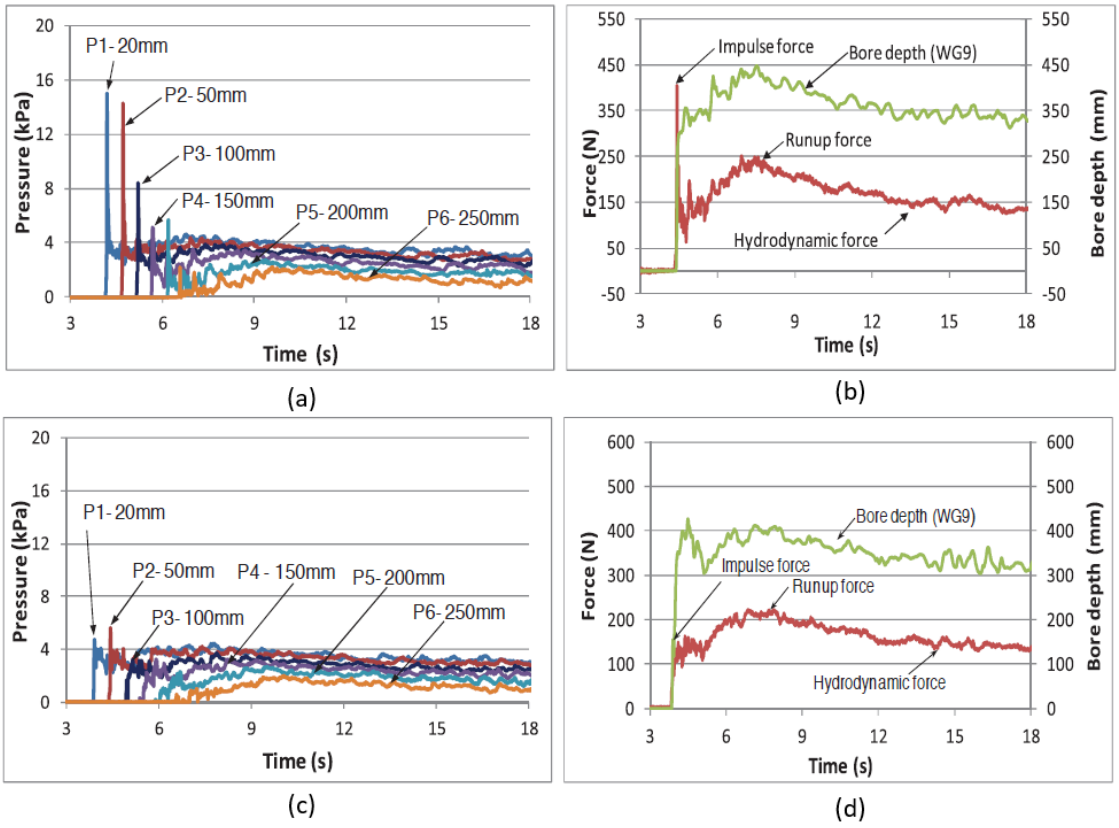

Figure 2-5: Al-Faesly, et al. (2012) Dry vs Wet Bed Condition Results

Another conclusion found by this research was that experimental forces varied significantly from the predictive equations for force found in FEMA P646 and SMBRT. It was found that FEMA

P646 drastically under predicted the base shear exerted on the structural model, while SMBRT tended to over predict the base shear. These results are shown in Figure 2-6.

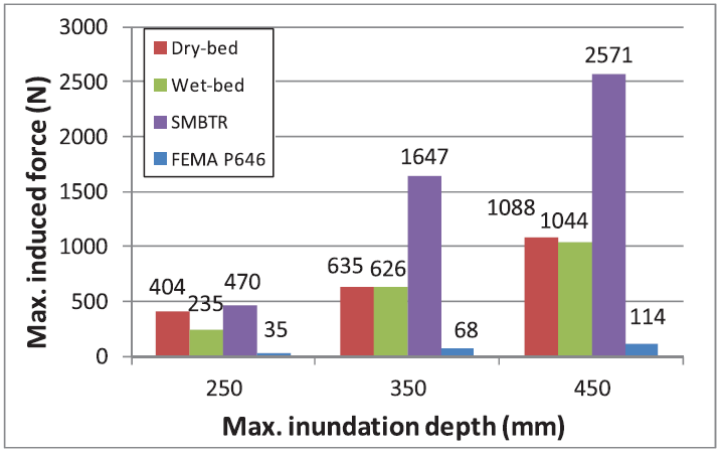

Figure 2-6: Comparison of Experimental Forces to Design Equations.

Similar to Shafiei, et al. (2016), Al-Faesly, et al. (2012) showed that for small test specimens a six axis load cell supporting the base of the structure works well to measure the forces and moments on the structure, providing a realistic fixed boundary conditions for the test specimen. Unfortunately the test specimens were both very small and light and not representative of realistic structure but rather characterized how a tsunami wave might load a structure with a similar shape. Al-Faesly, et al. (2012) did not present an attempt to show the force on the structure by integrating the pressures over the front face of the specimen, however from previous experiments examined this likely could be done with the number of pressure sensors used and the given size of the specimen.

2.3 Wienke and Oumeraci (2005) Breaking Wave Impact Force on a Vertical and Inclined Slender Pile—Theoretical and Large-Scale Model Investigations

Wienke and Oumeraci (2005) conducted a series of tests in the large wave flume (GWK) of the Coastal Research Centre (FZK) in Hanover, Germany to investigate the impact force of waves hitting an inclined steel cylinder. The objectives of this research were to improve the ability to predict wave impact forces on offshore structures.

2.3.1 *Test Specimen and Setup*

The test specimen consisted of a steel pile with a diameter of 0.7 m and a length of about 8 m. The specimen was fixed to the flume with a multi-axis load cell. The pile was also fixed to a cross girder near the top of the specimen to reduce total loads on the bottom load cell. This method of fixing the specimen at the top and the bottom gave fixed-fixed end boundary conditions representative of a section of a pile in a larger offshore structure. A diagram of the specimen and instrumentation is shown in Figure 2-7.

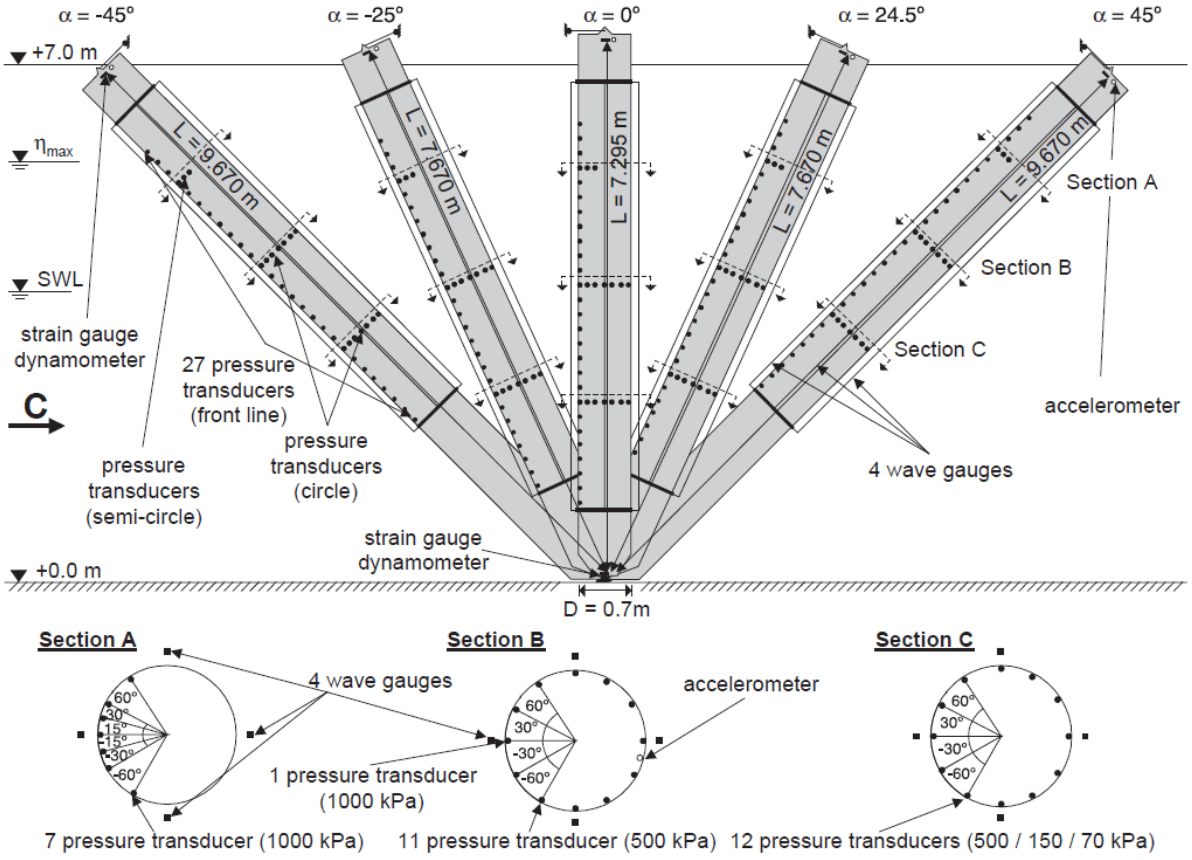

Figure 2-7: Wienke and Oumeraci (2005) Test Setup and Instrumentation

2.3.2 *Instrumentation*

Strain gauges were placed in the connection to the top cross girder to measure loads at the top of the specimen. A multi-axis load cell was used at the base of the specimen to measure loads. Pressure sensors were placed over the front face of the structure to measure forces locally. Accelerometers were placed at the specimen's connection points as well as in the center of the pile

to characterize the dynamic effects of the wave impact. Wave gauges were also placed around the structure to characterize the wave height during impact.

2.3.3 *Loading*

Load cases for this research consisted of changing the yaw angle of the test specimen from -45 degrees to +45 degrees as shown in Figure 2-7. Loading was also varied by changing the location that waves broke before hitting the pile. Broken waves in this test were generated by the method of constructive interference.

2.3.4 *Takeaways*

This test showed a good method for supporting a realistic structure with realistic boundary conditions. Forces were able to be measured both at a global level with load cells and at a local level with pressure sensors. Using a multi-axis load cell below a specimen could work for testing a scale model of a vertical evacuation structure, however as this test showed when a multi-axis load cell is used with a large scale structure it may be necessary to restrain the top of the specimen as was done in this test.

2.4 LINTON, GUPTA, COX, VAN DE LINDT, OSHNACK AND CLAUSON (2013) EVALUATION OF TSUNAMI LOADS ON WOOD-FRAME WALLS AT FULL SCALE

Linton, et al. (2013) conducted a series of tests on full scale wood framed walls subject to tsunami like waves at the Hinsdale Wave Research Laboratory at OSU. The objective was to investigate how a wooden structure preforms when subjected to a solitary wave bore and to then compare the measured forces to predictive equations from literature.

2.4.1 *Test Specimen and Setup*

The test specimens examined consisted of three different wall specimens with three different methods of framing. The first specimen (1A and 1B) was typical to an exterior residential wall, constructed out of 2 x 6 lumber with studs spaced 16” on center and sheathed with ½” plywood. The second specimen (2A and 2B) was constructed the same as the first except 2 x 4’s were used in the place of 2 x 6’s. The third specimen (3A) was constructed the same as the first except the

studs were spaced at 24” on center rather than 16”. All three of the specimens were 12’ wide, spanning the entire width of the flume, and 7’ tall. The wall specimens were supported with a series of four uni-axial load cells attached to the corners of the wall and anchored into the concrete walls that make the sides if the flume. This allowed for measurement of the total load on the wall however provided somewhat unrealistic boundary conditions for a wooden wall that would likely be attached at many more points in a real structure. For example the base plates would be attached to floor and roof diaphragms, the ends of the wall would likely have stiff corners that would deform less than simply having framing 16 or 24 inches on center. In some tests conducted the base plate for the wall was secured down to the flume floor, however there was no instrumentation to measure the forces in these anchors and so for those tests the total load on the wall was unknown. Figure 2-8 shows an installed specimen and supporting instrumentation.

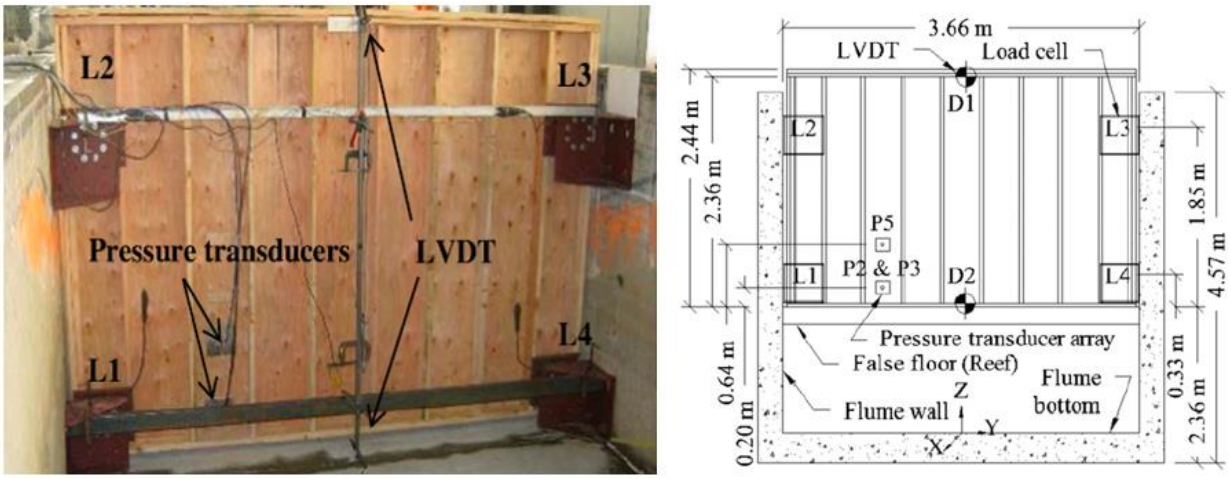

Figure 2-8: Wall Specimen and Instrumentation

2.4.2 *Instrumentation*

Each of the wall specimens was instrumented with four uni-axial load cells placed in the corners of the wall and connected to the walls of the flume to provide a rigid support. LVDTs were installed in the center of the wall on the top and bottom plates of the wall. The specimens were also instrumented with three pressure sensors near the bottom of the wall to help get an idea of the pressure distribution on the wall. A typical wall configuration with dimensions and instrumentation can be found in Figure 2-8.

2.4.3 *Loading*

Load cases for the specimens varied for the different framing methods. Overall wave heights varied between .1 m. and 1 m. Load cases for the different specimens are shown in Table 2-3.

Table 2-3: Linton et al. (2013) Load Cases

Experiment	Trials	Wave heights H_2 (m)	Specimen	Anchored	Load cells	Failure
TW 1	12	0.10–0.87	1A	No	4	Yes
TW 2	7	0.10–0.65	2A	No	4	No
TW 3	6	0.20–0.78	3A	No	4	Yes
TW 4	11	0.15–1.04	1B	Yes	4	No
TW 5	11	0.14–0.93	1B	Yes	2 top	No
TW 6	4	0.25–0.68	2B	Yes	4	No
TW 7	4	0.26–0.71	2B	Yes	2 top	No
TW 8	5	0.09–0.48	2B	No	4	Yes

2.4.4 *Takeaways*

Linton et al. (2013) showed one example of how to test a wall type structure in the Large Wave Flume at OSU. The test however provided unrealistic boundary conditions for the specimen and deflections of the wall were most likely much greater than they would be for a wall incorporated into a building. The test lacked redundant measurements of force due to the limited number of pressure sensors placed on the face of the wall. It was shown that three pressure sensors was not enough to characterize the pressure distribution across the face of a 12’ wide by 7’ high wall.

2.5 GILLS (2018) TSUNAMI WAVE PRESSURES AND FORCES ON AN ELEVATED STRUCTURE

Gills (2018) conducted a series of tests to improve the understanding of tsunami-structure interaction by subjecting an elevated steel structure to a series of tsunami like waves and recording the forces and pressures excreted on the structure by the wave. The primary objective of this study was to develop sets of measured forces and pressure distributions on elevated structures for numerical model validation. Testing was conducted at the Hinsdale Wave Research Laboratory at Oregon State University (OSU).

2.5.1 *Test Specimen and Setup*

The test specimen used for this research was a rectangular steel box approximately 1m x 1m in plan and .6m tall. The box was supported on piles .27m tall, however the piles were elevated slightly off the ground so that no force was being transferred down into the concrete slab below the specimen.

Loads imparted on the specimen by waves were transferred up to the top of the specimen into an instrumented support frame that was capable of measuring forces in three dimensions. The support frame however provided unrealistic boundary conditions for the specimen as in a realistic structure the loads would be transferred down through the piles and into a foundation below the structure. The support frame utilized a series of linear rollers to restrain the specimen with load cells. These rollers allowed the specimen to move only in the directions of load cells so that load could be measured however the rollers provided some friction and lead to disagreements in force between the load cells and the integration of pressures on the front face of the specimen. The specimen and support frame are illustrated in Figure 2-9.

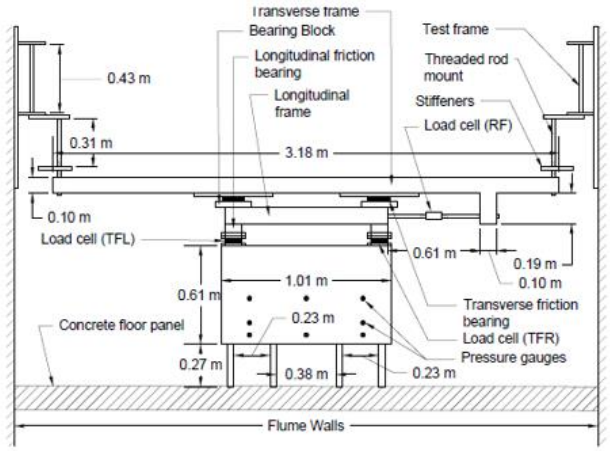

(a) Front View

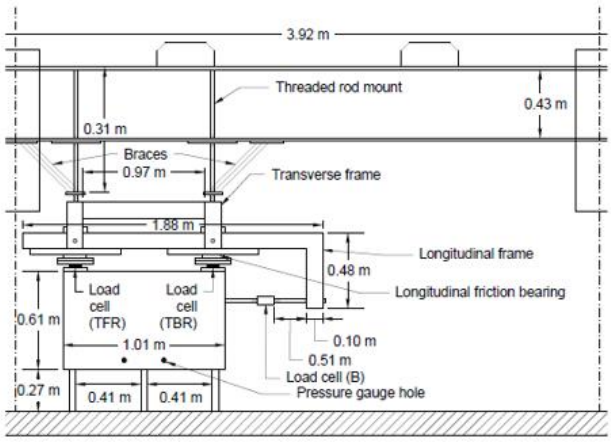

(b) Side View

(c) Isometric View as Built

Figure 2-9: Gills (2018) Test Specimen and Support Frame

2.5.2 *Instrumentation*

Two different methods of measuring loads, load cells and pressure sensors, were utilized in this research program. A series of uniaxial load cells were connected between the structure and reaction frame to measure loads in three directions. Four pancake type load cells were connected between the top of the specimen and the reaction frame to measure uplift forces. Two rod end (threaded) load cells were used to measure transverse forces on the structure and restrain twisting in the setup. One rod end load cell was connected to the rear of the structure to measure total stream-wise force on the system. Additionally two of the piles below the structure had load pancake type load cells attached to them to measure the forces in the piles. Photographs of the installed load cells can be seen in Figure 2-10.

(a) Vertical Sandwich Load Cell

(b) Column Sandwich Load Cell

(c) Horizontal Threaded Load Cell

(d) Transverse Threaded Load Cell

Figure 2-10: Gills (2018) Installed Load Cells

A series of pressure sensors were used to characterize the pressures on the front, bottom, back and side faces of the test specimen. Due to a limited number of pressure sensors available multiple different configurations of sensors were used to characterize the pressures on the different faces of the specimen. 17 pressure sensors locations were cut into the front face of the specimen, eight locations were used on the bottom, two on each of the sides and one on the back of the specimen. Using three different configurations of pressure sensors the pressures on each face of the specimen were recorded and used to determine the total load on the specimen by integrating the pressures over the different faces of the specimen.

2.5.3 *Loading*

Gills (2018) examined two different wave load cases, one of an unbroken solitary wave and one of a broken bore type wave. The two different waves provided different total loads on the structure as well as different pressure distributions over the face of the structure. It was found that when integrating the broken wave a bi-quadratic pressure distribution provided the closest results to the experiment, while for the unbroken wave a bi-linear distribution provided more realistic results.

2.5.4 *Takeaways*

Gills (2018) provided an example of how to measure forces on a test specimen in three dimensions. This research also showed that pressure sensors could be used as a redundant way to measure force and that data from multiple pressure sensor layouts could be combined together to characterize pressures on the same face of a specimen. The test however failed to provide realistic boundary conditions for the specimen. Another way the setup could be improved would be to find a way to reduce the friction in the sliders used which caused a reduction in the total force in the load cells. For a test specimen like the one used in this test the friction might not be a large factor because the weight of the specimen is rather small, however it could be a larger issue if a heavier test specimen were used, like one made of concrete.

2.6 WILSON, GUPTA, VAN DE LINDT, CLAUSON, AND GARCIA (2009) BEHAVIOR OF A ONE-SIXTH SCALE WOOD-FRAMED RESIDENTIAL STRUCTURE UNDER WAVE LOADING

Wilson, et al. (2009) completed a series of tests examining the performance of a 1:6 scale wood framed residential structure subject to tsunami like waves at the Hinsdale Wave Research Laboratory at OSU. The objective of this research were to examine the loads on and structural response of a wood framed structure under different load conditions and structural orientations.

2.6.1 *Test Specimen and Setup*

The test specimen was a scale model of a typical residential wood framed structure. The structure had plan dimensions of 240 cm. by 110 cm. with a height of 120 cm. The structure was tested in two different configurations, one with the long side facing the tsunami wave and the other with the short side facing the wave. The specimen was supported from below by four uni-axial load cells in the corners of the structure.

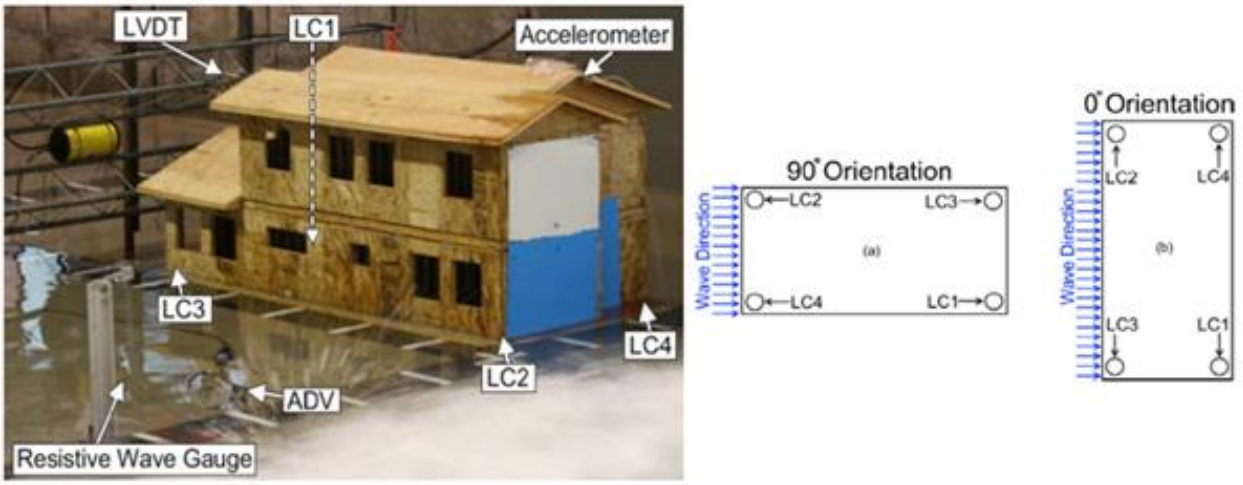

Figure 2-11: Wilson, et al. (2009) (a) Test Specimen and Instrumentation (b) Orientations Examined

2.6.2 *Instrumentation*

The test specimen was instrumented with a series of four uni-axial load cells below the structure to measure uplift forces and base moment on the structure. The structure was also instrumented with an accelerometer on the roof to measure accelerations due to wave impact. It was also instrumented with a linear variable differential transformer (LVDT) on the roof of the structure to measure deformations during testing. Unlike the previous tests discussed no pressure sensors were used and there were no instruments capable of measuring the total base shear on the structure.

2.6.3 *Loading*

Load cases for the test specimen consisted of running a series of wave that varied in height from 10 cm. to 60 cm. Other variables examined were the effects of closing the door and window openings on the structure, raising the water level in the flume to simulate a second tsunami wave that would come after the ground has been inundated, and elevating the structure slightly off the ground to examine how the forces changed on an elevated structure.

2.6.4 *Takeaways*

Wilson, et al. (2009) showed a good example of a realistic structure and were able to measure deformations and overturning moment on a 1:6 scale residential wood framed structure. However

they were unable to get an estimate of the total force on the structure from the tsunami wave without pressure sensors of a load cell oriented in the direction of wave loading.

2.7 Overall Takeaways

After an extensive review of current literature it was found that there is a significant lack in testing of large scale structures subjected to tsunami loads with realistic boundary conditions. While some tests have been conducted that measure forces in all directions as well as structural response they are primarily small structures constructed out of unrealistic building materials (Shafiei, eat al. (2016), Al-Faesly, et al. (2012)). These small scale tests showed that a six axis load cell works well to provide a realistic fixed boundary condition at the base of the structure, however when structures become larger and heavier the can require additional restraints as seen in Wienke and Oumeraci (2005). Linton, et al. (2013) was successful at measuring tsunami force on a wall at full scale, however the boundary conditions were not representative of a full-scale structure. Numerous tests showed that pressure sensors on the front face of a test specimen can be used to measure the demands on the system (Shafiei, eat al. (2016), Al-Faesly, et al. (2012), Wienke and Oumeraci (2005)). Gills (2018) showed that multiple pressure sensor layouts can be used and integrated together for larger structures. All tests examined used load cells to measure forces on the system, the challenge however is how to utilize the load cells to provide realistic boundary conditions and be able to measure forces in all directions, this is the challenge this research hopes to provide a new solution for.

Chapter 3. DESIGN OF PROTOTYPE VES WITH CORE WALLS

This chapter details the structural archetype design of a vertical evacuation structure that was completed in order to determine an appropriate size for scale models that could be tested. The chapter presents a summary of existing vertical evacuation structures in both the United States and Japan. It then summarizes the design of the full-scale structure accounting for both tsunami loading and earthquake loading without ductility. It concludes by describing the selected geometry of the scale model to be tested as well as the anticipated loads on the scale model.

3.1 BACKGROUND ON VERTICAL EVACUATION STRUCTURES

As communities in the Pacific Northwest of the United States come to recognize the threat of the Cascadia Subduction Zone and its potential to produce both large magnitude earthquakes as well as tsunamis along the northwest coast, coastal communities are taking many measures to protect their people and infrastructure from the devastating effects of a tsunami. There are many ways to protect coastal residents from tsunamis, most of which originate from Japan where the threat of tsunamis has been part of community planning for many years. The safest method to mitigate loss of life during a tsunami is to get to high ground where the water will not reach. In many cases however high ground could be miles away, for this reason other concepts have been used to protect people. One of these concepts is to construct a large berm (artificial high ground) along the coast that people can flee to in the event of tsunami. Another solution is to build tall structures that can withstand the force of a tsunami where people can evacuate to the upper levels when a tsunami occurs. These are henceforth referred to as vertical evacuation structures (VESs).

FEMA P646 (2008) lists a number of VESs constructed in Japan that could be used to influence the design of VESs in the United States. A list of these structures is provided in Table 3-1. Structures currently constructed or in the final planning phases in the United States are also included in this list.

Table 3-1: Vertical Evacuation Structures Examined

Name	Location	Open/Closed	Lateral Force Resisting System	Comments
Tasukaru Tower		Open	Steel Moment Frame	
Nishiki Tower	Kise, Japan	Closed	Concrete Core Walls	
Aonae Elementary School	Aonae, Japan	Hybrid	Concrete Core Walls	breakaway walls below innundation depth
Kaifu Tsunami Refuge	Kaifu, Japan	Open	Concrete Core Walls	
Shirahama Beach Resort Refuge Shelter	Shirahama, Japan	Open	Concrete Moment Frame	
Ocosta Elementary School	Westport WA, USA	Closed	Concrete Core Walls	
OSU Marine Science Building	Newport, OR, USA	Closed	Concrete Core Walls	
Tokeland Evacuation Tower	Tokeland, WA, USA	Open	Steel Moment Frame	

There are two methods historically used in VESs to resist tsunami loading (FEMA P646, 2008). The first is to design an open structure that allows the water to pass through, such as the Tasukaru Tower in Japan (Figure 3-1(a)), providing only a small area for water to apply pressure to and reducing the overall force on the system. The second method is to use a strong and stiff closed structural system such as thick reinforced concrete walls like the Nishiki Tower in Japan (Figure 3-1(b)). Both of these systems need to be designed robustly enough to withstand the forces of a large magnitude earthquake, tsunami and any potential debris that may impact the structure. The structures are designed to provide shelter on the top levels while simultaneously resisting large tsunami forces at the lower inundated levels. Furthermore because tsunami forces can be much greater than the force of the preceding earthquake the walls or columns used in the lateral system must remain elastic during the earthquake.

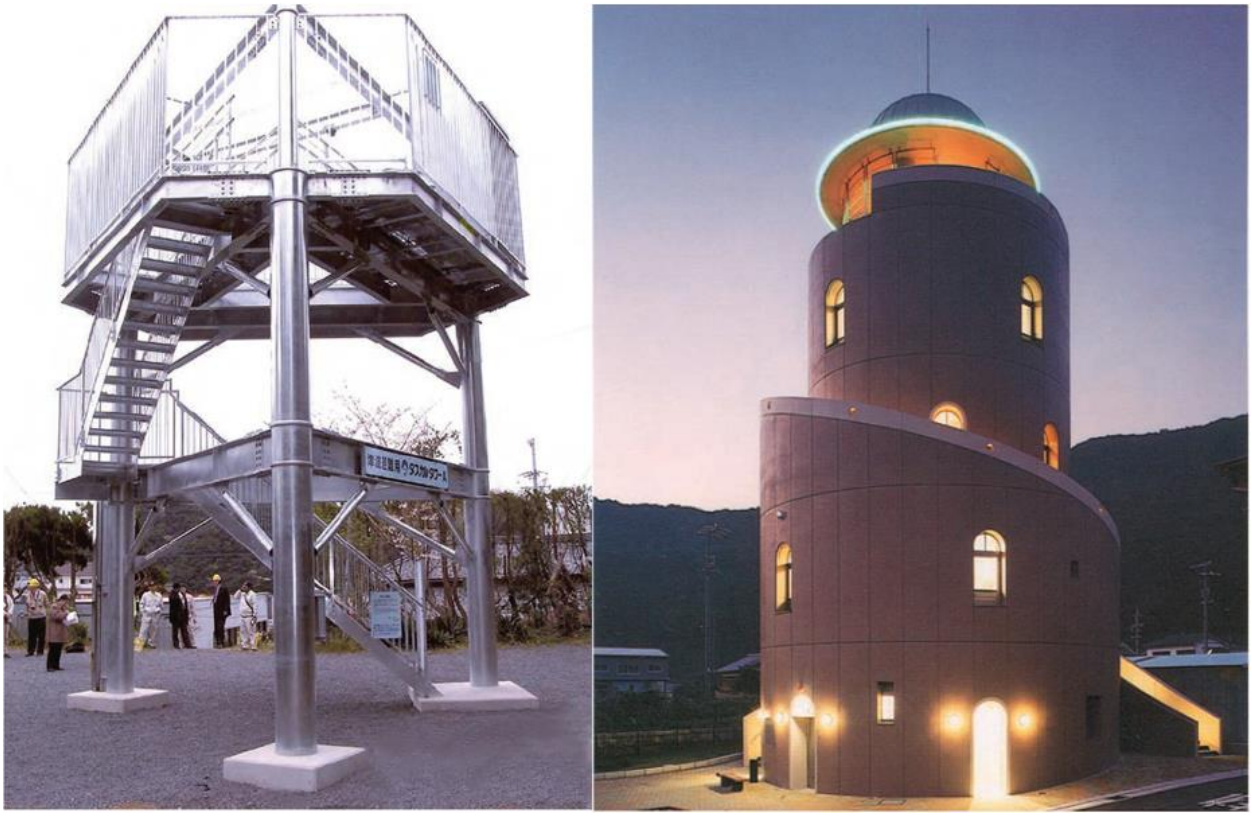

(a) (b)

Figure 3-1: (a) Tasukaru Tower and (b) Nishiki Tower (FEMA P646, 2008)

Other examples of VES's constructed in Japan include a VES integrated into an elementary school designed with reinforced concrete structural walls as the LFRS (Figure 3-2(a)). The top stories serve as the evacuation shelter while the lower stories have breakaway walls to reduce the tsunami forces on the structure. Other examples include elevated platforms constructed out of reinforced concrete with open bases to allow water to pass through (Figure 3-2(b) and (c)).

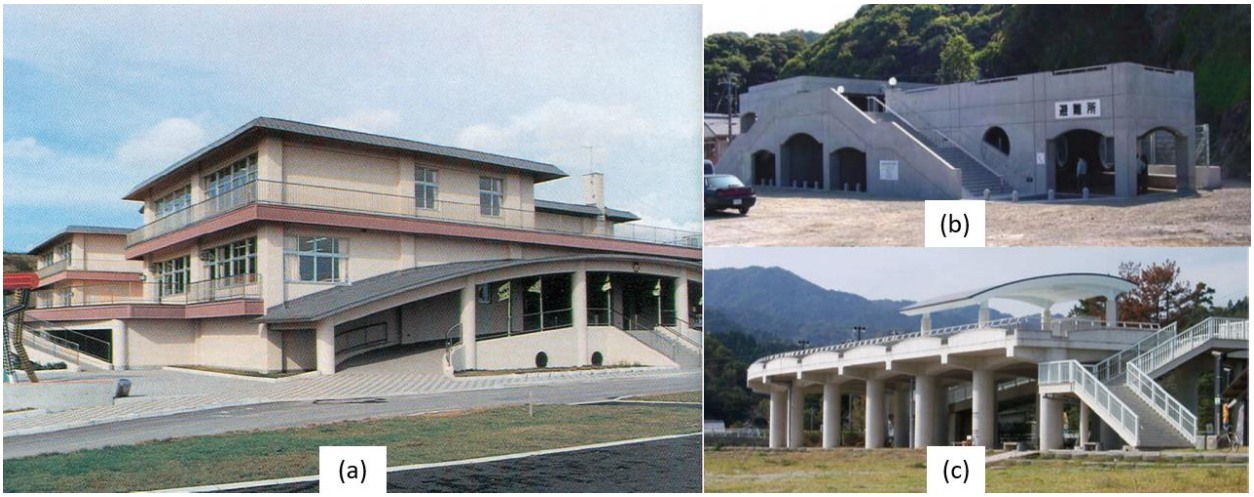

Figure 3-2: Additional Japanese VESs, (a) Aonae Elementary School, (b) Kaifu Tsunami Refuge, (c) Refuge Shelter at Shirahama Beach Resort (FEMA P646, 2008)

As communities across the coastal northwest begin to plan for the threat of tsunamis a number of VESs have been planned and to date one such structure has been built. The first VES constructed in the United States is located in Westport, Washington. Completed in 2016 the Ocosta Elementary was built as an addition onto the community's existing elementary school shown in Figure 3-3: Ocosta Elementary VES (a) Photograph and (b) Overview Rendering of Building

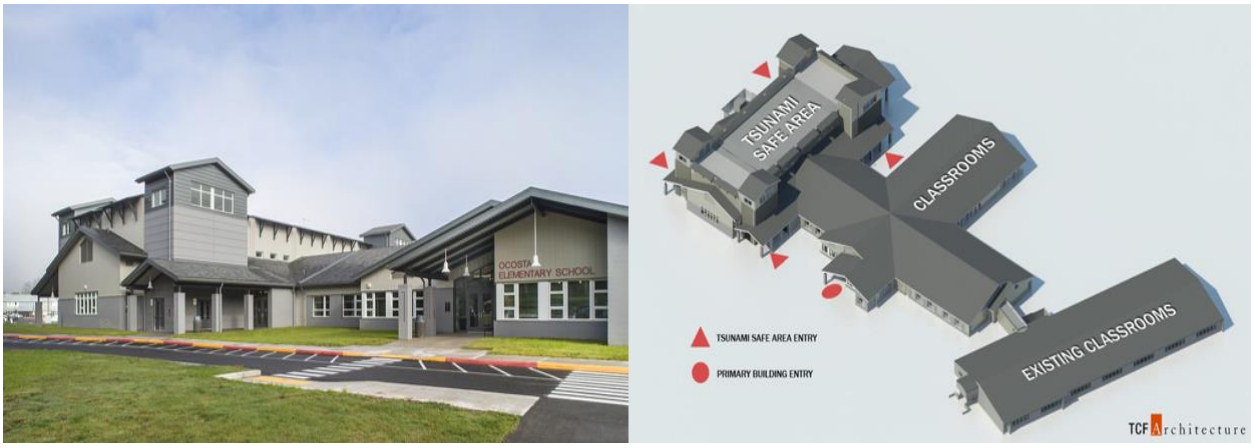

(a) (b)

Figure 3-3: Ocosta Elementary VES (a) Photograph and (b) Overview Rendering of Building

The tsunami evacuation shelter is located on the roof of the school's new gymnasium. A schematic of the structural system can be seen in Figure 3-4. The structure utilizes four special reinforced concrete core walls as the main lateral-force resisting system. The cores serve a dual purpose as both the lateral system and a protective housing for stairwells that allow people onto the roof in the event of a tsunami. The roof of the structure spans between the four concrete cores. Gravity

loads from the shelter platform are carried by the core walls as well as a number of concrete encased columns. The girders that transfer the shelter loads were designed with redundancy such that if any one of the columns supporting it were to fail the girder would still be able to hold up the shelter platform. The foundation for the school was constructed out of a series of 24" piles driven deep into the ground to avoid liquefaction issues present at the site. The piles were interconnected with a series of pile caps and grade beams. (Ash, 2015)

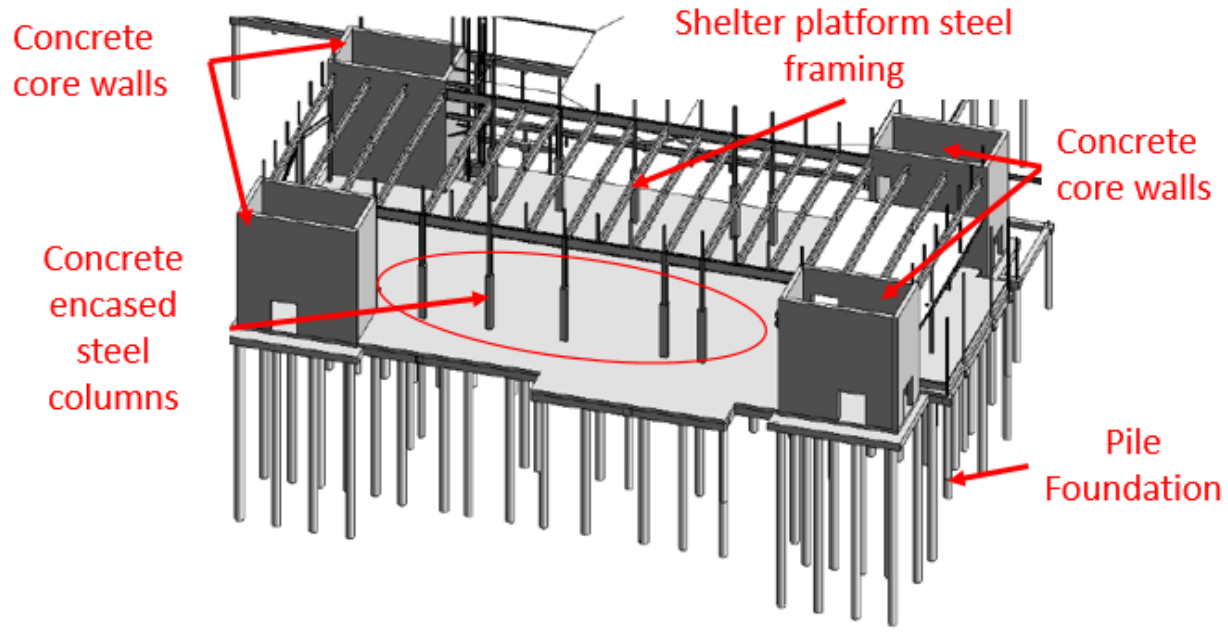

Figure 3-4: Ocosta Elementary School Structural Framing Model (Ash, 2015)

Another VES (shown in Figure 3-5) is currently being constructed in Newport Oregon. This structure is being built into a new marine studies building for Oregon State University. The building will consist of new laboratory, academic and research spaces as well a large community space. The building is designed such that the roof of the building can be used as a safe refuge in the event of a tsunami. The shelter will be accessible by a large ramp built into the outside of the building as well as a number of stair cores and elevators. The stair cores and elevator shafts serve the dual purpose of transporting people to the shelter while also providing a location for building cores to be placed that will act as the main lateral force resisting system for the structure.

Figure 3-5: Rendering of Planned Newport, Oregon VES

In addition to the previously discussed structures is a planned VES located in Tokeland, WA. This structure is currently being designed as an open platform similar to the Tasukaru Tower in Japan. The structure will utilize a steel moment frame system as its lateral force resisting system. While the structure will offer refuge to the community in the event of a tsunami the tower offers limited utility at other times and civilians will not be allowed to enter the tower unless there is an impending tsunami.

Figure 3-6: Planned Tokeland WA VES

After a review of the structures built to date in both the Pacific Northwest and Japan a few common trends were found:

- Incorporating a VES into a building is how the first two evacuation structures in the Northwest were designed.
- In buildings closed systems with large stiff concrete walls were used to carry lateral loads from both earthquakes and tsunamis.
- Evacuation towers that utilize an open system to reduce tsunami loading are another common method used for VESs however they offer limited utility outside of tsunami refuge.
- There have been limited attempts to date to incorporate an open system into a building.

Based on the construction of the VES in Westport, Washington and Newport, Oregon, a structural archetype was designed into a building utilizing reinforced concrete core walls as the main lateral force resisting system.

3.2 Demand Analysis and Prototype Building Design

The purpose of the archetype design was to be able to determine site specific loading for a VES in the Pacific Northwest. The loads on the archetype structure could then be applied to different structural systems in order to compare open and closed systems. This research is focused on the design and testing of a VES that utilizes reinforced concrete core walls as the lateral force resisting system. In addition to improving the understanding of the response of a closed VES to tsunami-type loading, this also serves as the reference structure and specimen for a new open-type concrete-filled steel tube framing system. The archetype could also be used to investigate a system that utilizes breakaway slabs to reduce the uplift forces due to tsunami inundation.

The objectives of the prototype building design were as follows:

- Determine site-specific loading for a vertical evacuation structure on the coast of the Pacific Northwest.
- Select a building site and geometry such that tsunami loading was the controlling design loading
- The geometry and site specific loading characteristics of the archetype structure can be used to investigate different lateral force resisting systems.

The following process was used to design the archetype structure:

1) Select location
2) Select geometry
3) Evaluate earthquake loading
4) Evaluate tsunami loading
5) Reiterate geometry so that tsunami controls over earthquake loading

A location was needed for the site in order to determine site specific tsunami and earthquake loading. An overall geometry of the building was also needed to determine loading on the structure. After a location and geometry were selected earthquake and tsunami loading at the site were determined. After the first iteration it was found that for certain geometries at the selected site earthquake loading was greater than tsunami loading. The geometry of the building was then adjusted so the tsunami loading was the controlling load and the lateral system was then designed for both tsunami and earthquake loading, while tsunami loading was the controlling load case in the on shore direction.

3.2.1 *Location Selection*

The following criteria were used when selecting a location for the vertical evacuation structure:

- Inundation depth greater than 20 feet to ensure it exceed the second-story slab
- Previous modeling of the site available

In order to investigate the potential of using breakaway slabs as a way to reduce the upward forces on the buildings substructure an inundation depth of at least 20’ was needed. This would allow for full inundation of the first story of the building while allowing the upper stories to be used as an evacuation shelter similar to the Aonae Elementary School in Japan.

The ASCE 7-16 code requires a numerical model to determine the inundation depth for the design of VESs in the United States. Due to the complexity and work involved in creating this type of model, it was decided that the VES archetype should be located in a place where this modelling has already been completed. With this criteria in mind, Seaside, Oregon was selected as a potential site to place the evacuation structure as the town has been examined by prior research projects to determine potential tsunami depths in the city (Reuben et al., 2010). Inundation depths in the city were investigated and it was determined that locating the structure on the block between Avenue

A, Avenue C, Franklin Street, and Edgewood Street would meet the criteria for site requirements. Figure 3-7 provides an image of the site as well as latitude and longitude.

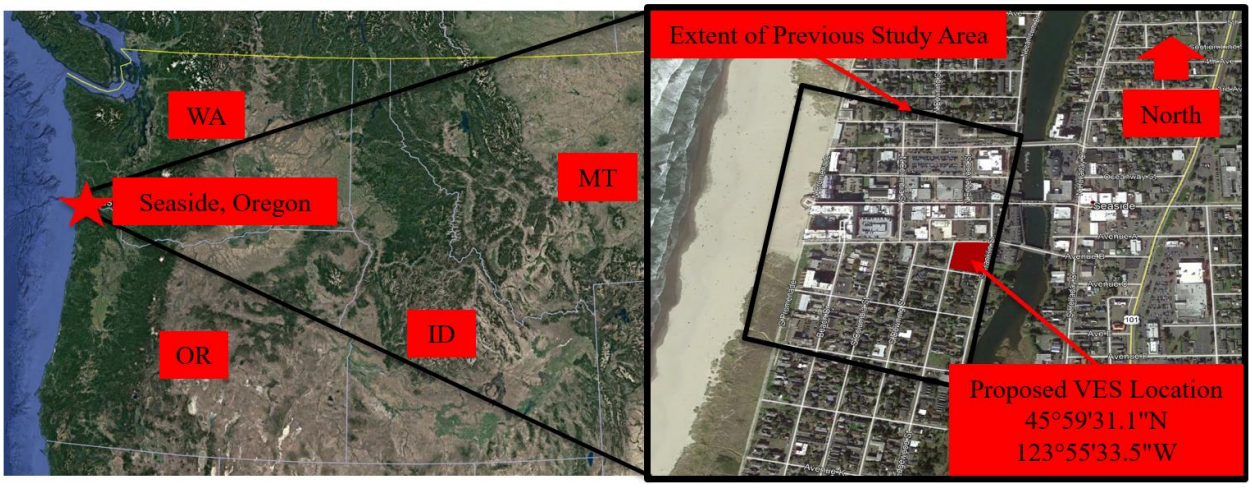

Figure 3-7: Proposed Site Location

3.2.2 *Initial Geometry Selection*

After selecting a location for the structure, geometries for the building were selected. The following criteria was used to determine the geometry of the structure:

- Representative of large hotel since a primary industry in the location is tourism.
- Tsunami loading controls over earthquake loading with response modification factor (R)=1
- Core walls frame typical central elevator shafts and stairwell openings

The geometry for the building, including height and floor plan, was selected to achieve the functionality and force level. The functionality of the structure was to ensure that the upper levels could be used for evacuation during the tsunami while the first level of the structure could be "sacrificial" during the tsunami such as lobby space, parking, or other open shared spaces. This lowest level of the building would allow the water to pass through. The upper levels would house the guest rooms, restrooms, etc. and serve as the evacuation shelter.

The first geometry investigated is shown in Figure 3-8 with the following dimensions and loading properties:

- A footprint of 150 ft. x 150 ft.
- A height of 75 ft.
- 5 stories with a story height of 15 ft.
- A seismic weight of 3,375 kips per story (150 psf. x building width x building depth)

The seismic weight for the structure was determined assuming a 10 in. thick, two-way, reinforced concrete slab with mild reinforcement (without prestressing), would be used as the floor system at each level including the roof. The core walls were to resist the unreduced earthquake and tsunami loads on the structure.

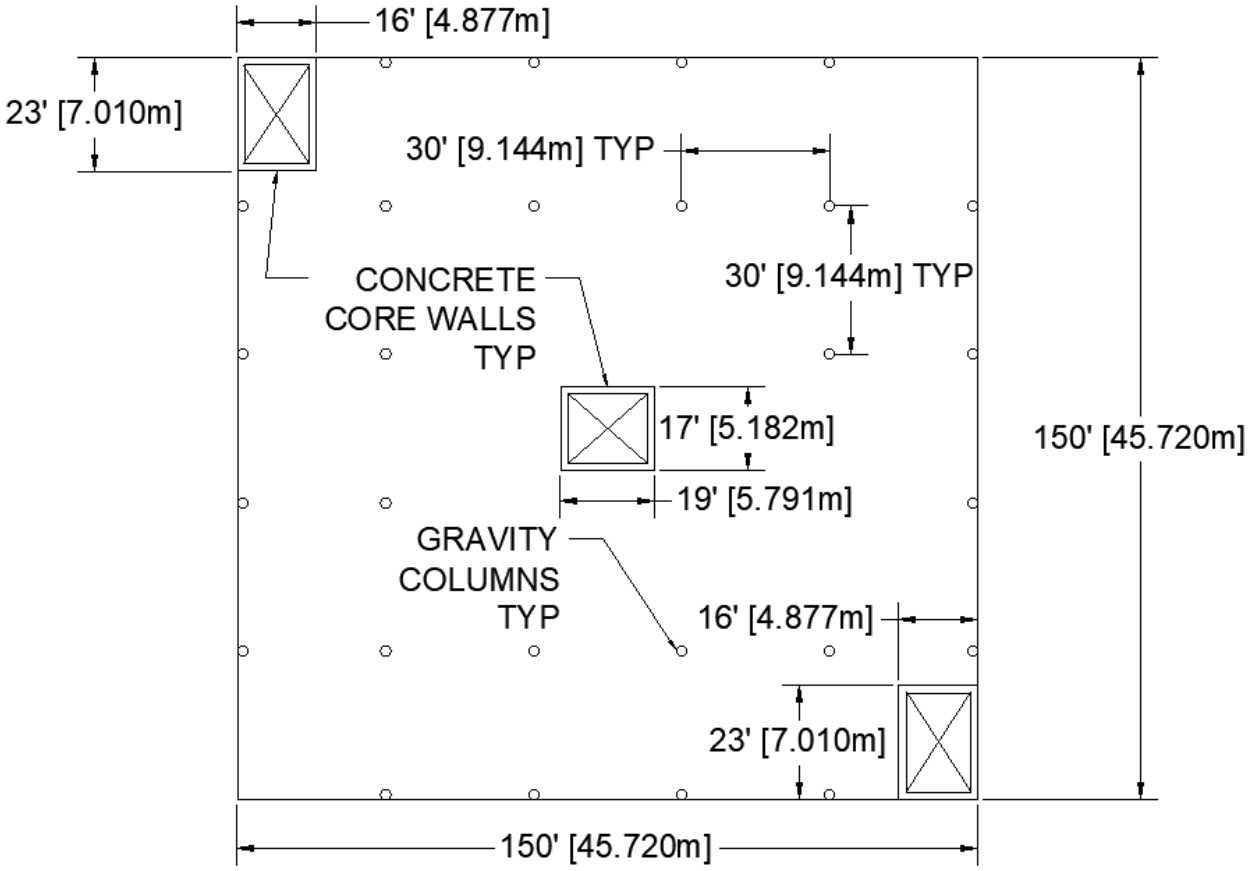

Figure 3-8: Plan Geometry 1

3.2.3 *Determination of Earthquake Load*

Once a geometry and site for the VES were selected earthquake and tsunami loads were evaluated. Earthquake loading was determined using the Equivalent Lateral Force (ELF) method. The following parameters were used to evaluate earthquake loading on the structure:

- Risk category IV (I_e = 1.5) (ASCE 7-16 Table 1.5-2)
    - Vertical evacuation structures must be Risk Category IV
- T_1= 16 s, S_1 = 0.7, S_s = 1.3 (from ASCE 7-16 Figures 22-14, 22-1, and 22-2 respectively)
- F_a = 1, F_v =1.7 (from ASCE 7 Tables 11.4-1 and 11.4-2 respectively)

- Site class D (worst-case scenario) was assumed due to lack of site-specific soil information.

- R=1
  - R was assumed to be 1 to ensure the structure would not lose any capacity and still be fully functional after the earthquake. Because R is a measure of the ductility of the structure setting R=1 means that very limited will occur in the structure and it will still have nearly its full capacity when the tsunami strikes.
- Natural period (T) for structure was found to be .6036s (per ASCE 7 section 12.8)
- C_s=1.95
  - C_s was evaluated per ASCE 7 12.8 and found to be nearly 2, meaning the structure will undergo nearly 2 times the force of gravity on it in the lateral direction. This large C_s value results from R = 1 and I = 1.5 as well as the worst-case scenario due to uncertainties in soil conditions.
- Total base shear V_{EQ} = W * C_s = (16875 kips) * 1.95 = 32,906 kips
  - W – Seismic weight of the structure = (5 stories) * 3,375 kips = 16,875 kips.

A full summary of calculations can be found in Appendix A.

3.2.4 *Determination of Tsunami Load*

After an evaluation of Earthquake loading on the structure was complete, tsunami loading was investigated. Tsunami loads were calculated using ASCE 7-16 Ch. 6. This chapter provides two different methods for calculating tsunami forces on a structure, both of which must be determined for a VES.

The first method is the Energy Grade Line method detailed in ASCE 7-16 Section 6.6. This method calculates inundation depths and flow velocities at a specific site based on the run-up elevation of an incoming tsunami. This analysis uses topographical data to work backward from the run-up elevation of the maximum credible tsunami to the proposed site, taking into account energy losses in the tsunami from changes in elevation and surface friction along the ground, as illustrated in Figure 3-11.

To obtain topographical data, run up elevations, and ground subsidence at the site *asce7tsunami.online* was used. Figure 3-10 illustrates the topography of the three transects with

the site location indicated (between 2000 and 2200 ft. from the shoreline) and Table 3-2 provides the run up elevation and ground subsidence values used in the analysis from *asce7tsunami.online.* The code requires that three topographical transects be used, one perpendicular to the shoreline and the other two ±22.5° from the first. This is done to account for tsunamis coming at different directions to the shoreline. Each of the transects must span from beyond the mean high water line on the offshore side to beyond the run up elevation and must pass through the proposed site, as illustrated in Figure 3-9. Land shaded in blue in this figure depicts areas that will be inundated by the tsunami. The orange triangles are points where the run up elevation is given. The maximum inundation depth at the site from the three transects is used for design. The code requires that the analysis takes into account the effects of ground subsidence due to a Cascadia Subduction Zone earthquake. The Juan de Fuca Plate is currently sub-ducting under the North American Plate causing the ground to rise, when the North American Plate slips off the Juan de Fuca Plate a large magnitude earthquake will be produced and the ground will go down.

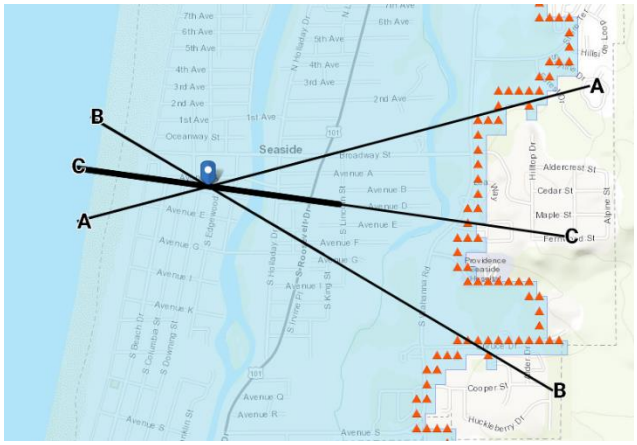

Figure 3-9: Topographical Transects Used in EGL analysis

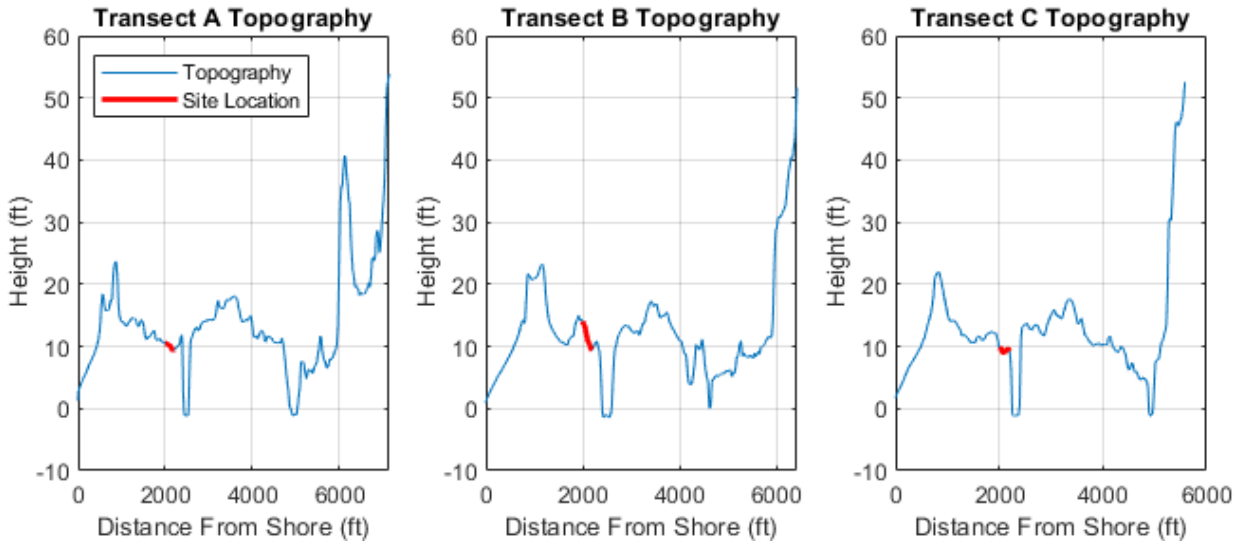

Figure 3-10: Topography of transects

Table 3-2: Transect run up elevations and ground subsidence

Transect	A	B	C
Run Up Elevation	54.7	52.0	54.1
Ground Subsidence	4.5		

With this data, ASCE 7-16 Equation 6.6-1 ($E_{g,i} = E_{g,i-1} + (\varphi_i + s_i)\Delta x_i$

Equation 3-1) was used to determine the inundation depth at the proposed site.

$$E_{g,i} = E_{g,i-1} + (\varphi_i + s_i)\Delta x_i \qquad \text{Equation 3-1}$$

Where:
$E_{g,i}$ = Hydraulic head at point $i = h_i + u_i^2/2g = h_i(1 + .5F_{ri}^2)$
h_i = Inundation depth at point i
u_i = Maximum flow velocity at point i
φ_i = Average ground slope between points i and $i-1$
F_{ri} = Froude number = $u/(gh)^{1/2}$ at point i
$\Delta x_i = x_{i-1} - x_i$, the increment of horizontal spacing
x_i = Horizontal inland distance from NAVD 88 shoreline at point i
s_i = Friction slope of the energy grade line between points i and $i-1$
$s_i = (u_i)^2/((1.49/n)^2 h_i^{4/3} = gF_{ri}^2/((1.49/n)^2 h_i^{1/3}$
n = Manning coefficient for terrain segment being analyzed

Flow velocity at the site is determined by $F_r = \alpha(1 - \frac{x}{x_r})^{.5}$

Equation 3-2:

$$F_r = \alpha(1 - \frac{x}{x_r})^{.5} \qquad \text{Equation 3-2}$$

Where:
α = Coefficient to account for tsunami bore velocities

For the proposed site tsunami bores were required to be considered so $\alpha = 1.3$. Figure 3-11 provides a depiction of the variables listed above.

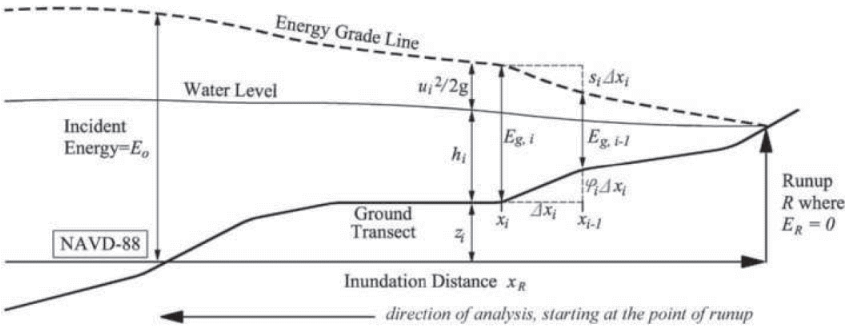

Figure 3-11: Depiction of Variables in $E_{g,i} = E_{g,i-1} + (\varphi_i + s_i)\Delta x_i$

Equation 3-1

Using the aforementioned equations inundation depths and flow velocities at the site were analyzed for the three transects. The greatest inundation depths and velocities were found from Transect C and a plot of inundation depth, flow velocities and topography for Transect C is shown in Figure 3-12. The maximum inundation depth and flow velocity along the three transects at the site are listed in Table 3-3.

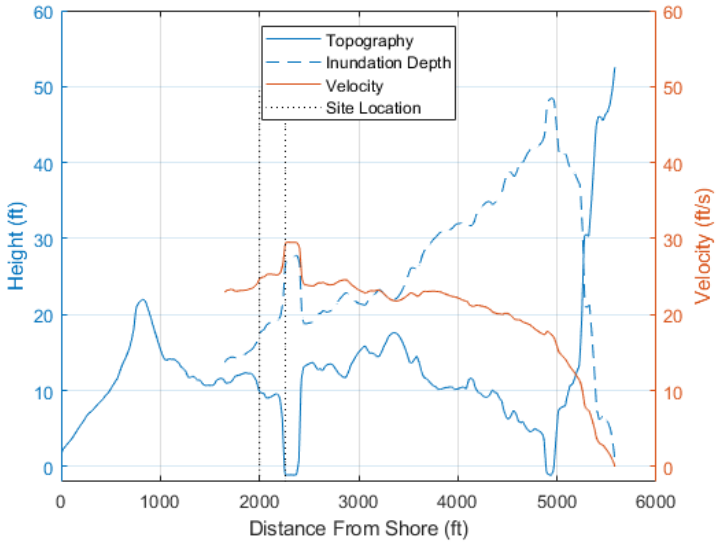

Figure 3-12: Inundation Depth, Velocity, and Topography Transect C

Table 3-3: Max Inundation Depth and Flow Velocity for Transects at Site Location

Transect	A	B	C
Inundation Depth (ft)	12.6	14.7	26.2
Flow Velocity (ft/s)	21.8	23.0	29.2

After completing the energy grade line analysis, the results were compared to a numerical model. As required by ASCE 7-16 Section 6.7. Here, the results of a prior study were used. Rueben et al. (2010) completed a study based on a 1:50 scale model of the section of Seaside Oregon. Scaled structures were placed on a flat beach to investigate how a tsunami bore would propagate through a built environment. The flow depths and velocities from this numerical study were used for comparison to the EGL. Figure 3-13 shows a plan view of the experimental model of Seaside. Numerous gauges to measure flow depth and velocity were placed in the landscape and are labeled in the figure with a white square including a letter and number to indicate the location.

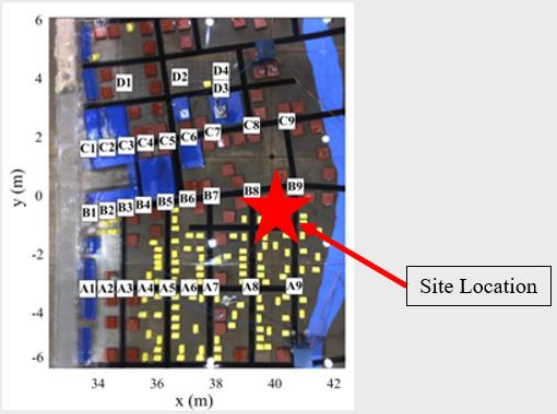

The location of USWG and ADV on the flat section

	USWG1/ADV1(A)		USWG2/ADV2(B)		USWG3/ADV3(C)		USWG4/ADV4(D)	
Position	X (m)	Y (m)	X (m)	Y (m)	X (m)	Y (m)	X (m)	Y (m)
1	33.611	-3.193	33.721	-0.588	33.809	1.505	35.124	3.712
2	34.103	-3.194	34.218	-0.533	34.553	1.604	36.684	3.888
3	34.534	-3.184	34.679	-0.467	35.051	1.686	38.086	4.070
4	35.040	-3.181	35.176	-0.406	35.556	1.769	38.141	3.585
5	35.544	-3.194	35.747	-0.317	36.050	1.845	N/A	N/A
6	36.355	-3.199	36.635	-0.229	37.047	1.988	N/A	N/A
7	37.767	-3.201	37.773	-0.068	38.243	2.193	N/A	N/A
8	39.223	-3.204	39.218	0.135	39.208	2.338	N/A	N/A
9	40.676	-3.228	40.668	0.269	40.400	2.582	N/A	N/A

Figure 3-13: Instrument Locations in Seaside Model from Reuben et al. 2010

Results of this study varied significantly from the results of the energy grade line analysis. Figure 3-14 shows the flow depth and velocity at various locations along the B line of the experiment. Location B9 was the closest to the proposed VES site. As shown the flow depth and velocity were significantly higher near the shore, Location B1 saw the highest inundation depth and velocity, and from that location inland the velocities and flow depths decreased, counter to what the EGL

analysis showed. It was determined that this was likely due to the inclusion of a large berm near the shore in the EGL that was not included in the experiment.

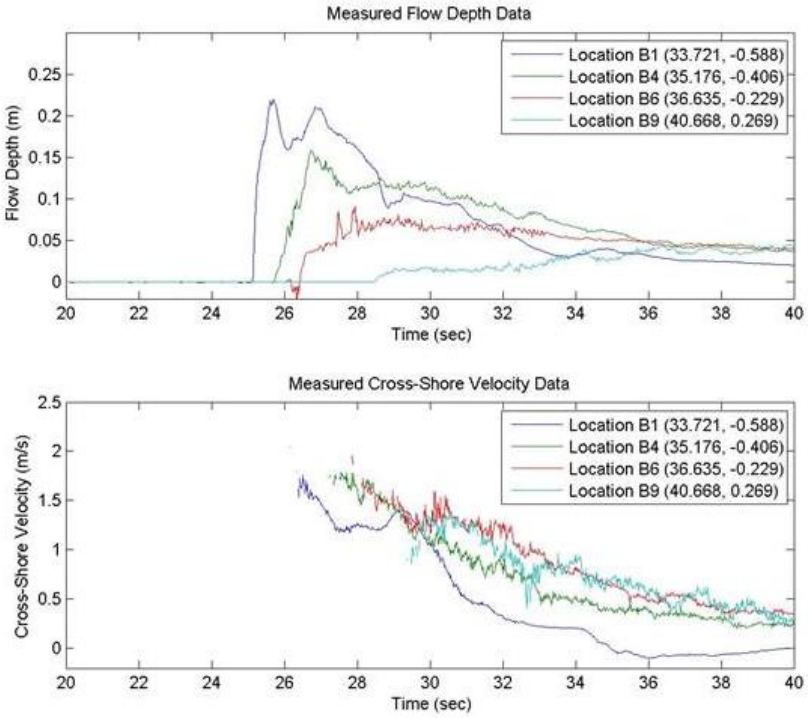

Figure 3-14: Flow Depth and Velocity from Reuben et al. 2010

Due to significant differences between the modeling and the EGL, inundation depths and flow velocities from the EGL were used to evaluate the tsunami loads on the structure. To determine the tsunami load, ASCE 7 assumes a uniform pressure acts over the face of the structure that is closest to the shore. The magnitude of this pressure was determined using $p_{uw} = 1.25 * I_{TSU} * \gamma_s * H_{max}$ Equation 3-3.

$$p_{uw} = 1.25 * I_{TSU} * \gamma_s * H_{max} \quad \text{Equation 3-3}$$

Where:

$p_{uw} =$ Pressure on the onshore face of the structure due to a tsunami = 2,887.5 psf

$I_{TSU} =$ Importance factor for tsunami loading (from ASCE 7 table 6.8-1) = 1.25 for VES

$\gamma_s =$ The density of seawater = 64 lb/ft^3 *k_s

Where:

k_s = 1.1 to account for suspended solids and other small debris in the tsunami flow

$H_{max} =$ Maximum inundation depth at the site =26.25 ft.

The total load of the tsunami on the building was then calculated using $P_{TSU} = p_{uw} * 1.3 * H_{max} * b_w$ Equation 3-4, assuming that the entire front face of the building will transfer load to the lateral force resisting system.

$$P_{TSU} = p_{uw} * 1.3 * H_{max} * b_w \quad \text{Equation 3-4}$$

Where:

p_{uw} = Pressure from the tsunami wave found using puw=$1.25 * I_{TSU} * \gamma_s * H_{max}$ Equation 3-3

b_w = The width of the face of the building closest to the shore = 150 ft.

3.2.5 *Geometry Iterations*

Assuming that the pressure acts upon the entire 150 ft. width of the building the tsunami load was calculated to be 14,780 kips. For this particular building geometry the earthquake loading was nearly twice the magnitude of tsunami loading. Without changing any other input parameters the building's depth was then decreased in order to reduce the seismic weight of the structure and lower the earthquake demands. To determine a geometry that would provide a controlling tsunami loading, the depth was decreased in 30 ft. increments (one typical bay depth) unit. Table 3-4 provides a summary of the building characteristics and demands from the different iterations. It was found that a structure with a footprint of 150 ft. wide by 60 ft. deep was controlled by tsunami loading, when the tsunami load acts upon the 150 ft. side of the building.

Table 3-4: Comparison of EQ and Tsunami Loads for Different Design Iterations

Iteration	**1**	**2**	**3**	**4**
Building Width (ft)	150	150	150	150
Building Depth (ft)	150	120	90	60
Tsunami Load (kips)	14,780	14,780	14,780	14,780
Earthquake Load (kips)	32,906	25,272	18,954	12,636
Tsu Load/Eq Load	0.44	0.58	0.77	1.17

Once loading was determined the concrete core walls of the building were sized to resist shear forces from both tsunami and earthquake loading. The geometry of the cores was determined assuming the concrete cores could carry a maximum shear force of $10*\sqrt{f'c} * A_v$ where $f'c$ is

the 28 day compressive strength of the concrete in psi and A_v is the $0.8A_g$, where A_g is the total area of the web of the concrete core walls. Earthquake and tsunami forces were distributed to the different cores based on the ratio of stiffness values of the different core walls.

Tsunami loading was the controlling load case for the onshore direction (perpendicular to the 150 ft. side of the building), while earthquake loads were the controlling load case for the cross-shore direction. Reinforcement was then determined for the core walls for both shear and flexural demands. A complete calculation package for this design can be found in Appendix A. The final building geometry is illustrated in Figure 3-15.

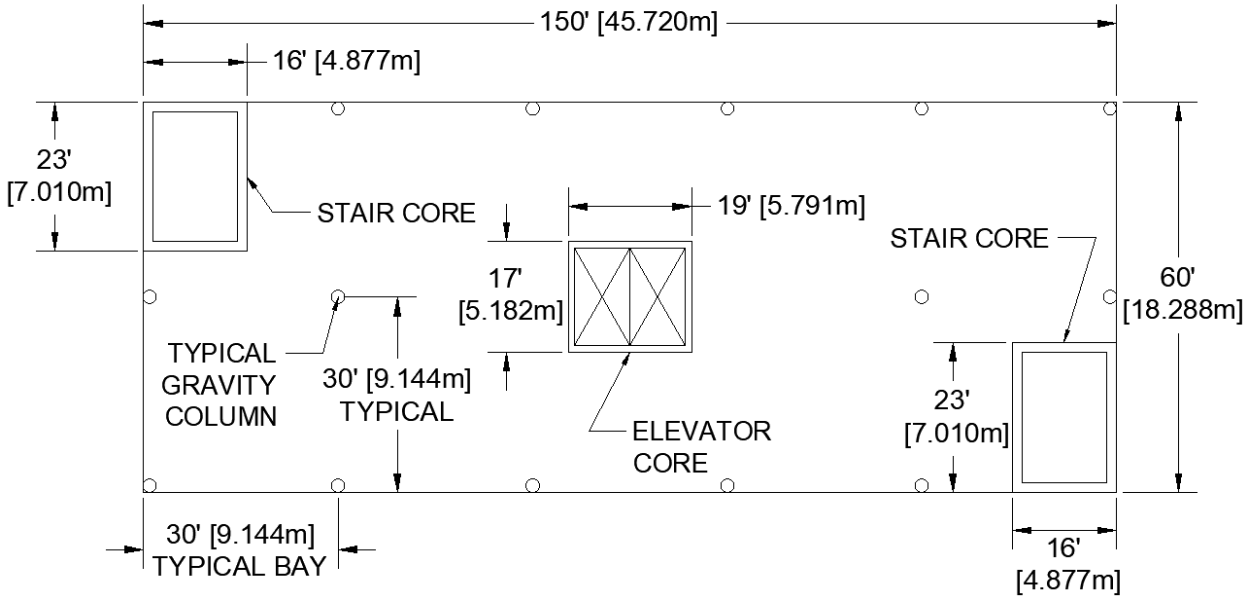

Figure 3-15: Final VES Plan Geometry

Chapter 4. EXPERIMENTAL PROGRAM

Experimental work was conducted by a collaborative team from the University of Washington and Oregon State University led by master's students Christopher Pyke and Kenneth Sullivan, in the Large Wave Flume (LWF) at Oregon State University's O.H. Hinsdale Wave Research Laboratory. This chapter details the test specimen design, experimental setup, instrumentation, and test conditions.

4.1 EXPERIMENT SET UP

4.1.1 *Test Facility*

The LWF is 104 m (342 ft) long, 3.7 m (12 ft) wide, and 4.6 m (15 ft) deep. Waves are generated by a piston-type wave maker on the upstream end of the flume. The wave maker is capable of producing regular, irregular, and tsunami-like waves. Tsunami waves are created by generating a solitary wave and then using the bathymetry of the flume or an unstable wave height (a height that cannot propagate indefinitely) to creating the breaking effect of a tsunami wave when it approaches shore. Its maximum stroke is 4 m (13.1 ft) at a speed of 4 m/s (13.1 ft/s). The maximum still water depth in the flume that a tsunami wave can be generated in is 2 m (6.5ft). The maximum wave height the facility is capable of creating given these constraints is a 1.4 m (4.6 ft) solitary wave.
The LWF utilizes a series of movable concrete 3.66 m. (12 ft.) x 3.66 m. (12 ft.) x 0.152 m. (6in.) slabs in order to adjust the bathymetry inside the flume for different experiments. Adjusting the bathymetry changes the way the wave propagates and breaks.

4.1.2 *Preliminary Modeling*

To determine what bathymetry and wave height would produce the largest force on the test specimen a series of preliminary analyses were performed using a numerical model of the flume. This modeling was also used to determine the approximate forces that would act upon the test specimen in order to design the test setup. A parametric study on test specimen location and bathymetric slope was completed using the OpenFOAM software to determine where the structure should be placed in the flume and what slope should be used to achieve the largest possible wave

and wave force. For this study “largest wave” was defined as the wave have the greatest free surface elevation at the top of the ramp.

Several different ramp steepness’s and test specimen locations were tested and are listed in Table 4-1. For each possible combination of ramp slope and distance a 1.4 m. solitary wave was generated in 2 m. of still water by the wave maker and the resulting wave heights at the top of the ramp were recoded.

Table 4-1: Parametric Study Variables

Ramp slopes	Distance from wave maker neutral position to top of ramp (m)
2:2	20
2:5	30
2:10	40
2:20	50
2:30	60
	70

From this study it was found that the farther down the flume the ramp is located the lower the wave height. According to solitary wave theory, this variation in wave height should be minimal or nonexistent, however due to inaccuracies in the numerical model a difference appeared. It was also found that the steeper the slope of the ramp, the larger the wave generated was at the top of the ramp. From this study it was decided that a ramp with a slope of 1:1 should be used and the specimen should be placed as close to the wave maker as possible. Because the LWF utilizes concrete slabs with a length of 12 ft. (3.66 m.) to create bathymetries in the flume, to avoid having to build a custom slope the final ramp slope ended up being 6.56:10 or 33.1°, this corresponds to a triangle with a hypotenuse of 12 ft. (3.66 m.) and a height of 6.56 ft. (2 m.). Upon discussions with staff from the LWF it was decided that the structure should be placed between bays 9 and 10 in the flume, approximately 134 ft. (40.77 m.) from the neutral position of the wave maker. This gave the wave time to fully develop after generation as well as room to place wave instruments before the slope to help characterize the wave. The flume bathymetry and specimen location used in testing is shown in Figure 4-1.

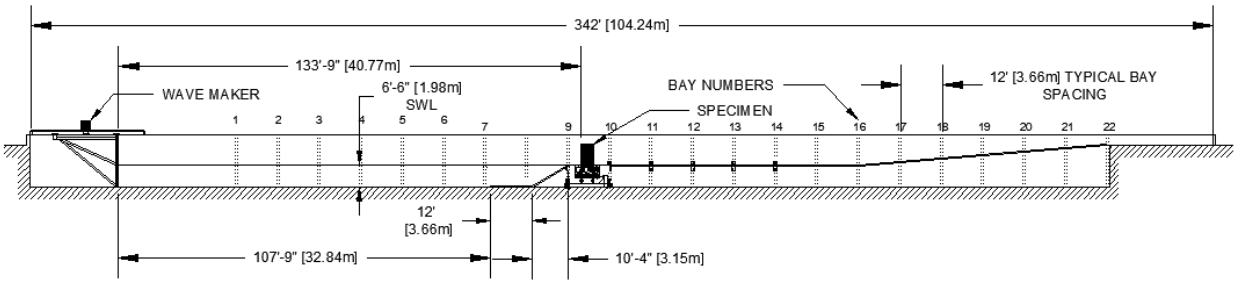

Figure 4-1: Large Wave Flume Bathymetry

4.1.3 *Test Structure and Support Frame*

After the design of the full scale structure was completed geometry for a scale model that could be tested in the LWF was determined. The goal was to test the largest scale model possible and generate the largest force possible on the model. It was determined that a 1:6 scale was the most appropriate and achievable with the given limitations of the flume. The maximum achievable wave height in the flume is 4.6 ft. (1.4 m) at 1:6 scale this translates to a 27.6 ft. (8.4 m) wave at full scale similar to the inundation depth determined for the archetype structure. Another limitation is the 12 kip maximum lifting capacity of the LWF laboratory crane. Due to this limitation, the test specimen and anything permanently fixed to it would need to weigh less than 12 kips. The test specimen was made square so that the same supports could be used for this specimen and another specimen representative of one square bay of the archetype structure, built out of concrete filled steel tubes. The geometry of the specimen was based off taking the longest wall, the 23 ft. (7 m.) side of the exterior core wall, and then making a square box. This translated to a test specimen that was 3 ft. 10 in. (1.168 m) by 3 ft. 10 in. (1.168 m) with 5 in. (0.127 m) thick walls. In order to cut down the weight of the specimen the height of the specimen was reduced from 12.5 ft. (3.81 m) (75 ft. (22.86 m) at full scale / 6) to 6 ft. (1.83 m). The specimen also had a 6.5 in. (0.165 m.) slab at the base of the walls, representative of a structural slab that would transfer lateral loads to the substructure. The final geometry of the test specimen is illustrated in Figure 4-2. The concrete shear wall was supported by four concrete filled steel tube piles located under the corners of the wall. These piles were embedded into a 6.5 in. (.165 m.) concrete slab that was used to transfer loads from the test specimen to a series of load cells. The slab also had threaded rods embedded into the sides of it that allowed steel walls to be fixed to the sides of the slab and create a soil box

that could be filled to investigate how different levels of soil around the structure affected the loading.

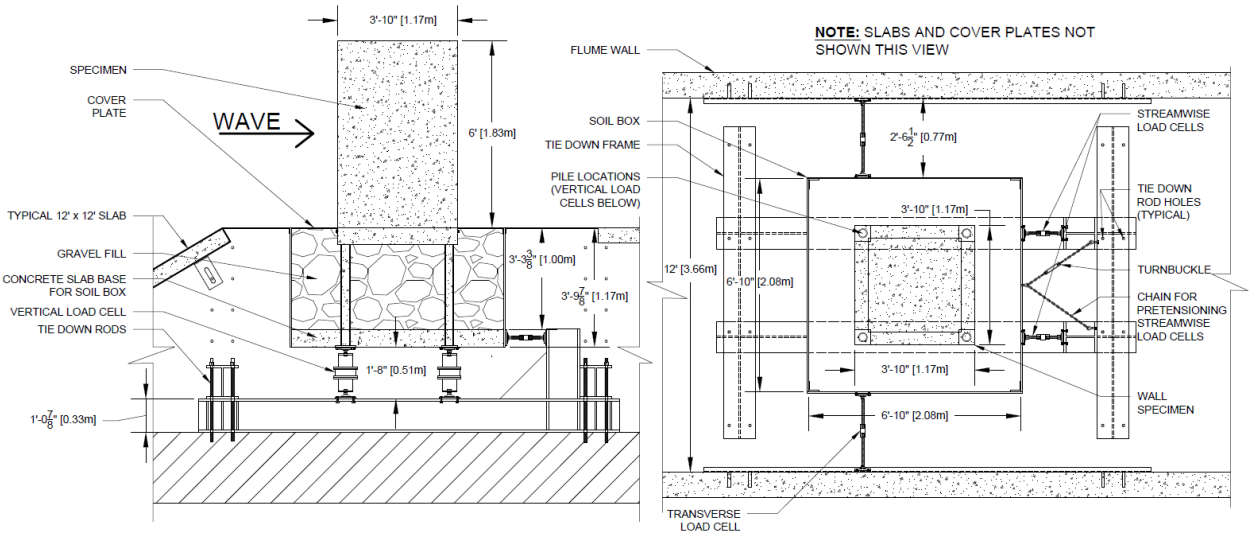

Figure 4-2: Test Specimen

Testing in the wave flume posed a unique question not found in most structural testing, what load is being put into the structure? Most structural testing involves using a calibrated actuator with a load cell to directly measure the force being put into the test specimen. In this case because the applied load comes from a wave rather than a conventional actuator measuring the reactions in all directions on the structure was paramount to knowing the applied load. After examining existing literature, detailed in Chapter 2, no good method for supporting a specimen of this size and weight while accurately measuring applied loading was found. The closest solution found was to use a series of uniaxial load cells with sliders, similar to Gills (2018), so the load cells do not interfere in directions they are not measuring. Other methods like using a six axis load cell under the slab of the structure were considered however they were found to be expensive and would not provide the necessary resolution in the stream wise and transverse directions. Because the weight of the structure, nearly 20 kips when the soil box was full, was so much greater than the anticipated load on the structure, around 5 kips, a load cell with a high vertical capacity was needed while capacity in the stream wise direction needed to be significantly lower. Measuring load in the transverse direction also posed an issue because loading in this direction was found to be close to zero during preliminary modeling. To overcome these challenges a plan to support the structure with a series of load cells with different capacities in the different directions being measured was developed. Keeping in mind that load cells should not be used to measure less than 5% of their capacity

accurately four 50 kip pancake type load cells were used to measure vertical forces, two 10 Kip rod-end load cells were used to measure stream wise forces, and two 2 Kip rod-end load cells were used to measure transverse forces.

To avoid conflicts between the load cells, load cells carrying loads other than axial compression or tension, load cells were connected as a series of truss elements with pin connections on each end to eliminate the transfer of shear and moment forces into the load cells. Truss elements were slightly different for the vertical load cells compared to the stream wise and transverse load cells due to their required capacity and load cell connection points. For all of the load cells the truss elements consisted of an element with 1 in. diameter threaded rods that connected the ends of the element into a rotational bearing. These bearings were welded to a 6 in. (0.152 m.) x 6 in. (0.152 m.) steel plate with holes to allow the plate to be fastened to the test specimen on one end of the element and the reaction frame on the other end. The vertical pancake type load cells, illustrated in Figure 4-3, were connected to a steel plate with holes to accommodate the load cell bolting pattern. This plate was welded to a piece of round HSS with another plate welded to the other end with a threaded hole that allowed for the connection to a threaded rod that could then thread into the previously described ball bearing. This was done to prevent buckling the 1 in rod under the gravity loads of the test specimen. The stream wise and transverse truss elements simply consisted of a 1 in. (0.025 m.) diameter rod threaded into the load cells and then threaded into the ball bearing.

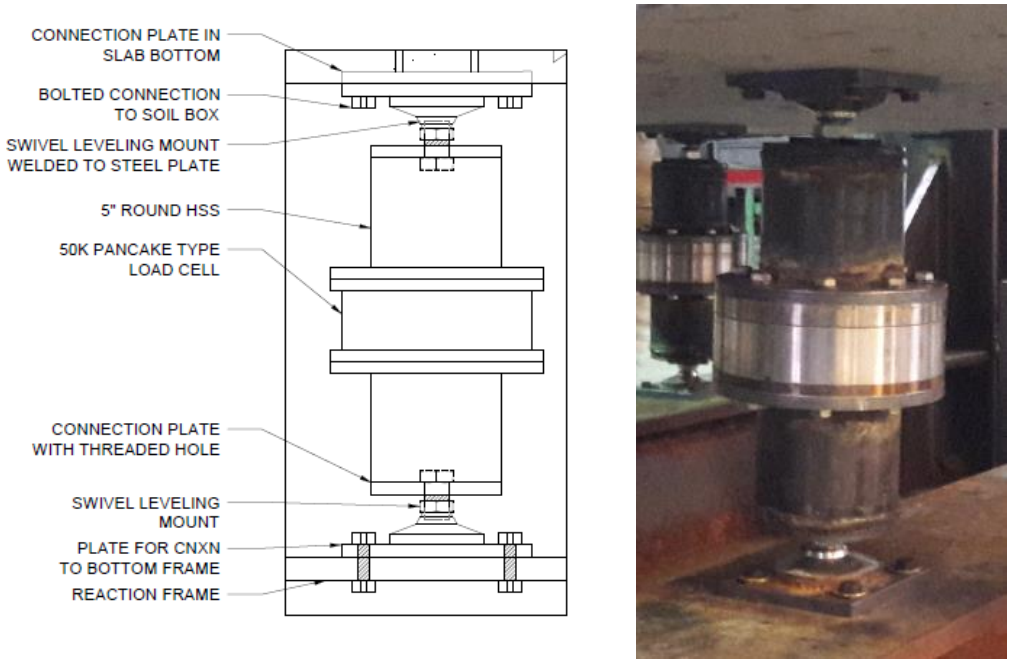

Figure 4-3: Typical Load Cell Connection

Load cells below and behind the structure were connected to a reaction frame that was then anchored to the flume floor. The reaction frame consisted of two W12x106 beams running parallel to the length of the flume. These beams then had another section welded upright to them with a complete joint penetration weld in order to connect the stream-wise load cells. Two other W12x106 beams were then placed transversely over the lower beams to accommodate more tie down holes for tensioning the assembly to the flume floor. The reaction frame was designed to remain rigid during testing. In order to ensure these beams were adequate and would not deflect under wave loading on the structure a model was created using RISA 2D to check deflection. Deflection at the top of the cantilever was checked assuming a 5 Kip point load was applied at the load cell connection, this equal the anticipated load on the entire structure found during preliminary modeling and therefore twice the load either of the given reaction beams were expected to experience during testing, assuming that load is evenly distributed between the two stream wise load cells. Total deflection at the end of the cantilever was found to be .002in, which was determined to be negligible and the beams deemed adequate. Channels were attached to the flume walls on either side of the specimen that the transverse load cells could be secured to.

4.1.4 *Specimen Construction*

After a plan for the dimensions of the test specimen and its supporting fixture were developed the structure was constructed by a team of graduate and undergraduate researchers in the Structures Lab at the University of Washington (UW). Forms for the shear wall were built by constructing a solid base out of ¾ in. plywood with 4 in. x 4 in. beams under it. An enclosed box was then built out of plywood and 2 in x 6 in studs to form the inside of the wall, illustrated in Figure 4-4(a). The wall was cast upside down to avoid issues of consolidating the slab at the bottom of the wall. Number 4 reinforcing bars were placed in the structure, Figure 4-4(b), with a reinforcement ratio of 2%. Based on the applied loads to the structure reinforcement demands were controlled by temperature and shrinkage requirements, not structural requirements. Due to the geometry of the wall the concrete was not expected to crack under wave loading. After reinforcement was placed the steel tubes used for the piles were placed inside the rebar cage and ran to ¾ in. from the top of the wall. Braces were attached to the piles to stiffen them before the base slab was connected and to prevent damage to the piles during lifting and transportation. Walls were constructed around the rebar cage to create the exterior face of the wall, Figure 4-4(c). To further avoid consolidation issues in the 5 in. thick walls with 2 curtains of rebar a 3/8" pea gravel concrete mix with a high slump was used. Detailed construction drawings can be found in Appendix B.

(a) (b) (c)

Figure 4-4: Construction Photos

After the concrete for the wall was cast and cured for seven days the exterior forms were removed and the specimen was lifted off the base of the forms, placed on its side, and the forms that made

the inside walls of the box were removed. The specimen was then flipped upright and placed in a form constructed to cast the 6.5 in. base slab at the bottom of the piles. While the test specimen was being constructed the reaction beam frames were fabricated. After the test specimen and reaction frame beams were constructed the system was assembled at UW and a test was conducted to ensure the setup worked to accurately measure applied loads on the system, see section 4.3: Setup Validation Testing. After the setup was validated the test specimen and reaction frame were shipped to OSU on a flatbed truck.

Figure 4-5: Test Specimen on Truck for Shipping

The test specimen was then unloaded and setup in the flume. The construction sequence was:

1. Place the reaction frame into the flume
2. Tension the reaction frame to the flume floor
3. place and secure beams for the transverse load cells to the flume walls
4. Bring the specimen into the flume and place it on blocks on top of the reaction frame
5. Connect the transverse and stream wise load cells to the test specimen
6. Attach bottom load cells to the reaction frame
7. Lift the specimen just enough to remove the blocking and connect the bottom load cells
8. Place concrete slabs for the sloped section and any other sections of bathymetry that were removed to facilitate installing the structure
9. Construct a deck around the test specimen to act as a beach around the structure with the soil box sitting below grade
10. Fill the soil box with gravel
11. Place covers of the gravel in the soil box

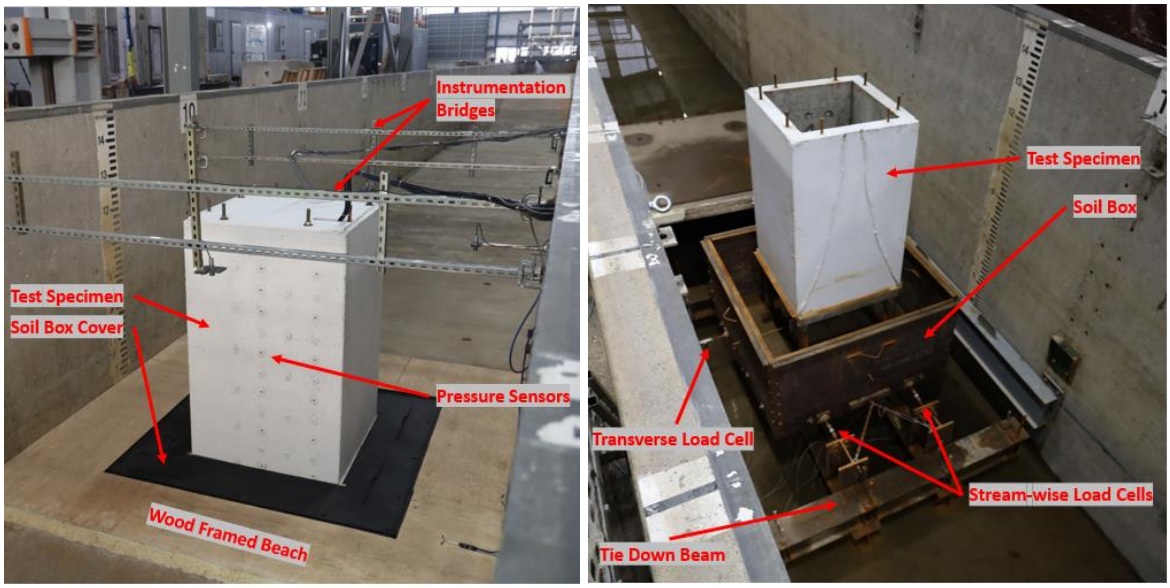

(a) Tested Condition (b) Covers Removed

Figure 4-6: Test Specimen

During testing the soil box was filled with a 3/8" pea gravel. Pea gravel was selected because it was readily available at OSU and was not likely to be removed from the soil box by wave action. The specimen was first tested with the soil box full, then half full and then empty in order to investigate how the loss of soil around the piles affects load transfer and loss of restraint and stiffness when soil is removed. Gravel was loaded into the soil box with buckets and attempts were made to compact the gravel as best possible by hand using a steel plate welded to the end of a rod that could be dropped repeatedly on the gravel.

(a) (b)

Figure 4-7: (a) Gravel Used in Testing (b) Soil Box Being Filled with Gravel

During installation of the test specimen a few issues arose with the setup. Primarily there was difficulty getting the load cells to distribute load evenly. This was not a major issue during preliminary testing at UW, however once installed in the flume one of the transverse load cells and one of the stream wise load cells seemed to be taking all the load in their respective directions. This was likely due to a small amount of axial movement in the rotational bearings of the truss elements. The original design of the load cell setup had both the transverse load cells on the same side of the flume. Under ideal conditions with this setup the stream wise load cells could both be pre-compressed to a very similar load by simply turning the threaded rods that connect them. Having a nearly similar pre load in the load cells causes the applied forces to distribute evenly. This then put one of the transverse load cells into compression and the other in tension to balance out the forces on the system. This was what was able to be done with the preliminary testing at UW however once the specimen was assembling in the flume it was impossible to get both of the stream wise load cells to pre-compress. In order to resolve this issue one of the transverse load cells was moved to the opposite side of the flume and a chain with a turnbuckle in it was attached to the test specimen and the uprights of the reaction frame as shown in Figure 4-2. This allowed both the stream wise load cells and the transverse load cells to be pre-compressed to a nearly even load and distribute the forces on the system evenly between the different load cells acting in the same directions.

4.2 INSTRUMENTATION

4.2.1 *Wave Measurements*

A series of wave gauges and velocimeters were installed in the flume and used to measure flow characteristics. Six wire resistance wave gauges were placed between the specimen and the wave maker to track wave propagation. Around the structure four acoustic wave gauges were placed to track the wave height as it breaks and interacts with the test specimen. The location of the wave gauges is shown in Figure 4-8. Figure 4-9 shows the two different types of wave gauges used. The naming convention for the wave gauges is wg or uswg followed by the instrument number, where "wg" indicates a wire type wave gauge and "uswg" indicates an ultrasonic wave gauge. The gauges were then numbered starting closest to the wave maker and moving downstream.

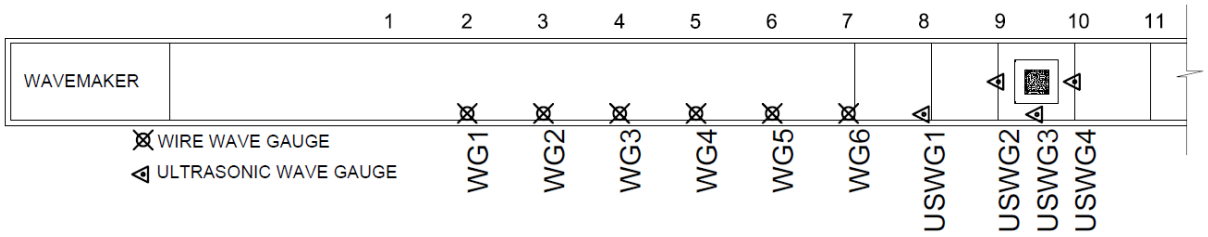

Figure 4-8: Wave Gauge Location Plan

(a) Ultrasonic Wave Gauge (b) Wire Wave Gauge

Figure 4-9: Typical Wave Gauges

Four Acoustic Doppler Velocimeters (ADV) were placed between the wave maker and the test specimen in order to measure changes in local velocities as the wave propagates toward the structure. The locations of the ADVs is illustrated in Figure 4-10. A typical ADV is shown in Figure 4-11. ADVs were also numbered according to their position starting closest to the wave maker and increasing in the downstream direction.

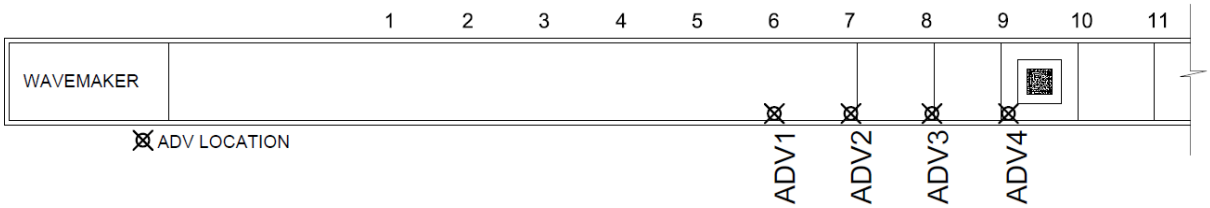

Figure 4-10: ADV Location Plan

Figure 4-11: Typical ADV

A survey of the flume was conducted in order to determine the exact location of instruments relative to the flume. Coordinates for each of the ADVs and wave gauges were found using the following coordinate system. The x-axis starts at the front face of the wave maker when it is in an at rest position and goes parallel to the length of the flume. The y-axis is transverse to the length of the flume with zero being at the centerline of the wave maker paddle. The z-axis is zero at the flume floor and positive going up in elevation from there. Table 4.1 lists the location of each instrument in this coordinate system.

Table 4-2: Wave Instrument Locations

Instrument name	x (m)	y (m)	z (m)
wg1	13.957	-1.389	1.325
wg2	17.620	-1.391	1.319
wg3	21.284	-1.389	1.309
wg4	24.934	-1.383	1.324
wg5	28.588	-1.380	1.323
wg6	32.237	-1.376	1.324
uswg1	36.044	-1.373	3.632
uswg2	39.967	-0.030	3.820
uswg3	41.427	-1.335	3.642
uswg4	43.569	-0.047	3.624
adv1	28.579	-1.451	0.916
adv2	32.220	-1.454	0.932
adv3	36.078	-1.460	0.926
adv4	39.738	-1.466	2.465

4.2.2 *Load Measurements*

Load cells and pressure sensors were both used to determine the total force on the structure due to the wave impact. The load cell layout, shown in Figure 4-12, consisted of four pancake type load cells below the structure and four rod-end load cells connected to the stream-wise and transverse directions of the flume. The naming convention for the load cells consists of a letter indicating the direction of load the load cell is measuring (vertical (V), transverse (T) or stream-wise (S)) followed by a letter and or number indicating what grid line (e.g., A, B) the load cell sits on.

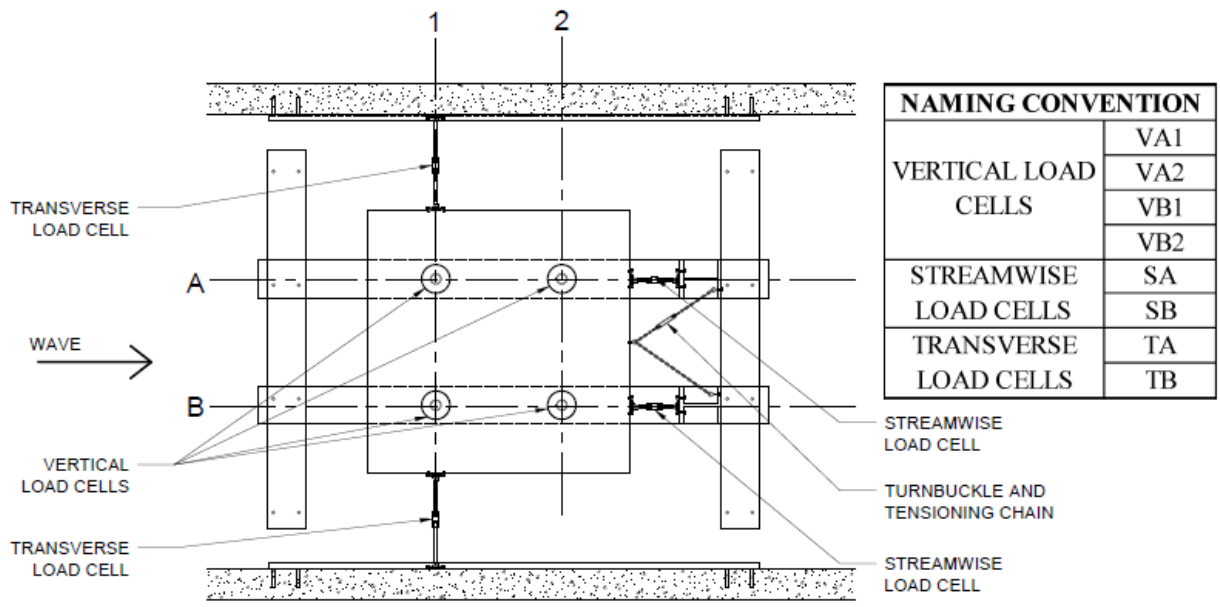

NAMING CONVENTION	
VERTICAL LOAD CELLS	VA1
	VA2
	VB1
	VB2
STREAMWISE LOAD CELLS	SA
	SB
TRANSVERSE LOAD CELLS	TA
	TB

Figure 4-12: Load Cell Layout

Stream-wise forces were measured using two rod end load cells connected to the soil box and then connected to the base reaction frame. A chain and turnbuckle connected to the soil box and then the reaction frame uprights were used to pre-compress the stream-wise load cells so that loads were evenly split between the load cells. Figure 4-13 shows the stream-wise load cells connected to the structure.

Figure 4-13: Stream-Wise Load Cells and Tensioning Chain

Uplift and overturning forces were measured by four pancake type load cells placed under the structure. Each load cell's swivels were connected to the soil box via embedded plates cast into the bottom of the soil box base slab and welded to the bottom of the piles the structure sits upon.

The other swivel was then attached to the base frame. Figure 4-14 shows the vertical load cells connected to the structure.

Figure 4-14: Vertical Load Cells

Two rod-end load cells were used to measure the transverse forces on the structure. The load cells were placed to oppose each other on grid line 1. The load cell's swivels were attached to the soil box walls and then connected to a channel connected to the wall of the flume. Because the two load cells do not sit on unique grid lines they were named according to their closest stream-wise grid line. Figure 4-15 shows the transverse load cells connected to the structure during preliminary testing at UW.

Figure 4-15: Transverse Load Cells

4.2.3 *Pressure Measurements*

Pressure measurements were taken with a series of Druck PDCR 830 pressure transducers available at the LWF. These gauges are designed to be mounted flush against a surface and can

accurately measure pressures from wave impacts. Unfortunately the manufacturer of the gauges has gone out of business and therefor only the gauges on hand at OSU could be used and no more could be ordered. According to researchers from OSU they are the best gauges available for measuring wave impact forces and they do not yet have a solution for replacing the gauges when they break over time. At the beginning of testing 13 of these gauges were working however during the course of testing one gauge was broken. The preliminary modeling of the structure was used to help determine the best locations to place the available sensors. It was found that beyond 5 ft. up the wall from the beach pressures were negligible so no sensors were located higher than this. It was also found through modeling that the pressures were the same on either side of the walls centerline so if the pressure distribution was characterized well for one side of the wall that pressure distribution could be applied to both halves of the wall to compute the total force on the wall from the wave. To validate this assumption one line of the pressure sensor grid was split between the two halves of the front face to confirm that the pressures could be mirrored across the walls centerline. The pressure sensors were located as close to the edges of the wall on the sides and bottom as physical limitations would allow. To avoid conflicts with the side walls of the specimen the closest row to the edge of front wall was placed 7 ½ in. from the side of the specimen. To avoid conflict with the base slab inside the wall the bottom row of pressure sensors was placed approximately ¾ in. up from the level of the beach. With these assumptions and limitations a grid of 33 pressure sensors was developed, as shown in Figure 4-16(a). To characterize the entire face of the wall five different pressure layouts were used. Originally it was planned that only three different layouts would be needed, consisting of three pressure sensors that would stay in the same location across the different layouts to confirm that pressures were consistent across trials, and 10 moving sensors that would be placed in different locations across the wall. However because one of the pressure sensors was broken over the course of testing two other pressure layouts were added to account for the lost sensor. The different pressure layouts are illustrated in Figure 4-16(b).

To connect the pressure sensors to the structure a series of PVC pipes were cast into the concrete. Standard PVC pipe caps were machined so they could be removed by hand after being installed. The caps then had a hole drilled and tapped in their centers that the pressure sensors could thread into. With this solution the pipe caps and pressure sensor heads projected out of the face of the wall about ¼ in., approximately the thickness of the head of the pipe cap. This connection is detailed in Figure 4-17(b) This was done so that the pressure sensors could easily be threaded into

the pipe caps and then placed into the wall without twisting the pressure sensor and its attached cable that ran to the data acquisition system.

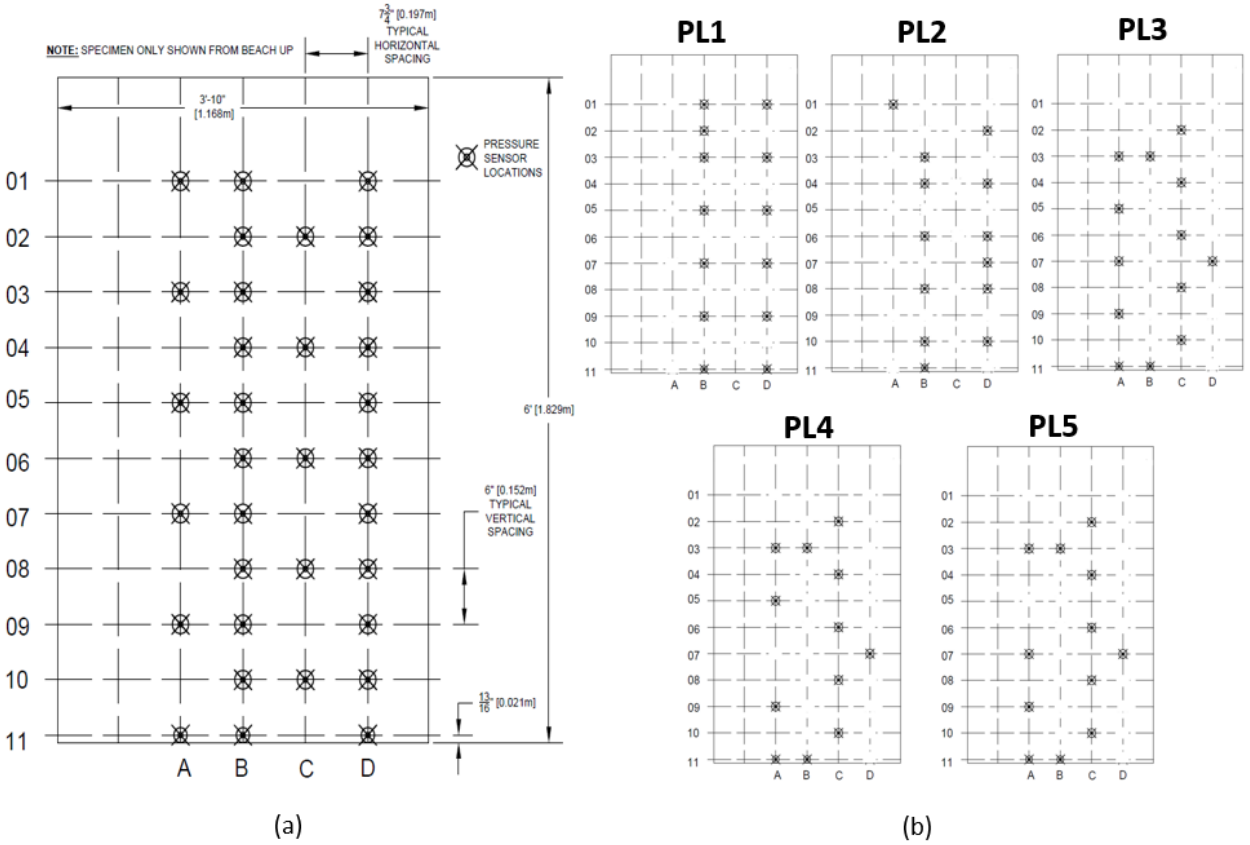

Figure 4-16: (a) Pressure Sensor Locations and (b) Pressure Sensor Layouts

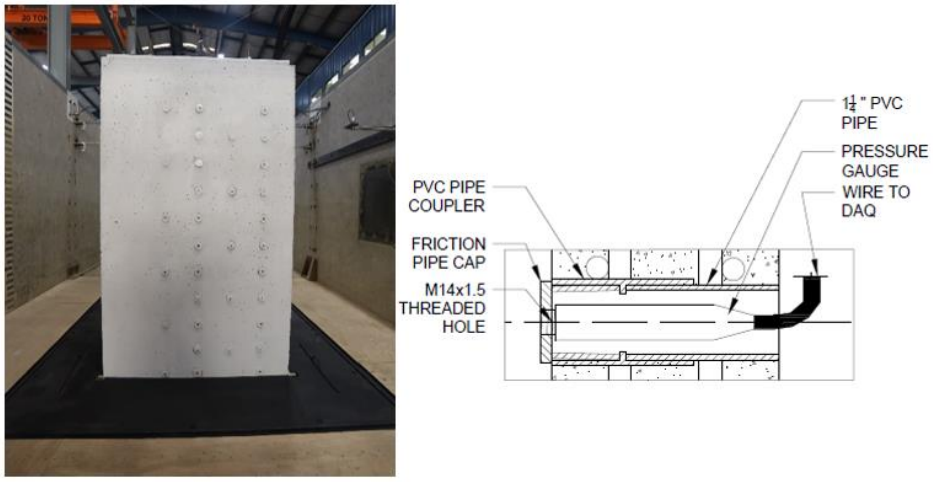

Figure 4-17: (a) Installed Pressure Sensors and (b) Pressure Sensor Install Schematic

4.2.4 *Strain Measurements*

Strain gauges were used to measure the force being transferred through the piles supporting the wall. The primary goal of the gauges was to determine if there was a change in the force in the piles when the soil box was full of soil as opposed to when it was half full and empty. Two Tokyo YFLA type strain gauges were attached to the front and back of each of the steel piles below the test specimen's slab and above the soil box slab for a total of four gauges on each pile. To simplify the section analysis the gauges were placed above and below mounting brackets used to attach the temporary moving braces to the test specimen.

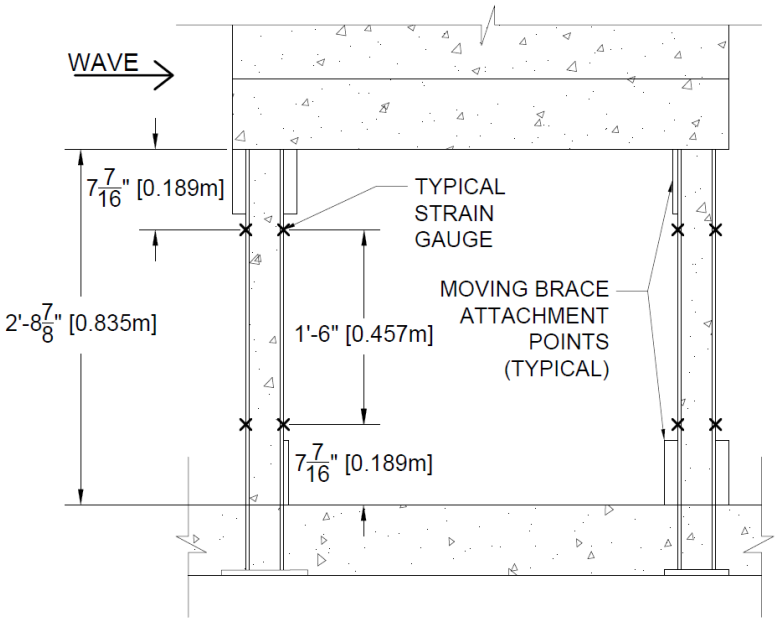

Figure 4-18: Strain Gauge locations

The strain gauges were then protected from the water using a series of protective products. First Micro Measurements Mcoat B was placed over the gauge. Once dried a layer of Mcoat W, a wax film, was placed over the gauge and up the wire a few inches. Next a piece of Mastik tape was placed over the gauge to protect from the mechanical hazard of placing soil around the piles. Finally the wires for the gauges were routed up the back of the structure. The wires were then coated in Vulcan polyurethane sealant which acted both to seal the wires from water and attach the wires to the wall.

Figure 4-19: Strain Gauge Wires with Sealant Applied

Strain gauges were used to calculate the total shear force in the piles by finding the bending moment and axial load in the pile at the upper and lower positions where gauges were placed. Strain Gauges placed on piles B1 and B2 in the upper front positions were broken during transport and installation of the specimen so strains from their corresponding gauges on columns A1 and A2 were assumed to be the same as the strain in the broken gauges.

A section analysis was performed at the level of each pair of gauges by breaking the section into 100 slices and assuming a linear strain distribution between the extreme fibers the gauges were placed on. The force in each slice was determined by finding the area of steel and concrete in each slice, then multiplying each area by the strain and the appropriate elastic modulus. Total axial force on the cross section was found by summing the forces at each slice. Total moment on the cross section was found by multiplying the force in each slice by the distance from the neutral axis to the centroid of each slice and then summing the values. The neutral axis for the cross section was found by taking the difference in strains in the extreme fibers and dividing by the length between the gauges to obtain the curvature of the section. The neutral axis was then determined by dividing the strain in one of the gauges by the curvature. For this analysis the strength of the concrete was taken as 4,473 psi after conducting a 28 day compression strength test on concrete cylinders cast with the same mix that was in the piles. The elastic modulus and cracking stress were found using equations 19.2.2.1b and 19.2.3.1 respectively from ACI 318-19. Cracked concrete (concrete with a stress higher than the cracking stress) was assumed to carry no tensile force. The total shear was

then calculated by taking the difference in the moments at the top and bottom of each pile and dividing by the length between the gauges. The total base shear on the structure was then calculated by adding together the shear in each of the four piles.

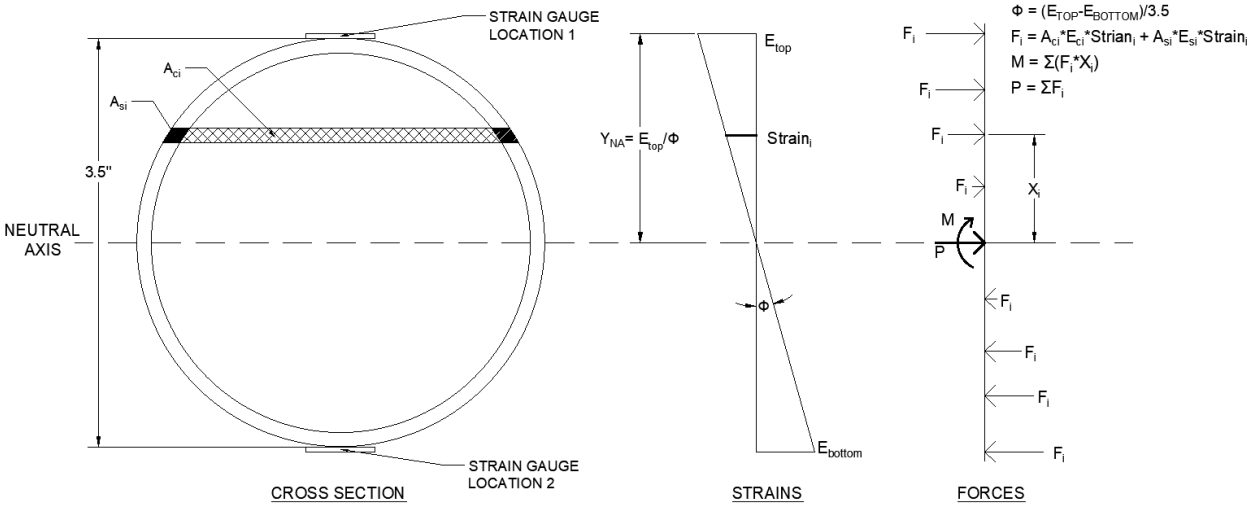

Figure 4-20: Depiction of Strain Section Analysis Variables

4.2.5 *OSU Data Acquisition*

During all testing at OSU a National Instruments PXI architecture data acquisition system (DAQ) was used. 51 channels were used to collect data from the 13 pressure sensors, 8 load cells, 16 strain gauges, four ultrasonic wave gauges, six wire wave gauges, and gauges in the wave maker that determine its displacement, water level in front of the paddle, and start time. A separate DAQ was setup and synchronized to collect data for the ADVs, as they require a special proprietary software to change their signal into usable velocity data. Data was sampled at a rate of 100 hz. The data acquisition system was not setup in such a way that data could be viewed live from any of the sensors, data had to be recorded over a period of time and then after collection was over the data could be examined. This was not an issue during wave testing but presented some unique challenges during validation tests performed at OSU.

4.3 SETUP VALIDATION TESTING

To ensure that this unique setup was capable of accurately measuring the total force on the system a series of static tests were conducted at both UW and OSU. The tests were conducted using a 5

ton Enerpac hydraulic jack to push on the structure in the stream wise direction. A load cell was placed between the jack and the structure to measure the force put into the system. The jack load cell was then compared to the load read by the stream wise load cells (SA and SB, see Figure 4-12).

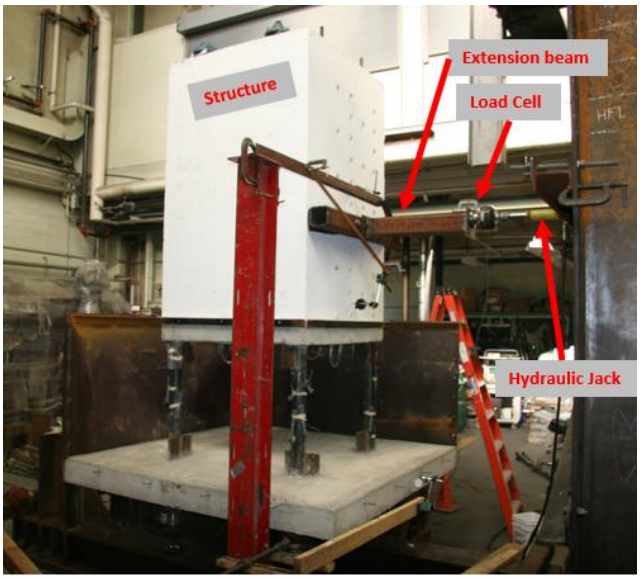

Figure 4-21: Static Test Setup

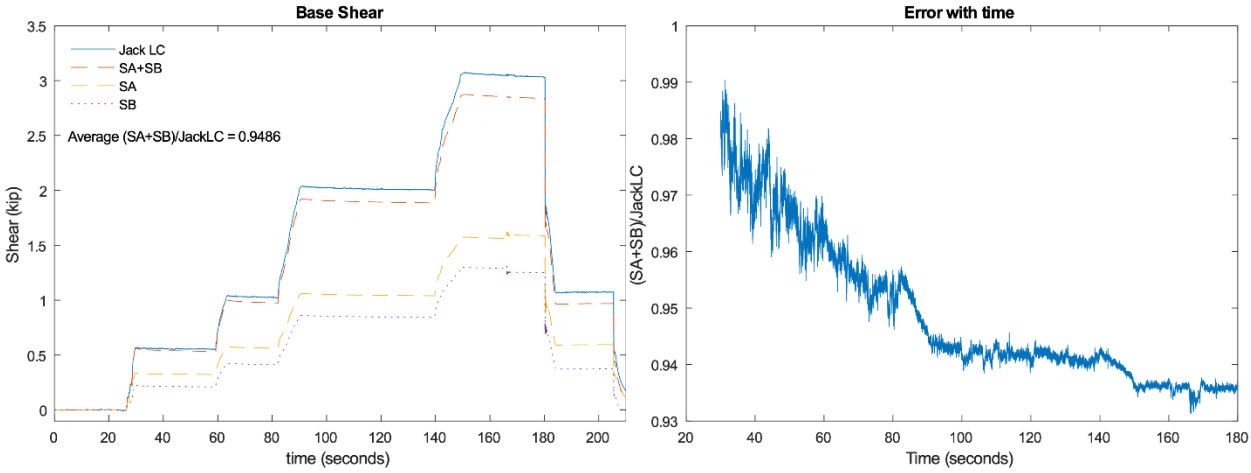

(a) (b)

Figure 4-22: (a) Force Measured with Time and (b) Error with Time

This testing was used to ensure that the setup could accurately measure the stream wise force put into the system. It was discovered that small changes in the length of the rods that connect the load cells to the structure could have a significant effect on the distribution of forces. To ensure even distribution of forces both load cells were put into compression with roughly the same magnitude in each load cell. It was found that the load cells tracked well to the input load and captured the

total load in the system with about 5% error. During this testing data was collected through a National Instruments data acquisition system that provided live read outs from all the load cells via Lab View software.

A similar series of tests were conducted with the structure in place in the flume to confirm that all the load cells were working once they were submerged in water and that load was being taken evenly between load cells in the stream wise and transverse directions when loading in either of those directions alone. Although the load cells being used were supposedly "waterproof" when the flume was filled for the first time one of the load cells no longer worked and the flume had to be drained to replace the load cell, adding about a days delay to the testing to allow time for the flume to empty and fill. At OSU tests were performed in both the stream wise and transverse direction with the intention of making sure all load cells were responding, tracking with the jack load cell, and distributing loads relatively evenly. These tests were conducted using a 5 ton hydraulic jack and load cell reacting against a beam that spanned the length of the flume in the stream wise direction and reacting against the flume wall in the transverse direction. During these tests data was collected via the OSU DAQ described in section 4.2.5, however to view the loads in the load cells during testing and while installing and pre compressing the load cells a voltmeter was attached through the DAQ to measure the voltage output of the load cell. The voltage output was then multiplied by the gain factor to find the load in the load cell in real time. The results of these tests can be found in Appendix C.

4.4 TEST CONDITIONS

4.4.1 *Wave generation*

The hydraulic wave maker in the Large Wave Flume was used to create two different test waves. First a 1.4 m solitary wave was investigated thoroughly. From previous OpenFOAM modeling this was determined to be the tallest wave that could be generated by the wave maker at the position of the specimen. From modeling it was anticipated that the wave would break at the top of the slope in bathymetry and strike the specimen as a broken bore, however little breaking was observed for this wave generation technique. This wave is referred to as the 1.4 m wave. After testing this wave it was suggested that another approach to wave generation be used to create an unstable wave that would be slightly higher and break on itself before it reached the slope in bathymetry and then

approach the structure as a broken bore. This wave is referred to as the 1.45 m wave. Wave maker displacement histories for both waves are provided in Figure 4-23, where a displacement of zero is the paddles neutral position.

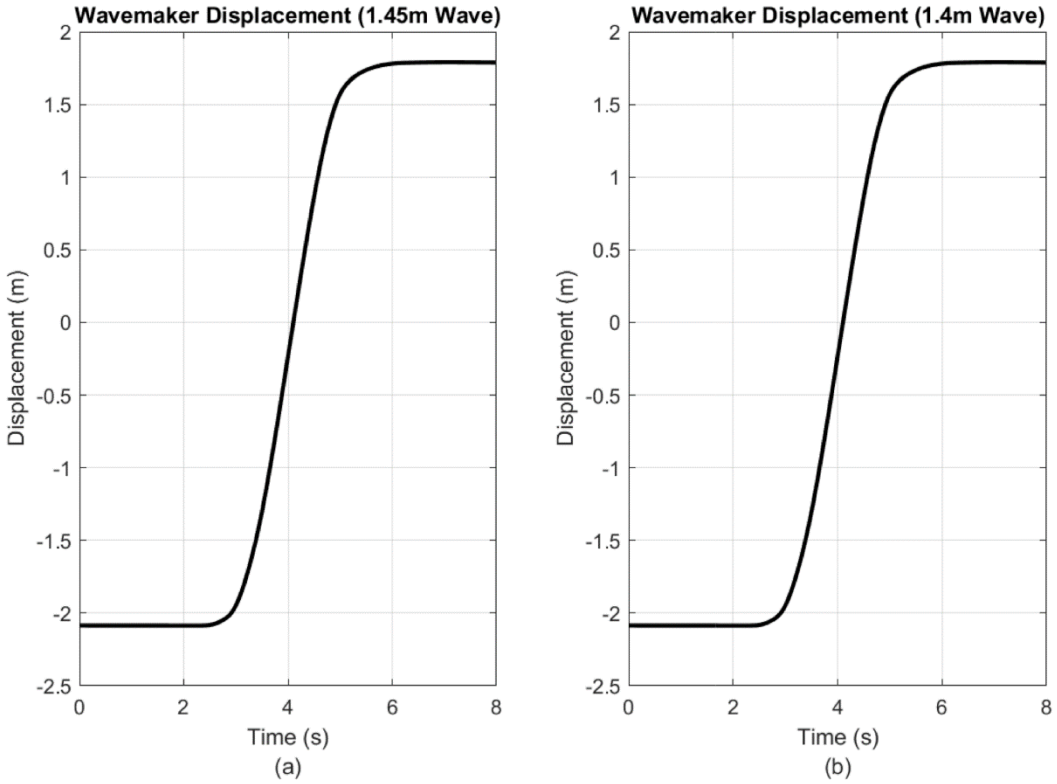

Figure 4-23: Wave Maker Displacement Histories

Chapter 5. EXPERIMENTAL RESULTS

The testing of the wall structure was conducted to measure the demands and reactions for different wave heights and soil conditions. This testing took place from October 14th through November 15th, 2019. The chapter describes the test procedure and measured results. For each test, measured results are presented, categorized by wave height and soil condition. The total base shear is measured in three ways: (1) directly from the stream-wise load cells, (2) by integrating the pressures measured by the pressure sensors, and (3) from the moments measured on the piles using the strain gages. All raw test data is available on DesignSafe-CI.org under the project title "Vertical Evacuation Structures Subjected to Sequential Earthquake and Tsunami Loadings".

This chapter begins by discussing the test matrix and test conditions. It then describes a typical test procedure. Data from wave gauges and ADVs is then examined to determine the repeatability of individual waves run. The chapter then discusses the assumptions made to integrate pressures over the front face of the wall. It concludes with data from the four different experiments conducted: a 1.4m wave with a full, half-full, and empty soil box, as well as a 1.45m wave with an empty soil box. For each experiment data from the pressure sensors, strain gauges, and load cells is presented.

5.1 TEST MATRIX

Experiments presented in this chapter are listed in Table 5-1 and Table 5-2. An experiment was defined as all the waves run for a combination of wave height and soil level. A trial was defined as a single wave run during an experiment. Three experiments were conducted for the 1.4m wave height, investigating forces in the system with the soil box full, half-full, and empty. For each experiment a minimum of three pressure sensor layouts were required to fully characterize pressures across the front face of the specimen. For the first experiment, the 1.4m wave with the soil box full, 10 trials were run for each pressure sensor layout to ensure repeatability of the pressures. After the first experiment one of the pressure sensors was damaged and required a fourth pressure sensor layout to make up for the damaged sensor. For the remaining experiments four pressure layouts were used, however fewer trials were run for the fourth layout because only one pressure sensor was changing location. For the final experiment, the 1.45m wave with the soil box

empty, only 5 trials were run for each pressure layout due to the repeatability of pressure measurements that were observed in the first three experiments. Only one soil condition was used for the 1.45m wave because the soil was shown to have minimal effect in the 1.4m wave height experiments. A total of 30 trials were run for the 1.4m wave with the soil box empty, 35 trials were run for the 1.4m wave with the soil box half-full, 37 trials were run for the 1.4m wave with the soil box empty, and 20 trials were run for the 1.45m wave with the soil box empty.

Table 5-1: 1.4m waves

wave height (m)	soil level	pressure layout	Number of trials	OSU Experiment name	Trial numbers
1.4	Full	PL1	10	Wall_Full_PL1_Day3	1:10
		PL2	10	Wall_Full_PL2_Day1	1:10
		PL3	10	Wall_Full_PL3_Day2	1:10
	Half	PL1	10	Wall_Half_PL1_Day1	2:11
		PL2	10	Wall_Half_PL2_Day1	1:10
		PL3	10	Wall_Half_PL3_Day1	1:10
		PL4	5	Wall_Half_PL4_Day1	1:05
	Empty	PL1	10	Wall_Empty_PL1_Day1	1:10
		PL2	10	Wall_Empty_PL2_Day1	1:10
		PL3	10	Wall_Empty_PL3_Day1	1:10
		PL5	7	Wall_Empty_PL5_Day1	1:07

Table 5-2**:** 1.45m waves

wave height (m)	soil level	pressure layout	Number of trials	OSU Experiment name	Trial numbers
1.45	Empty	PL1	5	Wall_Empty_PL1_Day2	1:05
		PL2	5	Wall_E_PL2_Day2	1:05
		PL3	5	Wall_E_PL3_Day2	1:05
		PL5	5	Wall_E_PL5_Day1	8:12

5.2 TEST PROCEDURE

For each experiment, the structure was subjected to a minimum of 20 waves (each wave is termed a “trial”) and took place over several days. After testing began it was possible run a maximum of 20 waves a day with the same soil level. Changing the soil level took a few hours and on days this was required fewer trials were run. A typical test day consisted of the following steps:

1. The hydraulics were initiated; testing was not started until they reached their operating temperature.
2. The data acquisition system was activated.
3. The wave was generated 30 seconds after the data acquisition system was activated.

4. The wave was observed visually for consistency, most importantly when running breaking waves to make sure that the bore was forming in relatively the same location along the length of the flume for each trial.
5. After the wave was generated at the paddle, it travelled down the length of the flume with a relatively consistent shape and height until it reached the ramp before the specimen. Upon reaching the ramp, the waves would gain amplitude and then strike the structure, sending a plume of water upward while the remaining water would flow around the specimen.
6. The data acquisition system would turn off 60 seconds after the trial began and the water in the flume would begin to settle.
7. It took approximately twenty minutes until the water level in the flume was still enough to run another wave (with variation in the free surface elevation around +/-1cm). Once the water level was again still the procedure was repeated until the day was over.

The initial experiments consisted of more trials to demonstrate consistency between measurements. For example, the first experiment, the 1.4m wave with the soil box full, had 10 trials (waves) for each unique pressure-sensor layout. Those results were analyzed for consistency, with a goal of having a coefficient of variation less than 5%.

Figure 5-1 shows the typical propagation of the 1.4m, unbroken, wave down the length of the flume and Figure 5-2 shows a plot of selected wave gauges during a single trial (1.4m wave, full soil box, pressure layout 1, trial 1). Figure 5-3 shows the typical propagation of the 1.45m, broken, wave down the length of the flume and Figure 5-4 shows wave a plot of selected wave gauges illustrating the propagation of one trial (1.45m wave, empty soil box, pressure layout 2, trial 1). In Figures 5-2 and 5-4 it can be seen that the maximum wave height occurs at the wavemaker wave gauge (wmwg),the wave then loses height as it propogates down the flume as shown by wave gauges 1-6 (wg1-6), the wave height then increases as the wave interacts with the sloped ramp (as shown by the untrasonic wave gauges (uswg1 and 2). Wave gauge locations and naming convention are shown in Figure 4-8.

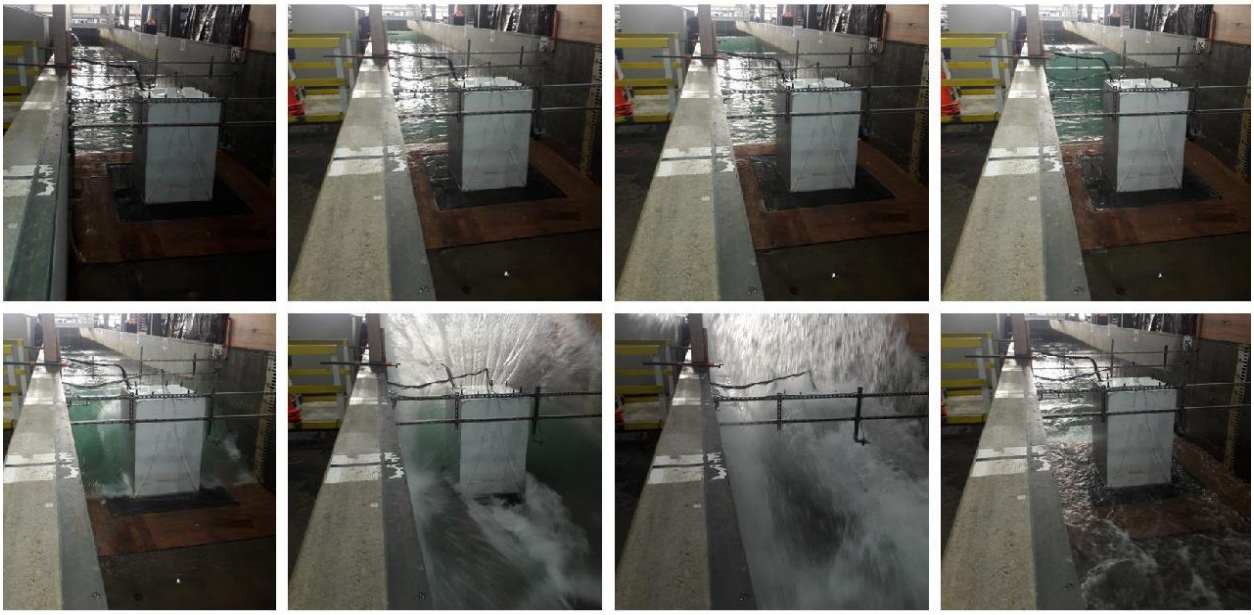

Figure 5-1: Typical 1.4m Wave Propogation

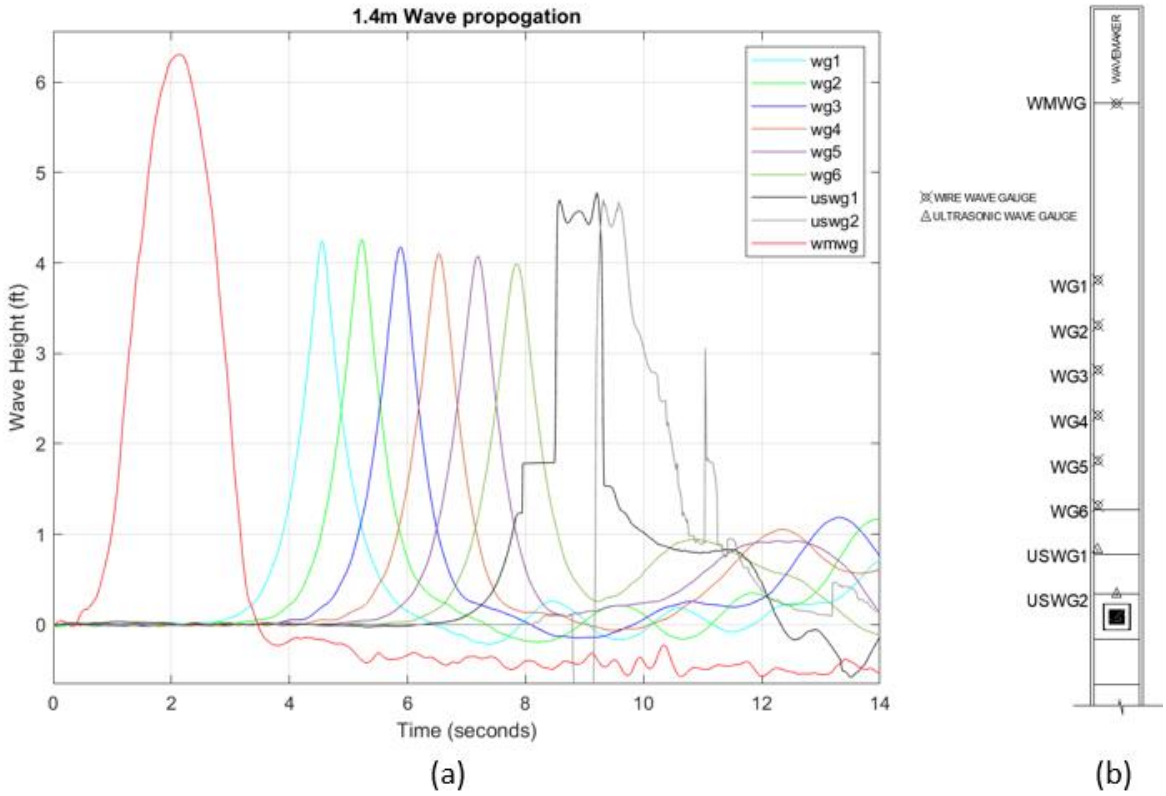

Figure 5-2: (a) Typical 1.4m Wave Height Trend along Flume (b) Wave Gauges Locations Shown in Figures 5-2(a) and 5-4.

Figure 5-3: Typical 1.45m Wave Propagation

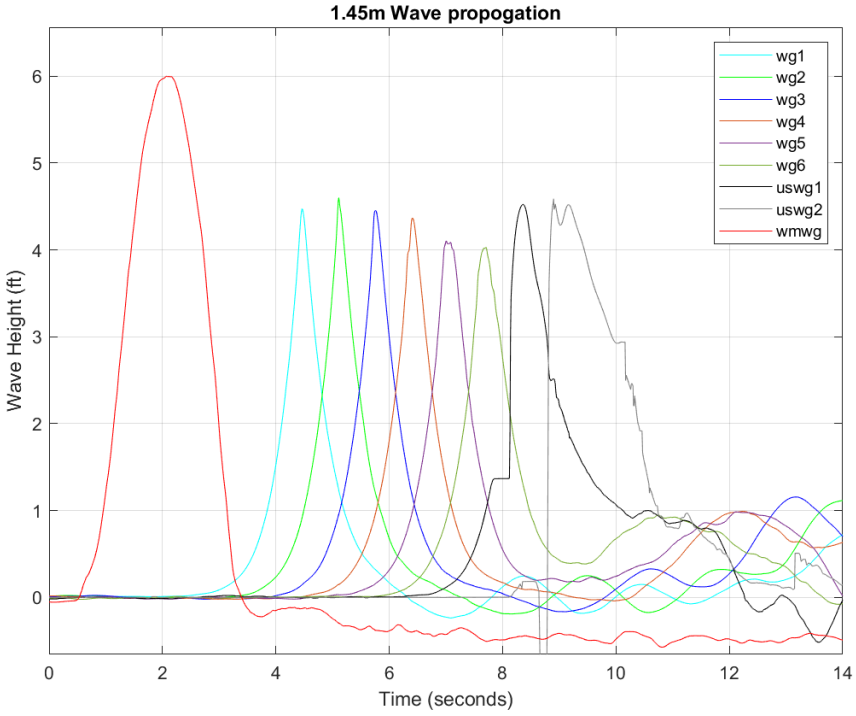

Figure 5-4: Typical 1.45m Wave Height Trend along Flume

5.3 EXPERIMENT REPEATABILITY

This section details the wave measurements taken that demonstrate the repeatability of the waves generated. To demonstrate repeatability both free surface elevations and particle velocities were evaluated upstream from the test specimen to confirm that a similar wave would strike the test specimen in each trial. A wave was deemed to be repeatable if across all trials for the same wave height the coefficient of variation was less than 5%. This goal was achieved for most of the instruments however some instruments had higher coefficients of variation due to issues with their placement and issues with the sensors themselves, not necessarily the wave.

5.3.1 *1.4m Wave*

For the 1.4m wave height all three experiments were examined together for consistency as nothing about the wave generation or propagation should have been changing between experiments, the only variable changing was the level of soil present in the soil box. This resulted in a total of 102 trials being averaged together to examine consistency.

5.3.1.1 Wave Gauge Measurements

Wave gauges were used to measure the wave height along the length of the flume. Time histories were examined for each trial. The average, standard deviation and coefficient of variation were determined for the maximum wave height at each gauge across all trials and are presented in Table 5-3. The 1.4m wave demonstrated good repeatability in the wave gauges with each of the wire wave gauges having a coefficient of variation below the acceptance criteria of 5%. The ultrasonic wave gauges yielded higher coefficients of variation, however this was due to errors in the gauges. When water would splash from the waves it would sometimes get on the surface of the ultrasonic gauges, blocking the sound signal emitted from the face of the gauges resulting in erroneous readings. Locations of the wave gauges can be found in Figure 4-8.

The measurements from the wire wave gauges (wg1-wg6) are shown in Figure 5-5 (b) through (g) where the thin grey lines that represent individual trials are barely noticeable behind the thick black line indicating the average free surface elevation at each time step. Time histories for the wave maker wave gauge (wmwg), and ultrasonic wave gauge 1 (uswg1) are also provided in Figure 5-5(a) and (h) respectively.

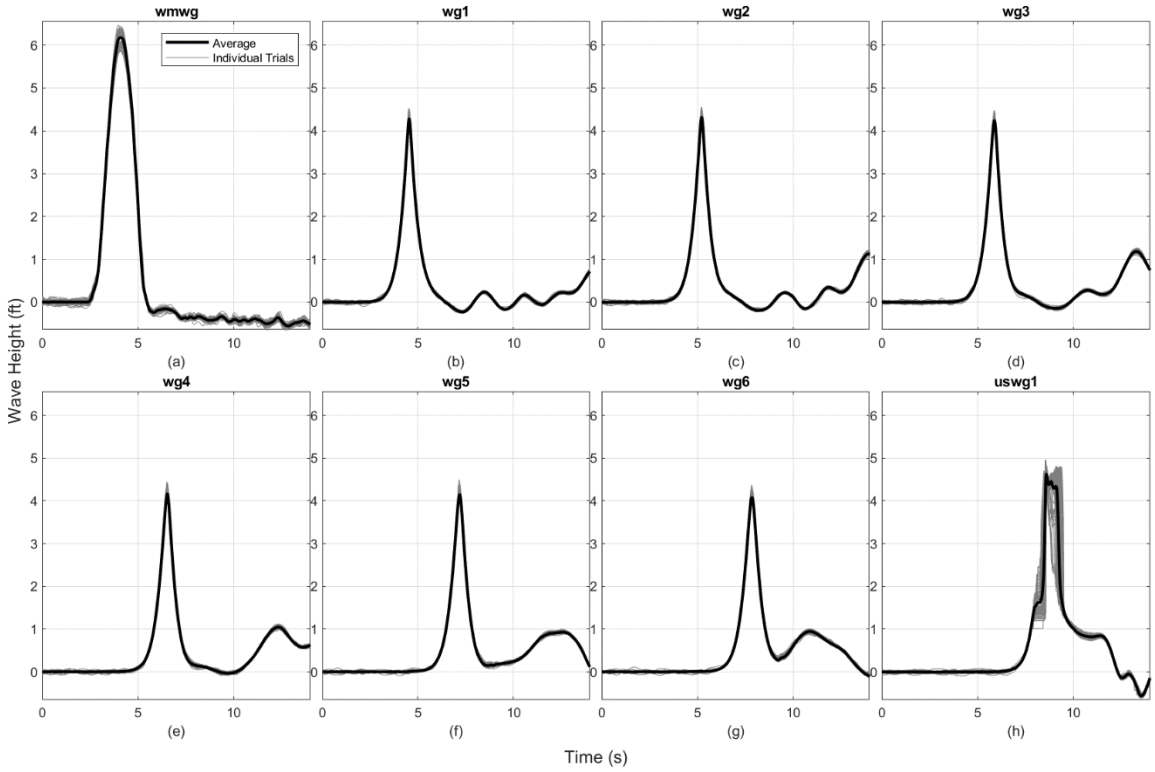

Figure 5-5: Wave Gauge Time Histories (1.4m Wave)

Table 5-3: Wave Heights for 1.4m Wave

Instrument	No. of Trials	Average Max (ft)	Standard Deviation (ft)	COV (%)
wmwg	102	6.19	0.17	2.8%
wg1	102	4.29	0.08	1.9%
wg2	102	4.32	0.08	1.9%
wg3	102	4.25	0.08	1.9%
wg4	102	4.18	0.09	2.1%
wg5	102	4.16	0.09	2.2%
wg6	102	4.09	0.08	2.0%
uswg1	102	4.76	0.07	1.5%
uswg2	102	4.57	0.83	18.1%
uswg3	102	4.23	2.03	48.0%
uswg4	102	4.14	1.21	29.3%

5.3.1.2 Velocity Measurements

Velocities were recorded in the 3 principal flume directions using a series of Acoustic Doppler Velocimeters. The stream-wise velocity time histories are shown in Figure 5-6 and statistics for the maximum velocities are provided in Table 5-4. ADV1 is likely the most reliable because there

were no changes in bathymetry close to where the sensor was placed. ADV2 was placed above a small step up in bathymetry where a toe slab was used to hold the sloped slab in place (see Figures4-1 and 4-10). ADV3 was at the bottom of the sloped slab and ADV4 was placed at the top of the slope where it was dry until the wave inundated the beach around the structure. ADV 1 showed adequate repeatability however the other ADV sensors showed less repeatability in the wave, likely due to inconsistencies in the flume bathymetry causing differences in the particle velocities between waves. ADV4 provides the most variability due to it being places on the dry beach before being inundated with water. This change from dry to wet conditions at the ADV lead to erroneous readings according to OSU's instrumentation manager. Sudden changes in bathymetry also can lead to increased variability in the particle velocities as evidenced by ADV3, which was placed near the intersection of the ramp with the bed of the flume. Locations of the ADVs can be found in Figure 4-10. Due to the consistent results of the wave gauges and the most offshore ADV the 1.4m wave was deemed to be repeatable.

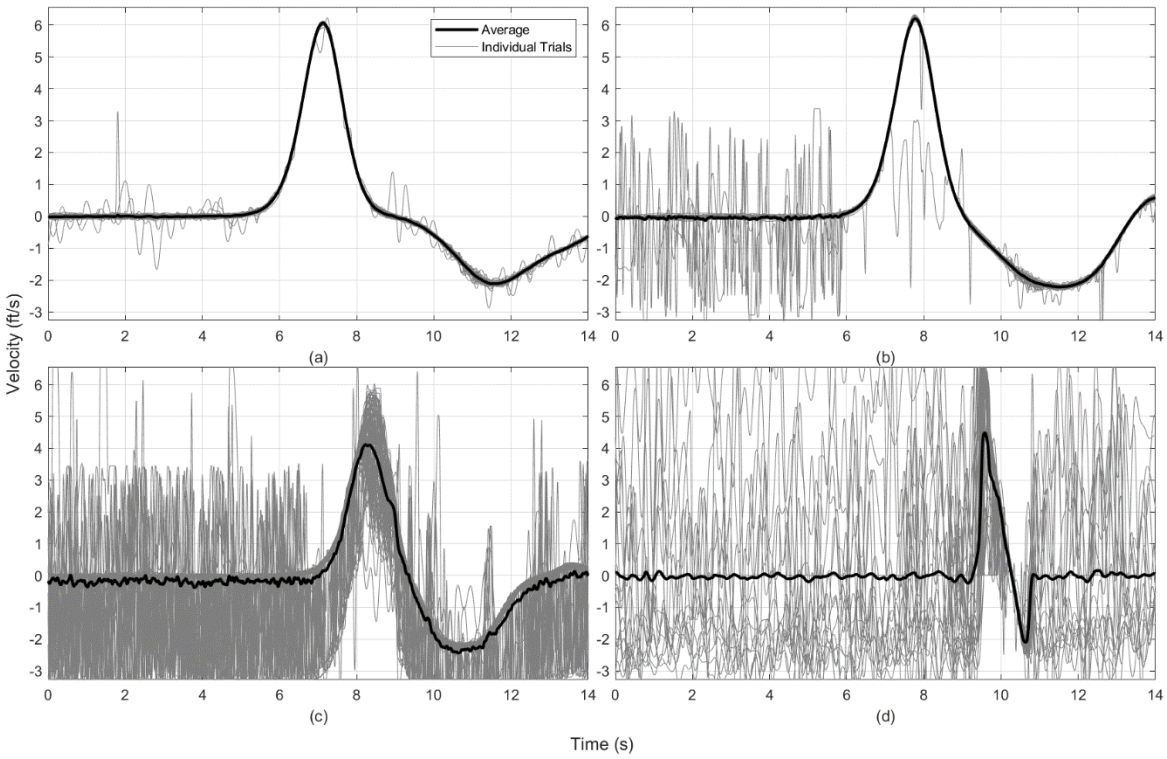

Figure 5-6: Stream-wise Velocity Time History (1.4m Wave) (a) ADV1 (b) ADV2 (c) ADV3 (d) ADV4

Table 5-4: ADV Statistics (1.4m Wave)

Instrument	No. of Trials	Average Max Velocity (ft/s)	Standard Deviation (ft/s)	COV
ADV1	94	6.078	0.01	0.6%
ADV2	101	6.201	0.10	5.1%
ADV3	101	5.001	0.21	13.6%
ADV4	101	5.719	0.60	34.2%

5.3.2 *1.45m Wave*

The 1.45m Wave was run after the completion of the 1.4m wave. After confirming consistency in the wave from previous experiments only 20 trials were run for the 1.45m wave experiment, five trials in four different pressure configurations. The only soil condition used for the 1.45m wave tests was the empty soil box condition.

5.3.2.1 Wave Gauge Measurements

The 1.45m wave gauges provide similar reliability to the 1.4m wave gauges with slightly more variability as the wave got close to the structure. In each trial the wave was observed to start breaking between bays four and five in the flume, between wg3 and wg4. Time histories for each wave gauge are presented in Figure 5-7 and statistics for the wave gauges are provided in Table 5-5.

Due to the turbulent nature of the wave bore after it breaks wave gauges after wg4 showed more variability in the 1.45m wave than in the 1.4m wave. Ultrasonic wave gauges generally provided better data for this wave as well, however uswg3 was directly in the splash zone and provided poor accuracy, therefor it was omitted from Figure 5-7. In Table 5-5 it can be seen that each wave gauge had a coefficient of variation less than the 5% acceptance criteria, with the exception of uswg3. Locations of the wave gauges can be found in Figure 4-8.

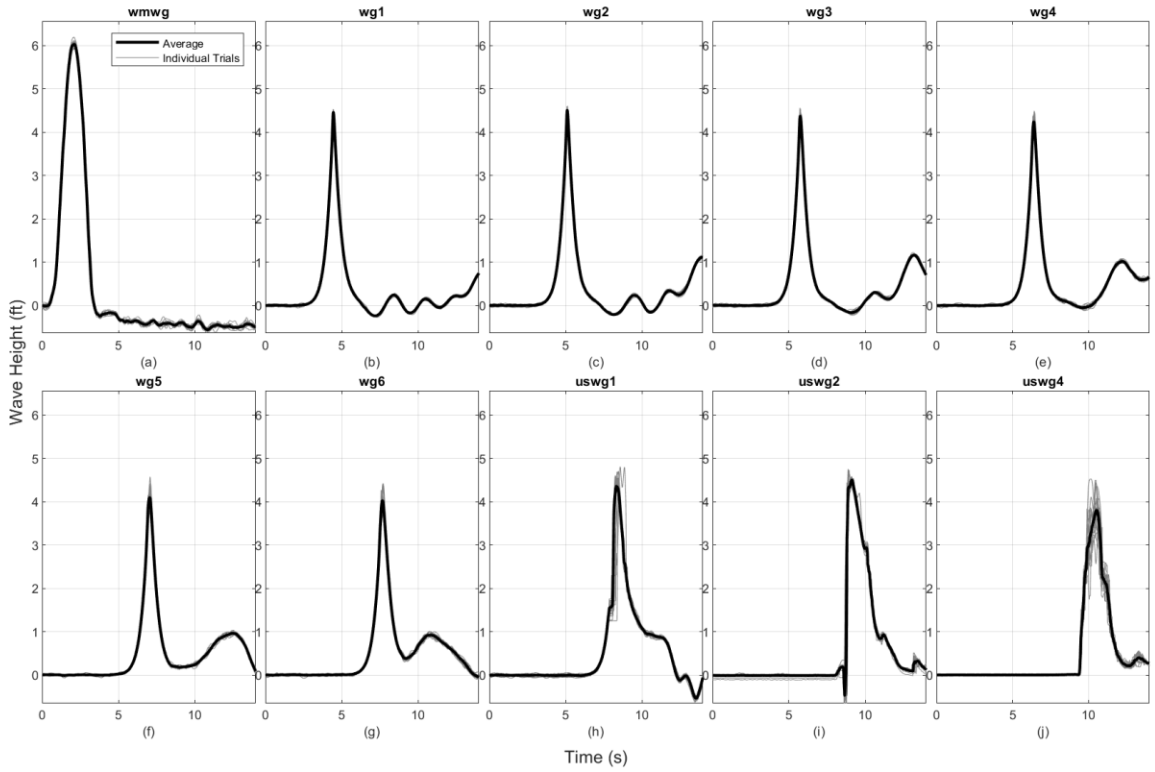

Figure 5-7: Wave Gauge Time Histories (1.45m Wave)

Table 5-5: Wave Gauge Statistics (1.45m Wave)

Instrument	No. of Trials	Average Max (ft)	Standard Deviation (ft)	COV (%)
wmwg	20	6.05	0.05	0.8%
wg1	20	4.48	0.04	0.9%
wg2	20	4.53	0.06	1.4%
wg3	20	4.42	0.08	1.8%
wg4	20	4.29	0.12	2.9%
wg5	20	4.15	0.17	4.1%
wg6	20	4.08	0.18	4.4%
uswg1	20	4.54	0.07	1.6%
uswg2	20	4.57	0.11	2.3%
uswg3	20	3.03	2.54	83.6%
uswg4	20	4.02	0.35	8.6%

5.3.2.2 Velocity Measurements

Similar to the 1.4m wave, the 1.45m wave velocity measurements from ADV1 and ADV2 provided very consistent data. A time history of the stream-wise velocities is provided in Figure 5-8 while the statistics for the max values are shown in Table 5-6. ADVs 1 and 2 had coefficients

of variation below the acceptance criteria, however for similar reasons to the 1.4m wave ADVs 3 and 4 had coefficients of variation significantly greater than the acceptance criteria. Locations of the ADVs can be found in Figure 4-10. Due to the consistent results of the wave gauges and ADVs 1 and 2 the 1.45m wave was deemed to be repeatable.

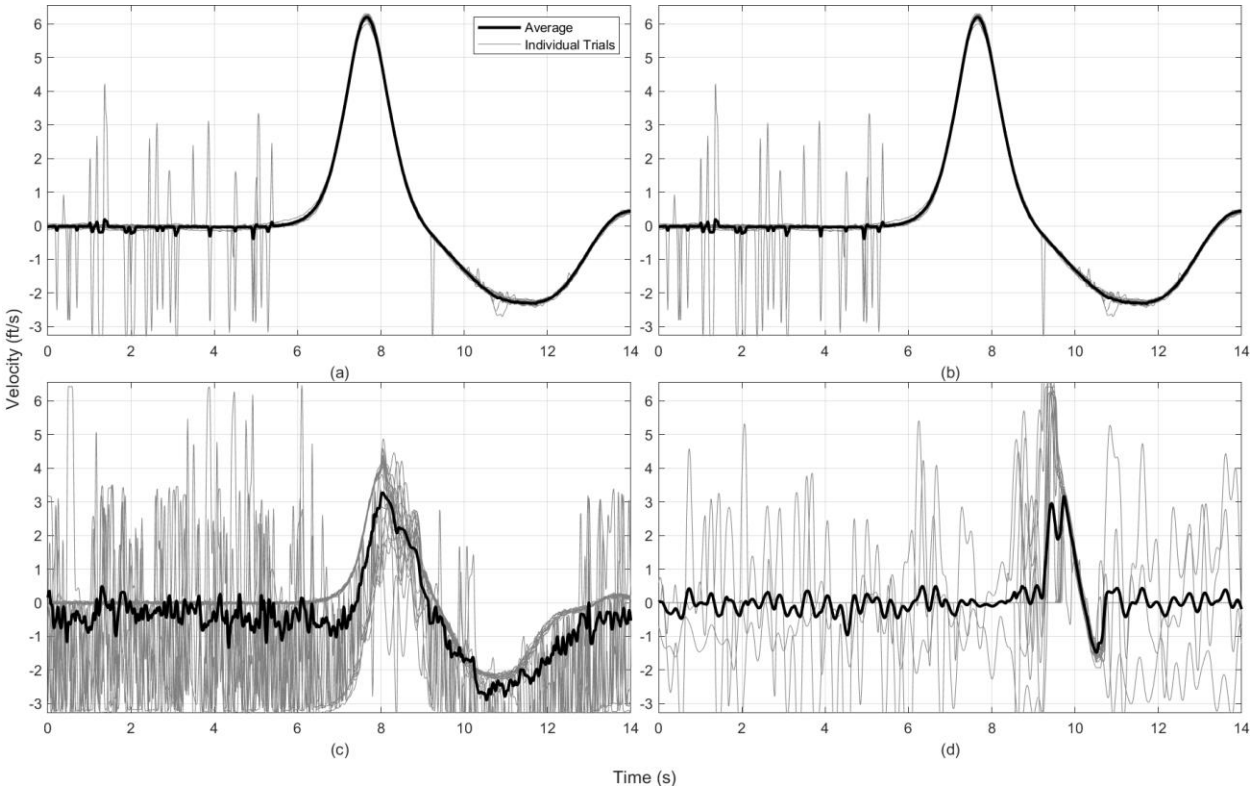

Figure 5-8: Stream-wise Velocity Measurements (1.45m Wave) (a) ADV1 (b) ADV2 (c) ADV3 (d) ADV4

Table 5-6: ADV Statistics (1.45m Wave)

Instrument	No. of Trials	Average Max Velocity (ft/s)	Standard Deviation (ft/s)	COV
ADV1	10	6.088	0.01	0.6%
ADV2	20	6.204	0.02	1.3%
ADV3	20	4.570	0.27	19.6%
ADV4	20	4.735	0.51	35.2%

5.4 EVALUATION OF PRESSURES

This section details the assumptions that allowed for the integration of pressures over the front face of the specimen. Two major assumptions were made and later validated by test data. The first is that different pressure layouts can be combined together to provide an adequate characterization of pressures over the entire face of the test specimen. The second was that pressures could be mirrored across the centerline of the test specimen. Pressure sensor locations can be found in Figure 4-16.

Due to the limited number of pressure sensors available and the size of the wall multiple pressure sensor layouts were required to characterize the pressure distribution over the entire face of the wall. In order to confirm that the pressures were repeatable across the tests, three sensor locations (B03, D07, B11) had a sensor in them in every layout and the remaining locations only had sensors in them for one pressure sensor layout. The average pressures from the sensor locations that did not move were then compared across the different layout to confirm that the pressures at a given location were the same when the same wave was run with sensors in different locations. The average values for these sensors for different layouts is provided in Table 5-7. Pressure sensors in location A11 and D07 show very consistent results from layout to layout, while sensor B03 has slightly more variability. This is likely due to B03 being closer to the top of the wave where pressures are less consistent from the water/air interaction taking place.

Another important assumption in order to be able to integrate pressures over the face of the wall was that the pressures were the same on either side of the centerline of the wall. To confirm this pressures from the A column and the C column were put in order from top to bottom and compared to how the pressure changes with height in the B column. Figure 5-9 provides a plot of this comparison for the case of the 1.4m wave with the soil box full, however this trend was consistent across wave heights and soil levels. It can be seen that when the A and C lines are combined that the trend up the height of the wall is very similar to the trend in the B column, confirming that this is an adequate assumption. This assumption was also used to mirror the D line across the wall's centerline.

Table 5-7: Static pressure sensors, Average max values for different sensor layouts

Sensor	Average max pressure (psi)		
	PL1	PL2	PL3
B03	1.685	1.664	1.559
D07	2.051	2.097	2.008
A11	2.928	2.912	2.911

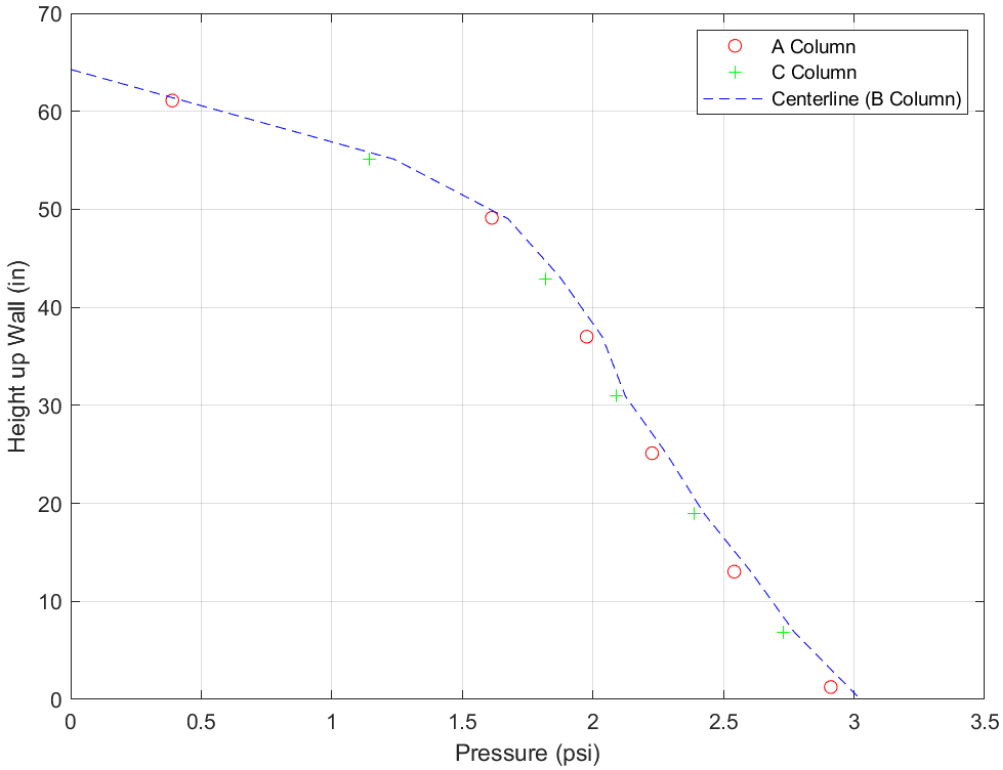

Figure 5-9: A/C Column and B Column Pressure Distributions

In order to integrate the pressures over the front face of the specimen the following assumptions were made. The pressures can be mirrored across the centerline of the wall, for reasons discussed previously, and that multiple pressure layouts could be combined together, as evidenced by the pressure sensors that did not move recording very similar values between pressure layouts. Due to constructability constraints the closest that a sensor could be placed to the outside edge of the wall was 7.5 inches from the edge. Linear extrapolation was used, continuing the trend of each numbered grid line from the centerline of the wall to the edge, in order to estimate the pressures along the edge of the wall. Similarly, the height corresponding to zero pressure was determined assuming a linear pressure distribution from the top two pressure sensors from their pressure to

zero. With this information and the measurements, a surface for the distributions were developed and integrated to find the total force being put into the system. Plots of force with time are presented separately for each wave height and soil condition in the next section.

5.5 EXPERIMENTAL MEASUREMENTS

This section summarizes the force and pressure measurements for each experiment. In this testing, force on the specimen was measured in three ways; by integrating pressures on the front face, measuring force being put into the system, by measuring strains in the piles that support the specimen, giving an idea of forces inside the system, and by measuring loads on the total system with load cells. In this section the pressure sensor, strain gauge, and load cell measurements are presented independently. Comparisons between experiments and force measuring techniques are then made in Chapter 6.

5.5.1 *1.4m Height, Full Soil Box*

The 1.4m wave, soil box full was the first experiment conducted. It consisted of running 30 waves in order to demonstrate the repeatability of the wave and resulting forces and pressures. 10 trials were run for each of the three pressure sensor layouts used.

5.5.1.1 Pressure Measurements

Pressures were recorded on the front face of the structure in order to characterize the pressure distribution and then integrate the pressures over the face of the wall to figure out the force on the specimen from the wave.

Figure 5-10 shows a time history of the average pressures at different locations on the wall for nine of the 33 pressure sensor locations. The selected sensors are located along the three primary vertical lines of pressure sensors at the top, middle, and bottom of the pressure grid to give an idea of the changes in pressure over the height of the wall. The location of pressure sensors can be found in Figure 4-16. Table 5-8 gives the average maximum, standard deviation and coefficient of variation across all trials for this experiment, for the pressure sensors shown in Figure 5-10. The pressure sensors near the bottom and middle of the wall showed good repeatability with coefficients of variation less than 5%. The pressure sensors near the top of the wall showed slightly

higher variability. It can be seen in Figure 5-10 that some of the pressure sensors recorded a short instance of negative pressure directly before the wave impact. This was explained by OSU's instrumentation manager Tim Maddux to be due to a flaw in the pressure sensors when water with entrapped air strikes the sensors. The negative values from the sensors were assumed to be zero when used to calculate force time histories from the pressures.

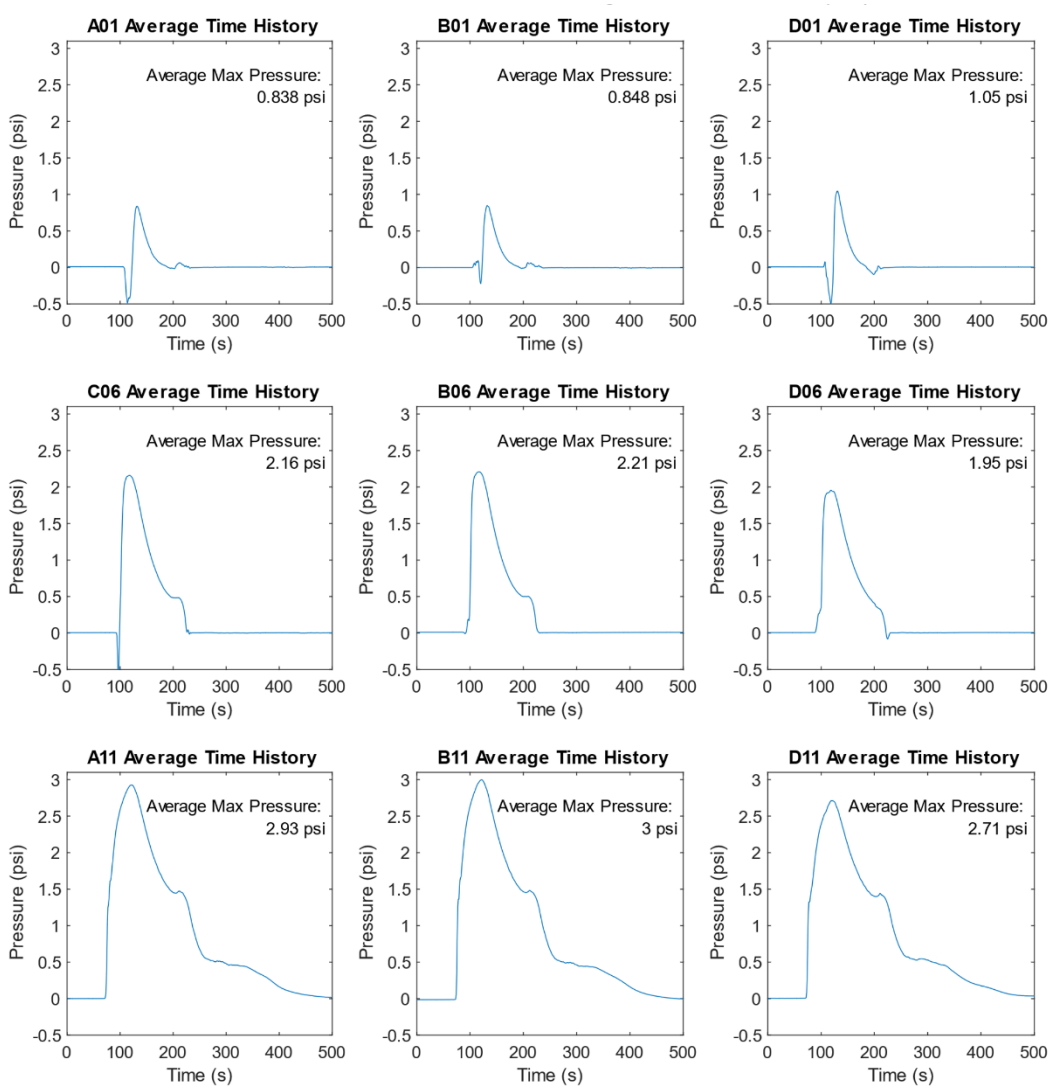

Figure 5-10: Average Pressure Time Histories at Selected Sensors (1.4m Wave, Full)

Table 5-8: Pressure Sensor Statistics at Selected Sensors (1.4m Wave, Full)

Sensor Name	Average Max Pressure (psi)	Coefficient of Variation	No. of Trials
A01	0.838	9%	10
B01	0.848	8%	10
D01	1.047	18%	10
C06	2.159	1%	10
B06	2.207	2%	10
D06	1.955	3%	10
A11	2.928	0%	10
B11	2.997	0%	30
D11	2.711	1%	10

After examining pressures at individual sensor locations the different pressure layouts were combined and integrated to find the total force acting on the wall from the wave. The average pressure at each gauge location was used to evaluate the force on the test specimen. Figure 5-11 provides a time history of the force from the pressures as well as the average maximum force on the wall.

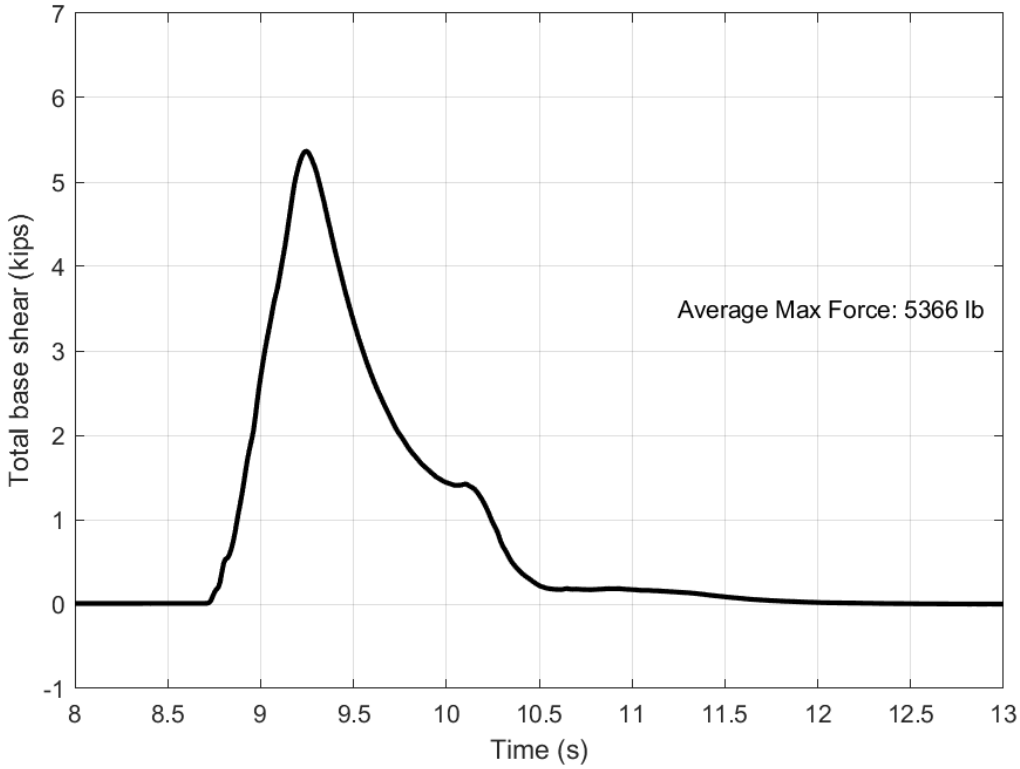

Figure 5-11: Force Time History from Pressures (1.4m Wave, Full)

5.5.1.2 Strain Gauge Measurements

A time history of axial forces in each pile at the top and bottom strain gauge locations are provided in Figure 5-12 and Figure 5-13 respectively. An explanation of how strains are transformed into forces on the cross section is available in Section 4.2.4. The maximum force, standard deviation and coefficient of variation for each gauge location in each pile can be found in Table 5-9, as well as the sum of the axial forces in at the top and bottom of the piles. Negative values in this table indicate compression in the section. It can be observed that the strain gauges provided reliable data for axial in the piles as evidenced by coefficients of variation being below 5% for all gauge locations with the exception of the lower gauge location on pile B1. This location had a very low maximum relative to the other locations while having about the same standard deviation, leading to a higher coefficient of variation.

In general the results for the axial force make sense, with the piles on the back face of the specimen going into compression while the piles on the front face go into compression. It was discovered however that the total axial force measured on the specimen was not the same at the top and bottom strain gauge locations, as would be expected. The top gauges gave a total axial force of 1.15 Kips in compression, while the bottom gauges give a total axial force of .24 Kips in compression. There could be some axial force present in the piles from the weight of the wave acting on the cover plate placed around the specimen to keep the soil contained. This plate was supported by angles that ran around the walls of the soil bow and by angles connected to the specimen. This would explain an axial force being present in the piles, however the axial force should be constant between the top and bottom strain gauges. It could be possible that the soil around the piles was taking some of the axial force in the piles through skin friction around the pile, however this theory was disproven when examining the axial force in the empty soil box condition, where the axial force was also changing. Without other strain gauges to measure the axial force at different points in the pile it is difficult to make a determination of why the axial force is changing over the length of the pile. Another observation can be made that the axial force is not the same in each of the piles. This indicates that the specimen was twisted somewhat in the flume and did not evenly distribute forces to the support piles.

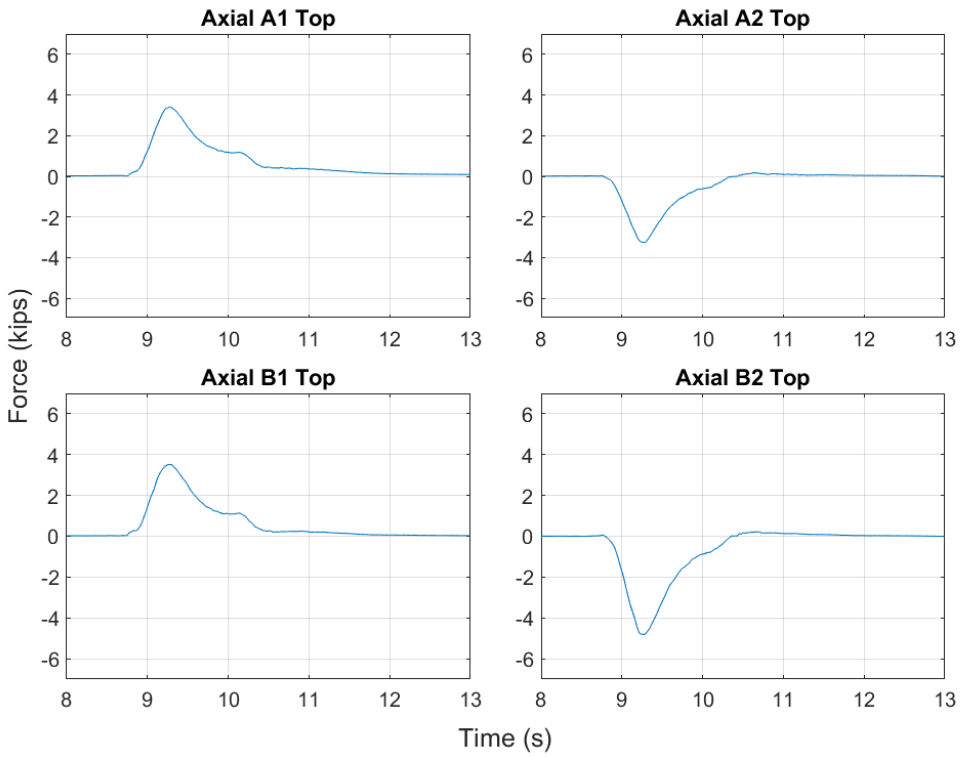

Figure 5-12: Time History for Axial Force at Top Gauge Locations (1.4m Wave, Full)

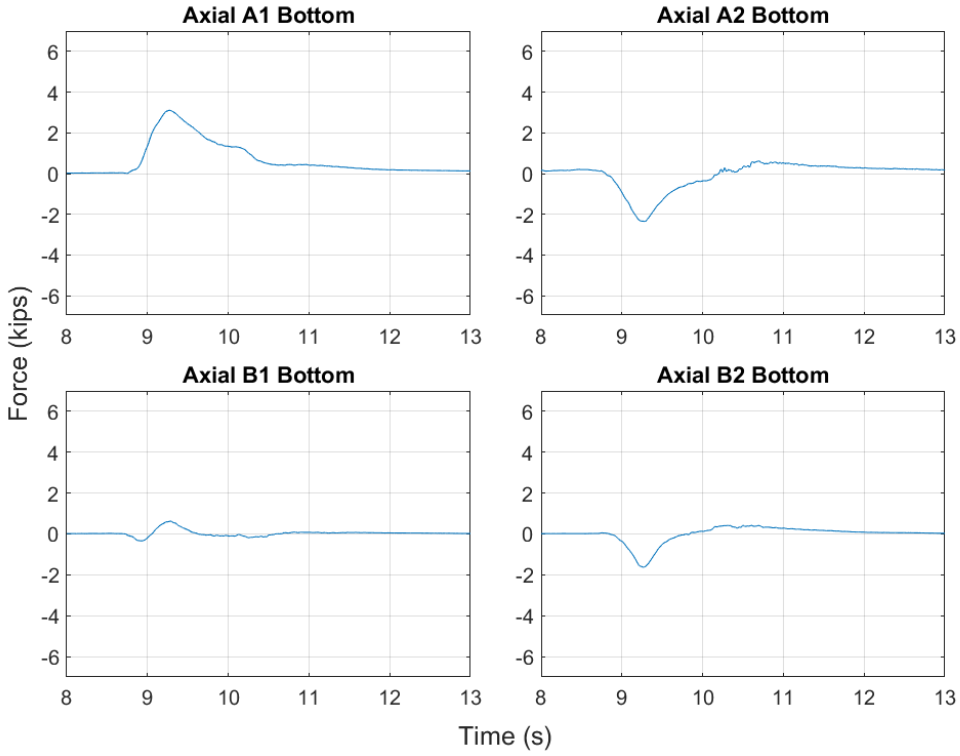

Figure 5-13: Time History for Axial Force at Bottom Gauge Locations (1.4m Wave, Full)

Table 5-9: Statistics for Axial Force at Gauge Locations on Individual Piles (1.4m Wave, Full)

Gauge Location	Pile Location	Axial Force (kips)		
		Max	Standard Deviation	COV
Top	A1	3.41	0.07	2.0%
	B1	3.52	0.07	2.0%
	A2	-3.26	0.07	2.1%
	B2	-4.82	0.08	1.7%
	sum	-1.15		
Bottom	A1	3.11	0.07	2.2%
	B1	0.63	0.07	10.9%
	A2	-2.35	0.06	2.5%
	B2	-1.63	0.08	4.9%
	sum	-0.24		

A time history of the moment at each gauge location at the top and bottom of each pile are presented in Figure 5-14 and Figure 5-15 respectively. Maximum values and statistics for these plots can be found in Table 5-10. From these plots it can be seen that double bending is occurring in the piles with positive moments at the top of the piles and negative moments at the bottom of the piles as would be expected for a member with fixed-fixed boundary conditions as is the case for the piles, as they were embedded into the concrete of the base slab and the specimen. The moment in the piles is not distributed evenly between the piles. Because each of the piles was constructed out of the same materials they should all have the same stiffness and distribute load evenly, however like with the axial force this is evidence that the specimen was not placed symmetrically in the flume and therefore an even distribution of forces did not occur. The strain gauges provided very consistent data for the maximum moment in the piles, as evidenced by every strain gauge location having a coefficient of variation well below 5%.

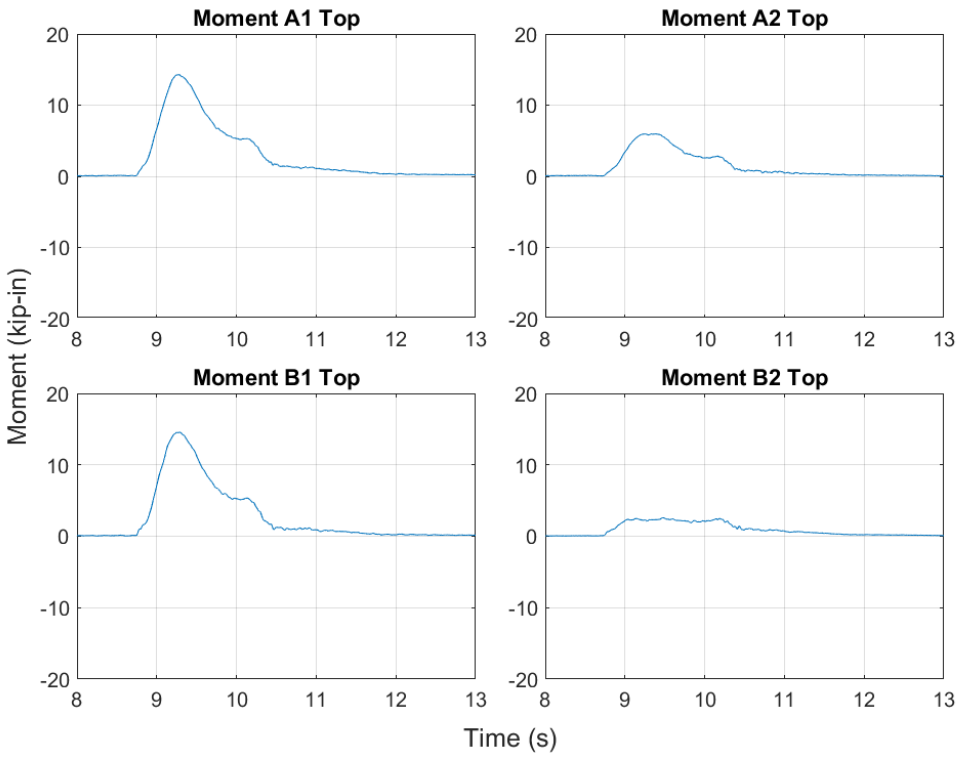

Figure 5-14: Time History for Moment at Top Gauge Locations (1.4m Wave, Full)

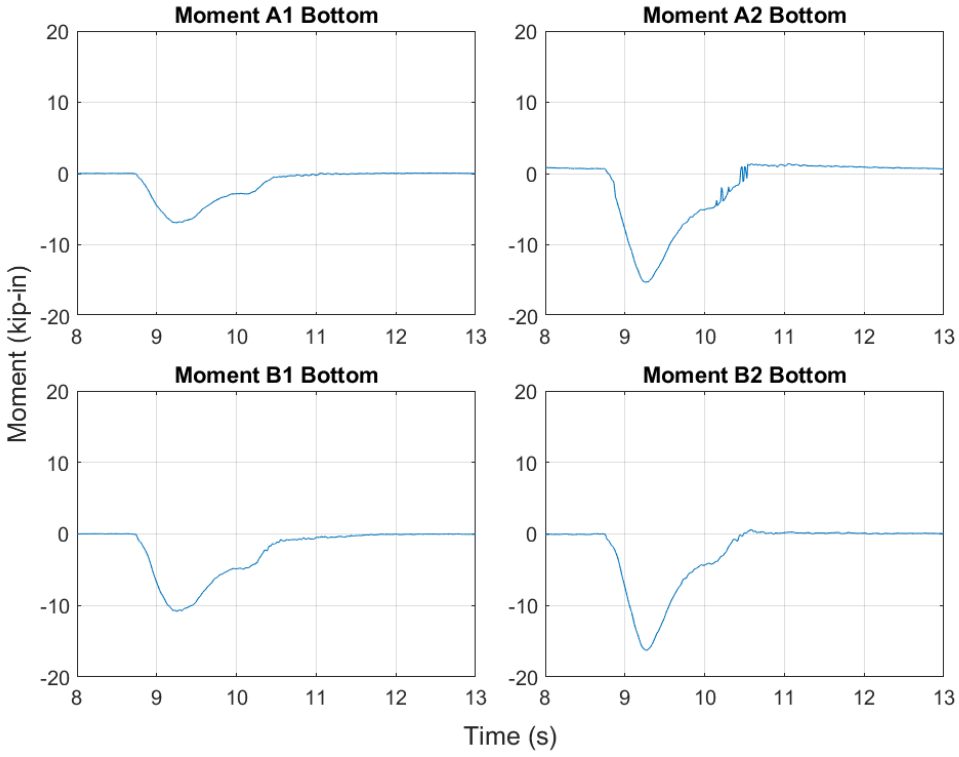

Figure 5-15: Time History for Moment at Bottom Gauge Locations (1.4m Wave, Full)

Table 5-10: Statistics for Moment at Gauge Locations on Individual Piles (1.4m Wave, Full)

Gauge Location	Pile Location	Moment (k-in)		
		Max	Standard Deviation	COV
Top	A1	14.3	0.080	0.6%
	B1	14.6	0.051	0.3%
	A2	6.0	0.045	0.8%
	B2	2.6	0.064	2.5%
	sum	37.4		
Bottom	A1	-6.9	0.081	1.2%
	B1	-10.8	0.081	0.7%
	A2	-15.3	0.078	0.5%
	B2	-16.3	0.080	0.5%
	sum	-49.3		

A time history of shear in the individual piles is presented in Figure 5-16 and a time history of the total base shear on the structure is provided in Figure 5-17. The maximum values and statistics for shear in the individual piles as well as on the entire structure are provided in Table 5-11. The shear in the piles showed lower repeatability than the moment and axial measurements as evidenced by higher coefficients of variation for the shear values. This could be due to the combining the uncertainties of the moment measurements. Unlike the axial and moment measurements on the piles, the total shear in the piles was distributed more evenly between the piles.

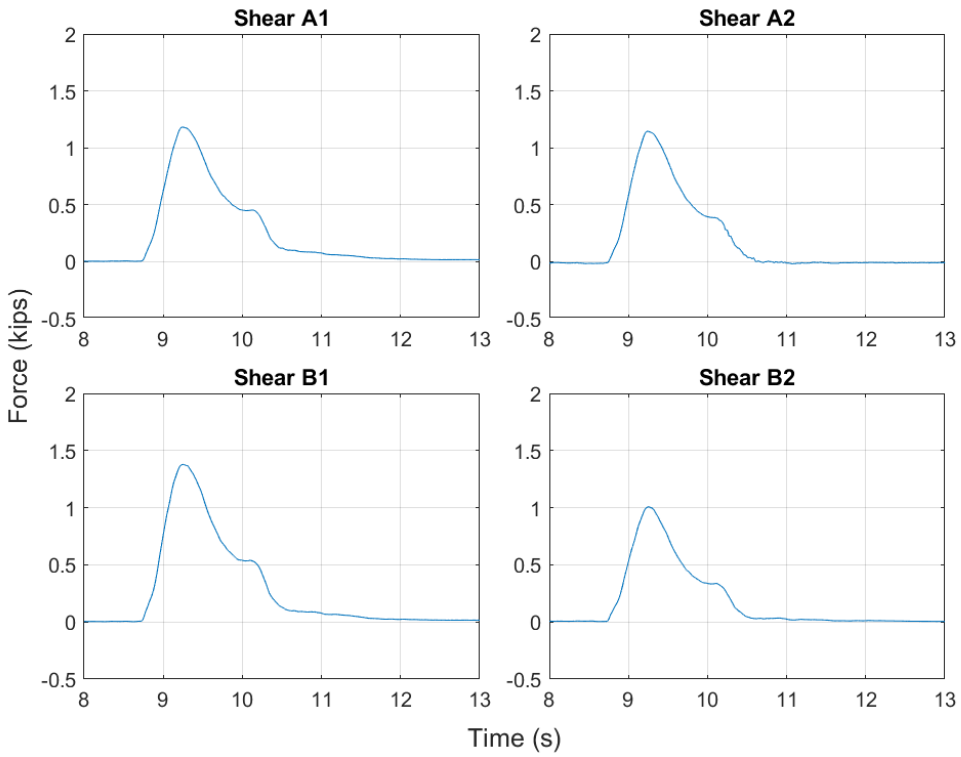

Figure 5-16: Time History for Shear in Individual Piles (1.4m Wave, Full)

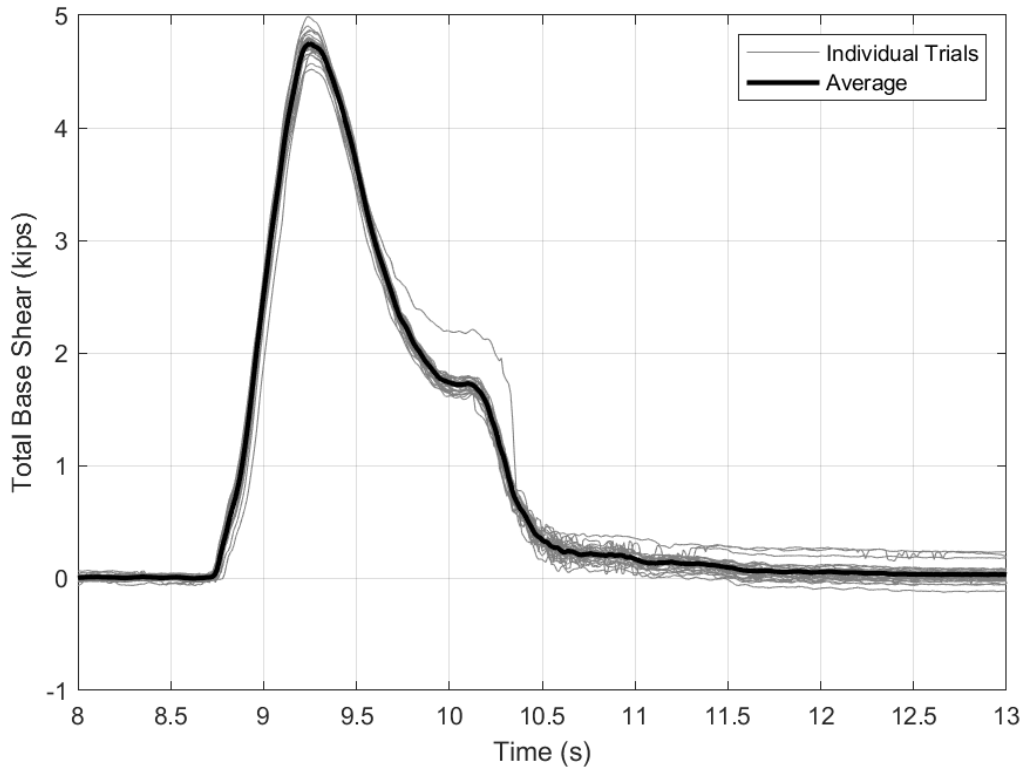

Figure 5-17: Combined Pile Shear Time History (1.4m Wave, Full)

Table 5-11: Statistics for Pile Shear Measurements (1.4m Wave, Full)

Pile Location	Shear (kips)		
	Max	Standard Deviation	COV
A1	1.18	0.08	6.6%
A2	1.15	0.08	7.0%
B1	1.38	0.08	5.6%
B2	1.01	0.08	7.7%
Combined	4.71	0.43	9.1%

5.5.1.3 Load-Cell Measurements

Loads on the structure were measured in the stream-wise, transverse, vertical load cells over all 30 trials for the experiment. A diagram of the load cell configuration can be found in Figure 4-12. For all load cell plots the sign convention is positive when the load cell is in compression.

Load Cells SA and SB measured the stream-wise horizontal reactions at the base of the structure. A time history for the total force is shown in Figure 5-18. Statistics for the individual load cells as well as when they are combined is provided in Table 5-12. The stream-wise load cells provided good repeatability as evidenced by their coefficients of variation both being below 5%. The maximum force from the load cell measurements was within 300lbf of the total stream-wise force as measured by the strain gauges, with the load cells showing greater force than the strain gauges.

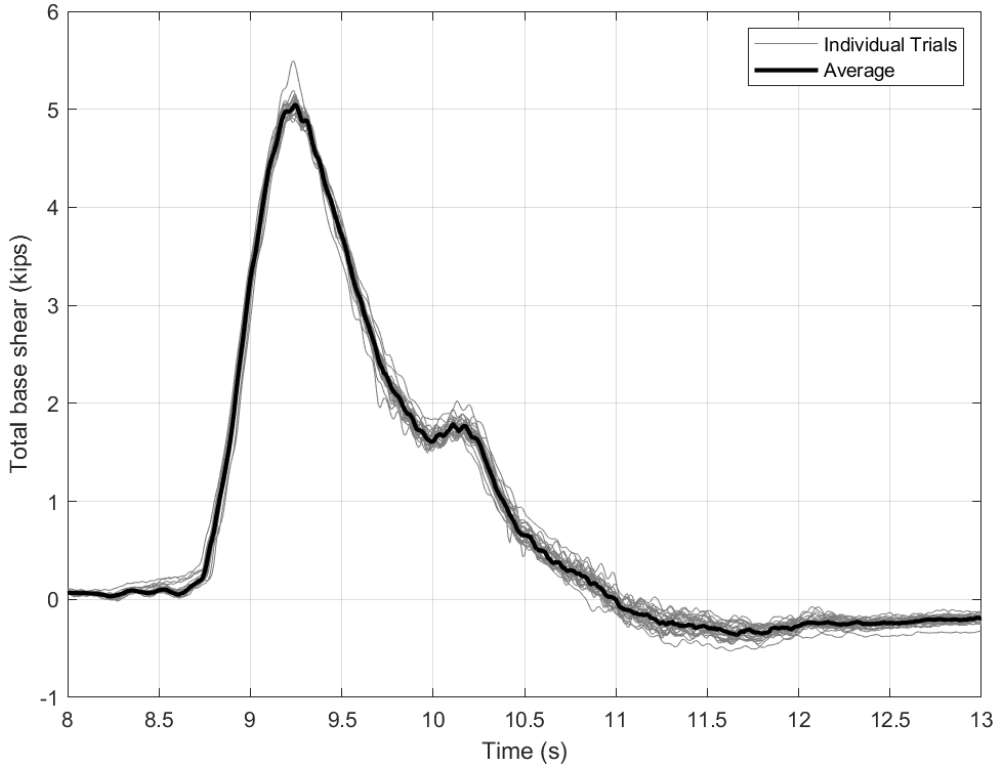

Figure 5-18: Stream-wise Load Cell Time History (1.4m Wave, Full)

Table 5-12: Statistics for Stream-wise Load Cells (1.4m Wave, Full)

Soil Condition	Load Cell	1.4m Wave			
		No. of Trials	Average Max (lbf)	Standard Deviation (lbf)	COV
Full	SA+SB	30	5,058	102	2.0%
	SA	30	2,163	43	2.0%
	SB	30	2,895	58	2.0%

Vertical forces on the structure were measured using the four vertical load cells. A time history for each of these load cells is provided in Figure 5-19. Due to the design of the setup and the wooden framing for the beach bearing on the outside rim of the soil box load cells VA1 and VB1 located on the side of the structure the wave impacts first see a small increase in force where the front load cells go into compression as the weight of the wave moves onto the beach before the structure is impacted. As the structure is impacted the force in the load cells goes down, however on average not reaching below zero and into tension, while the back load cells go into compression (around time 9.25s). Because the Average value at this time step is so close to zero yet there is some variability in the data, the standard deviation is greater than the average resulting in very large values for the coefficient of variation, however the repeatability of the data seems adequate based

on how closely the individual trials follow to the average. Plots for VA2 and VB2 show about the same amount of variability in the peak as VA1 and VB1, but have much lower COV values.

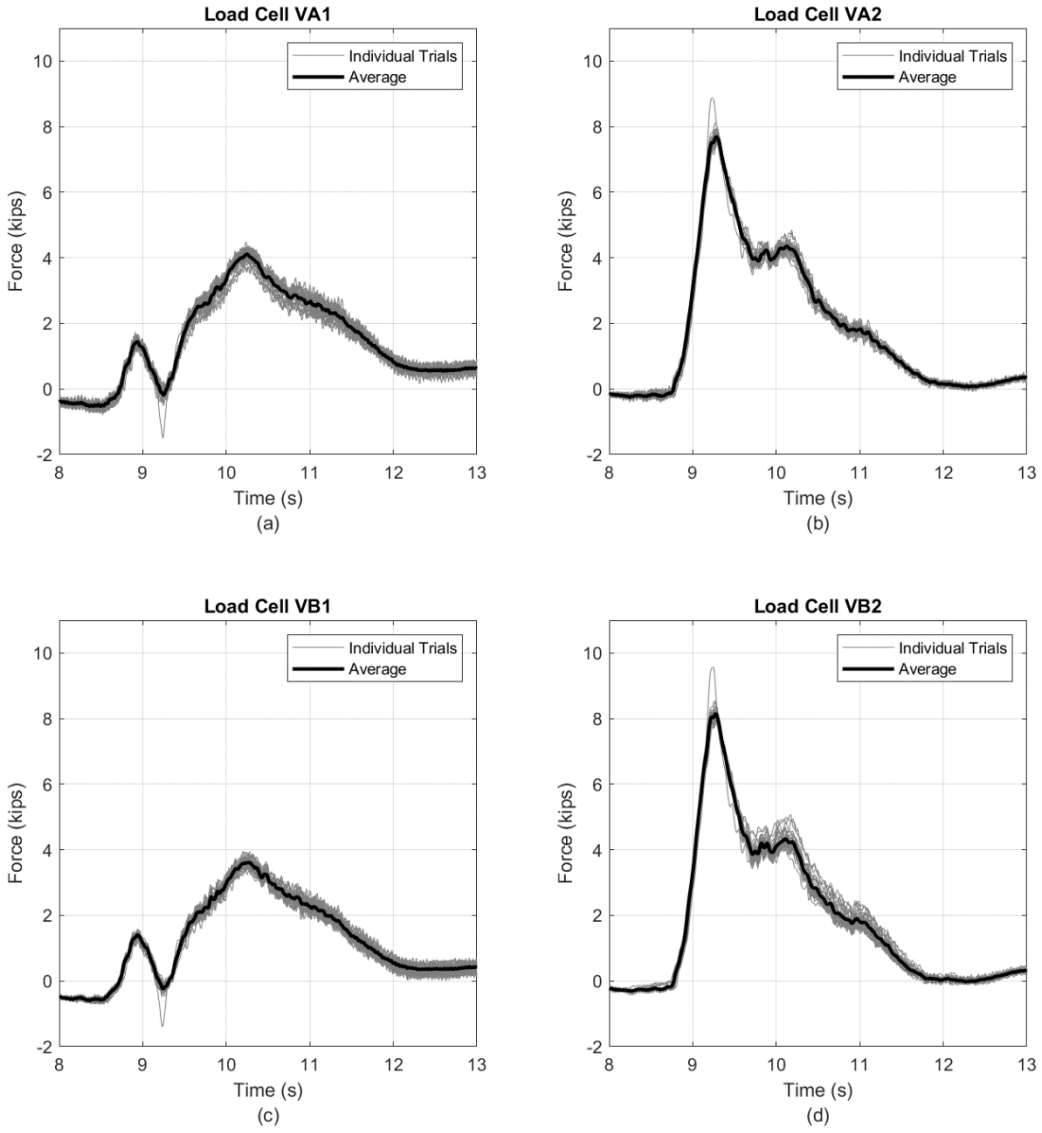

Figure 5-19: Bottom Load Cell Time Histories (1.4m Wave, Full)

Table 5-13: Bottom Load Cell Statistics (1.4m Wave, Full)

Soil Condition	Load Cell	1.4m Wave			
		No. of Trials	Average Max (lbf)	Standard Deviation (lbf)	COV
Full	VA1	30	-19.5	167	-859%
	VB1	30	-159	134	-84%
	VA2	30	7,695	172	2%
	VB2	30	8,148	173	2%

Transverse forces were measured with load cells T1 and T2. A plot of the sum of the forces in these load cells is provided in Figure 5-20. Loads in the transverse direction were an order of magnitude lower than those observed in the stream-wise and vertical directions. Ideally there would be no transverse force on the system however there is some due to issues with the setup such as the structure not being placed perfectly in the middle of the flume and issues getting it perfectly square to the flume walls during the installation. The transverse load cells showed significantly more variation than the load cells in other directions likely due to the smaller loads being measured. Because this was the first experiment conducted there also could have been some movement in the structure from the first few waves before the structure found a stable alignment.

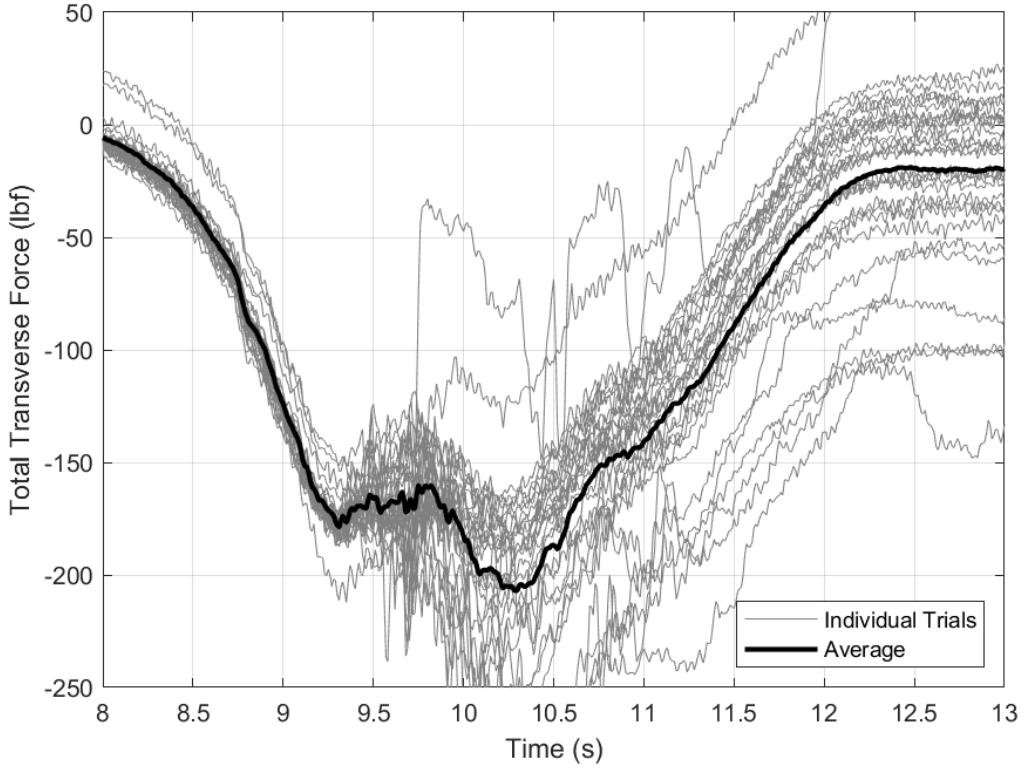

Figure 5-20: Transverse Load Cell Time History (1.4m Wave, Full)

Table 5-14: Transverse Load Cell Statistics (1.4m Wave, Full)

Soil Condition	Load Cell	1.4m Wave			
		No. of Trials	Average Max (lbf)	Standard Deviation (lbf)	COV
Full	TA+TB	30	-207	59	-28.4%
	TB	30	-87	12	-13.6%
	TA	30	-120	52	-43.0%

5.5.2 *1.4m Height, Half Full Soil Box*

The 1.4m wave, soil box half full was the second experiment conducted. It consisted of running 35 waves in order to demonstrate the repeatability of the wave and resulting forces and pressures. 10 trials were run for each of the first three pressure sensor layouts used, and five trials were run for the fourth pressure sensor layout used.

5.5.2.1 Pressure Measurements

Figure 5-21 shows a time history of the average pressures at different locations on the wall for nine of the 33 pressure sensor locations. The selected sensors are located along the three primary vertical lines of pressure sensors at the top, middle, and bottom of the pressure grid to give an idea of the changes in pressure over the height of the wall. The location of pressure sensors can be found in Figure 4-16. Table 5-15 gives the average maximum, standard deviation and coefficient of variation across all trials for this experiment, for the pressure sensors shown in Figure 5-21. The pressure sensors near the bottom and middle of the wall showed good repeatability with coefficients of variation less than 5%, with the exception of sensor D01 which was located at the bottom outside corner of the wall. The pressure sensors near the top of the wall showed significantly higher variability than they did for the 1.4m wave, full experiment. This could be due to the action of the wave breaking towards the top of the wall and causing air bubbles in the water to change the pressures applied to the structure.

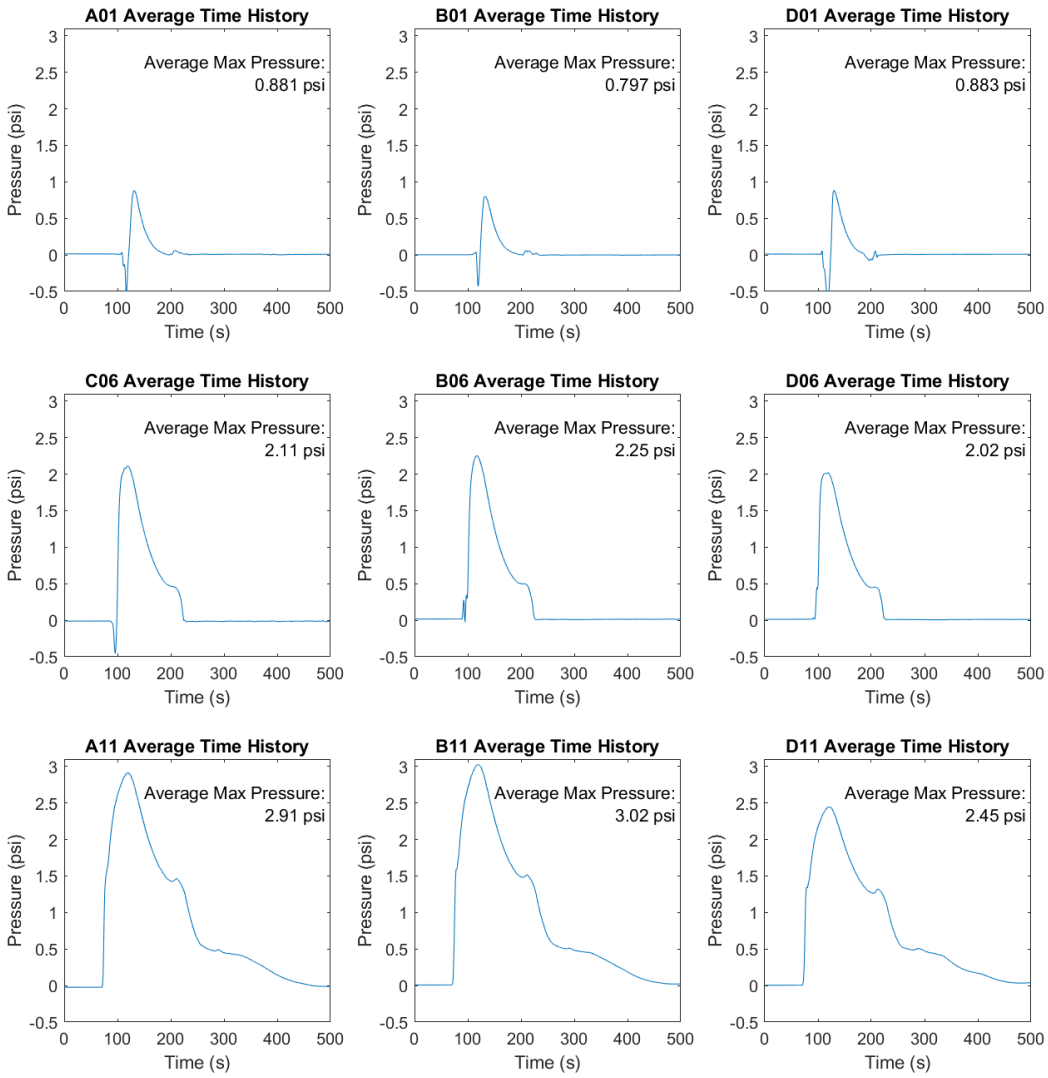

Figure 5-21: Average Pressure Time Histories at Selected Sensors (1.4m Wave, Half)

Table 5-15: Pressure Sensor Statistics at Selected Sensors (1.4m Wave, Half)

Sensor Name	Average Max Pressure (psi)	Coefficient of Variation	No. of Trials
A01	0.881	5%	10
B01	0.797	35%	10
D01	0.883	41%	10
C06	2.108	2%	15
B06	2.253	4%	10
D06	2.020	4%	10
A11	2.912	1%	15
B11	3.023	1%	35
D11	2.448	33%	10

After examining pressures at individual sensor locations the different pressure layouts were combined and integrated to find the total force acting on the wall from the wave. The average pressure at each gauge location was used to evaluate the force on the test specimen. Figure 5-22 provides a time history of the force from the pressures as well as the average maximum force on the wall.

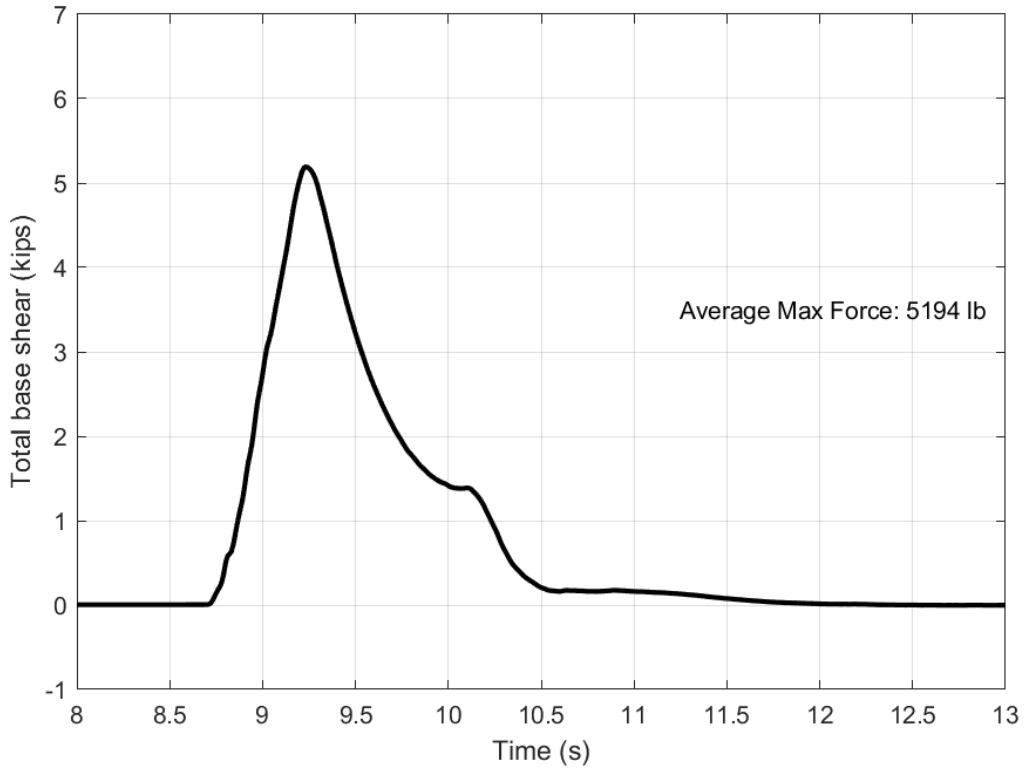

Figure 5-22: Force Time History from Pressures (1.4m Wave, Half)

5.5.2.2 Strain Measurements

A time history of axial forces in each pile at the top and bottom strain gauge locations are provided in Figure 5-23 and Figure 5-24 respectively. The maximum force, standard deviation and coefficient of variation for each gauge location in each pile can be found in Table 5-16, as well as the sum of the axial forces in at the top and bottom of the piles. Negative values in this table indicate compression in the section. It can be observed that the strain gauges provided reliable data for axial in the piles as evidenced by coefficients of variation being below 5% for all gauge locations with the exception of the lower gauge location on pile B1. This location had a very low maximum relative to the other locations while having about the same standard deviation, leading to a higher coefficient of variation.

Similar to the 1.4m wave, full, generally the results for the axial force make sense, with the piles on the back face of the specimen going into compression while the piles on the front face go into compression. Also similar to the 1.4m wave full, for the 1.4m wave half full there was a total axial force applied to the specimen, in this case averaging slightly higher than the axial force for the previous experiment. Finally the axial forces are different in each pile similar to the previous experiment, further showing that the structure was not sitting perfectly square, plumb, and level in the flume.

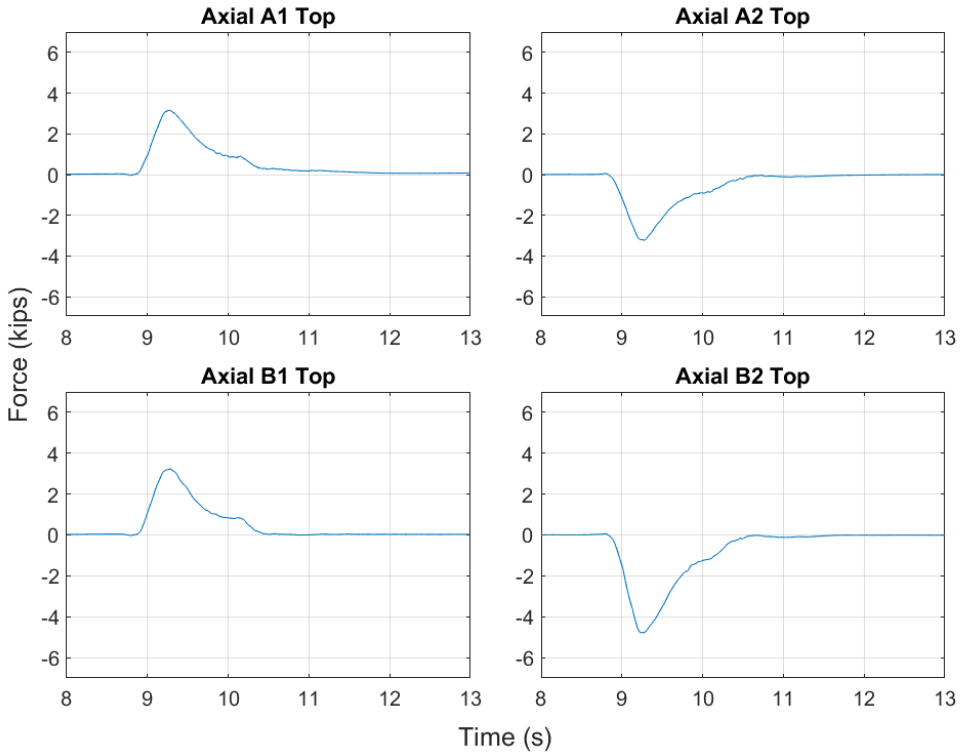

Figure 5-23: Time History for Axial Force at Top Gauge Locations (1.4m Wave, Half)

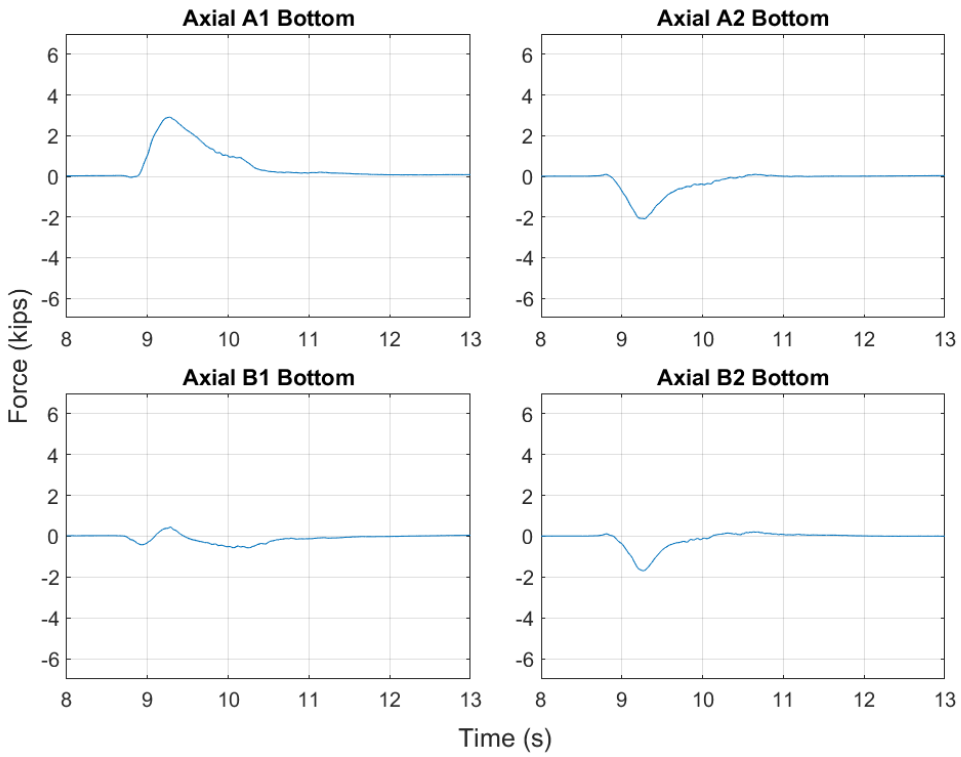

Figure 5-24: Time History for Axial Force at Bottom Gauge Locations (1.4m Wave, Half)

Table 5-16: Statistics for Axial Force at Gauge Locations on Individual Piles (1.4m Wave, Full)

Gauge Location	Pile Location	Axial Force (kips)		
		Max	Standard Deviation	COV
Top	A1	3.16	0.09	2.8%
	B1	3.23	0.08	2.6%
	A2	-3.22	0.08	2.6%
	B2	-4.78	0.09	1.8%
	sum	-1.62		
Bottom	A1	2.91	0.09	3.0%
	B1	0.45	0.08	18.6%
	A2	-2.09	0.08	4.0%
	B2	-1.69	0.09	5.2%
	sum	-0.42		

A time history of the moment at each gauge location at the top and bottom of each pile are presented in Figure 5-25 and Figure 5-26 respectively. Maximum values and statistics for these plots can be found in Table 5-17. Similar to the prior experiment moment in the piles is positive at the top gauge locations and negative at the bottom gauge locations. The repeatability of the

moment measurements also appears to be very good with coefficient of variation values all below 5%. Again the time history for moment in pile B1 is rather flat compared to the other moment time histories, indicating that the readings from the prior experiment were not erroneous and that something is happening to reduce the moment in pile B1 at the top compared to other locations.

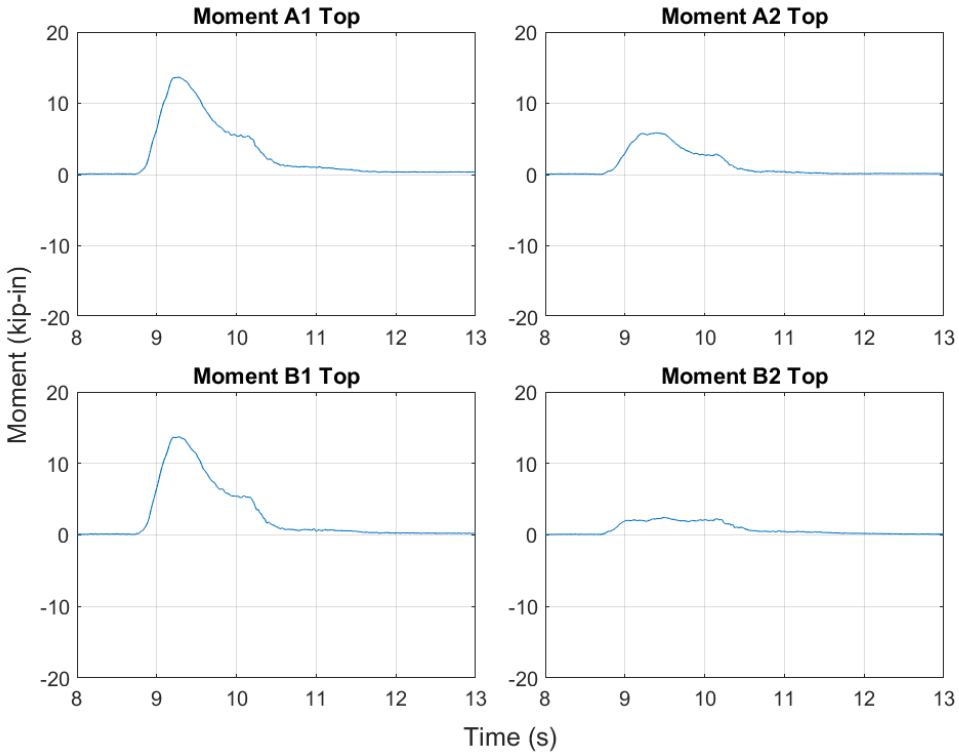

Figure 5-25: Time History for Moment at Top Gauge Locations (1.4m Wave, Half)

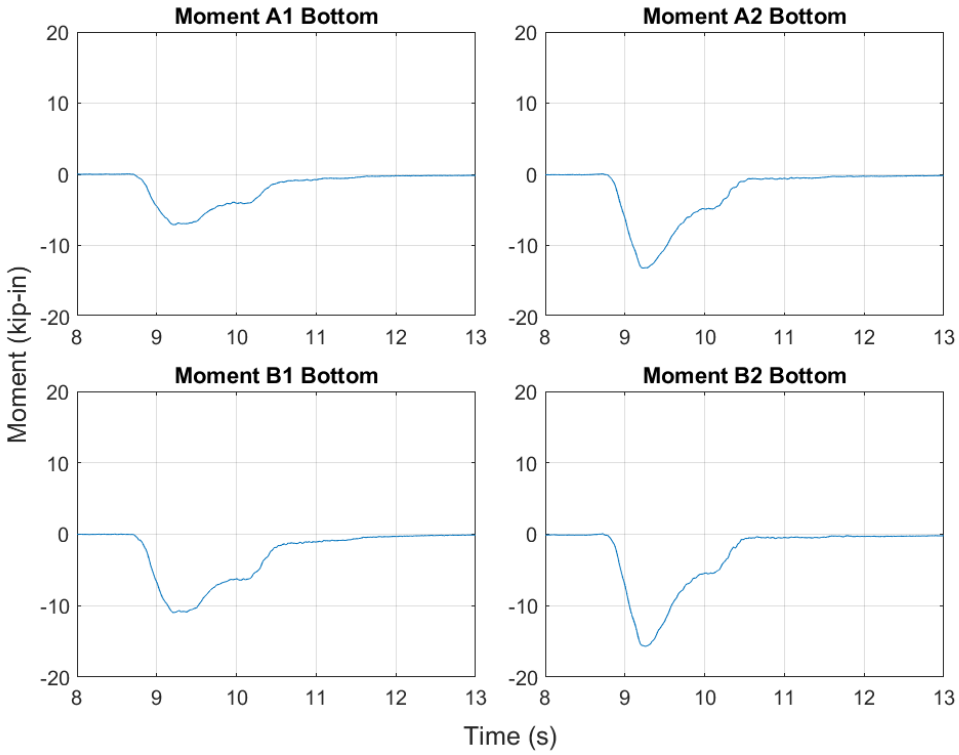

Figure 5-26: Time History for Moment at Bottom Gauge Locations (1.4m Wave, Half)

Table 5-17: Statistics for Moment at Gauge Locations on Individual Piles (1.4m Wave, Empty)

Gauge Location	Pile Location	Moment (k-in)		
		Max	Standard Deviation	COV
Top	A1	13.7	0.088	0.6%
	B1	13.7	0.084	0.6%
	A2	5.8	0.106	1.8%
	B2	2.5	0.101	4.1%
	sum	35.7		
Bottom	A1	-7.1	0.168	2.4%
	B1	-11.0	0.168	1.5%
	A2	-13.2	0.133	1.0%
	B2	-15.7	0.096	0.6%
	sum	-46.9		

A time history of shear in the individual piles is presented in Figure 5-27 and a time history of the total base shear on the structure is provided in Figure 5-28. The maximum values and statistics for shear in the individual piles as well as on the entire structure are provided in Table 5-18. Similar to the previous experiment the variation in shear on the piles is slightly higher than the variation

of other strain gauge measurements. The total base shear for the half full soil box condition shows slightly lower force than for the full condition. If the soil was taking any of the load in the piles the force would be lower for the full soil box condition. This could be used to show that the soil in the soil box is not taking load from the piles and the total base shear is being transferred into the base slab for the test specimen.

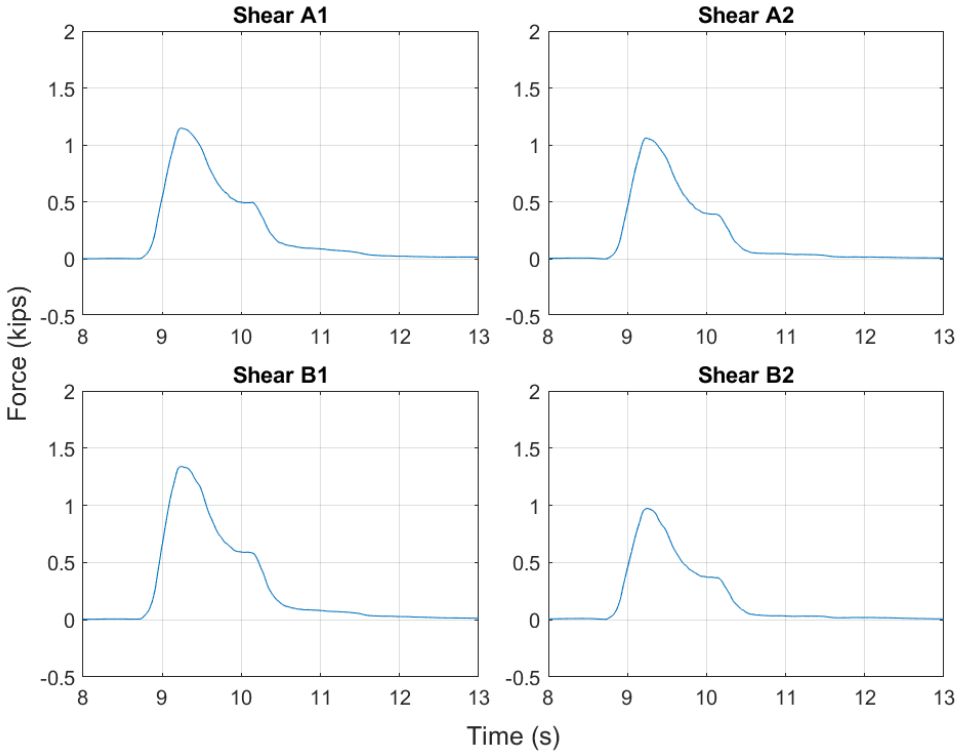

Figure 5-27: Time History for Shear in Individual Piles (1.4m Wave, Half)

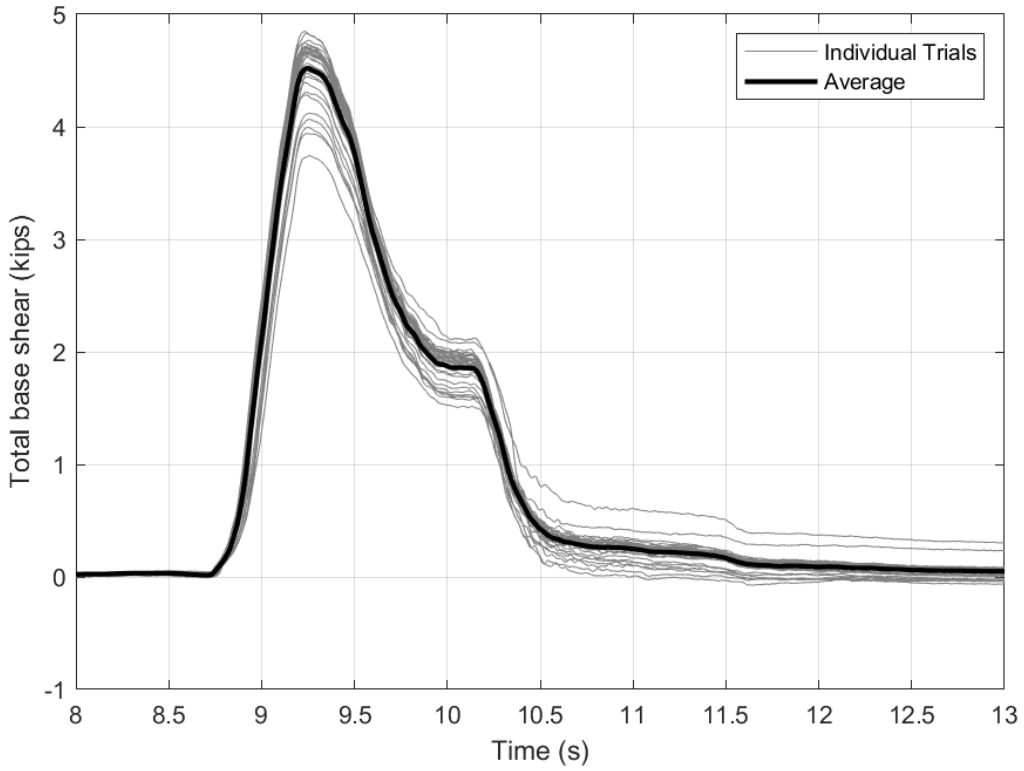

Figure 5-28: Combined Pile Shear Time History (1.4m Wave, Half)

Table 5-18: Statistics Pile for Shear Measurements (1.4m Wave, Half)

Pile Location	Shear (kips)		
	Max	Standard Deviation	COV
A1	1.15	0.10	8.6%
A2	1.06	0.10	9.3%
B1	1.34	0.10	7.2%
B2	0.97	0.10	9.9%
Combined	4.52	0.27	6.0%

5.5.2.3 Load Cell Measurements

Loads on the structure were measured in the stream-wise, transverse, vertical load cells over all 35 trials for this experiment. A diagram of the load cell configuration can be found in Figure 4-12. For all load cell plots the sign convention is positive when the load cell is in compression.

Load Cells SA and SB measured the stream-wise horizontal reactions at the base of the structure. A time history for the total force is shown in Figure 5-29. Statistics for the individual load cells as well as when they are combined in provided in Table 5-19. Similar to the previous experiment

the stream-wise load cells provided good repeatability with coefficients of variation for both load cells below 5%.The maximum force from the load cell measurements was within 400lbf of the total stream-wise force as measured by the strain gauges, with the load cells showing slightly more force than the shear measured by the strain gauges.

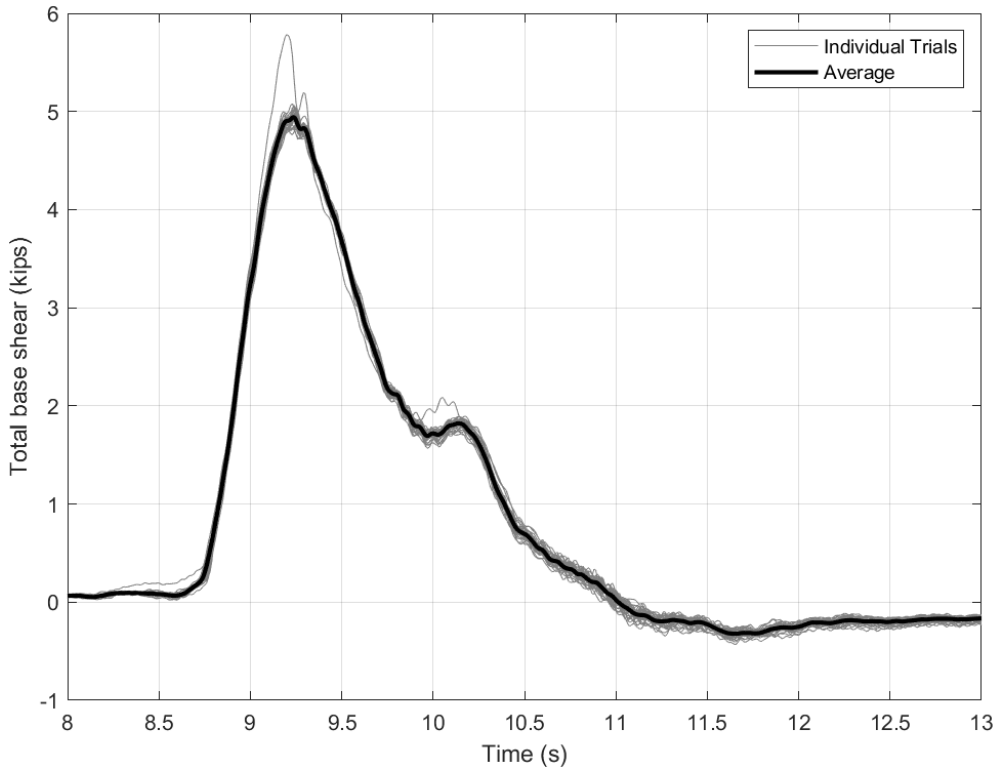

Figure 5-29: Stream-wise Load Cell Time History (1.4m Wave, Half)

Table 5-19: Statistics for Stream-wise Load Cells (1.4m Wave, Half)

Soil Condition	Load Cell	1.4m Wave			
		No. of Trials	Average Max (lbf)	Standard Deviation (lbf)	COV
Half	SA+SB	35	4,948	156	3.1%
	SA	35	2,079	65	3.1%
	SB	35	2,869	90	3.1%

Vertical forces on the structure were measured using the four vertical load cells. A time history for each of these load cells is provided in Figure 5-30 and maximum values and statistics for the load cells are provided in Table 5-20. Similar to the previous experiment the front load cells (VA1 and VB1) do not go into tension due to the weight of the wave acting on the test setup. The back load cells provide very reliable data with coefficients of variation below 5%. The front load cells have

much higher coefficients of variation, however from looking at the individual trials again it seems like this is due to the low mean value for the load cells rather than the wave not being repeatable.

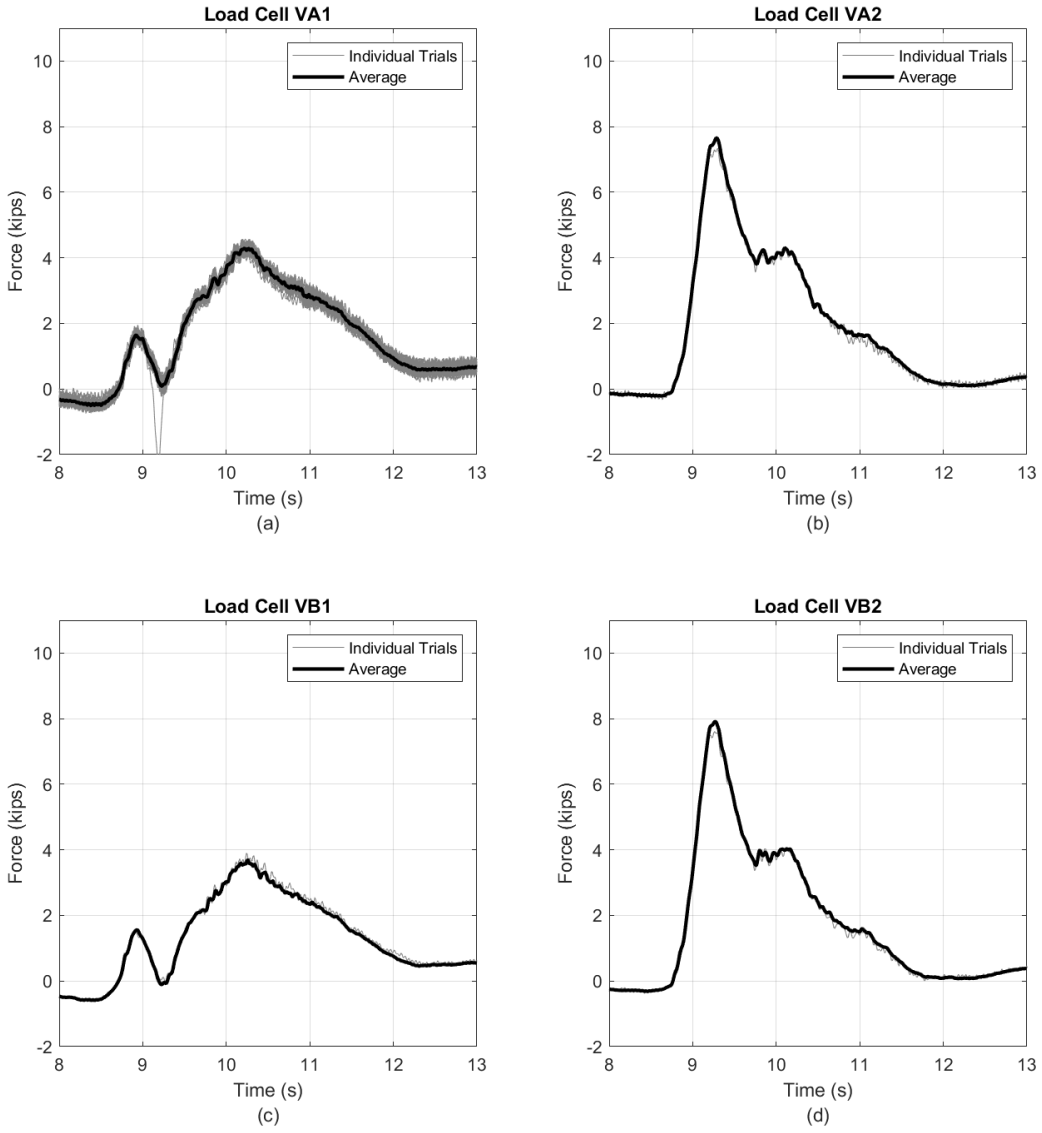

Figure 5-30: Bottom Load Cell Time Histories (1.4m Wave, Half)

Table 5-20: Bottom Load Cell Statistics (1.4m Wave, Half)

Soil Condition	Load Cell	1.4m Wave			
		No. of Trials	Average Max (lbf)	Standard Deviation (lbf)	COV
Half	VA1	35	311	149	48%
	VB1	35	-39.0	83	-214%
	VA2	35	7,653	173	2%
	VB2	35	7,916	162	2%

Transverse forces were measured with load cells T1 and T2. A plot of the sum of the forces in these load cells is provided in Figure 5-31 and mean values and statistics are provided in Table 5-21. Unlike the previous experiment the time history for the half full experiment shows much less variability in the data, with the grey lines following the same trend as the average line. This is also reflected in the individual load cell statistics, T2 and T1+T2 both have significantly lower coefficients of variation, while the coefficient of variation for T1 increased slightly. This shows that the test specimen was able to move slightly during the first experiment, however by the second experiment it seems to be in a stable condition and provide repeatable data.

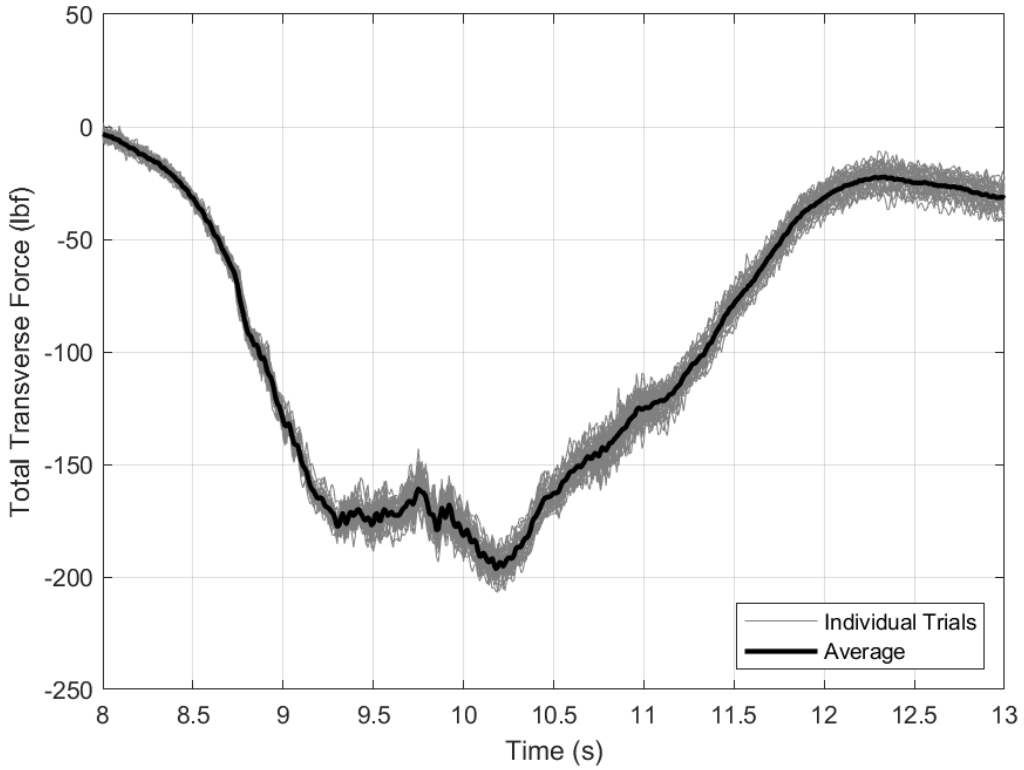

Figure 5-31: Transverse Load Cell Time History (1.4m Wave, Half)

Table 5-21: Transverse Load Cell Statistics (1.4m Wave, Half)

Soil Condition	Load Cell	1.4m Wave			
		No. of Trials	Average Max (lbf)	Standard Deviation (lbf)	COV
Half	TA+TB	35	-196	4.5	-2.3%
	TB	35	-62	11.0	-17.7%
	TA	35	-134	11.8	-8.8%

5.5.3 *1.4m Height, Empty Soil Box*

The 1.4m wave, soil box empty was the third experiment conducted. It consisted of running 37 trials. 10 trials were run for each of the first three pressure sensor layouts used, and seven trials were run for the fourth pressure sensor layout used.

5.5.3.1 Pressure Measurements

Figure 5-32 shows a time history of the average pressures at different locations on the wall for nine of the 33 pressure sensor locations. The selected sensors are located along the three primary vertical lines of pressure sensors at the top, middle, and bottom of the pressure grid to give an idea of the changes in pressure over the height of the wall. The location of pressure sensors can be found in Figure 4-16. Table 5-22 gives the average maximum, standard deviation and coefficient of variation across all trials for this experiment, for the pressure sensors shown in Figure 5-32. The pressure sensors near the bottom and middle of the wall showed good repeatability with coefficients of variation less than 5%. The pressure sensors near the top of the wall showed similar variability to the 1.4m wave, full experiment, and slightly less variability than the 1.4m wave, half experiment.

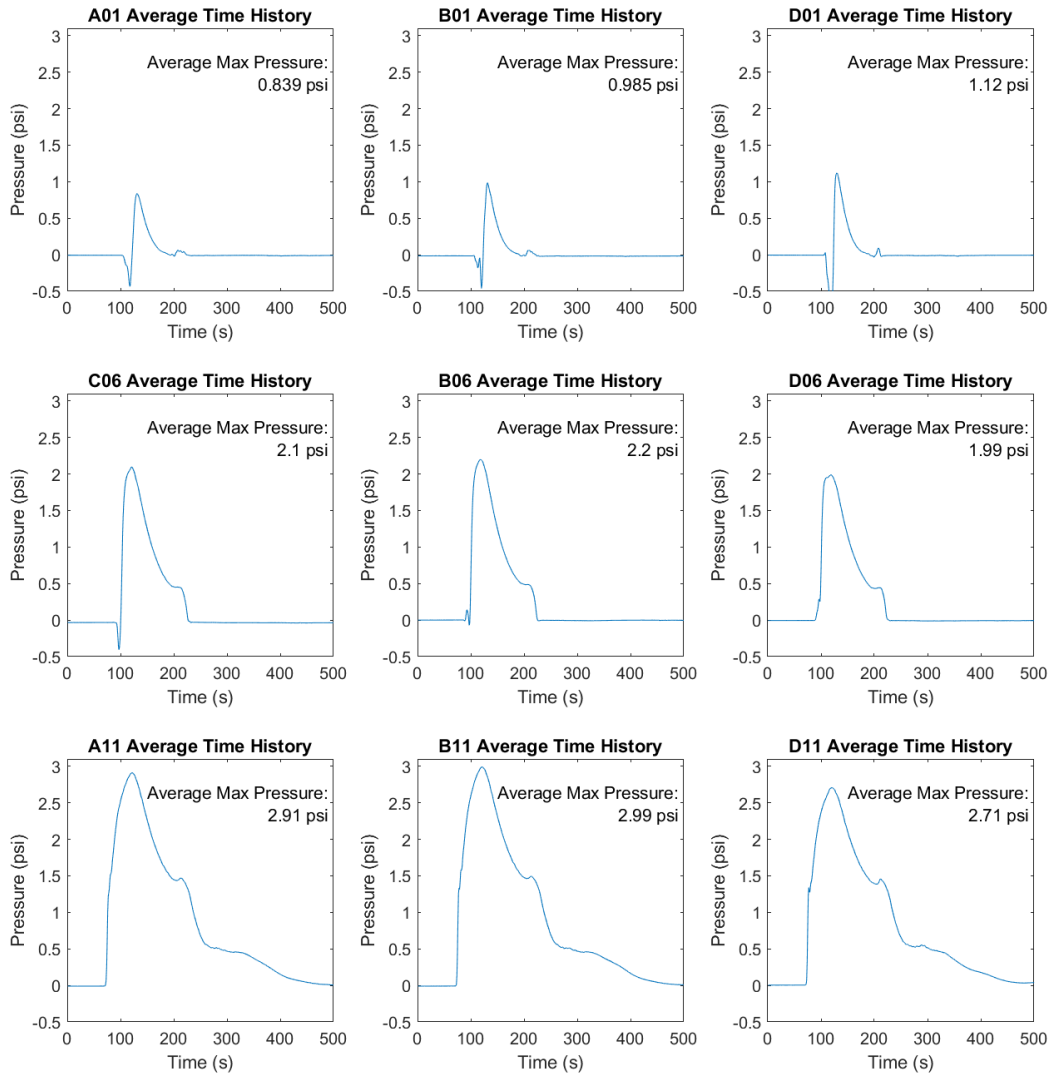

Figure 5-32: Average Pressure Time Histories at Selected Sensors (1.4m Wave, Empty)

Table 5-22: Pressure Sensor Statistics at Selected Sensors (1.4m Wave, Empty)

Sensor Name	Average Max Pressure (psi)	Coefficient of Variation	No. of Trials
A01	0.839	9%	10
B01	0.985	15%	10
D01	1.119	5%	10
C06	2.098	6%	17
B06	2.196	1%	10
D06	1.988	1%	10
A11	2.911	2%	17
B11	2.989	2%	37
D11	2.706	1%	10

After examining pressures at individual sensor locations the different pressure layouts were combined and integrated to find the total force acting on the wall from the wave. The average pressure at each gauge location was used to evaluate the force on the test specimen. Figure 5-33 provides a time history of the force from the pressures as well as the average maximum force on the wall.

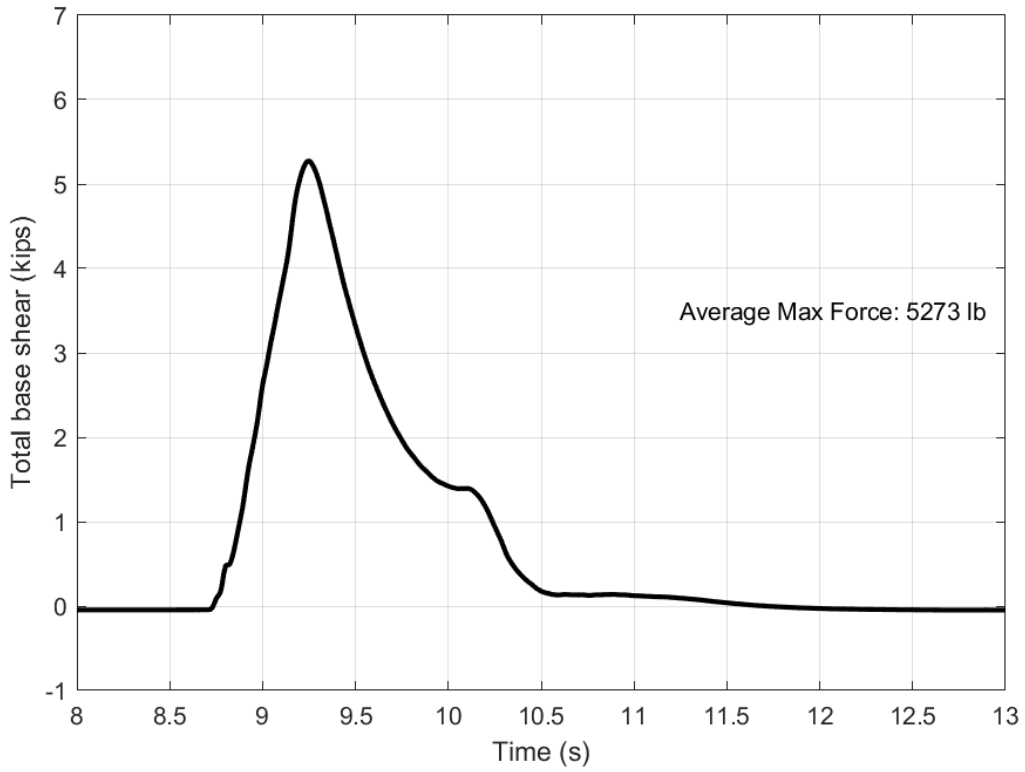

Figure 5-33: Force Time History from Pressures (1.4m Wave, Empty)

5.5.3.2 Strain Measurements

A time history of axial forces in each pile at the top and bottom strain gauge locations are provided in Figure 5-34 and Figure 5-35 respectively. The maximum force, standard deviation and coefficient of variation for each gauge location in each pile can be found in Table 5-23, as well as the sum of the axial forces in at the top and bottom of the piles. Negative values in this table indicate compression in the section. It can be observed that the strain gauges in the top locations all provided very reliable data with coefficients of variation all below 5%. Gauges on the bottoms of the piles had slightly more variability for this experiment than the previous two discussed.

Similar to the prior two experiments, in general the results for the axial force make sense, with the piles on the back face of the specimen going into compression while the piles on the front face go

into compression. The top gauges gave a total axial force of 1.64 Kips in compression, while the bottom gauges give a total axial force of .76 Kips in compression. These two values provide about the same change in axial force along the length of the pile as the 1.4m wave, full soil box experiment and because for this experiment the soil box was empty show that the axial force is not being taken by the soil. As previously noted more gauges on the piles would be necessary to get a better idea of why the axial force in the piles is changing.

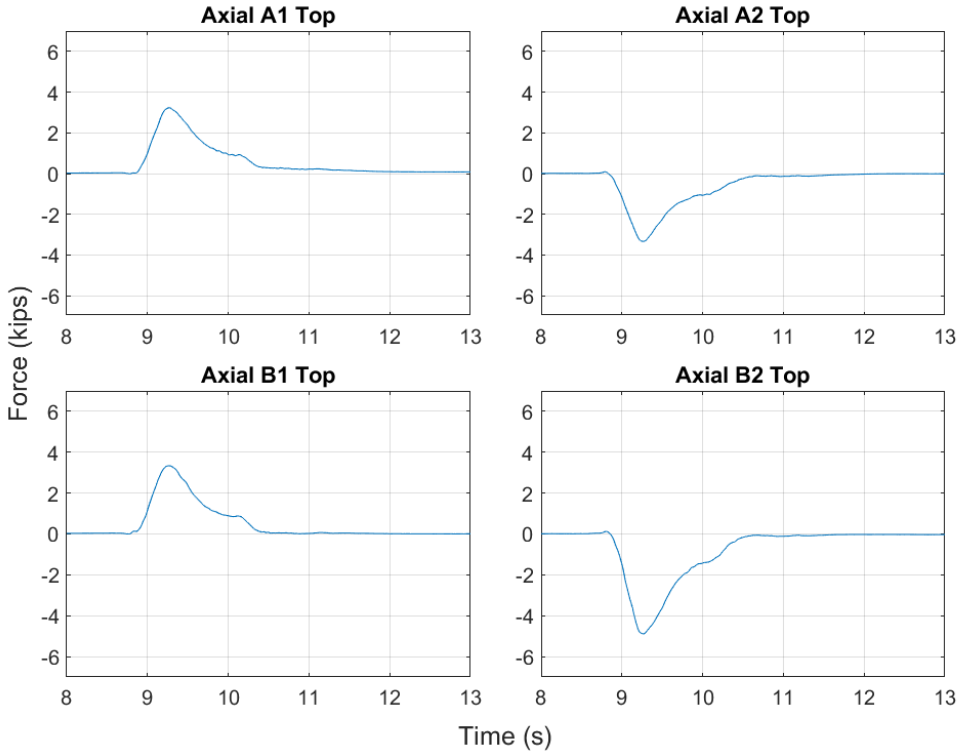

Figure 5-34: Time History for Axial Force at Top Gauge Locations (1.4m Wave, Empty)

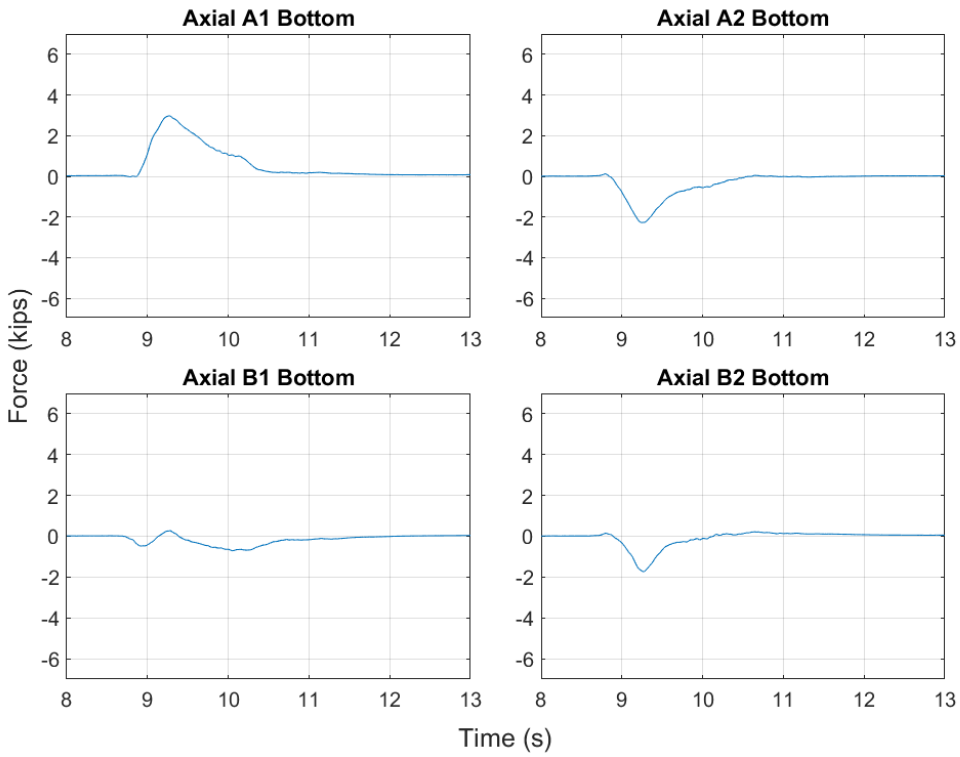

Figure 5-35: Time History for Axial Force at Bottom Gauge Locations (1.4m Wave, Empty)

Table 5-23: Statistics for Axial Force at Gauge Locations on Individual Piles (1.4m Wave, Empty)

Gauge Location	Pile Location	Axial Force (kips)		
		Max	Standard Deviation	COV
Top	A1	3.24	0.15	4.6%
	B1	3.34	0.15	4.5%
	A2	-3.33	0.15	4.5%
	B2	-4.89	0.15	3.0%
	sum	-1.64		
Bottom	A1	2.98	0.15	5.0%
	B1	0.27	0.11	41.4%
	A2	-2.27	0.20	8.9%
	B2	-1.74	0.15	8.6%
	sum	-0.76		

A time history of the moment at each gauge location at the top and bottom of each pile are presented in Figure 5-36 and Figure 5-37 respectively. Maximum values and statistics for these plots can be found in Table 5-24. Moment time histories and statistics appear very similar to the prior two experiments discussed, with positive moment in the top of the piles and negative moment

in the bottom of the piles. The shape of the time history for moment in pile B2 at the top of the pile is still relatively flat, as it was in the other experiments, compared to the other moment time histories for this experiment. The variability in the maximum moment applied is also very good for this experiment with all strain gauge locations having a coefficient of variability less than 5%. Total moment at the top and bottom of the piles is also very similar across all three 1.4m wave experiments.

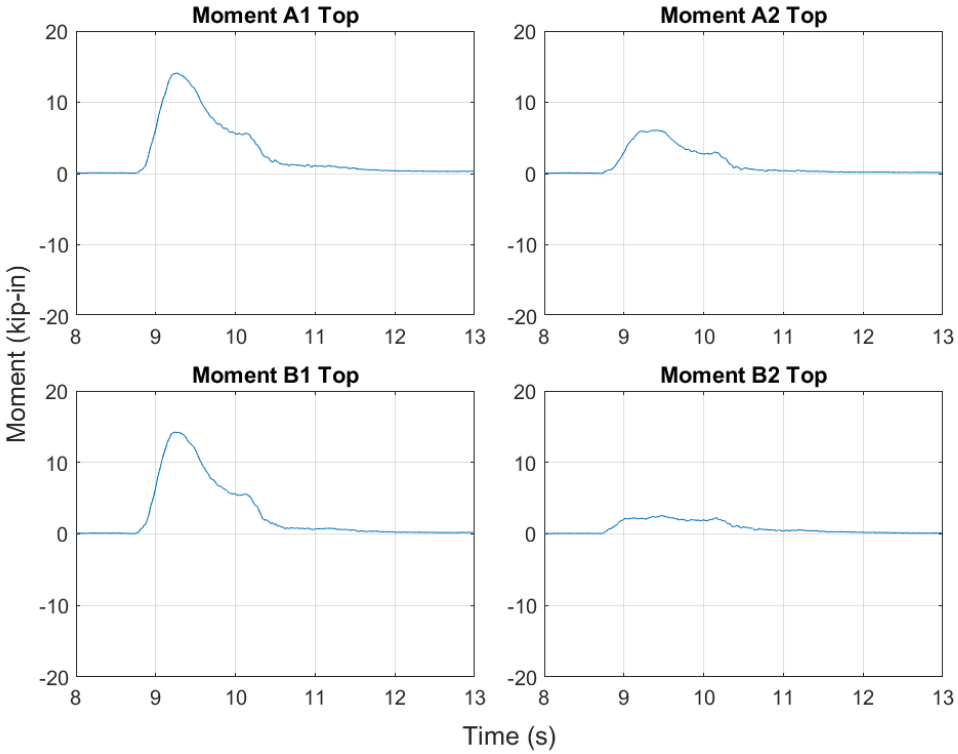

Figure 5-36: Time History for Moment at Top Gauge Locations (1.4m Wave, Empty)

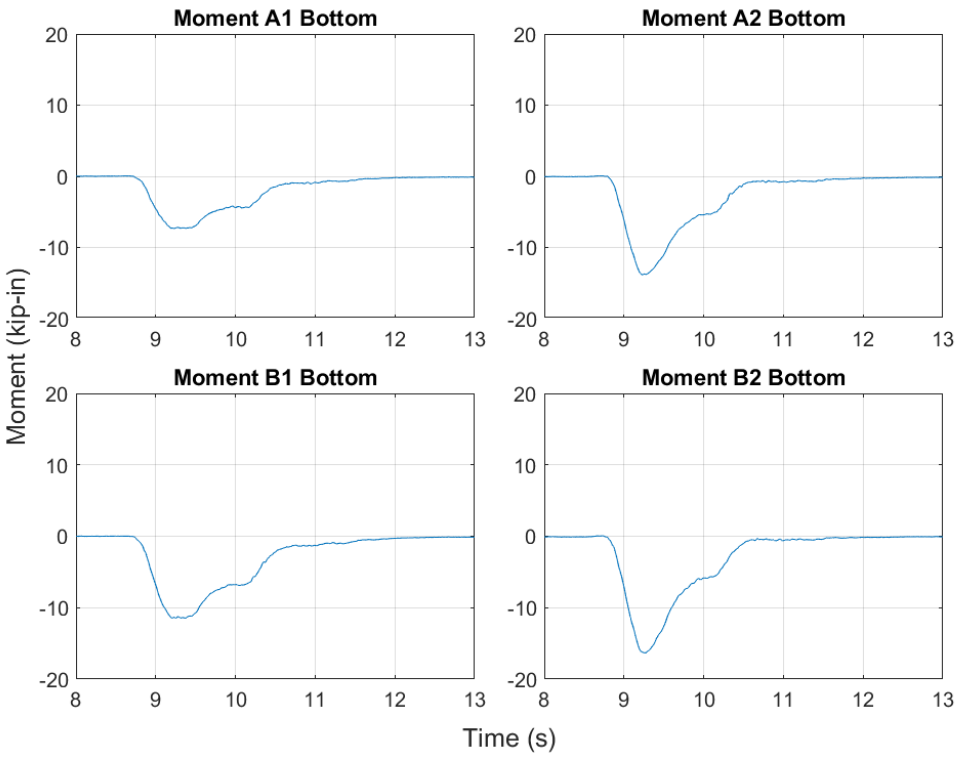

Figure 5-37: Time History for Moment at Bottom Gauge Locations (1.4m Wave, Empty)

Table 5-24: Statistics for Moments at Gauge Locations on Individual Piles (1.4m Wave, Empty)

Gauge Location	Pile Location	Moment (k-in)		
		Max	Standard Deviation	COV
Top	A1	14.1	0.149	1.1%
	B1	14.2	0.209	1.5%
	A2	6.1	0.075	1.2%
	B2	2.6	0.068	2.6%
	sum	37.0		
Bottom	A1	-7.3	0.205	2.8%
	B1	-11.5	0.202	1.8%
	A2	-13.8	0.205	1.5%
	B2	-16.3	0.149	0.9%
	sum	-49.0		

A time history of shear in the individual piles is presented in Figure 5-38 and a time history of the total base shear on the structure is provided in Figure 5-39. The maximum values and statistics for shear in the individual piles as well as on the entire structure are provided in Table 5-25. Similar to the other two experiments for the 1.4m wave, the shear in the piles showed lower repeatability than the moment and axial measurements as evidenced by higher coefficients of variation for the shear values. This could be due to the combining the uncertainties of the moment measurements. Unlike the axial and moment measurements on the piles the total shear in the piles was distributed more evenly between the piles.

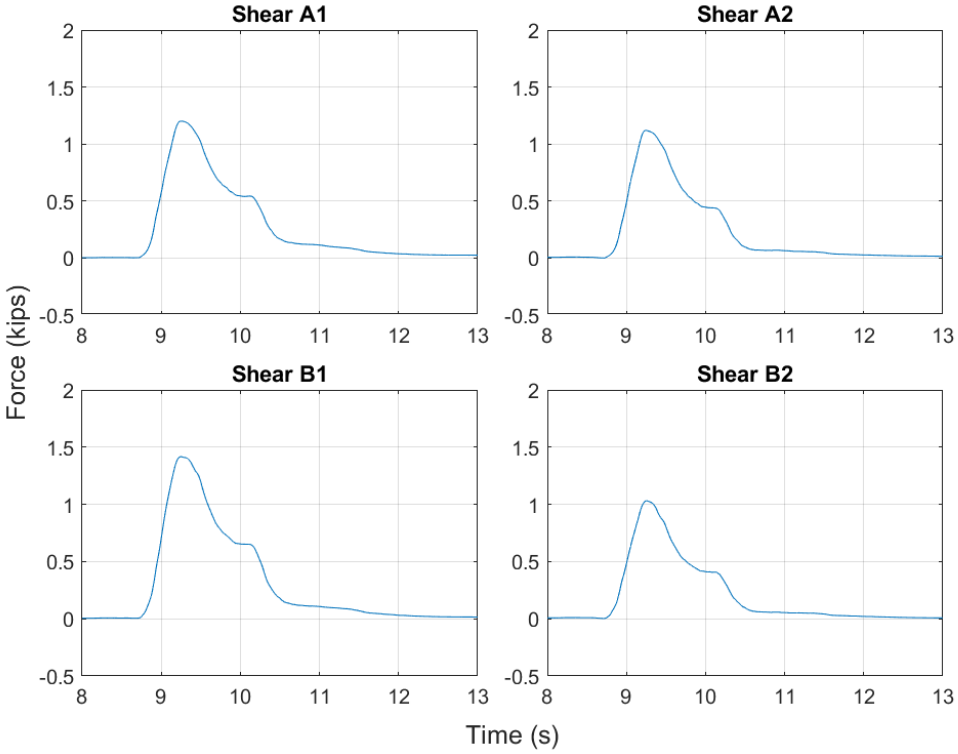

Figure 5-38: Time History for Shear Force in Individual Piles (1.4m Wave, Empty)

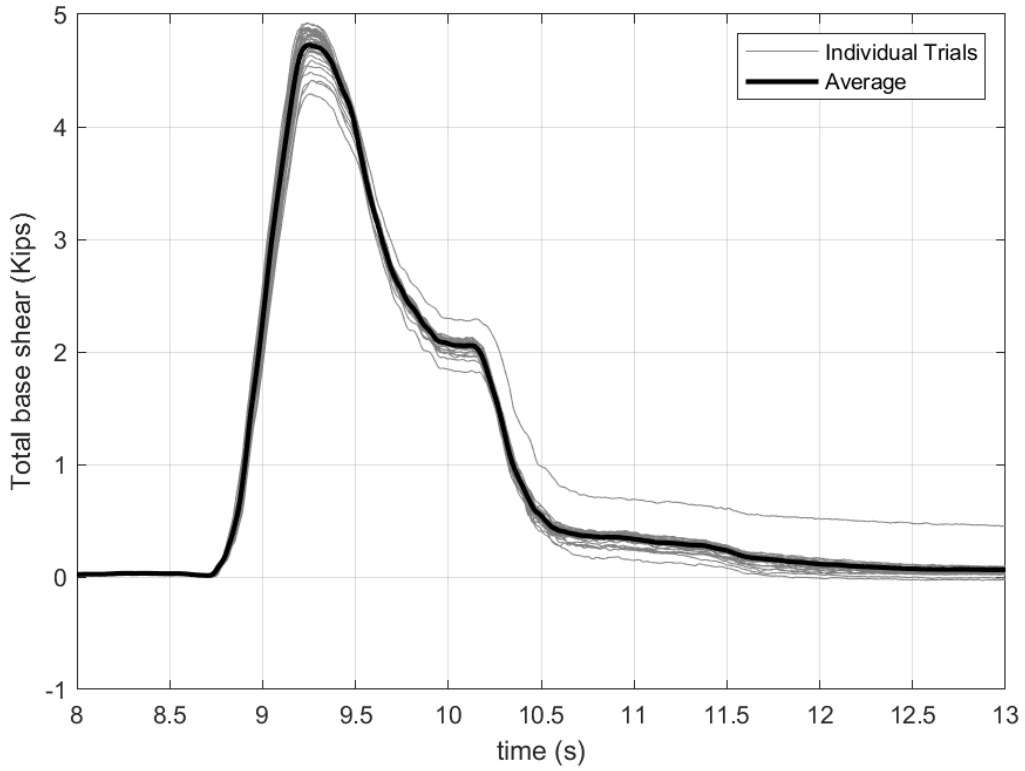

Figure 5-39: Combined Pile Shear Time History (1.4m Wave, Empty)

Table 5-25: Statistics for Pile Shear Values (1.4m Wave)

Pile Location	Shear (kips)		
	Max	Standard Deviation	COV
A1	1.20	0.18	15.1%
A2	1.12	0.21	18.6%
B1	1.42	0.20	14.2%
B2	1.03	0.20	19.5%
Combined	4.77	0.16	3.3%

5.5.3.3 Load Cell Measurements

Loads on the structure were measured in the stream-wise, transverse, vertical load cells over all 37 trials for the experiment. A diagram of the load cell configuration can be found in Figure 4-12. For all load cell plots the sign convention is positive when the load cell is in compression.

Load Cells SA and SB measured the stream-wise horizontal reactions at the base of the structure. A time history for the total force is shown in Figure 5-40. Statistics for the individual load cells as well as when they are combined in provided in Table 5-26. The stream-wise load cells provided

good repeatability as evidenced by their coefficients of variation both being below 5%.The maximum force from the load cell measurements was within 200lbf of the total stream-wise force as measured by the strain gauges.

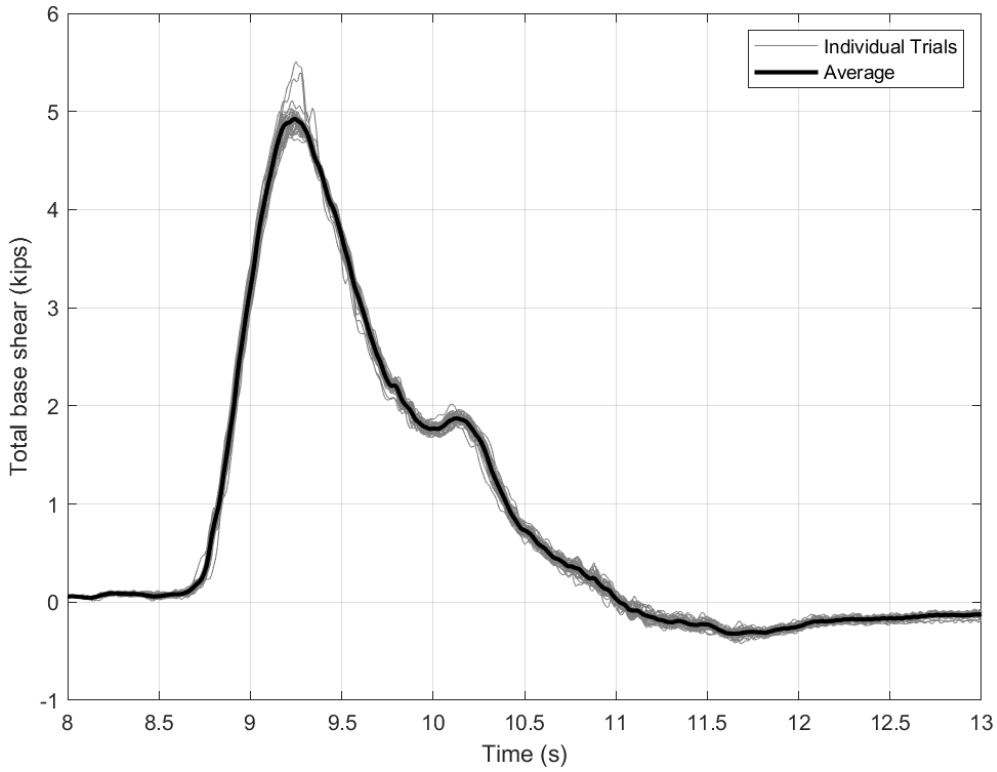

Figure 5-40: Stream-wise Load Cell Time History (1.4m Wave, Empty)

Table 5-26: Statistics for Stream-wise Load Cells (1.4m Wave, Empty)

Soil Condition	Load Cell	1.4m Wave			
		No. of Trials	Average Max (lbf)	Standard Deviation (lbf)	COV
Empty	SA+SB	37	4,926	141	2.8%
	SA	37	2,059	61	2.9%
	SB	37	2,867	84	2.9%

Vertical forces on the structure were measured using the four vertical load cells. A time history for each of these load cells is provided in Figure 5-41 and maximum values and statistics for the load cells are provided in Table 5-27. Similar to the previous experiments the front load cells (VA1 and VB1) do not go into tension due to the weight of the wave acting on the test setup. The back load cells provide very reliable data with coefficients of variation below 5%. The front load cells have

much higher coefficients of variation, however from looking at the individual trials again it seems like this is due to the low mean value for the load cells rather than the wave not being repeatable.

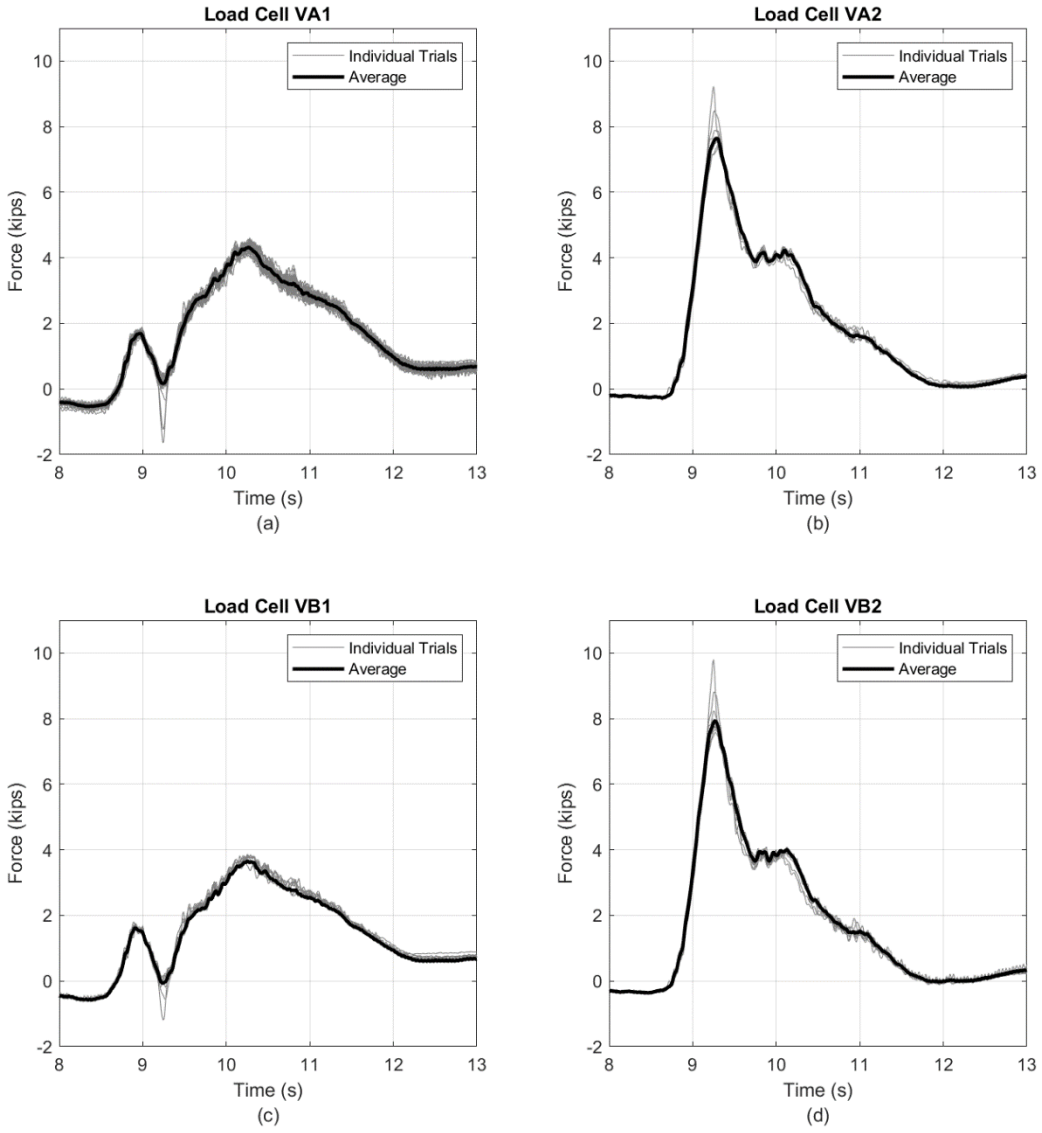

Figure 5-41: Bottom Load Cell Time Histories (1.4m Wave, Empty)

Table 5-27: Bottom Load Cell Statistics (1.4m Wave, Empty)

Soil Condition	Load Cell	1.4m Wave			
		No. of Trials	Average Max (lbf)	Standard Deviation (lbf)	COV
Empty	VA1	37	371	176	48%
	VB1	37	55.9	159	285%
	VA2	37	7,640	228	3%
	VB2	37	7,932	215	3%

Transverse forces were measured with load cells T1 and T2. A plot of the sum of the forces in these load cells is given in Figure 5-42 and mean values and statistics are provided in Table 5-28. Similar to the 1.4m wave half full experiment this experiment showed much better repeatability in the transverse load cell than the 1.4m wave full soil box experiment. Again the thin grey lines representing individual trials appear to follow the trend of the average line much better than they did for the 1.4m wave full soil box experiment. Coefficients of variation for this experiment were also around the same values as in the 1.4m wave half full soil box experiment. This shows that the test specimen was able to move slightly during the first experiment, however by the second and third experiments it seems to be in a stable condition and provide repeatable data.

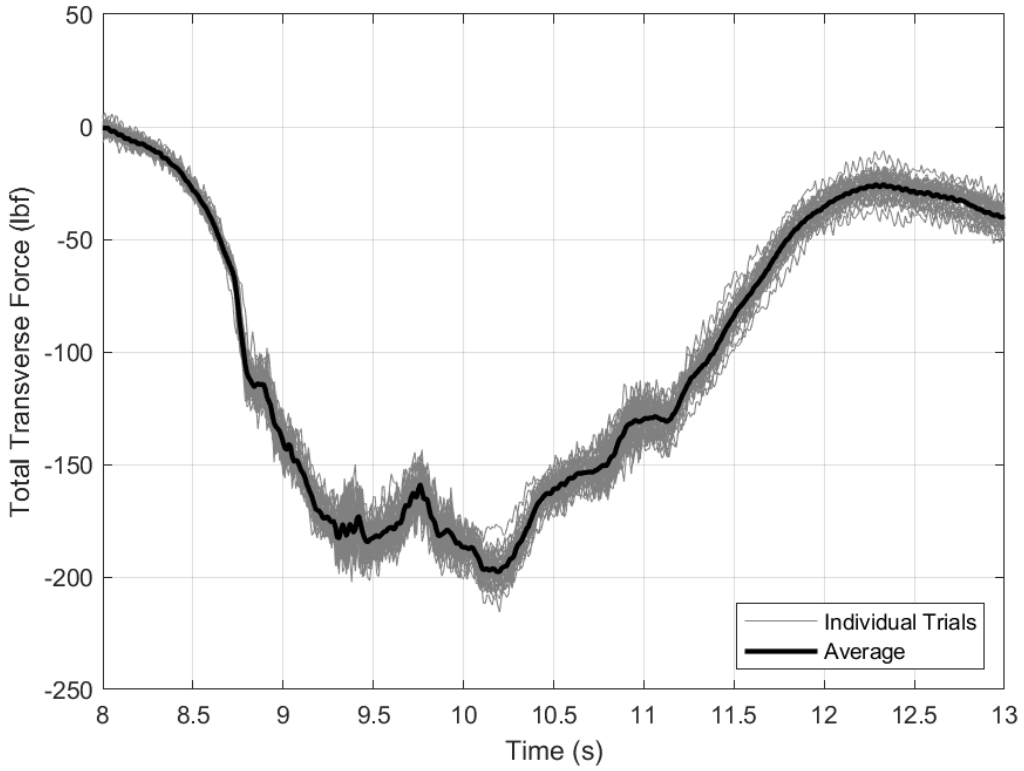

Figure 5-42: Transverse Load Cell Time History (1.4m Wave, Empty)

Table 5-28: Transverse Load Cell Statistics (1.4m Wave, Empty)

Soil Condition	Load Cell	1.4m Wave			
		No. of Trials	Average Max (lbf)	Standard Deviation (lbf)	COV
Empty	TA+TB	37	-198	7.2	-3.7%
	TB	37	-55	6.2	-11.3%
	TA	37	-143	5.5	-3.9%

5.5.4 *1.45m wave, Empty Soil Box*

The 1.45m wave, empty soil box experiment was the last experiment conducted. It consisted of running five trials for four different pressure sensor layouts. This was done to save time and validated by the repeatability of the waves demonstrated by the previous experiments.

5.5.4.1 Pressure Measurements

Pressures were measured across the front face of the specimen to characterize the pressure surface and use it to integrate the pressures to find the total force being put into the system. Figure 5-43 provides a pressure time history for the 1.45m wave at the same locations presented for the 1.4m wave experiments. Table 5-29 provides statistics for the average maximum pressure at each sensor location. The COV for the max pressures was much higher towards the top of the wall for the broken wave due to the turbulent nature of the bore as it interacts with the structure. While the lower sensors provide similar COV values to the 1.4m wave, however with slightly more variation. Overall the lowest row of sensors provided good repeatability while the middle and upper sensors showed more variation. On average pressures were slightly higher for this experiment than the 1.4m wave experiments conducted.

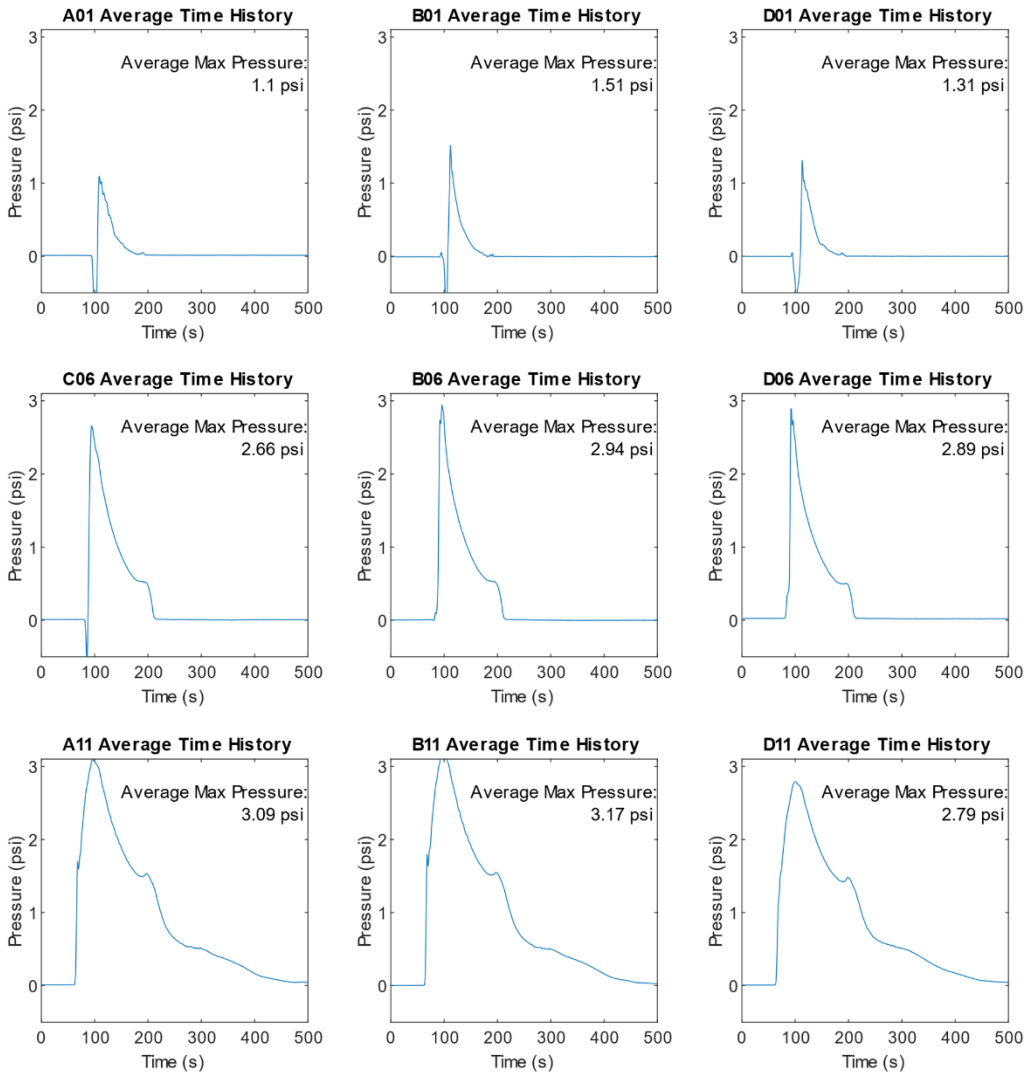

Figure 5-43: Average Pressure Time Histories at Selected Sensors (1.45m Wave, Empty)

Table 5-29: Pressure Sensor Statistics at Selected Sensors (1.45m Wave, Empty)

Sensor Name	Average Max Pressure (psi)	Coefficient of Variation	No. of Trials
A01	1.096	58%	5
B01	1.515	54%	5
D01	1.312	75%	5
C06	2.659	25%	10
B06	2.941	5%	5
D06	2.893	11%	5
A11	3.094	4%	10
B11	3.175	4%	20
D11	2.791	4%	5

After examining pressures at individual sensor locations the different pressure layouts were combined and integrated to find the total force acting on the wall from the wave. The average

pressure at each gauge location was used to evaluate the force on the test specimen. Figure 5-44 provides a time history of the force from the pressures as well as the average maximum force on the wall.

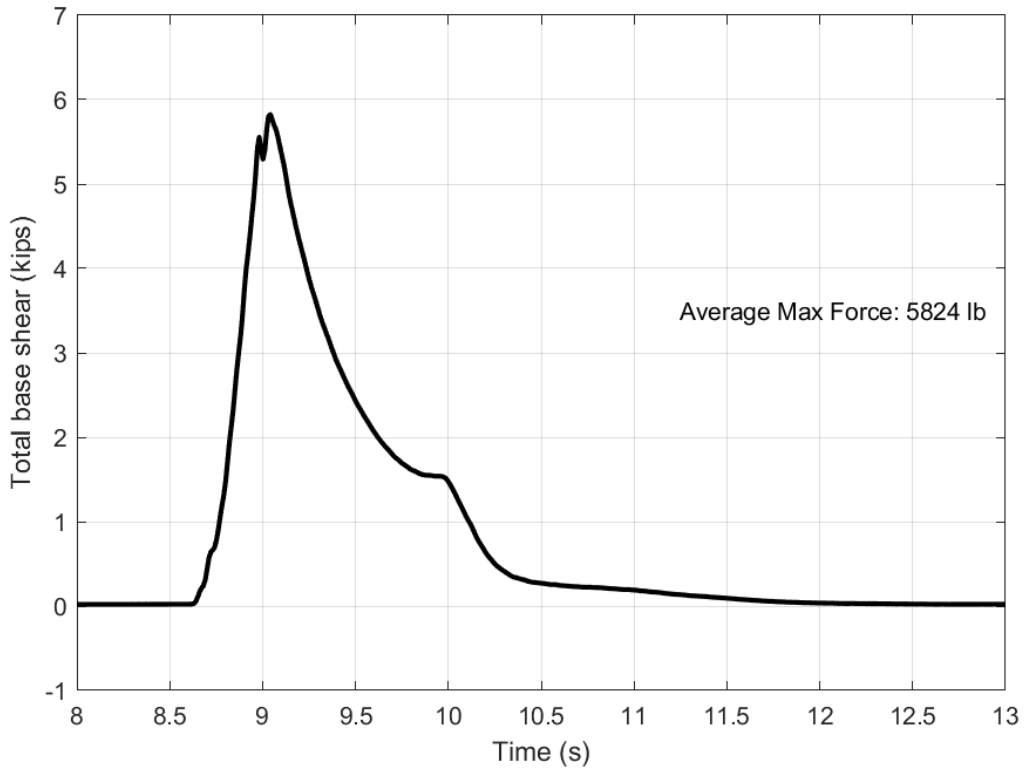

Figure 5-44: Force Time History from Pressures (1.45m Wave)

5.5.4.2 Strain Gauge Measurements

A time history of axial forces in each pile at the top and bottom strain gauge locations are provided in Figure 5-45 and Figure 5-46 respectively. The maximum force, standard deviation and coefficient of variation for each gauge location in each pile can be found in Table 5-30, as well as the sum of the axial forces in at the top and bottom of the piles. Negative values in this table indicate compression in the section.

For this experiment the strain gauges provided less consistent data with coefficients of variation higher than those found in the 1.4m wave experiments, only column B2 at the top gauge location had a coefficient of variation below 5% for the maximum axial force. The total axial force acting on the specimen is also higher for this experiment then the previous experiments examined, with around 3 kips of force at the top gauges and 1 kip of force at the bottom gauges. Furthermore the

axial force is still changing between the top and the bottom of the piles as was observed during all of the 1.4m wave experiments.

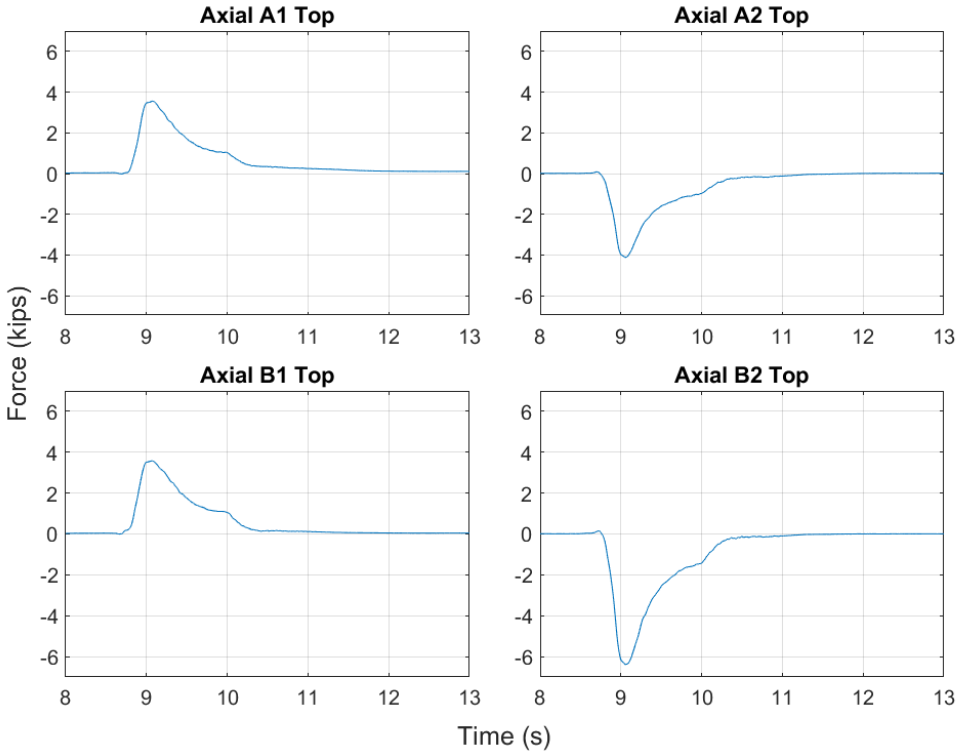

Figure 5-45: Time History for Axial Force at Top Gauge Locations (1.45m Wave)

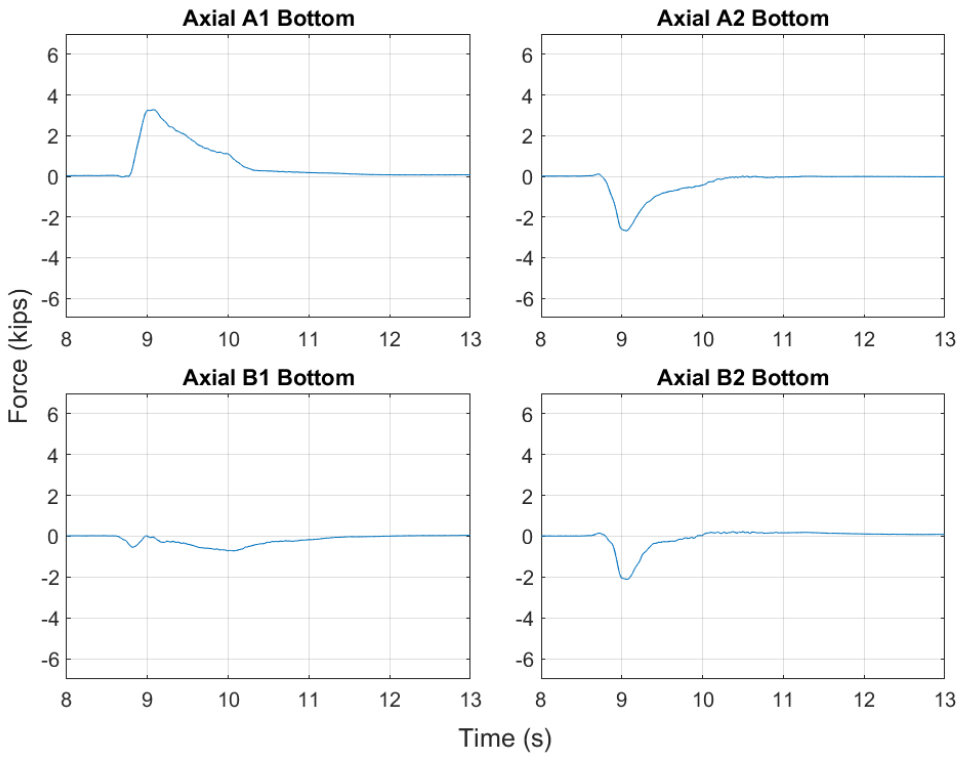

Figure 5-46: Time History for Axial Force at Bottom Gauge Locations (1.45m Wave)

Table 5-30: Statistics for Axial Force at Gauge Locations on Individual Piles (1.45m Wave)

Gauge Location	Pile Location	Axial Force (kips)		
		Max	Standard Deviation	COV
Top	A1	3.56	0.30	8.5%
	B1	3.58	0.29	8.1%
	A2	-4.12	0.28	6.8%
	B2	-6.38	0.28	4.4%
	sum	-3.36		
Bottom	A1	3.28	0.29	8.9%
	B1	0.13	0.03	19.9%
	A2	-2.68	0.28	10.5%
	B2	-2.11	0.28	13.3%
	sum	-1.38		

A time history of the moment at each gauge location at the top and bottom of each pile are presented in Figure 5-47 and Figure 5-48 respectively. Maximum values and statistics for these plots can be found in Table 5-31. For this experiment the coefficients of variation for the maximum moment were higher than those found for the 1.4m wave experiments. For this experiment only

five of the eight gauge locations had a coefficient of variation less than 5%, unlike the 1.4m tests where the values were all below 5% at each location for each of the experiments. The total moment at the top and bottom of the piles is also greater. The shape of the time histories is consistent with the previous experiments.

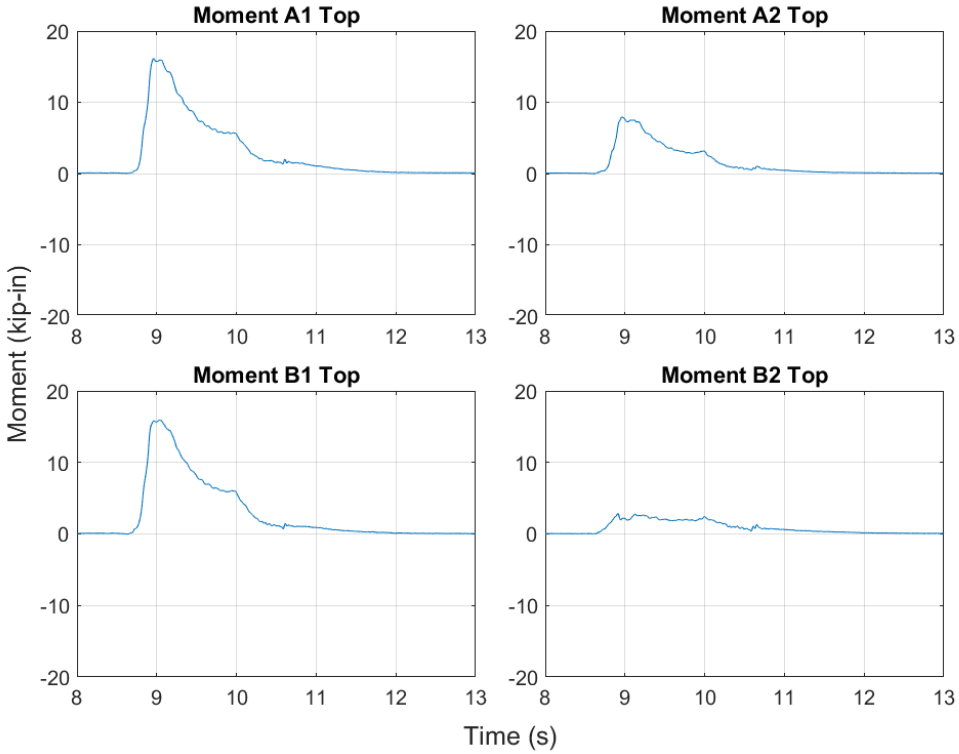

Figure 5-47: Time History for Moment at Top Gauge Locations (1.45m Wave)

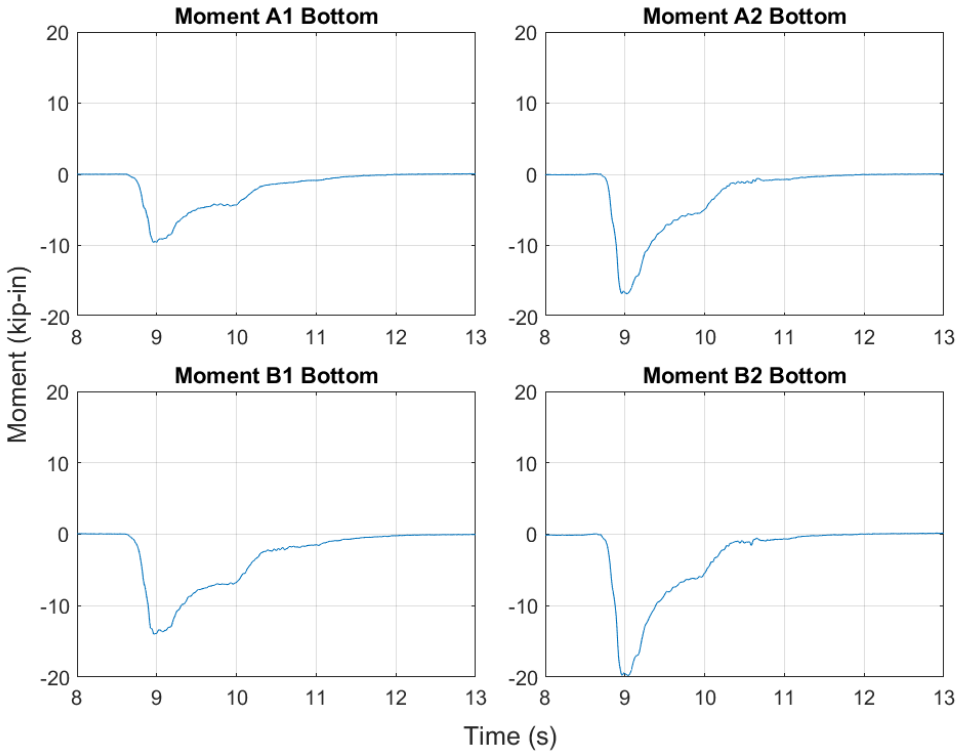

Figure 5-48: Time History for Moment at Bottom Gauge Locations (1.45m Wave)

Table 5-31: Statistics for Moments at Gauge Locations on Individual Piles (1.45m Wave)

Gauge Location	Pile Location	Moment (k-in)		
		Max	Standard Deviation	COV
Top	A1	16.2	0.642	4.0%
	B1	15.9	0.345	2.2%
	A2	7.9	0.642	8.1%
	B2	2.9	0.607	21.1%
	sum	43.0		
Bottom	A1	-9.6	0.642	6.7%
	B1	-14.0	0.620	4.4%
	A2	-16.8	0.642	3.8%
	B2	-19.8	0.345	1.7%
	sum	-60.1		

A time history of shear in the individual piles is presented in Figure 5-49 and a time history of the total base shear on the structure is provided in Figure 5-50. The maximum values and statistics for shear in the individual piles as well as on the entire structure are provided in Table 5-32. Similar to shear measurements for the other experiments, the shear in the piles showed lower repeatability

than the moment and axial measurements as evidenced by higher coefficients of variation for the shear values. For this experiment the total shear force on the structure was 1,000lb higher than the 1.4m experiments. The variation of the maximum shear force for this experiment was also higher than the variation in the 1.4m wave experiments. This is likely due to the turbulent nature of the 1.45m wave which was a broken bore when it hit the structure and inherently less repeatable.

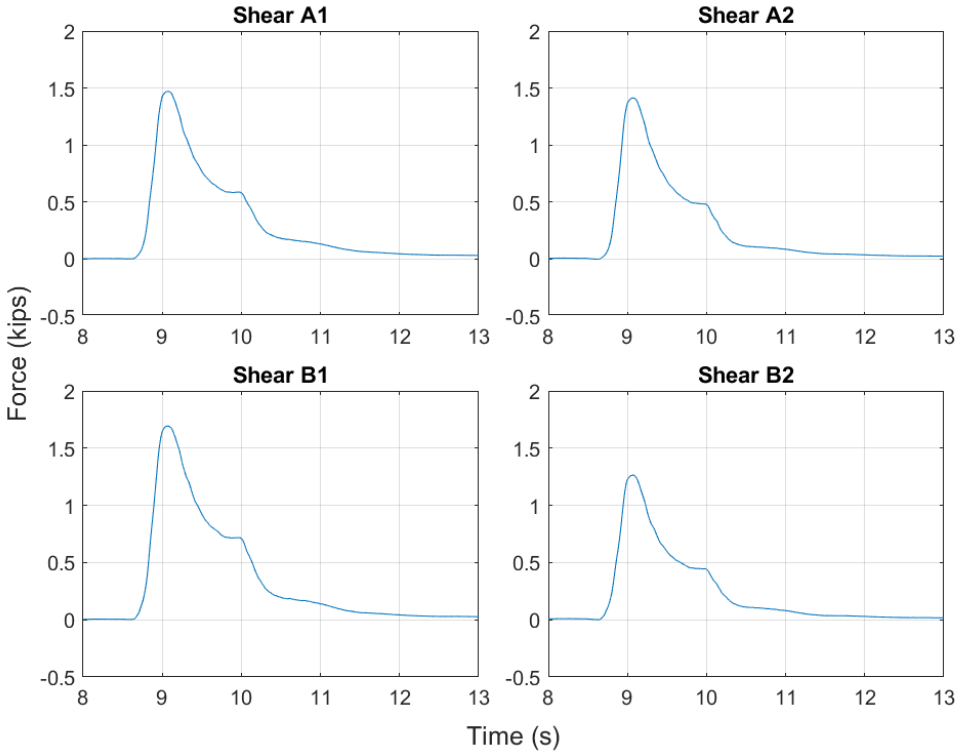

Figure 5-49: Time History for Shear in Individual Piles (1.45m Wave)

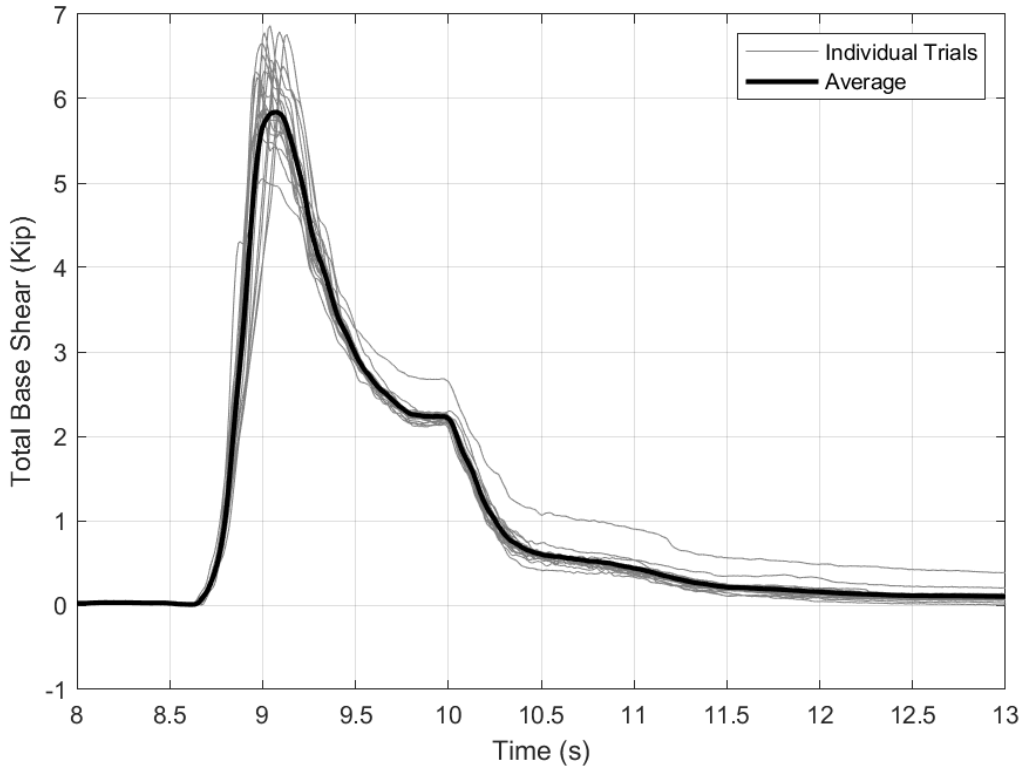

Figure 5-50: Combined Pile Shear Time History (1.45m Wave)

Table 5-32: Statistics for Pile Shear Measurements (1.45m Wave)

Pile Location	Shear (kips)		
	Max	Standard Deviation	COV
A1	1.47	0.30	20.7%
A2	1.41	0.29	20.6%
B1	1.69	0.29	17.2%
B2	1.26	0.29	23.0%
Combined	5.84	0.41	7.1%

5.5.4.3 Load Cell Measurements

The 1.45m wave produced a total stream-wise force that was about 600lb greater than that of the 1.4m wave on average. The wave did have more variability resulting in a higher coefficient of variation.

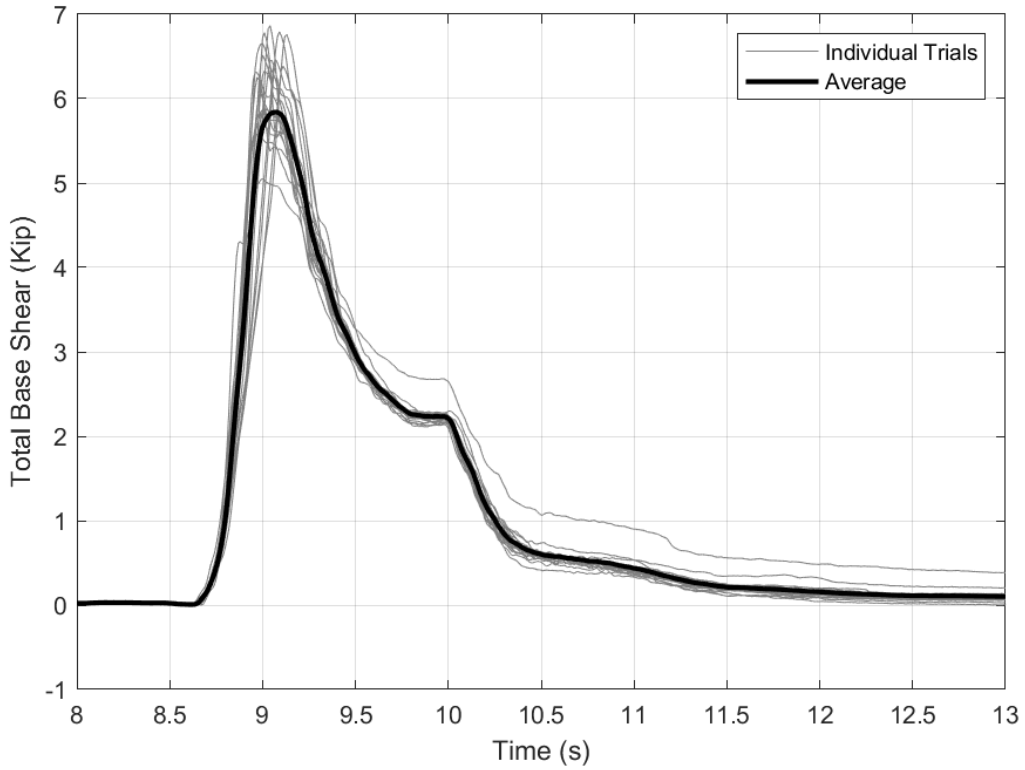

Figure 5-51: Stream-wise Load Cell Time History (1.45m Wave, Empty)

Table 5-33: Stream-wise Load Cell Statistics (Broken Wave)

Load Cell	No. of Trials	Average Force (lbf)	Standard Deviation (lbf)	COV
SA	20	2094	0.27	4.5%
SB	20	2874	0.27	4.5%
Combined	20	5580	0.27	4.5%

A time history of the force in the four vertical load cells for this experiment are presented in Figure 5-52 and maximum values and statistics are provided in Table 5-34. Similar to the stream-wise load cells the vertical load cells also saw greater load from the 1.45m wave experiment then the previous experiments examined. The coefficient of variation for the max forces was higher for load cells VA1 and VB1 similar to the previous experiments, however from looking at the time histories it seems like the variation in the front and back load cells should be about the same. For this experiment, unlike the previous experiments examined the front load cells (VA1 and VB1) do go about 1,000lb into tension.

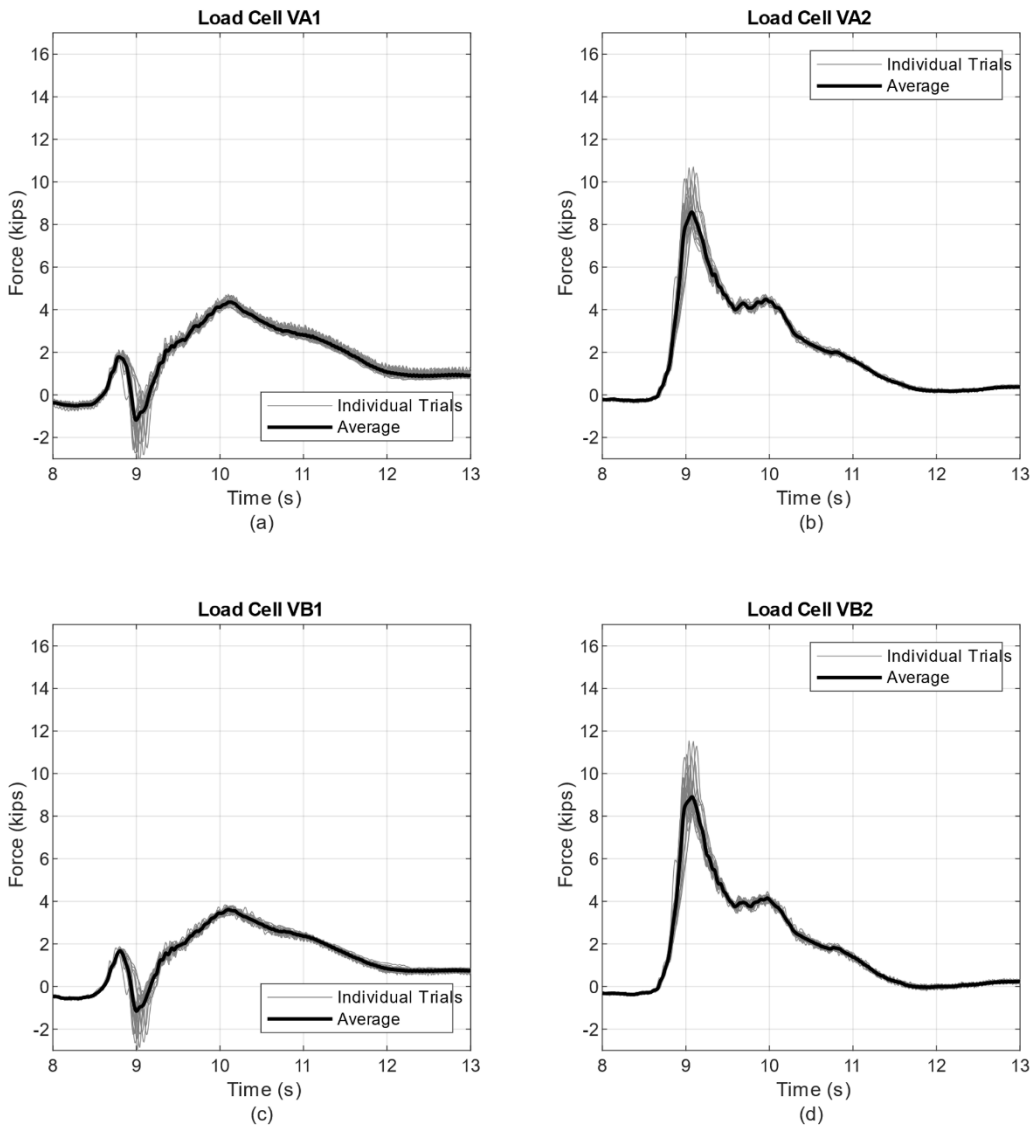

Figure 5-52: Bottom Load Cell Time History (1.45m Wave, Empty)

Table 5-34: Bottom Load Cell Statistics (1.45m Wave, Empty)

Load Cell	No. of Trials	Average Max (lbf)	Standard Deviation (lbf)	COV
VA1	20	-807	564	-25.3%
VB1	20	-927	502	-24.2%
VA2	20	8586	799	8.5%
VB2	20	8903	894	8.9%

A plot of the sum of the forces in the transverse load cells is given in Figure 5-53 and mean values and statistics for both load cells and the sum of the load cells are provided in Table 5-35. Similar to the last two 1.4m wave experiments the individual trials do a better job of following the average line than the 1.4m full soil box experiment.

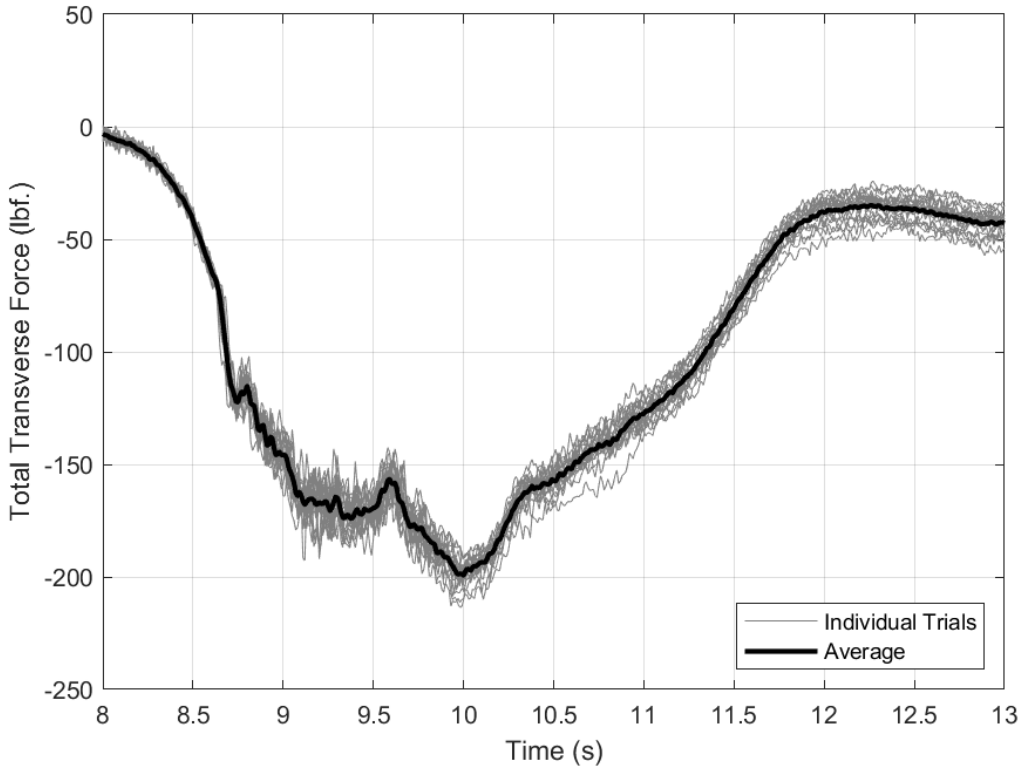

Figure 5-53: Transverse Load Cell Time History (1.45m Wave, Empty)

Table 5-35: Transverse Load Cell Statistics (1.45m Wave, Empty)

Load Cell	No. of Trials	Average Max Force (lbf)	Standard Deviation (lbf)	COV
TB	20	-62.2	12.8	-16.2%
TA	20	-152.2	8.47	-5.1%
Combined	20	-199.3	5.56	-2.7%

Chapter 6. EVALUATION OF EXPERIMENTAL RESULTS

This chapter makes comparisons among the different experiments conducted as well as simulated values from OpenFOAM and code equations. First, the results from the different methods of measuring force were compared to determine the impact of the two study parameters: soil height and wave height. Next, the measured responses were compared to OpenFOAM simulations. Finally, the experimental results were compared with provisions in ASCE 7-16.

6.1 Comparison of Experimental Force Measurements

This section describes comparisons between different methods of measuring force to evaluate the impact of the study parameters. First comparisons are made between load measurements for the 1.4m wave experiments with different soil heights to determine if the soil is resisting the load. Comparisons are then made between the load measurements from the 1.4m wave experiments and the 1.45m wave experiment to determine the change in force from the different wave heights and wave types.

6.1.1 *Comparisons for Different Soil Levels*

The 1.4m wave tests evaluated the impact of soil level. This section compares different force measurement results for the three 1.4m wave experiments to investigate the impact of the soil on the pile forces and base shear. Integrated pressure forces, strain gauge data and load cell data are presented. Forces from integrated pressures and load cells provide a base line for the experimental variation. The total shear from the strain gauges is then examined to determine if the soil is resisting the shear on the piles, by comparing the change in force to the typical experimental variation.

Centerline pressure distributions and total force from the integrated pressure sensors were examined across the three experiments for the 1.4m wave to confirm that the force being input into the system was nominally identical for of the 1.4m wave experiments. Figure 6-1 illustrates the centerline pressure distributions averaged across all trials for the 1.4m wave experiments at the instance of the maximum force. The average pressure distributions are similar in both shape and average values.

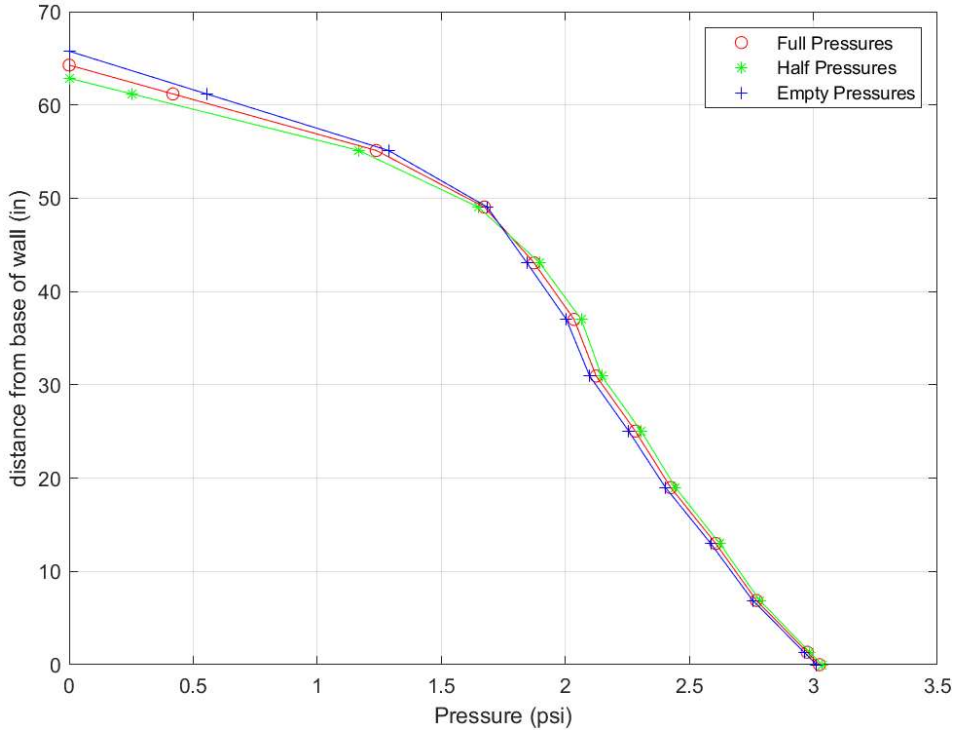

Figure 6-1: Centerline Pressure Distributions for 1.4m Wave Experiments

Table 6-1 presents results for the force from integrating the pressure sensors for the three different soil conditions, the soil box full, half full and empty. These measurements are expected to be the same since only the amount of soil was varied. The maximum difference between force measurements is about 200 lbf or 3.2% of the total force measured.

Table 6-1: Force from Integrated Pressures for Different Soil Conditions

Soil Condition	Force from Integrated Pressures (lbf)	$Force/Force_{Full}$
Full	5366	(reference)
Half	5194	0.97
Empty	5273	0.98

Moments at the base of the structure were examined however the results were not meaningful. Because the weight of the wave acts upon the test setup to get the overturning moment at the base it would be necessary to find how much of the weight is acting on each of the vertical load cells and then subtract it out to obtain the total vertical forces acting on the base from the horizontal force of the wave.

Table 6-2 presents average force across all trials for a given experiment as recorded by the load cells from the three experiments conducted using the 1.4m wave, at the instance of maximum stream-wise force. Negative values indicate the load cell is in tension. It can be observed that the stream wise load cells yield results that are within 3% of each other across experiments. Vertical load cells also give results that are within 3% of each other across experiments. Total vertical loads from the load cells here are positive in compression, indicating the weight of the wave acting over the soil box. Consistent results suggest that the same amount of water was present on top of the soil box in each experiment. The transverse load cells also show good agreement with a maximum difference of only 3lbf between experiments. The total stream-wise load from the integrated pressure sensors was slightly greater than the reactions measured using the load cells. The forces measured from the load cells and integrated pressures are within about 300 lbf of each other, a difference of about 6%, which is similar to the experimental error discussed in Section 4.3. From the load cell results it can be inferred that if the strain gauges provide maximum shear values within 3% of each other that there is essentially no difference in the measured shear. Moments at the base of the structure were examined however the results were not meaningful. Because the weight of the wave acts upon the test setup to get the overturning moment at the base it would be necessary to find how much of the weight is acting on each of the vertical load cells and then subtract it out to obtain the total vertical forces acting on the base from the horizontal force of the wave.

Table 6-2: Load Cell Measurements at Maximum Stream-wise Force for Different Soil Conditions, 1.4m Wave

Soil Condition	Direction of Reaction	Total Force (lbf)	$Force/Force_{Full}$
Full	Stream-wise	5,058	(reference)
	Transverse	-170	
	Vertical	15,664	
Half	Stream-wise	4,948	0.98
	Transverse	-169	0.99
	Vertical	15,841	1.01
Empty	Stream-wise	4,926	0.97
	Transverse	-173	1.02
	Vertical	15,999	1.02

Torsions on the test specimen were calculated by summing moments about the center of the test specimen. It was assumed that the stream-wise force of the wave acts at the center of the wall and was neglected from these calculations. Table 6-3 presents the torsion on the setup as well as the load cell values at the instance of maximum stream-wise force. Negative values indicate the load cell is in tension. The following equation was used to compute the torsion:

$$T = (SA + TB) * 20in - (SB + TA) * 20in$$

Where:

SA, SB, TA and TB are the measured load in load cells SA, SB, TA, and TB, at the instance of maximum stream-wise force, and 20 in. is the distance from each of the load cells to the center of the test setup as shown in Figure 6-2.

The total torsion on the test specimen increases with each test. This could indicate that the specimen moved slightly from one experiment to the next. The torsion values for the last two experiments however, is very similar indicating that this movement could have occurred during the first experiment before the structure found a stable orientation.

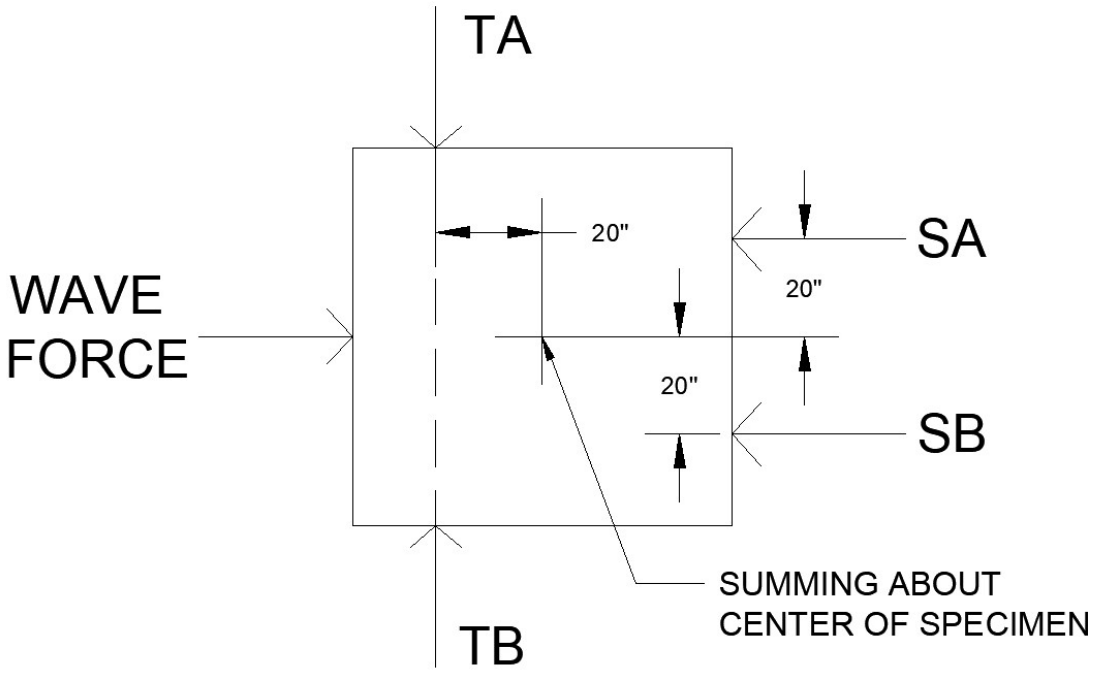

Figure 6-2: Dimensions and Locations of Forces Used for Torsion Calculations

Table 6-3: Torsion on Test Specimen for 1.4m Wave Experiments

Load Cell	Experiment		
	1.4m wave Full	1.4m wave Half	1.4m wave Empty
TA (lbf)	-111	-134	-141
TB (lbf)	-59	-35	-33
SA (lbf)	2158	2074	2058
SB (lbf)	2895	2869	2867
Total Torsion (lbf-ft)	-1315	-1490	-1528
$Torsion/Torsion_{Empty}$	0.86	0.98	reference

Table 6-4 presents the shear, moment and axial forces determined from the strain gage measurements. (Section 4.2.4 provides a description of how these forces were determined.) The difference in total base shear measured during the full soil box experiment to the empty soil box experiment was less than 2%; this likely indicates that the soil was not resisting the shear force. The total shear forces in the piles were lower than the forces measured by the load cells or integrated from pressure measurements; this trend was found for all soil conditions.

The moment in the top of the piles is within 5% of the full condition for all experiments indicating that similar loading is being applied in each experiment. Axial force shows the greatest change between experiments, however as seen in Chapter 5 the total axial load in the piles is unreliable due to the total axial force changing between the top and bottom of the piles.

Table 6-4: Top Strain Gauge Measurements for Different Soil Conditions, 1.4m Wave

Soil Condition	Reaction	Total Force (lbf)	$Force/Force_{Full}$
Full	Shear (lbf)	4,714	(reference)
	Axial (lbf)	-1,149	
	Moment (lbf-ft)	3,115	
Half	Shear (lbf)	4,522	0.96
	Axial (lbf)	-1,621	1.41
	Moment (lbf-ft)	2,976	0.96
Empty	Shear (lbf)	4,769	1.01
	Axial (lbf)	-1,643	1.43
	Moment (lbf-ft)	3,084	0.99

Table 6-5 shows a comparison of the stream-wise forces for the different experiments for the 1.4m wave. Forces from the integrated pressures are the demands; forces measured using the strain gauges and load cells are the total reactions. Due to experimental uncertainties, a range of values +/- one standard deviation from the mean was also examined and is shown in Table 6-6. Forces from integrating the pressure sensors were consistently higher than the other methods of measuring force. This could be due to inaccuracies in the integration technique. It could also be some of the force being imparted on the system by the wave being lost in the system as was seen by the load cells during the setup validation testing described in Section 4.3.

Forces determined from the strain gauges measurements recorded the lowest total stream-wise force. Forces measured from the integrated pressures were consistently the highest force measured. When examining the range of forces +/- one Standard deviation it can be seen that the high end of the range for the strain gauges and load cells is typically close to the low end of the range for the integrated pressured. This suggests that some of the force being put into the system is not being captured by the stream-wise load cells or strain gauges. Force in the load cells is expected to be about 5% lower than force from the pressures as demonstrated in the validation testing done on the setup detailed in Section 4.3. The strain gauges could be measuring lower force if they were not placed on the extreme fibers of the section, resulting in a lower strain distribution in the section. Another factor that could result in lower strain values is the placement of the strain gauges about 1.5 inches below angles welded to the piles to allow for the connection of braces to the piles during transportation. These angles would stiffen the piles locally and change the distribution of strains across the section. Because the gauges were placed relatively close to these angles the strains may not have redistributed evenly by the time they were measured at the gauges, invalidating the assumption that strains varied linearly between the gauges applied on the extreme fibers of the section.

Table 6-5: Stream-wise Forces from Different Instruments for 1.4m Wave Experiments

Soil Condition	Stream-wise force from: (lbf)			Standard Deviation: (lbf)		
	Pressures	Strain Gauges	Load Cells	Pressures	Strain Gauges	Load Cells
Full	5366	4,714	5,058	252	431	102
Half	5194	4,522	4,948	733	271	156
Empty	5273	4,769	4,926	251	157	141

Table 6-6: Range of Maximum Instantaneous Force Values +/- One Standard Deviation from Different Instruments for 1.4m Wave Experiments

Soil Condition	Range of Values (+/-1 standard deviation)		
	Pressures	Strain Gauges	Load Cells
Full	5,618-5,114	5,145-4,283	5,160-4,956
Half	5,927-4,461	4,792-4,251	5,104-4,792
Empty	5,524-5,022	4,927-4,612	5,076-4,785

6.1.2 *Force Comparisons for Different Wave Heights*

The tests using different wave heights were investigated. Pressure distributions, total forces and the centroids of the force were compared. The two waves were fundamentally different in how they struck the structure. The 1.4m wave held its shape and did not break before striking the structure. The 1.45m wave broke upstream of the structure and impacted the test specimen as a broken bore.

The total force determined from integrating the pressures for different wave heights are presented in Table 6-7. Force from the 1.4m wave was averaged across all experiments. The total force from the 1.45m wave is approximately 7% higher than the force from the 1.4m wave.

Table 6-7: Force from Integrated Pressures for Different Wave Heights

Wave height (m)	Max Force (kips)	$Force/Force_{1.4m}$
1.4	5.28	(reference)
1.45	5.66	107%

Centerline pressure distributions at the instance of maximum force are presented in Table 6-1. Due to similarities in pressures for the 1.4m wave experiments, shown in Figure 6-1, the distribution for the 1.4m wave consisted of averaging the pressures recorded from the three different 1.4m wave experiments. The 1.45m wave resulted in slightly larger pressures on the front face of the wall than the 1.4m wave. The 1.45m distribution also has a much sharper drop in pressures towards the top of the wall.

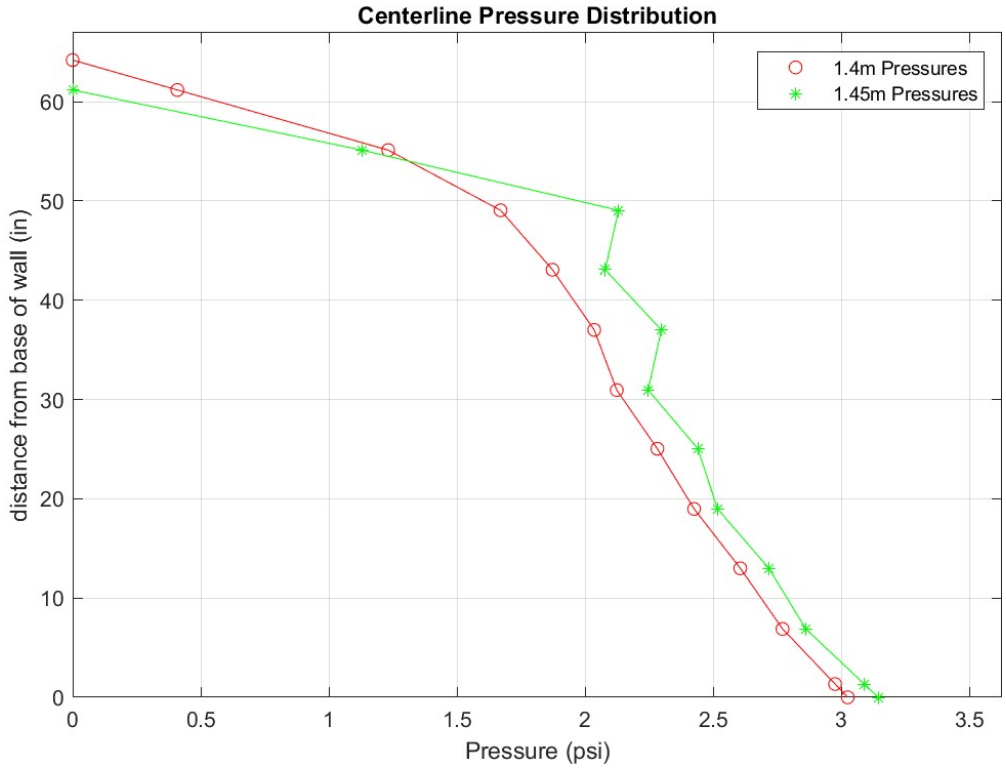

Figure 6-3: Centerline Pressure Distributions for Different Wave Heights

The computed values of the force centroid of the centerline pressure distributions is presented in Table 6-8; centroid values are given as the distance from the bottom of the wall above the cover plate for the soil to the centroid of force from the wave. Centroids were determined from both the pressure distribution on the front face of the wall as well as by summing the moments about the piles in column line 2 from the strain gauge measurements. The centroid height was determined using the following equation:

$$x = ((A_1 + B_1) * 40in + M_{tot})/V_{tot} - 14in$$

Where:

$x = Distance\ from\ the\ base\ of\ the\ wall\ to\ the\ centroid\ of\ force$

$A_1 = Axial\ force\ in\ pile\ A1$

$B_1 = Axial\ force\ in\ pile\ B1$

$M_{tot} = sum\ of\ the\ moments\ being\ resisted\ by\ each\ pile$

$V_{tot} = sum\ of\ the\ shear\ forces\ being\ resisted\ by\ each\ pile$

40 inches is the center to center distance between piles, and 14 inches is the distance from the gauge location to the bottom of the wall.

The centroid location for the 1.45m wave is slightly lower than the centroid location for the 1.4m wave, likely due to the steep drop off at the top of the pressure distribution as shown above. Centroid locations determined from the moments measured in the piles were consistently higher than from the pressure sensors, but were deemed less reliable as described in Chapter 5.

Table 6-8: Centroid Locations for Different Experiments

Wave Height	Soil Condition	Centroids from Integration	Centroids from Moments	Integration/Moments
		(in)	(in)	
1.4m	All	25.9	34.9	0.74
	Full	25.9	36.8	0.70
	Half	25.6	34.6	0.74
	Empty	26.3	33.4	0.79
1.45m	Empty	25.8	27.5	0.94

Loads measured by the load cells were compared in the stream-wise, transverse and vertical directions and are presented in Table 6-9. Loads from the 1.4m wave were averaged across the three experiments for this wave height. Transverse and vertical loads on the specimen are similar for both wave heights. The largest difference is in the stream-wise forces where there is a 12% increase in force from the 1.4m wave to the 1.45m wave. This is a greater increase than was seen from the integrated pressures. Both measurements however do agree that the 1.45m wave is putting more force into the system than the 1.4m wave.

Table 6-9: Load Cell Measurements for Different Wave Heights

Wave height (m)	Direction of Reaction	Total Force (lbf)	Force/Force$_{1.4m}$
1.4	Stream-wise	4,977	(reference)
	Transverse	-200	
	Vertical	15,835	
1.45	Stream-wise	5,580	1.12
	Transverse	-199	0.99
	Vertical	16,142	1.02

Loads measured by the strain gauges for the two different wave heights are presented in Table 6-10. Strain gauge measurements from the 1.4m wave were averaged across the three experiments for this wave height. Consistent with the results for the load cells and integrated pressures there is an increase in the stream-wise force as measured by the total shear in the piles. The total force in

the stream-wise direction as measured by the strain gauges is 25% higher for the 1.45m wave than the 1.4m wave.

This is likely due to the increased variability in the strain gauges as described in Chapter 5. The strain gauges also recorded an increase in the total moment in the piles. The increase in moment was a similar magnitude to the increase in shear force. This is consistent with the increased stream-wise force in the load cells, if more force is acting on the test specimen it will take a larger moment to resist the forces from the wave.

Table 6-10: Strain Gauge Measurements for Different Wave Heights

Wave height (m)	Reaction	Total Force (lbf)	Force/Force$_{1.4m}$
1.4	Shear	4,668	(reference)
	Axial	-1,471	
	Moment	3,058	
1.45	Shear	5,840	1.25
	Axial	-3,358	2.28
	Moment	3,580	1.17

6.2 Comparison of Measured and Simulated Results

Computational fluid dynamic (CFD) analyses of the experiments were conducted using OpenFOAM, focusing on the different wave heights and types. The objectives of these analyses were to calibrate the modeling approach. Initially, CFD models were used to determine the bathymetry of the flume testing as described in Section 4.1.2. Following the testing, these models were improved, as the initial models had total forces that were approximately twice the measured force. The following describes: (1) the modeling procedure, and (2) the measured and simulated pressure distributions, wave height, particle wave velocities and total forces for the different waves. It is of note that OpenFOAM utilizes the specimen as a boundary condition and therefore only the wall is modeled as a solid rectangular prism. The program as utilized in this project is not capable of modeling differences in soil height and therefore this study parameter is not addressed. A model of the Large Wave Flume that was calibrated with previous test data (Gills 2018) was used. The flume bathymetry, still water depth and structure location were replicated in the simulation. The measured paddle displacement time history from the experiments was used to

create the waves simulated. Unlike the simulations to determine the ramp slope, where the test specimen should be placed and the anticipated force on the structure described in Chapter 4, this simulation used a more accurate mesh. The mesh technique ensured that no elements were inverted or skewed around the structure such that numerical derivatives and calculations contingent on the determinant of the Jacobian do not result in numerical singularities/sinks which would change the energy distribution through the model. The turbulence model for the simulation was also changed from a standard k-epsilon (KE) model to a k-omega-shear-stress-transport (k-omega-sst) model. The primary difference between the two turbulence models is that the KE model does a good job of characterizing the mean turbulence of a general region of flow using two partial differential equations, while the k-omega-sst uses a different partial differential equation to characterize the turbulent kinetic energy. This equation does a much better job of capturing the turbulent kinetic energy generation near the wall, resulting in a higher resolution of shear stresses and forces imparted upon objects within the flow. The two turbulence models give nearly the same results for the case of general flow far from boundary conditions however the k-omega-sst does a much better job near the boundaries. Pressures from this analysis were recorded by placing probes that recorded pressures at the same locations as the pressure sensors in the experiment. Forces from the analysis were then found by integrating those pressures using the same integration method described in Chapter 5 for the experiment.

6.2.1 *Wave Height*

Time histories of the wave height at the locations of the six wire-type wave gauges are shown in Figure 6-4. Simulated time histories are plotted in red and indicated with the prefix "OF-" in the legend. The wire resistance gauges provided the most repeatable test data and therefore are used here. The maximum wave height values for both the simulation and experiment are presented in Table 6-11. The shape of the time histories and the maximum height of the wave in the simulation are similar to the measured results.

For the 1.45m wave, the breaking action in the simulation happens before the breaking action in the experiment. This is demonstrated as follows: the first wave gauge location shows good agreement in the wave height however at the second wave gauge location; it appears that the simulated wave has broken as evidenced by the lower maximum wave height, while this decrease in wave height in the experiment does not occur until the third or fourth wave gauge location. The

maximum difference for the 1.4m wave was about 4% while the maximum difference for the 1.45m wave was approximately 6%. For both wave heights, the experiment recorded higher free surface elevations at every wave gauge location with the exception of WG6 for the broken wave. A larger difference was expected for the 1.45m wave because it was a broken wave which introduces more uncertainty in terms of its the propagation.

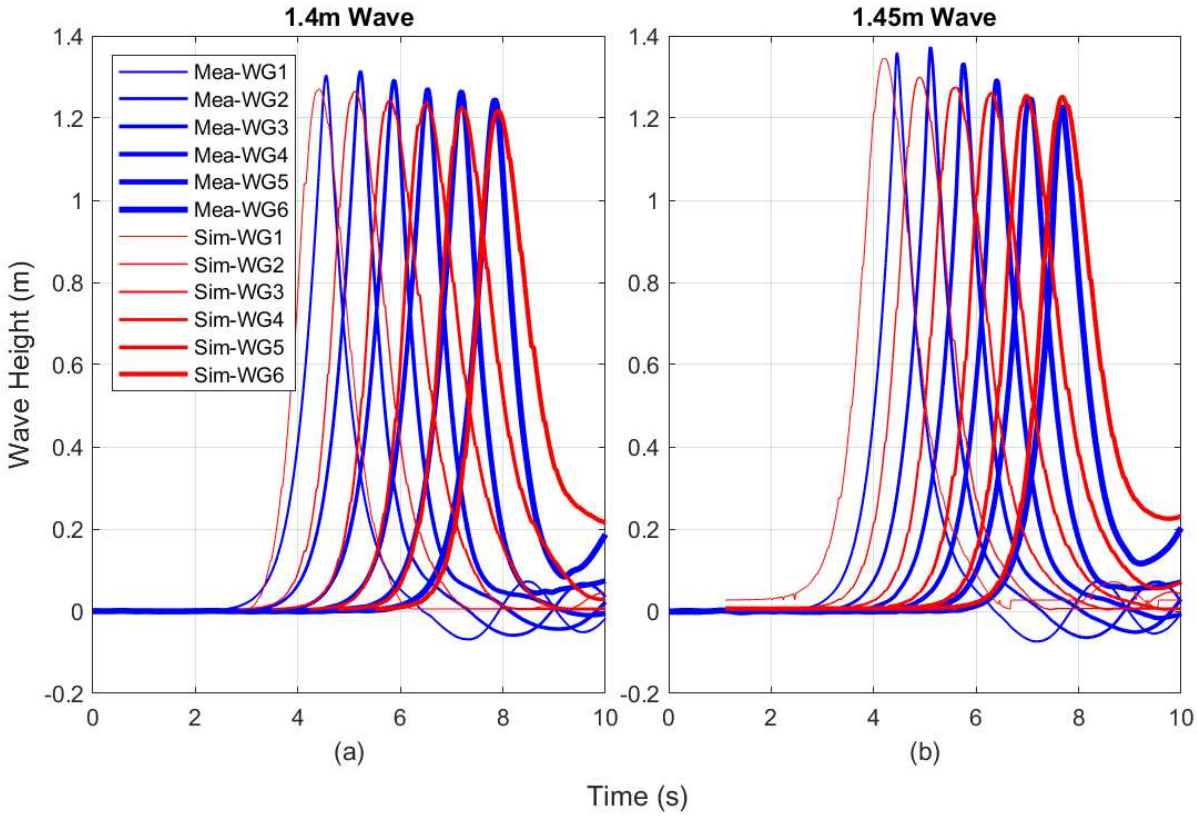

Figure 6-4: Wave Gauge Time History Comparison

Table 6-11: Comparison of Instantaneous Maximum Wave Height Values

Location	1.4m Wave Heights (ft)			1.45 m Wave Heights (ft)		
	Measured	Simulation	Measured/ Simulation	Measured	Simulation	Measured/ Simulation
wg1	4.29	4.17	1.03	4.48	4.42	1.01
wg2	4.32	4.15	1.04	4.53	4.26	1.06
wg3	4.25	4.08	1.04	4.42	4.18	1.06
wg4	4.18	4.06	1.03	4.29	4.14	1.04
wg5	4.16	4.02	1.03	4.15	4.12	1.01
wg6	4.09	3.99	1.02	4.08	4.11	0.99

6.2.2 *Water Particle Velocity*

The measured and simulated time histories of the water-particle velocity at the location of ADV1 are shown in Figure 6-5. The Instrument ADV 1 was selected for comparison because it had the most consistent results across trials (see low coefficient of variation for both waves in Tables 5-4 and 5-6). Table 6-12 provides the measured and simulated maximum instantaneous velocities. The shapes of the time histories are similar; the difference in maximum instantaneous velocities for both waves was less than 4%. Overall, the wave height and velocity measurements from the simulation agreed well with the measurements and were deemed accurate.

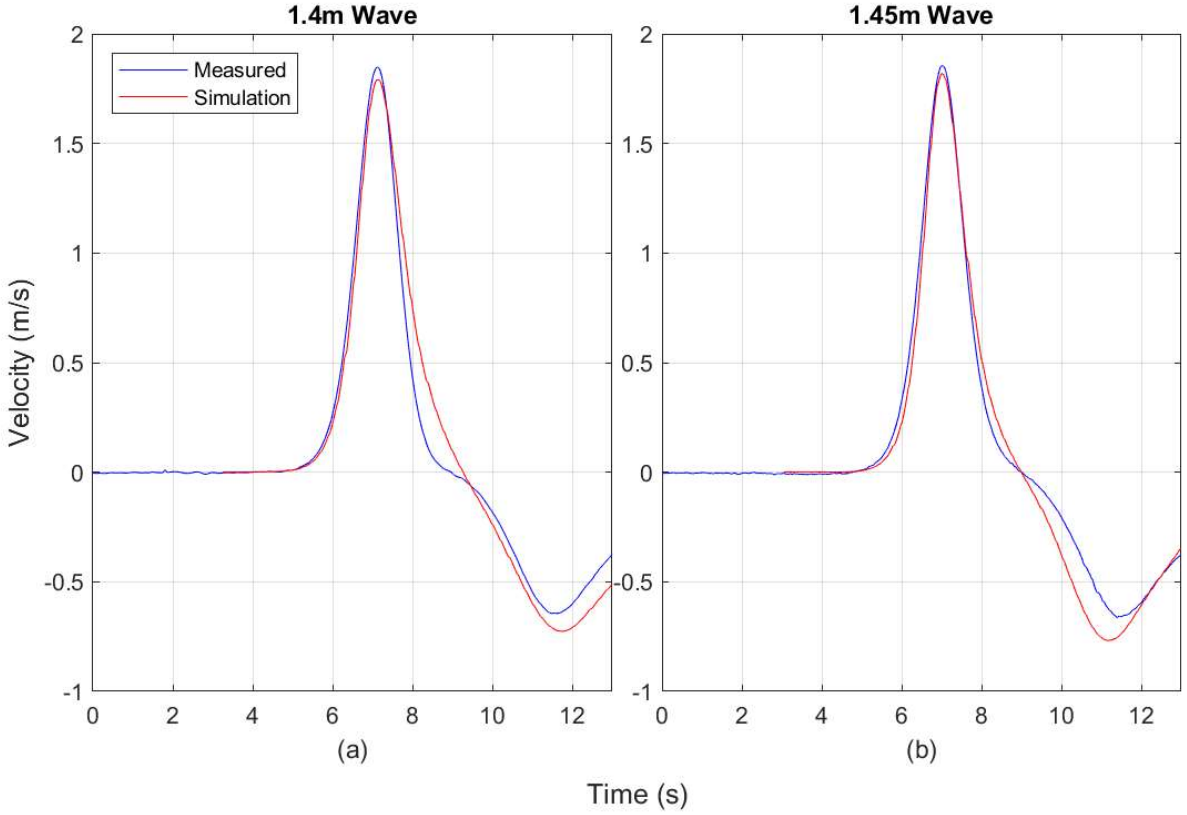

Figure 6-5: Velocity Time History Comparison at ADV1

Table 6-12: Comparison of Instantaneous Maximum Velocity Values at ADV1

Wave height (m)	Velocity (ft/s)		Measured/Simulation
	Simulation	Measured	
1.4	5.876	6.078	1.03
1.45	5.967	6.088	1.02

6.2.3 *Pressure Measurements*

The pressure fields on the front face of the wall were compared. The selected locations were along the wall centerline and the outermost line of pressure sensors (15.5 inches from the centerline), at the bottom, middle and top of the pressure sensor grid. A diagram showing the location of the sensors compared is given in Figure 6-6. Values for the maximum instantaneous pressures are shown in Table 6-13. Time histories for the different locations examined for the 1.4m and 1.45m waves can be found in Figure 6-7 and Figure 6-8 respectively.

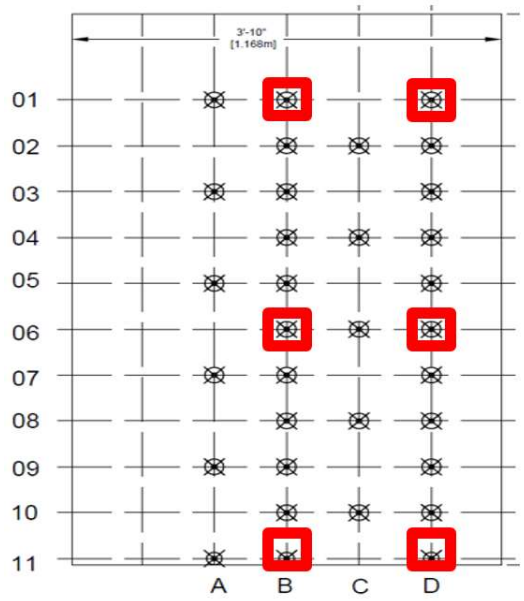

Figure 6-6: Pressure Sensor Locations for Comparison Shown in Table 6-12

Table 6-13: Maximum Pressures at Different Locations

Sensor Name	1.4m Wave Pressures (psi)			1.45m Wave Pressures (psi)		
	Simulation	Measured	Measured/ Simulation	Simulation	Measured	Measured/ Simulation
B01	0.84	0.88	1.04	1.37	1.51	1.10
D01	0.75	1.02	1.35	1.10	1.31	1.20
B06	4.52	2.22	0.49	4.00	2.94	0.73
D06	3.97	1.99	0.50	3.63	2.89	0.80
B11	3.57	3.00	0.84	3.42	3.17	0.93
D11	3.14	2.62	0.84	3.06	2.79	0.91

Comparing the measured and simulated responses shown in Table 6-13, the maximum pressure values deviate more than wave heights and velocities. The time histories have similar shapes, as illustrated by Figure 6-7 and Figure 6-8, indicating that the inundation phenomena are similar (as expected from the evaluation of the wave), however the maximum values are larger in the simulation for locations near the bottom and top of the wall. The sensors located about halfway up the wall have the largest error. Finally, the maximum pressures for the 1.45m wave had overall a lower percent difference than those of the 1.4m wave.

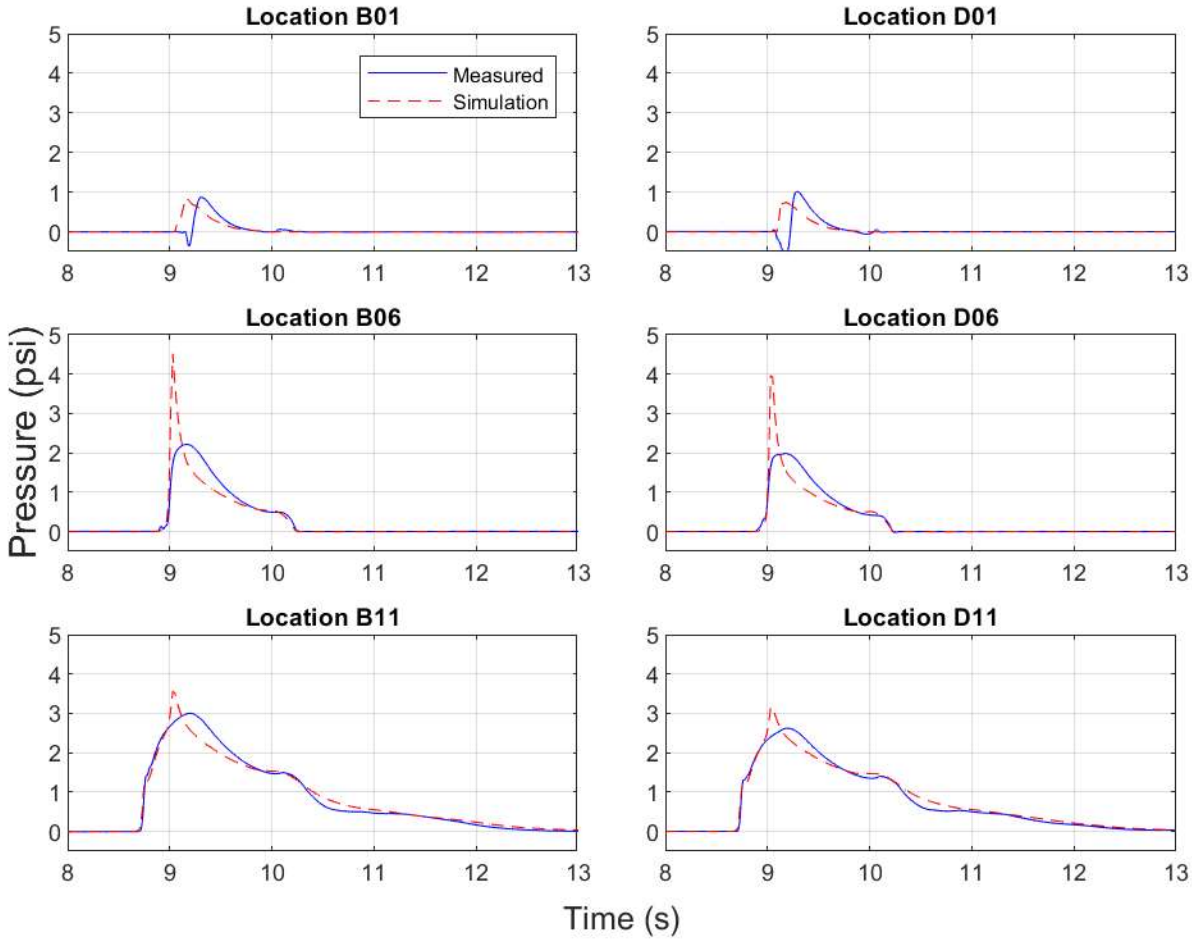

Figure 6-7: 1.4m Wave Pressure Comparison

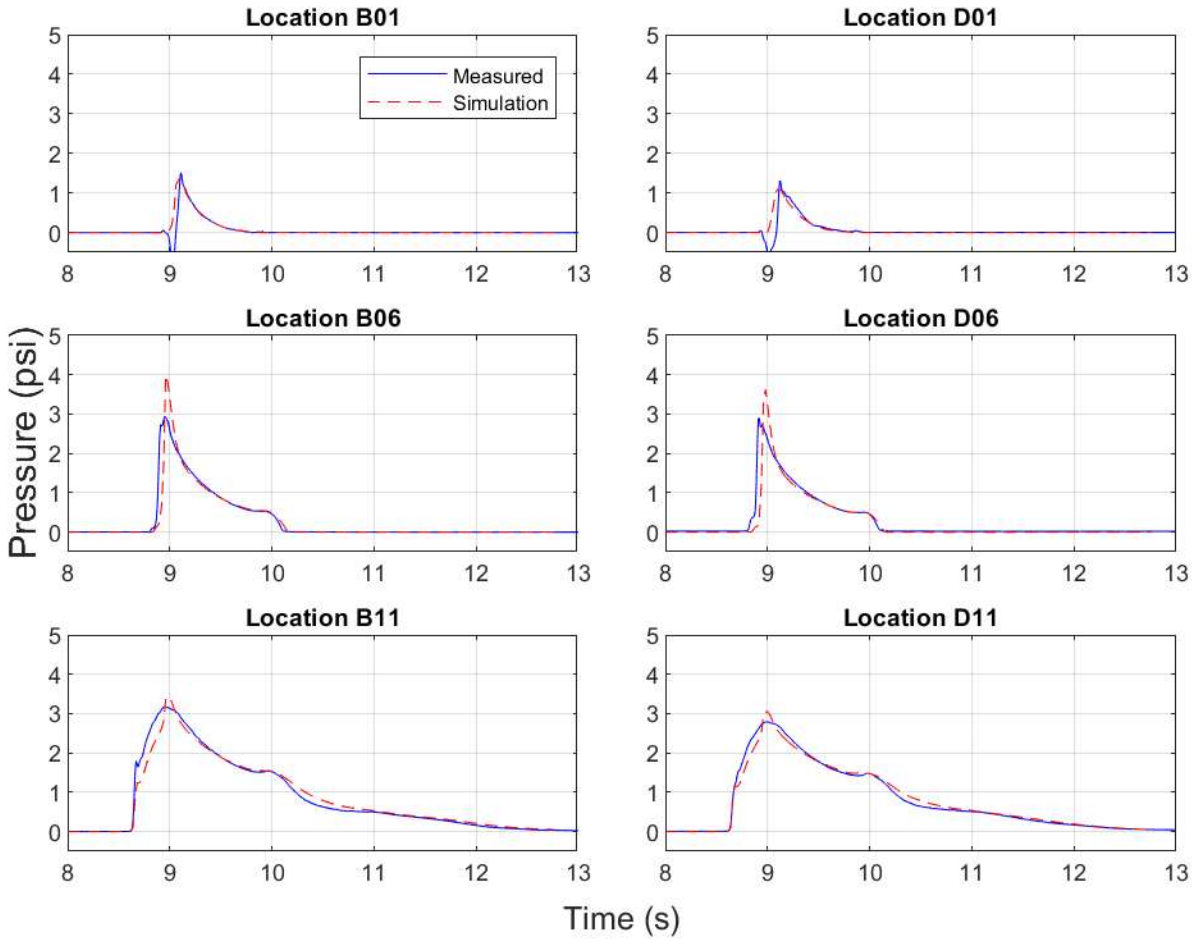

Figure 6-8: 1.45m Wave Pressure Sensor Time History Comparison

The simulated and measured pressure distributions at the centerline (pressure sensor column B in Figure 6-6) and the walls edge line of sensors (pressure sensor column D in Figure 6-6) are compared in Figure 6-9 for the 1.4m wave. It can be seen that the simulation is overestimating the pressures near the bottom of the wall. It also predicts that the pressure increase in the center of the wall will be nearly twice as large as the measured pressures during the experiment. Near the top of the wall the simulation underestimates the pressures. The simulation also predicts that the D line will have greater pressures near the middle of the wall than the centerline, another phenomenon that is not observed in the experimental data.

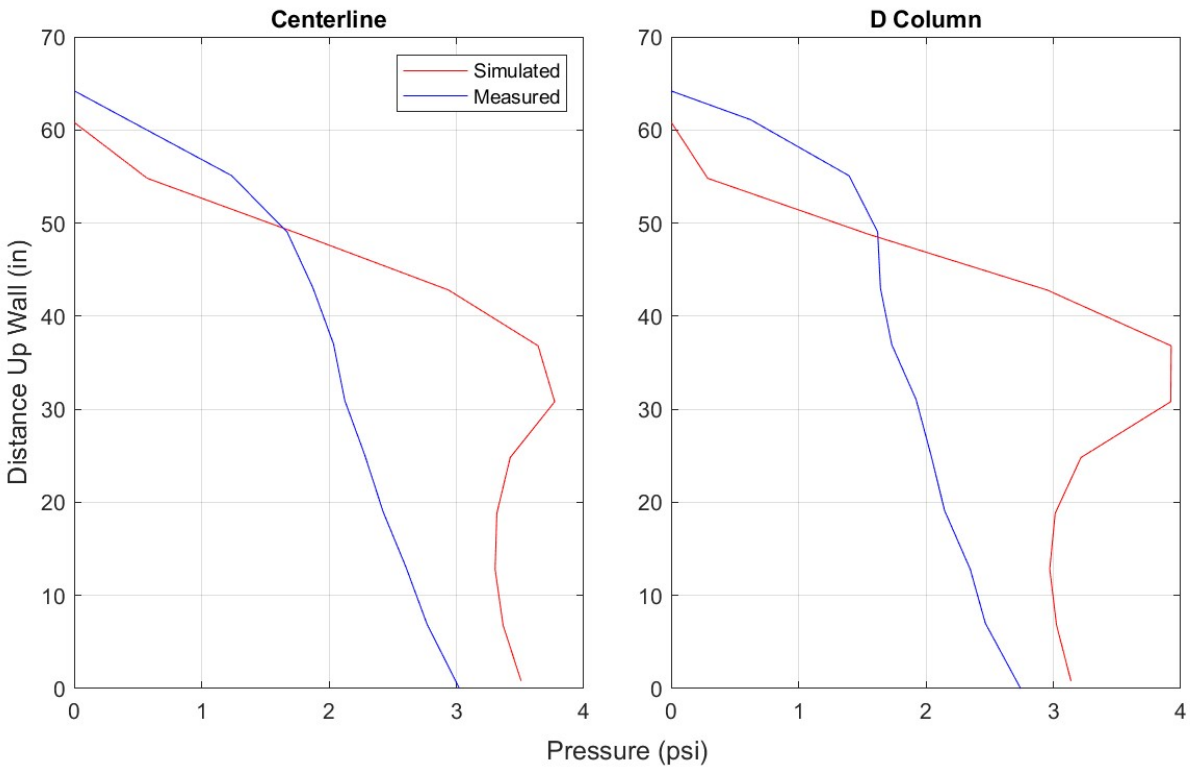

Figure 6-9: Pressure Distribution Comparison along Centerline (B column) and D Column (1.4m Wave)

Figure 6-10 compares the pressure distributions for the 1.45m wave, which are closer than the1.4m wave. It is interesting to note that the maximum pressures in the simulation for the 1.45m wave are slightly lower than the pressures for the 1.4m wave in the middle of the wall, which is the opposite of what was observed during the experiment, where pressures were consistently higher for the 1.45m wave. These differences in pressure distribution will undoubtedly lead to a greater force in the simulation than was observed during the experiment.

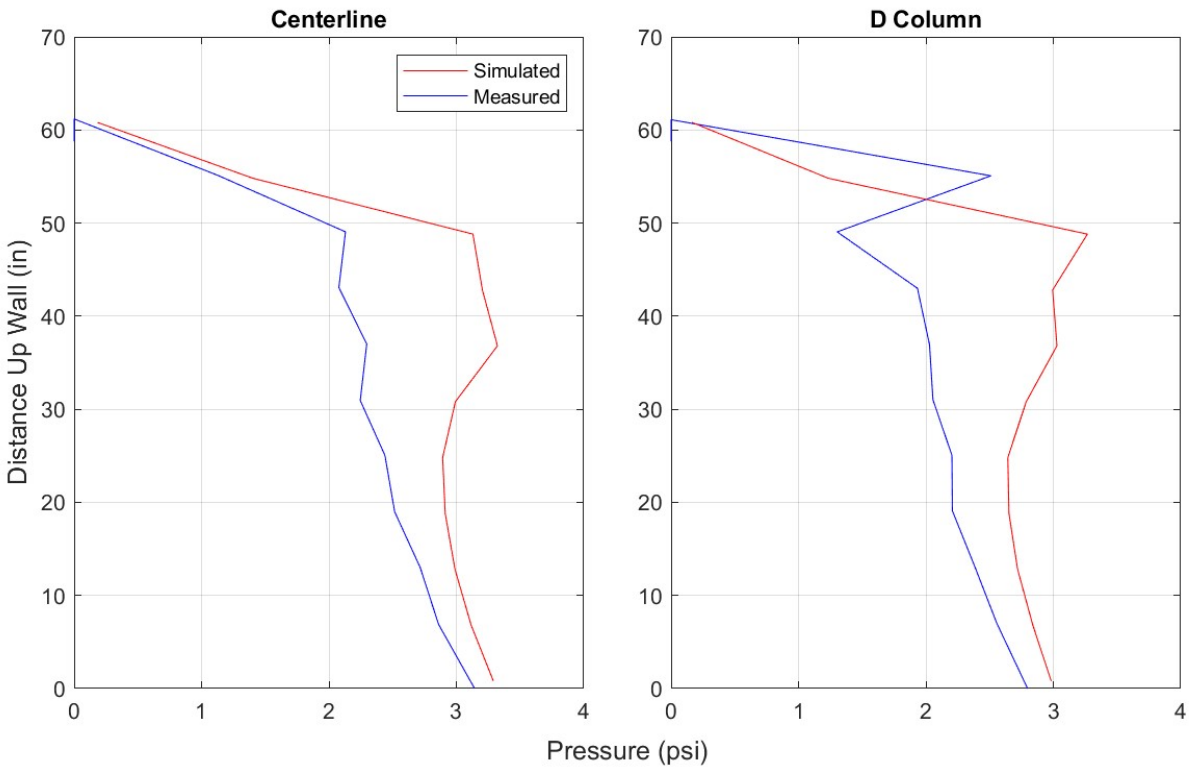

Figure 6-10: Pressure Distribution Comparison along Centerline (B column) and D Column (1.45m Wave)

6.2.4 *Force Measurements*

The force time histories and maximum values were also compared. Figure 6-11 presents stream-wise force time histories for both the 1.4 and the 1.45m waves. Table 6-14 and Table 6-15 compare the maximum instantaneous force determined by integrating the pressures in the simulation as well as load cells, strain gauges and integrated pressures from the experiment. The shapes of the time histories are similar but the simulated maximum values are 18% to 27% higher for the 1.4m wave and 10% to 13% higher for the 1.45m wave.

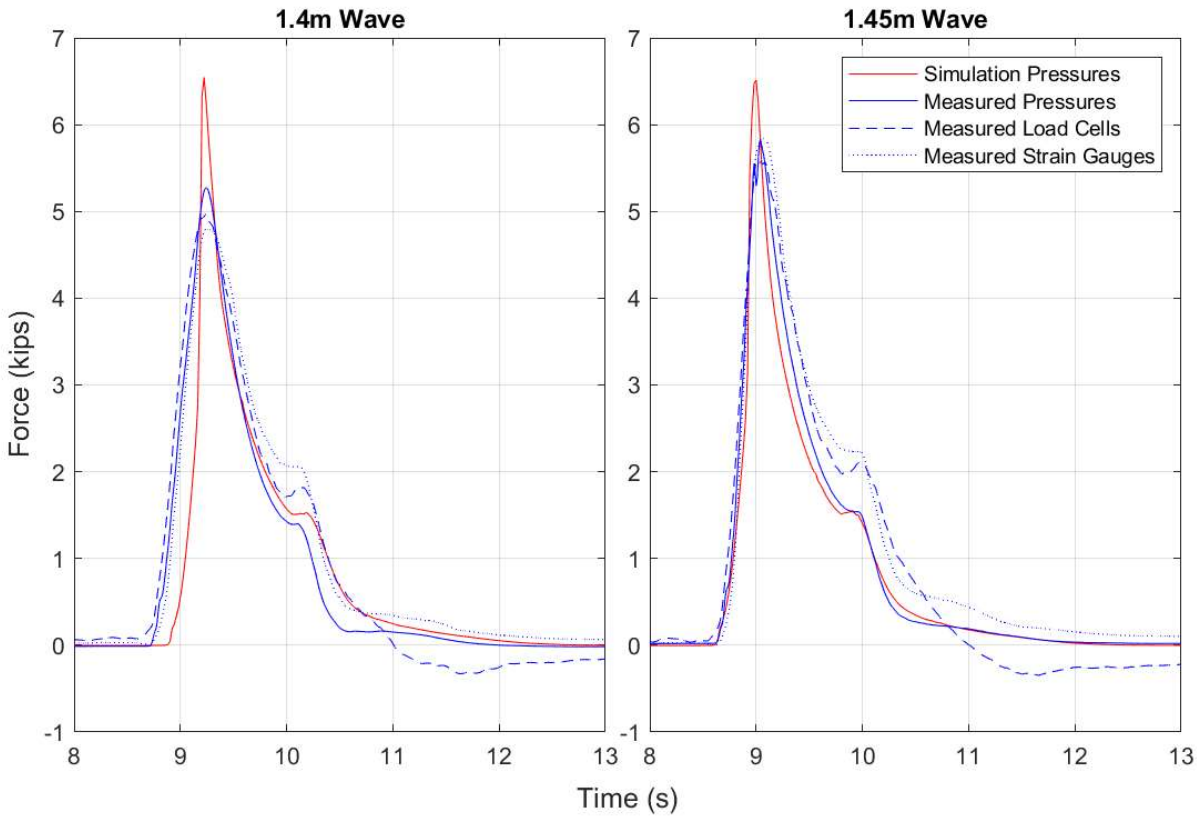

Figure 6-11: Stream-wise Force Time History Comparison

Table 6-14: Maximum Instantaneous Force Comparison, 1.4m Wave

	Measured			Simulation
	Load Cells	Strain Gauges	Pressures	
Max Force (kips)	5.378	4.77	5.38	6.545
Experiment/Simulation	0.82	0.73	0.82	1.00

Table 6-15 Maximum Instantaneous Force Comparison, 1.45m Wave

	Measured			Simulation
	Load Cells	Strain Gauges	Pressures	
Max Force (kips)	5.66	5.84	5.66	6.514
Experiment/Simulation	0.87	0.90	0.87	1.00

From these observations and the difference in pressure distributions, it is hypothesized the simulation is not capturing some of the physical phenomena occurring when the wave impacts the structure. The model predicted the propagation of the wave well, within a few percent for both wave heights and velocities, however further work needs to be done to refine the model to more

accurately represent the pressure distributions and forces observed in the stream-wise direction on the wall during the experiment.

6.3 ASCE7-16 FORCE COMPARISON

The measured forces were compared with theoretical forces using ASCE 7-16 and the experimental values for flow depth and velocity. Equations 3-3 and 3-4, shown below, were used to determine the estimated unbalanced hydrostatic loading described in Section 6.10.1 of ASCE 7-16.

$$p_{uw} = 1.25 * I_{TSU} * \gamma_s * H_{max} \quad \text{Equation 3-3}$$

Where:

p_{uw} = Pressure on the onshore face of the structure due to a tsunami

I_{TSU} = Importance factor for tsunami loading (from ASCE 7 table 6.8-1)

γ_s = The density of seawater = 64 lb/ft^3 *k_s

Where:

k_s = 1.1 to account for suspended solids and other small debris in the tsunami flow

H_{max} = Maximum inundation depth at the site = 4.57ft.

$$P_{TSU} = p_{uw} * 1.3 * H_{max} * b_w \quad \text{Equation 3-4}$$

Where:

P_{TSU} = Stream-wise force from tsunami inundation

p_{uw} = Pressure from the tsunami wave found using Equation 3-3

b_w = The width of the face of the building closest to the shore = 46 in.

For this comparison, the experimental wave height from the closest wave gauge to the structure (Gage uswg2) was used to calculate the total theoretical pressure and force on the structure without the 1.25 multiplier in Eq. 3-3, the 1.3 multiplier in Eq. 3-4 and I=1 (rather than 1.25). The results are shown in Table 6-16. The codified force from ASCE 7 for both waves is the same due to similarities in the measurements of wave height between the two waves at uswg2, each experiment recorded an average maximum wave height (H_{max} in Table 6-16) of 4.57 ft. The results show that the expressions estimate the force well, with a maximum difference between the theoretical force and the measured force of under 3%. With the amplification factors the applied force would be

approximately twice this value, ensuring that a VES would be able to withstand tsunami loads and add a significant factor of safety for the large uncertainties associated with flow depth and velocity at a given site.

Table 6-16: ASCE 7-16 Equation 6.10-1 Comparison

Wave Height (m)	H_{max} (ft)	I_{TSU}	γ_s (lbf/ft^3)	p_{uw} (lbf/ft^2)	B_w (ft)	P_{TSU} (kips)	Experiment Force (kips)	% difference
1.4	4.57	1	68.64	313.9	3.83	5.50	5.38	2.25%
1.45	4.57	1	68.64	313.9	3.83	5.50	5.660	2.87%

Chapter 7. CONCLUSION

This chapter is broken into three sections. The first presents a summary of the work completed and presented in this document. The second section draws conclusions from the result and comparisons presented in Chapter 5 and 6. The final section details additional future work that would further research in the field of tsunami-structure interaction.

7.1 SUMMARY

This thesis presents work done to investigate wave-soil-structure interaction through experimental testing in a large wave flume. The primary goal of this research was to measure the forces of a tsunami wave impacting a large scale structural model in three dimensions with realistic boundary conditions. Multiple methods of measuring stream-wise forces were used in order to provide redundancy in measurements. Primary test parameters investigated were the height of soil present in the soil box around the test specimen and the height of the wave impacting the test specimen.

To meet this goal a review of existing literature was conducted to determine how to set up a wave flume experiment that could be capable of measuring forces in three dimensions on a specimen while maintaining realistic boundary conditions. It was found that there is a lack of testing on large scale models subject to tsunami loads with the capability of measuring force in three dimensions with realistic boundary conditions. Some small-scale tests have measured force in three dimensions utilizing multi axis load cells at the base of the structure, however they typically utilized light, unrealistic building materials Large scale tests (1/6 scale or larger), where realistic building materials were used, were found to either present unrealistic boundary conditions or only measure force in a selected direction. It was determined that a new test setup design would be necessary to achieve the goals of this research.

To determine a reasonable geometry for the test specimen a full scale vertical evacuation structure was designed to the new code provisions in ASCE 7-16. The building was designed to site specific loads for a location in Seaside, Oregon, a popular coastal tourist location subject to tsunami inundation in the event of a Cascadia subduction zone earthquake. The building was designed to remain nearly elastic during a maximum credible earthquake, with R=1 and no 2/3 on the design accelerations at the site, to ensure it would have adequate strength to resist tsunami loads. Three

reinforce concrete core walls were used to resist loads from both tsunami inundation and the preceding earthquake. The walls were size to be 23ft x 16ft in plan with a wall thickness of 30 inches.

The core walls were then scaled down to a 1:6 scale in order to fit within the limitations of the test facility. A unique setup was designed to support the test specimen with a series of pin connected load cells oriented in the three principle directions. These load cells were assumed to act as truss elements and only take axial compression. The test specimen consisted of a core wall supported on piles. These piles were founded on a base slab that provided a rigid base that the load cells were attached to, allowing the measurement of reactions on the system. The base slab also facilitated the installation of steel walls used to create a soil box around the structure. The load cells were connected to the base slab and to a custom built stiff reaction frame that was anchored to the base of the flume. In addition to the load cells, loads were measured with a series of pressure sensors on the front face of the wall, and a series of strain gauges placed on the piles that support the wall. Four different experiments were conducted, a 1.4m tall wave with the soil box full, a 1.4m tall wave with the soil box half full, a 1.4m tall wave with the soil box empty, and finally a1.45m tall wave with the soil box empty. The soil levels were varied to investigate how changing the level of soil in the soil box changed the forces in the piles supporting the structure. The wave height was varied to investigate the difference in force from an unbroken wave and a broken bore type wave. Forces in the stream-wise direction were measured with three different methods, by integrating pressures over the front face of the wall, by utilizing strain gauges on the piles to determine the total shear being carried by the piles, and by load cells oriented in the stream-wise direction.

Comparisons were made between experiments to determine what effect changing the soil level and wave height had on total loads on the specimen. Comparisons were then made between the experiment and an OpenFOAM simulation of the experiment. Finally comparisons were made between the experiment and provisions used in ASCE 7-16 to determine the accuracy of the codified equations to predict the total stream-wise force from tsunami inundation.

7.2 CONCLUSIONS

The following conclusions were drawn from the experiments and comparisons:

- Changing the soil level had little effect on load transfer to the base slab. The total shear in the piles showed only a slight increase from the full to the empty soil box condition. Total shear also showed a decrease in force between the full and half full soil box experiments.
- More strain gauges need to be used to understand axial force in piles. The total axial force on the specimen as measured by the strain gauges varied between the top and bottom strain gauge locations indicating that something was off with their measurements. This could be due to the angles for attaching moving braces welded to the piles about 1.5 inches above the top strain gauges. Due to the close proximity of the strain gauges to this discontinuity in the section axial strains may have not redistributed evenly by the time they reached the top strain gauges, invalidating the assumption that strains varied linearly between the strain gauges on the front and back of the piles. Additional strain gauges placed in the middle of the piles would help to better understand the distribution of strains in the piles.
- 1.45m wave induces a greater stream-wise force on test specimen. All three methods of measuring stream-wise force showed an increase between the 1.4 and the 1.45m wave. The strain gauges recorded the largest increase in force, showing an increase of about 1200lbf, while the integrated pressures provided the smallest increase in force, about 300lbf. Load cells showed an increase in force of about 500 lbf. Load cells and pressures showed lower variation so the total increase in force was more likely around the 300 to 500lbf range.
- Similar center line pressure distributions and centroid locations were found for both wave types. The pressures recorded for the 1.45m wave were slightly higher however and showed a sharper decrease in pressures near the top of the wall. When examining the centroid location for the centerline distributions, centroids were found to be within .1 inch of each other.
- The OpenFOAM simulation did a good job of predicting the free surface elevation and velocity of the waves tested experimentally, with both free surface elevation and velocities showing a difference between the simulation and the experiment of less than 4% on average.
- The computed simulation pressures varied more from the experimental pressures, with large difference observed between the experimental pressure distribution and the simulated pressure distribution. While the experiment seemed to show a linear decrease up the height

of the wall the simulation showed lower pressures at the bottom of the wall and larger pressures in the middle of the wall.

- Total force from the experiment was overestimated in the OpenFOAM simulation by about 10% for the 1.45m wave and 20% for the 1.4m wave. In the simulation both wave heights provided similar results for total force on the specimen with a total difference in force of only 30 lbf, a factor of 10 lower than the smallest increase recorded experimentally. The total force from the simulated waves was also larger for the 1.4m wave than the 1.45m wave, the opposite of what was observed during test.
- It was found that Equations 3-4 taken from Section 6.10.1 of ASCE 7-16 did a good job of estimating the total force from the tsunami waves on the test specimen when the safety factors were removed from the equation. With the safety factors included the total force was about twice the measured experimental force, which would account for uncertainties associated with tsunami inundation depth and velocity in practice.

7.3 FUTURE WORK

The following are improvements that could be made to the test setup to increase the accuracy of the results for future works:

- Use more strain gauges. Placing strain gauges on the neutral axis in the middle of the section would give a better idea of the strain distribution between the measured extreme fibers. Placing another set of gauges in the vertical middle of the piles as well as at the top and bottom of the piles could also better help understand the axial forces present in the piles.
- Set up test in such a way that weight of the wave does not act on load cells. The plywood beach placed around the specimen was bearing on the outside of the soil box which caused the weight of the wave to act on the vertical load cells. The cover plates placed over the soil box also provided area for the weight of the wave to act upon. Now that it has been determined that changing the soil level does not change the load transfer mechanisms in the piles, it would be possible to build a new beach that would go over the soil box and be self-reacting so that the only loads measured by the load cells are induced by the lateral force of the wave.

- Install specimen using jacks and orient specimen to ensure it is centered, square, level, and plumb in the flume. Placement of the specimen is key to reducing interference between load cells. Using a system of hydraulic jacks below the specimen to set it in place and then connecting all load cells would allow for a simpler installation process and reduce the issues mentioned above.
- Using a larger wave flume would allow for the testing of larger waves on a larger specimen. This would give a better indication of structural performance at full scale during tsunami inundation. It could also be possible to instrument full scale structures in tsunami prone regions to measure their responses in the event of a tsunami, however this could be expensive and due to the uncertain nature of tsunamis the instrumentation could become outdated or inoperable before a tsunami ever strikes the building.

Additional future work should be done to investigate the following:

- The investigation of different structural systems. Often times in practice tsunami evacuation structures are designed as an open system to recede the demands on the lateral force resisting system. Testing of an open system would provide a good comparison between the total forces attracted on a closed core wall system and an open system.
- The investigation of a core wall with openings. It is very common for core walls in practice to have openings for doorways and other utilities that might run through the core. Testing of a core wall with openings would give a better idea of the response of a realistic building component
- More work should be done to better simulate the pressures observed during this testing. Although the free surface and velocities in the OpenFOAM simulation seem to do a good job of replicating observations made during the experiment, further work needs to be done to more accurately predict the pressures and total force on the test specimen.

REFERENCES

ASCE. (2017). *7-16 Minimum Design Loads and Associated Criteria for Buildings and Other Structures* .

Ash, C. (2015). Design of a Tsunami Vertical Evacuation Refugre Structure in Westport, Washington. *Structures Congress.*

David Linton, R. G. (2013). Evaluation of Tsunami Loads on Wood-Frame Walls at Full Scale. *JOURNAL OF STRUCTURAL ENGINEERING*, 1318-1325.

FEMA. (2019). *P646 Guidelines for Design of Structures for Vertical Evacuation from Tsunamis.*

Gills, C. (2018). *Experimental and Numerical Validation of Three-Dimensional Tsunami Wave Pressures and Forces on an Elevated Structure.* Masters Thesis, University of Washington.

Hyoungsu Park, D. T. (2013). Tsunami Innundation Modeling in Constructed Enviornments: A Physical and Numerical Comparison of Free-surface Elevation, Velocity, and Momentun Flux. *Coastal Engineering*, 9-21.

J. Wienke, H. O. (2005). Breaking wave impact force on a vertical and inclined slender pile—theoretical and large-scale model investigations. *Coastal Engineering*, 435-462.

Jebediah S. Wilson, R. G. (2009). Behavior of a One-Sixth Scale Wood-Framed Residential Structure under Wave Loading. *JOURNAL OF PERFORMANCE OF CONSTRUCTED FACILITIES*, 336-345.

Qin, X., Motley, M. R., & Marafi, N. A. (2018). Three-dimensional Modeling of Tsunami Force on Coastal Communities. *Coastal Engineering*.

Robertson, I. R. (2008). EXPERIMENTAL RESULTS OF TSUNAMI BORE FORCES ON STRUCTURES. *Proceedings of the ASME 27th International Conference on Offshore Mechanics and Arctic Engineering.* Estoril, Portugal.

Rueben, M. H. (2010). Optical Measurements of Tsunami Innundation through an Urban Waterfront Modeled in a Large-Scale Laboratory Basin. *Coastal Engineering*, 229-238.

Seyedreza Shafiei, B. W. (2016). Experimental investigation of tsunami bore impact force and pressure on a square prism. *Coastal Engineering*, 1-16.

Taofiq Al-Faesly, D. P. (2012). Experimental Modeling of Extreme Hydrodynamic Forces on Structural Models. *International Journal of Protective Structures*, 477-505.

APPENDIX A
FULL SCALE DESIGN CALCULATIONS

Author: Christopher Pyke Date: 7/11/2018

Tsunami Load Calculation worksheet

References:
1) ASCE 7-16 Ch.6

Water and wave properties:

Input Variables

$H_{max} := 26.25\ ft$ Maximum Inundation Depth at site

$U_{max} := 41.3\ \frac{ft}{s}$ Max Inundation Velocity at site

$K_s := 1.1$ Fluid Density factor per R1 section 6.8.4

$\gamma_s := K_s \cdot 64\ \frac{lbf}{ft^3}$ Seawater specific wieght

$\rho_s := K_s \cdot 2\ \frac{slug}{ft^3}$ Seawater mass density

Building properties:

$b_w := 150\ ft$ Building width

$h_{sx} := 15\ ft$ Average story height

$h_b := h_{sx} \cdot 5 = 75\ ft$ total height

$I_{TSU} := 1.25$ importance factor for structure

6.10.1 Simplified Equivalent uniform lateral static pressure

accounts for combination of unbalanced hydrostatic loads and hydrodynamic loads
use this section or 6.10.2 "detailed hydrodynamic lateral forces"

$p_{uw} := 1.25 \cdot I_{TSU} \cdot \gamma_s \cdot H_{max} = 2887.5\ \frac{lbf}{ft^2}$ total pressure on structure

$P_{TSU} := p_{uw} \cdot 1.3 \cdot H_{max} \cdot b_w = 14780.3906\ kip$ total load on structure THIS IS DESIGN LOAD

6.10.2.1 Overall Drag Force on Buildings and Other Structures

Buildings lateral force resisting system must be designed to resist overall drag forces at each level caused by incoming or outgoing flows at load case 2 (Umax, H=2/3Hmax)

$h := \frac{2}{3} \cdot H_{max}$ design inundation height per load case 2

$\frac{b_w}{h} = 8.5714$ width to inundation depth ratio (used to determine Cd)

$C_d := 1.25$ Drag coefficient per table 6.10-1

$C_{cx} := 1$ Max value from section 6.8.7 due to debris buildup and unknown number of windows/openings in structure (cannot be greater than 1 or less than .7)

$F_{dx} := \frac{1}{2} \cdot \rho_s \cdot I_{TSU} \cdot C_d \cdot C_{cx} \cdot b_w \cdot h \cdot U_{max}^2 = 7695.5936\ kip$ Overall drag force at each level below inundation depth

Max considered Earthquake Load

Reference: ASCE 7-16

$I_e := 1.5$ Importance factor for catagory 4 building from ASCE 7 table 1.5-2

$T_l := 16$ mapped long period transistion period from ASCE 7 figure 22-14

$S_s := 1.3$ .2s spectral response acceleration from ASCE 7 figure 22-1

$S_1 := .7$ 1s spectral response acceleartion from ASCE 7 figure 22-2

$R := 1$ R=1 for MCE

$h_n := 60$ structural height of structure

$C_t := .02$ period parameters per table 12.8-2

$x := .75$

$C_u := 1.4$ upper limit period coefficient per table 12.8-1

$T_a := C_t \cdot h_n^{\,x} = 0.4312$ Approximate fundemental period of the structure

$T := C_u \cdot T_a = 0.6036$ Maximum natural period allowed per section 12.8.2

Spectral acceleration and Seismic coeffiecinet

$F_a := 1$

$F_v := 1.7$

Site coefficients assuming site class D (soil class unknown)
From ASCE 7 tables 11.4-1&2

$S_{MS} := F_a \cdot S_s = 1.3$

$S_{M1} := F_v \cdot S_1 = 1.19$

Max Considered spectral acceleration parameters
per ASCE 7 EQs 11.4-1 & 2

$$C_s := \min\left(\left[\frac{S_{MS}}{\left(\frac{R}{I_e}\right)} \quad \frac{S_{M1} \cdot T_l}{T^2 \cdot \left(\frac{R}{I_e}\right)} \quad \frac{S_{M1}}{T \cdot \left(\frac{R}{I_e}\right)}\right]\right) = 1.95$$

Without R factor C.s=1.3 close to value given from Seth during 8/7 call

Seismic weight and load

$A := 150\ \text{ft} \cdot 60\ \text{ft} = 9000\ \text{ft}^2$ Building Footprint

$SW := 150\ \text{psf}$ Assumed self weight of each floor

$FW := SW \cdot A = 1350\ \text{kip}$ weight of each floor

$RW := 120\ \text{psf} \cdot A = 1080\ \text{kip}$ weight of the roof

$W := 4 \cdot FW + RW = 6480\ \text{kip}$ Total weight of structure

$K := .75 + .5 \cdot T = 1.0518$ must be 1 < K < 2.5

$V_{EQ} := C_s \cdot W = 12636\ \text{kip}$ total base shear on the structure

Final Building Geometry:

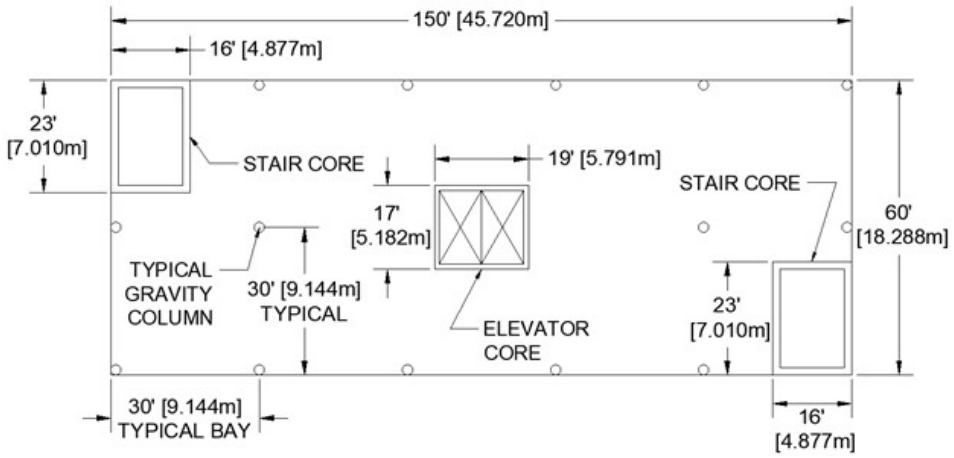

Exterior cores

$b_e := 16\ ft$ length and width of core
assuming each core as typ stairwell

$l_e := 23\ ft$

$t_e := 30\ in$ core wall thickness

$A_{ge} := b_e \cdot l_e - \left(b_e - 2 \cdot t_e\right) \cdot \left(l_e - 2 \cdot t_e\right) = 170\ ft^2$ Area of exterior core

$I_{gxe} := \frac{b_e \cdot l_e^{\,3}}{12} - \frac{\left(b_e - 2 \cdot t_e\right) \cdot \left(l_e - 2 \cdot t_e\right)^3}{12} = 93.8762\ m^4$ Gross moment of inertia in X direction exterior core

$I_{gye} := \frac{l_e \cdot b_e^{\,3}}{12} - \frac{\left(l_e - 2 \cdot t_e\right) \cdot \left(b_e - 2 \cdot t_e\right)^3}{12}$ Gross moment of inertia in Y direction exterior core

$I_{exe} := .7 \cdot I_{gxe} = 1.5788 \cdot 10^8\ in^4$ Effective moment of intertia from ACI table 6.6.3.1.1a

$I_{eye} := .7 \cdot I_{gye} = 8.4974 \cdot 10^7\ in^4$

Interior cores

$b_i := 19\ ft$ Width of interior core

$l_i := 17\ ft$ length of interior core

$t_i := 30\ in$ thickness of interior core

$A_{gi} := b_i \cdot l_i - \left(b_i - 2 \cdot t_i\right) \cdot \left(l_i - 2 \cdot t_i\right) = 155\ ft^2$ gross area of core

$I_{gxi} := \frac{b_i \cdot l_i^{\,3}}{12} - \frac{\left(b_i - 2 \cdot t_i\right) \cdot \left(l_i - 2 \cdot t_i\right)^3}{12} = 49.7396\ m^4$ Gross moment of inertia in X direction exterior core

$I_{gyi} := \frac{l_i \cdot b_i^{\,3}}{12} - \frac{\left(l_i - 2 \cdot t_i\right) \cdot \left(b_i - 2 \cdot t_i\right)^3}{12}$ Gross moment of inertia in Y direction exterior core

$I_{exi} := .7 \cdot I_{gxi} = 8.365 \cdot 10^7\ in^4$ Gross moment of intertia from ACI table 6.6.3.1.1a

$I_{eyi} := .7 \cdot I_{gyi} = 1.0121 \cdot 10^8\ in^4$

Determine demands based on stiffness of cores:

from AISC table 3-23 Core was assumed to be a cantilever beam with a point load, K=P/Δ

$b := 647.8\ in$ moment arm for EQ load, base moment/base shear

$f'c := 6\ ksi$ compressive strength of concrete

$E_c := 57000 \cdot \sqrt{f'c\ psi} = 4415.201\ ksi$ Elastic Modulus of Concrete

Stiffness of interior and exterior cores in X and Y directions

$$k_{yi} := \frac{3 \cdot E_c \cdot I_{gxi}}{b^3} = 5822.5902\ \frac{kip}{in} \qquad k_{xi} := \frac{3 \cdot E_c \cdot I_{gyi}}{b^3} = 7045.1195\ \frac{kip}{in}$$

$$k_{ye} := \frac{3 \cdot \left(E_c \cdot I_{gxe}\right)}{b^3} = 10989.2919\ \frac{kip}{in} \qquad k_{xe} := \frac{3 \cdot \left(E_c \cdot I_{gye}\right)}{b^3} = 5914.7851\ \frac{kip}{in}$$

$\alpha_{xi} := \frac{k_{xi}}{2 \cdot k_{xe} + 1 \cdot k_{xi}} = 0.3733$ $\alpha_{yi} := \frac{k_{yi}}{1 \cdot k_{yi} + 2 \cdot k_{ye}} = 0.2094$ stiffness ratios for center core X, and Y directions

$\alpha_{xe} := \frac{k_{xe}}{1 \cdot k_{xi} + 2 \cdot k_{xe}} = 0.3134$ $\alpha_{ye} := \frac{k_{ye}}{1 \cdot k_{yi} + 2 \cdot k_{ye}} = 0.3953$ stiffness ratios for exterior core X, and Y directions

$1 \cdot \alpha_{xi} + 2 \cdot \alpha_{xe} = 1$ $1 \cdot \alpha_{yi} + 2 \cdot \alpha_{ye} = 1$

Axial Demands:

$LL := 100\ psf$ Assembly live load for evacuation floors

$DL := 150\ psf$ Assumed dead load

$DLC_e := \left(b_e + l_e - 2 \cdot t_e\right) \cdot 2 \cdot t_e \cdot h_b \cdot 150\ \frac{lbf}{ft^3} = 1912.5\ kip$ weight of the exterior core

$DLC_i := \left(b_i + l_i - 2 \cdot t_i\right) \cdot 2 \cdot t_i \cdot h_b \cdot 150\ \frac{lbf}{ft^3} = 1743.75\ kip$ weight of the interior core

$A_{te} := (23\ ft) \cdot (26.5\ ft) = 609.5\ ft^2$

Assumed tributary area for core

$A_{ti} := (38.5\ ft) \cdot (60\ ft) = 2310\ ft^2$

$P_{ui} := 1.2 \cdot DL \cdot A_{ti} \cdot 5 + .5 \cdot LL \cdot A_{ti} \cdot 2 + 1.2 \cdot DLC_i = 4402.5\ kip$ total axial load assuming 5 floors with DL and 2 evacuation floors with LL

$P_{ue} := 1.2 \cdot DL \cdot A_{te} \cdot 5 + .5 \cdot LL \cdot A_{te} \cdot 2 + 1.2 \cdot DLC_e = 2904.5\ kip$ total axial load assuming 5 floors with DL and 2 evacuation floors with LL

EQ loads:

$V_{EQ} = 12636\ kip$ total base shear from EQ

$M_{EQ} := 682135\ kip\ ft$ Total moment from EQ = sum(story shear*story height) from excel calcs

Shears on interior cores

$V_{xi} := V_{EQ} \cdot \alpha_{xi} = 4716.4818\ kip$

$V_{yi} := V_{EQ} \cdot \alpha_{yi} = 2646.444\ kip$

moments on interior cores

$M_{xi} := M_{EQ} \cdot \alpha_{xi} = 2.5461 \cdot 10^5\ kip\ ft$

$M_{yi} := M_{EQ} \cdot \alpha_{yi} = 1.4286 \cdot 10^5\ kip\ ft$

Shears on exterior cores

$V_{ye} := V_{EQ} \cdot \alpha_{ye} = 4994.778\ kip$

$V_{xe} := V_{EQ} \cdot \alpha_{xe} = 3959.7591\ kip$

moments on exterior cores

$M_{ye} := M_{EQ} \cdot \alpha_{ye} = 2.6964 \cdot 10^5\ kip\ ft$

$M_{xe} := M_{EQ} \cdot \alpha_{xe} = 2.1376 \cdot 10^5\ kip\ ft$

$F_x := 101\ kip$

$F_y := 679.4\ kip$

additional shear in the y direction due to torsion (include for EQ in both directions) from excel calcs, forces only act on exterior cores

Compare to Tsunami loading (Y direction only):

Exterior (acts in Y dir)

$V_{te} := P_{TSU} \cdot \alpha_{ye} = 5842.4161\ kip$ Total Tsunami load on exterior building cores

$V_{ye} + F_y = 5674.178\ kip$ Total EQ load on exterior building cores

Interior (acts in Y dir)

$V_{ti} := P_{TSU} \cdot \alpha_{yi} = 3095.5584\ kip$ Total Tsunami force on interior building core

$V_{yi} = 2646.444\ kip$ Total EQ force on interior building core

Exterior Core Design (load acting in x-direction, 16' side)

$\varphi_v := .75$

area resisting shear

$A_{vxe} := .8 \cdot b_e \cdot 2 \cdot t_e = 9216\ in^2$

$\varphi V_{n\_maxex} := \varphi_v \cdot 10 \cdot \sqrt{f'c\ psi} \cdot A_{vxe} = 5354.0122\ kip$

demands (highlighted)

$V_{xe} + F_x = 4060.7591\ kip$

$A_{vxen} := \frac{V_{xe} + F_x}{\varphi_v \cdot 10 \cdot \sqrt{f'c\ psi}} = 6989.89\ in^2$

Utilization of max reistance

$\frac{V_{xe} + F_x}{\varphi V_{n\_maxex}} = 0.7585$

$M_{xe} = 2.1376 \cdot 10^5\ kip\ ft$

shear strength of concrete

$V_{cxe} := 2 \cdot \sqrt{f'c\ psi} \cdot A_{vxe} = 1427.7366\ kip$

$f_y := 60\ ksi$

rebar yield strength

area to spacing required

$ATS_{xe} := \frac{\left(V_{xe} + F_x\right) - \varphi_v \cdot V_{cxe}}{\varphi_v \cdot f_y \cdot .8 \cdot b_e} = 0.4326\ in$

Area of 4 #8 bars

$A_{vnxe} := 4 \cdot .79\ in^2 = 3.16\ in^2$

required spacing

$s_{min} := \frac{A_{vnxe}}{ATS_{xe}} = 7.3051\ in$

$s := 6\ in$

steel shear strength

$V_{sxe} := \frac{A_{vnxe} \cdot f_y \cdot .8 \cdot b_e}{s} = 4853.76\ kip$

23' side

$A_{vye} := .8 \cdot l_e \cdot 2 \cdot t_e = 13248\ in^2$

$\varphi V_{n\_maxey} := \varphi_v \cdot 10 \cdot \sqrt{f'c\ psi} \cdot A_{vye}$

$\varphi V_{n\_maxey} = 7696.3925\ kip$

$V_{ye} + F_y = 5674.178\ kip$

$V_{te} = 5842.4161\ kip$

$\frac{V_{ye} + F_y}{\varphi V_{n\_maxey}} = 0.7373$

$M_{ye} = 2.6964 \cdot 10^5\ kip\ ft$

$V_{cye} := 2 \cdot \sqrt{f'c\ psi} \cdot A_{vye} = 2052.3713\ kip$

$ATS_{ye} := \frac{\left(V_{ye} + F_y\right) - \varphi_v \cdot V_{cye}}{\varphi_v \cdot f_y \cdot .8 \cdot l_e} = 0.4162\ in$

$A_{vnye} := 4 \cdot .79\ in^2$

$s_{min} := \frac{A_{vnye}}{ATS_{ye}} = 7.5934\ in$

$V_{sye} := \frac{A_{vnye} \cdot f_y \cdot .8 \cdot l_e}{s} = 6977.28\ kip$

$\varphi V_{nxe} := \min\left(\left[\, 1 \cdot \varphi V_{n\_maxex} \;\; \varphi_v \cdot \left(V_{cxe} + V_{sxe}\right) \,\right]\right)$ section shear capacity $\varphi V_{nye} := \min\left(\left[\, 1 \cdot \varphi V_{n\_maxey} \;\; \varphi_v \cdot \left(V_{cye} + V_{sye}\right) \,\right]\right)$

$\frac{V_{xe} + F_x}{\varphi V_{nxe}} = 0.862$ total shear utilization of the section $\frac{V_{ye} + F_y}{\varphi V_{nye}} = 0.8379$

Exterior core: exterior dimmensions 16'x23' with 30" thick walls, shear reinforcement is #8 bars spaced 6" c/c flexural reinforcement is #7 bars spaced 8" c/c EF

Interior Core Design

13.5' side

$A_{vxi} := .8 \cdot b_i \cdot 2 \cdot t_i = 10944 \text{ in}^2$

$\varphi V_{n\_maxix} := \varphi_v \cdot 10 \cdot \sqrt{f'c \text{ psi}} \cdot A_{vxi} = 6357.8895 \text{ kip}$

$V_{xi} = 4716.4818 \text{ kip}$

$A_{vxen} := \frac{V_{xe} + F_x}{\varphi_v \cdot 10 \cdot \sqrt{f'c \text{ psi}}} = 6989.89 \text{ in}^2$

$\frac{V_{xi}}{\varphi V_{n\_maxix}} = 0.7418$

$M_{xi} = 2.5461 \cdot 10^5 \text{ kip ft}$

$V_{cxi} := 2 \cdot \sqrt{f'c \text{ psi}} \cdot A_{vxi} = 1695.4372 \text{ kip}$

$f_y := 60 \text{ ksi}$

$ATS_{xi} := \frac{\left(V_{xi}\right) - \varphi_v \cdot V_{cxi}}{\varphi_v \cdot f_y \cdot .8 \cdot b_i} = 0.4197 \text{ in}$

$A_{vnxi} := 4 \cdot .79 \text{ in}^2$

$s := \frac{A_{vnxi}}{ATS_{xi}} = 7.5292 \text{ in}$

$s := 5 \text{ in}$

$V_{sxi} := \frac{A_{vnxi} \cdot f_y \cdot .8 \cdot b_i}{s} = 6916.608 \text{ kip}$

$\varphi V_{nxi} := \min\left(\left[\, 1 \cdot \varphi V_{n\_maxix} \;\; \varphi_v \cdot \left(V_{cxi} + V_{sxi}\right) \,\right]\right)$

$\varphi V_{nxi} = 6357.8895 \text{ kip}$

$\frac{V_{xi}}{\varphi V_{nxi}} = 0.7418$

24.5' side

$A_{vyi} := .8 \cdot l_i \cdot 2 \cdot t_i = 9792 \text{ in}^2$

$\varphi V_{n\_maxiy} := \varphi_v \cdot 10 \cdot \sqrt{f'c \text{ psi}} \cdot A_{vyi} = 5688.6379 \text{ kip}$

$V_{yi} = 2646.444 \text{ kip}$ $V_{ti} = 3095.5584 \text{ kip}$

$\frac{V_{ti}}{\varphi V_{n\_maxiy}} = 0.5442$

$M_{yi} = 1.4286 \cdot 10^5 \text{ kip ft}$

$V_{cyi} := 2 \cdot \sqrt{f'c \text{ psi}} \cdot A_{vyi} = 1516.9701 \text{ kip}$

$ATS_{yi} := \frac{\left(V_{ti}\right) - \varphi_v \cdot V_{cyi}}{\varphi_v \cdot f_y \cdot .8 \cdot l_i} = 0.2666 \text{ in}$

$A_{vnyi} := 4 \cdot .79 \text{ in}^2$

$s_{max} := \frac{A_{vnyi}}{ATS_{yi}} = 11.8534 \text{ in}$

$V_{syi} := \frac{A_{vnyi} \cdot f_y \cdot .8 \cdot l_i}{s} = 6188.544 \text{ kip}$

$\varphi V_{nyi} := \min\left(\left[\, 1 \cdot \varphi V_{n\_maxiy} \;\; \varphi_v \cdot \left(V_{cyi} + V_{syi}\right) \,\right]\right)$

$\varphi V_{nyi} = 5688.6379 \text{ kip}$

$\frac{V_{ti}}{\varphi V_{nyi}} = 0.5442$

Interior core: exterior dimmensions 17'x19' with 30" thick walls, shear reinforcement is #8 bars spaced 5" c/c, flexural reinforcement is #7 bars spaced 8" c/c EF

APPENDIX B
CONSTRUCTION DRAWINGS

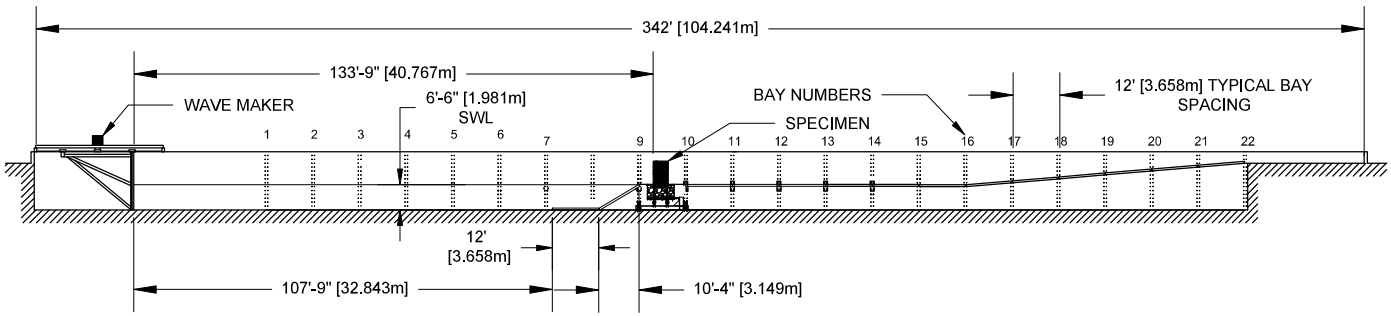

1 FLUME ELEVATION

Scale: N/A

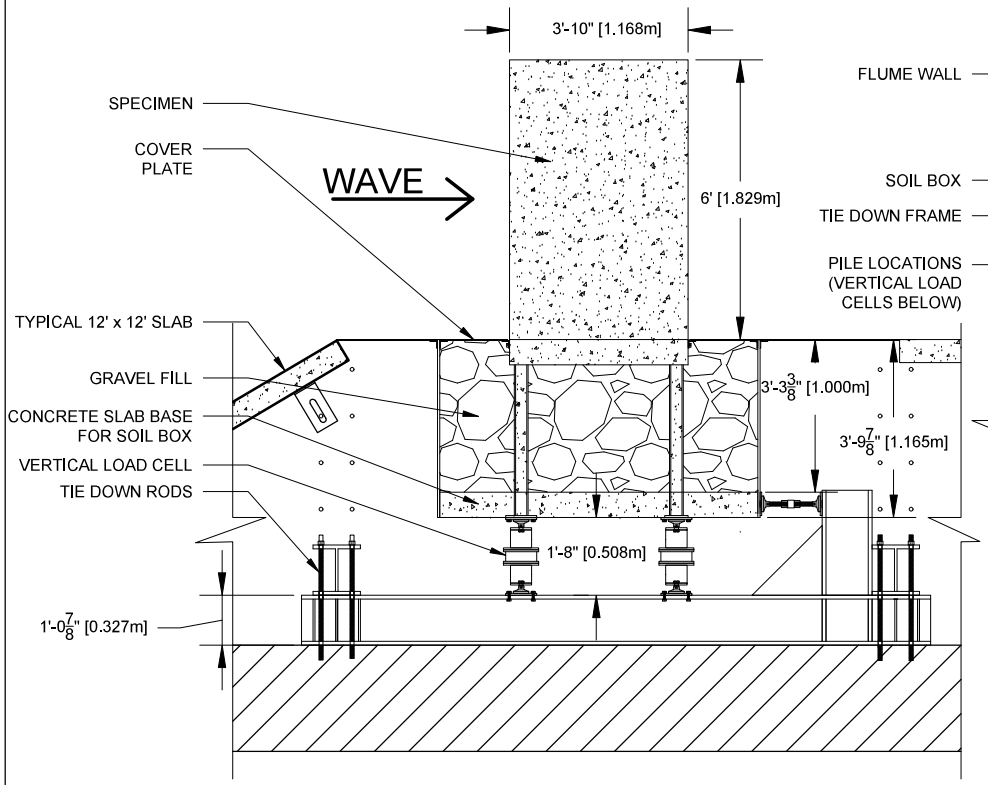

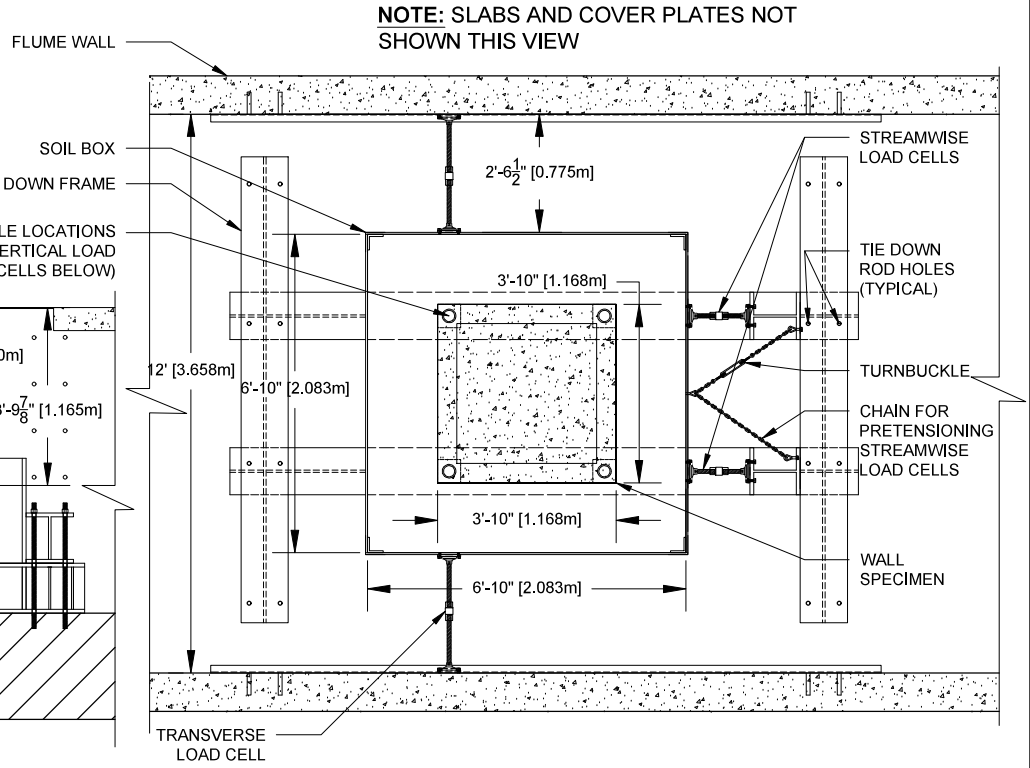

CIVIL & ENVIRONMENTAL ENGINEERING

General Notes

No.	Revision/Issue	Date

VERTICAL EVACUATION STRUCTURES

SETUP OVERVIEW

Project: NSF VES	Sheet: S101
Date: 6/26/19	
Scale: AS NOTED	

PRODUCED BY AN AUTODESK STUDENT VERSION

PRODUCED BY AN AUTODESK STUDENT VERSION

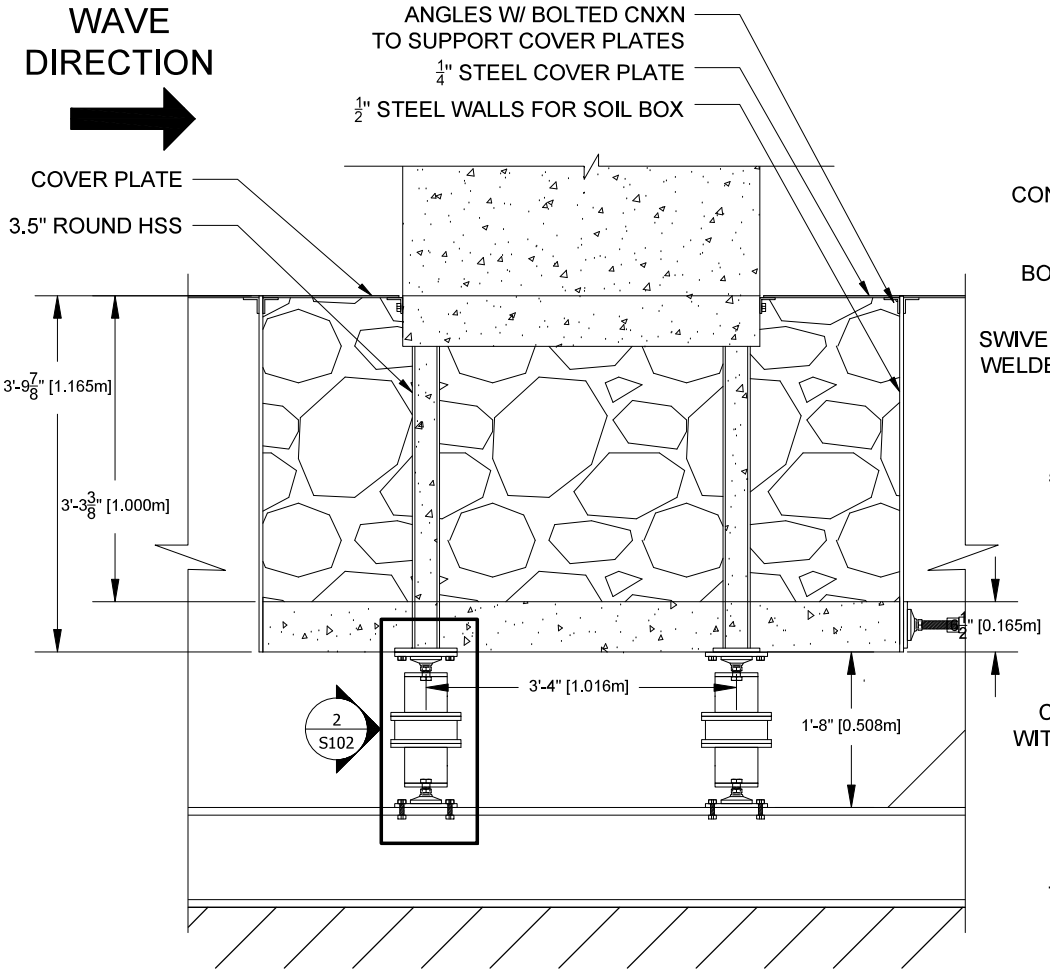

1 SOIL BOX ELEVATION

Scale: 3/4" = 1'

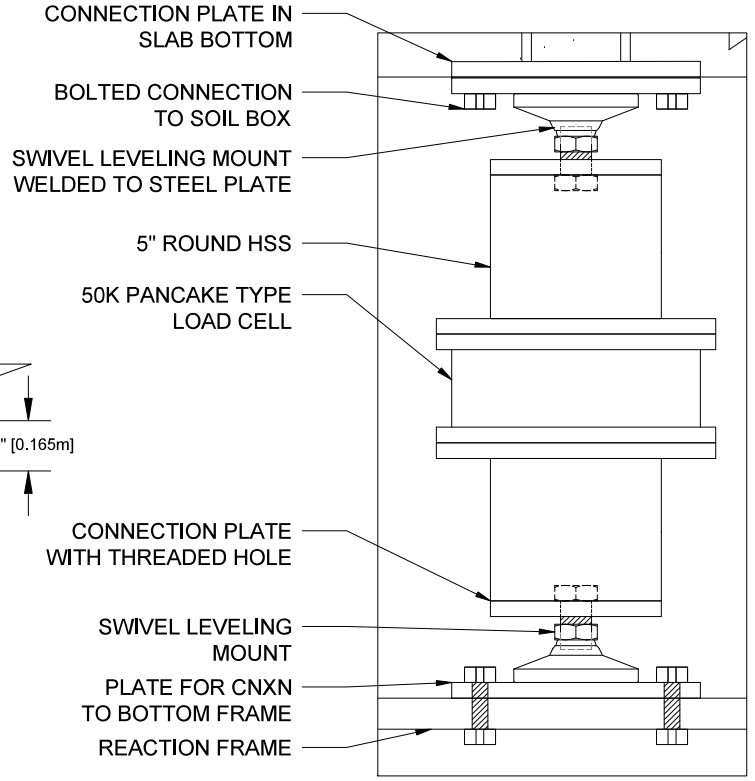

2 BOTTOM STRUT DETAIL

Scale: 3" = 1'

CIVIL & ENVIRONMENTAL ENGINEERING

General Notes

No.	Revision/Issue	Date

VERTICAL EVACUATION STRUCTURES

BOTTOM STRUT DETAIL

Project	Sheet
NSF VES	S102
Date: 6/26/19	
Scale: AS NOTED	

PRODUCED BY AN AUTODESK STUDENT VERSION

PRODUCED BY AN AUTODESK STUDENT VERSION

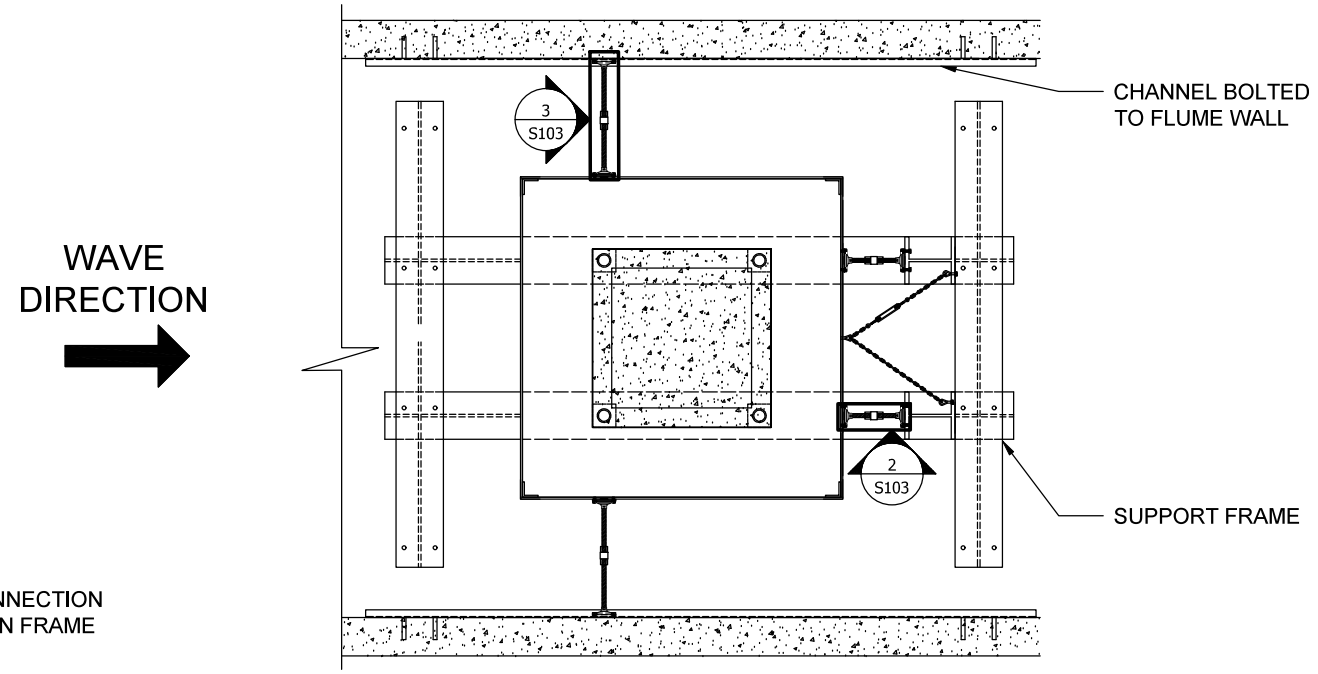

1 FLUME SETUP PLAN

Scale: 3/8" = 1'

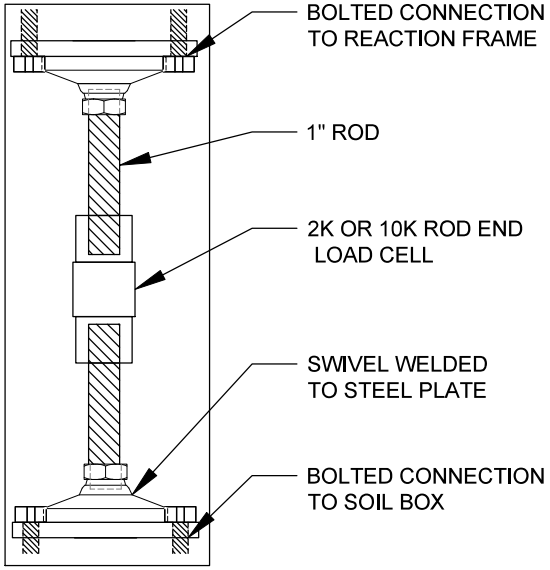

2 STREAMWISE LOAD CELL DETAIL

Scale: 1 1/2" = 1'

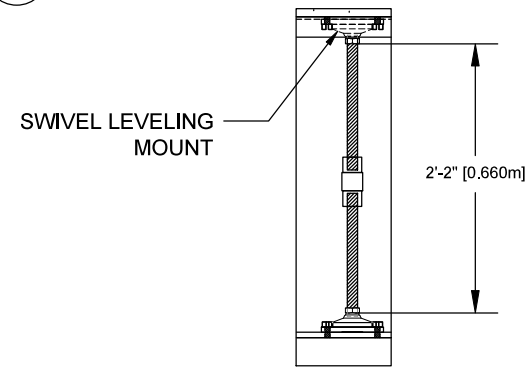

3 TRANSVERSE LOAD CELL DETAIL

Scale: 1" = 1'

CIVIL & ENVIRONMENTAL ENGINEERING

General Notes

NOTES:

- LEVELING MOUNTS ACCEPT 1"-8 RODS WHILE LOAD CELLS ACCEPT 1"-14 RODS
- WELD LEVELING MOUNTS TO PLATE AND THEN ATTACH WITH BOLTS

No.	Revision/Issue	Date

VERTICAL EVACUATION STRUCTURES

HORIZONTAL LOAD CELL DETAILS

Project	Sheet
NSF VES	S103
Date: 6/26/19	
Scale: AS NOTED	

PRODUCED BY AN AUTODESK STUDENT VERSION

PRODUCED BY AN AUTODESK STUDENT VERSION

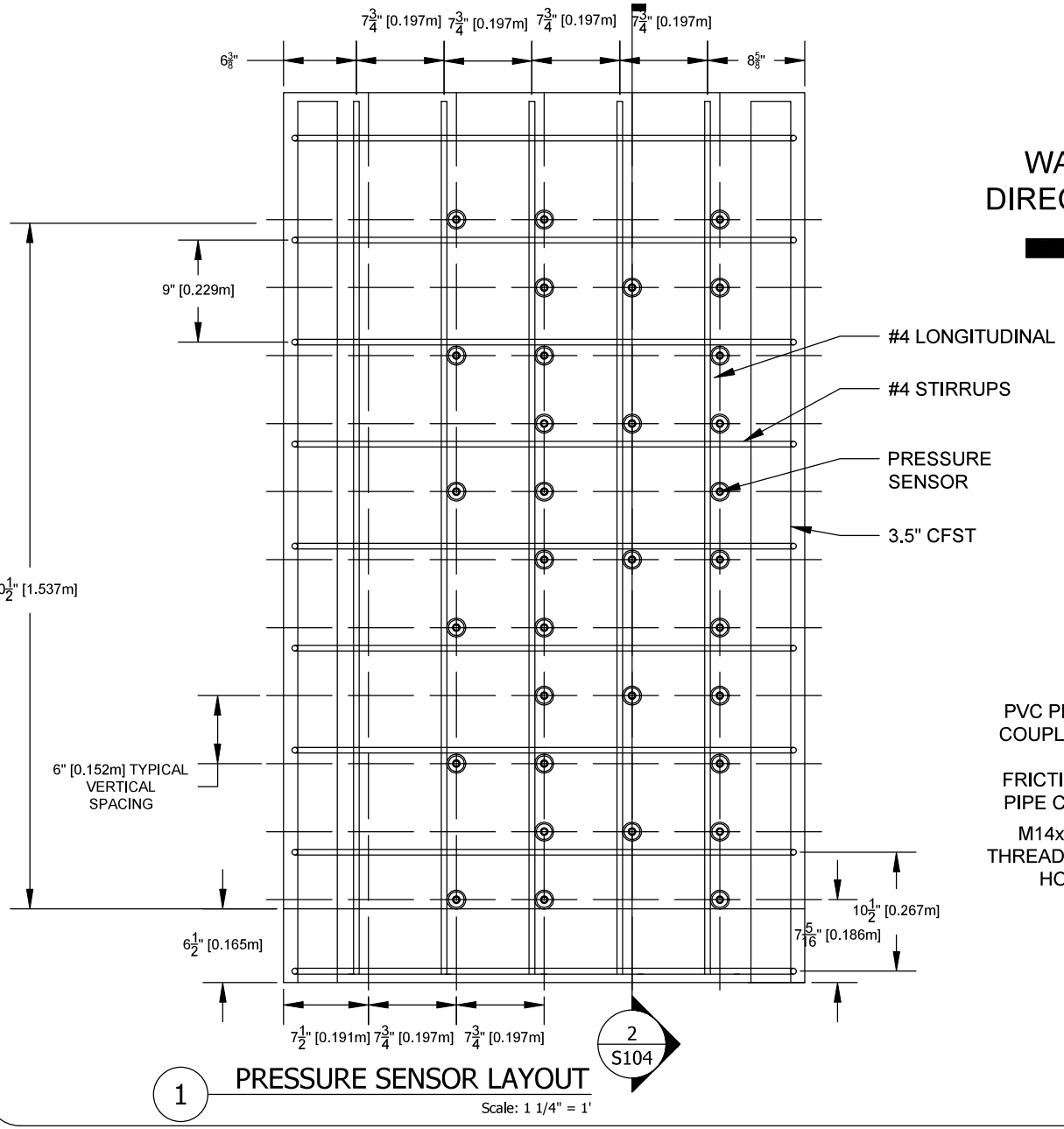

1 PRESSURE SENSOR LAYOUT

Scale: 1 1/4" = 1'

WAVE DIRECTION

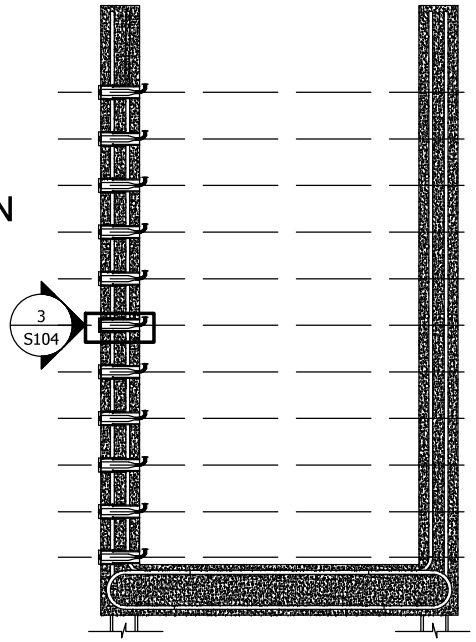

2 SECTION VIEW

Scale: 3/4" = 1'

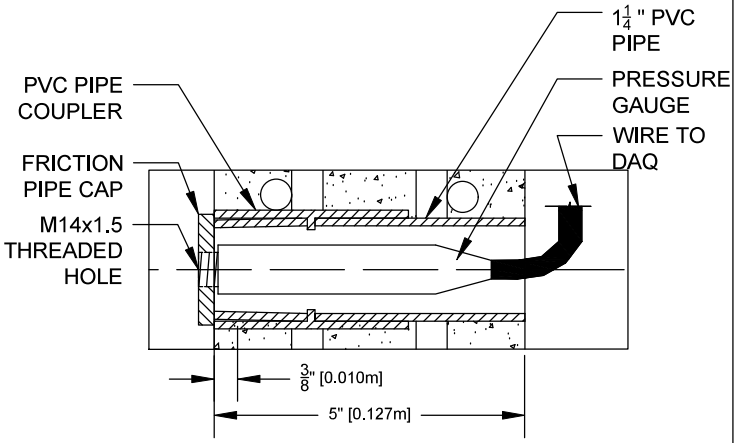

3 PRESSURE GAUGE DETAIL

Scale: 6"=1'

CIVIL & ENVIRONMENTAL ENGINEERING

General Notes

NOTES:

- ARRANGEMENT SHOWN USES 33 PRESSURE SENSORS
- WITH 13 GAUGES WILL NEED 3 RUNS PER WAVE
- MAX WAVE INUNDATION ASSUMED TO BE 4' 8"
- SENSOR LAYOUT IS SYMMETRIC ABOUT ℄

No.	Revision/Issue	Date

VERTICAL EVACUATION STRUCTURES

PRESSURE SENSOR DETAILS

Project: NSF VES	Sheet: S104
Date: 6/26/19	
Scale: AS NOTED	

PRODUCED BY AN AUTODESK STUDENT VERSION

PRODUCED BY AN AUTODESK STUDENT VERSION

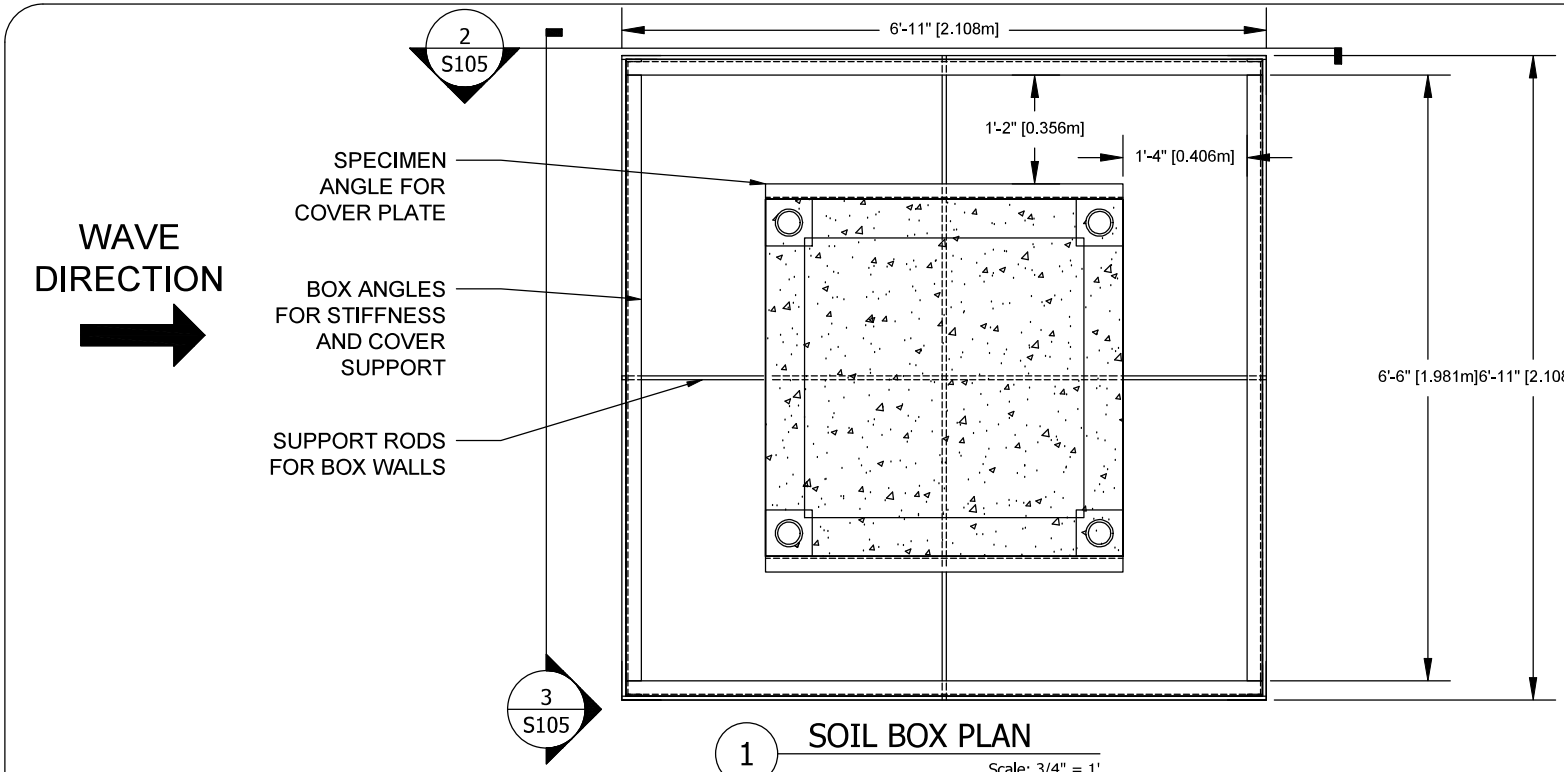

1 SOIL BOX PLAN
Scale: 3/4" = 1'

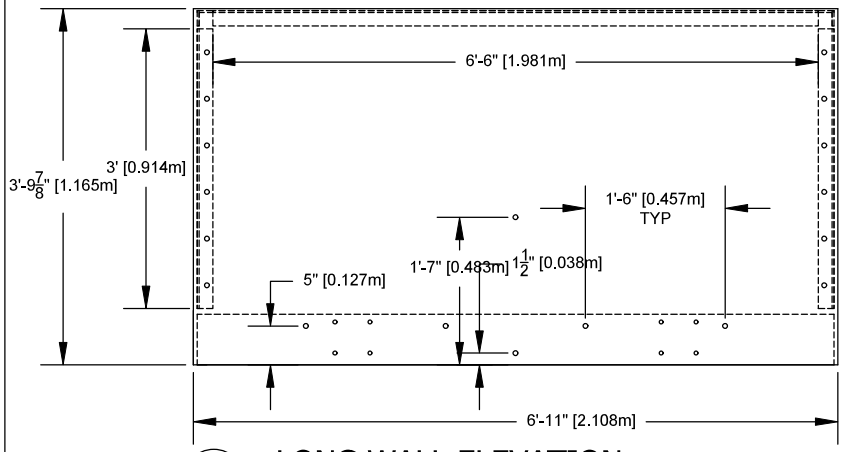

2 LONG WALL ELEVATION
Scale: 3/4" = 1'

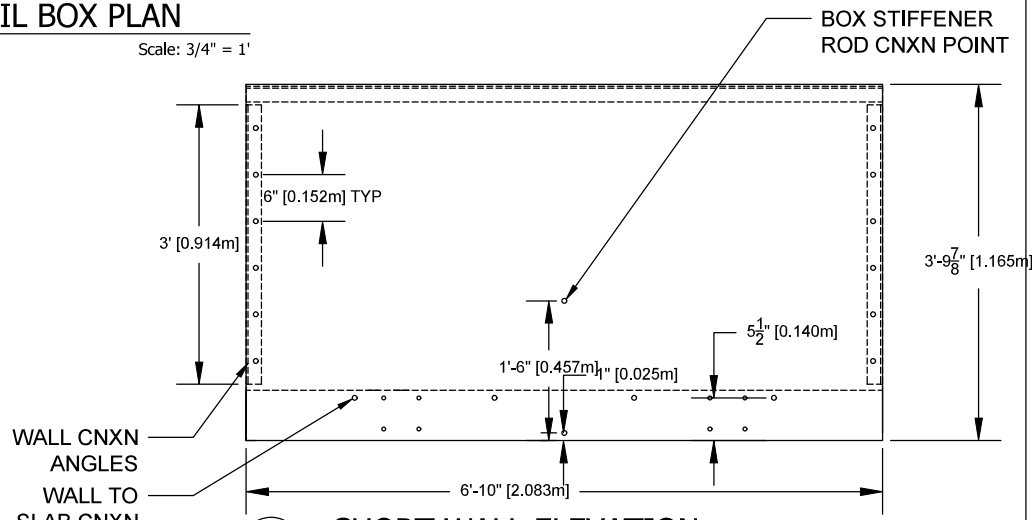

3 SHORT WALL ELEVATION
Scale: 3/4." = 1'

CIVIL & ENVIRONMENTAL ENGINEERING

General Notes

NOTES:

- ALL ANGLES ARE L2x2x.25
- ¾" COVER PLATE WILL SIT ON TOP OF ANGLES AROUND RIM OF SOIL BOX
- MAX SPAN FOR ¾" PLATE IS 16"
- ½" RODS WILL BE EMBEDDED IN THE BASE SLAB TO SECURE BOX WALLS
- ½" RODS WILL BE EMBEDDED IN SPECIMEN TO SECURE SUPPORT ANGLES

No.	Revision/Issue	Date

VERTICAL EVACUATION STRUCTURES

SOIL BOX WALL DETAILS

Project	Sheet
NSF VES	S105
Date: 6/26/19	
Scale: AS NOTED	

PRODUCED BY AN AUTODESK STUDENT VERSION

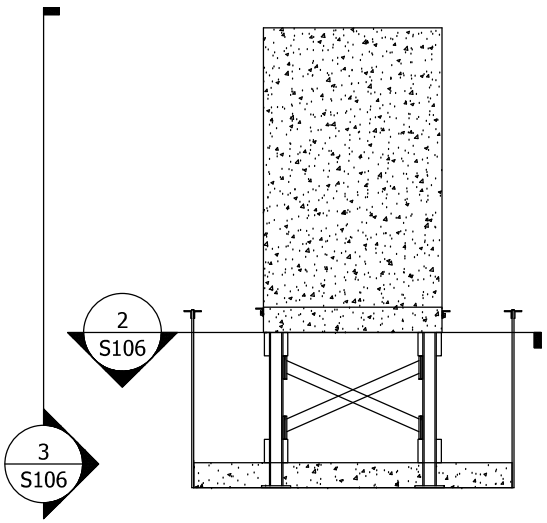

1 VIEW TITLE
Scale: 1:1

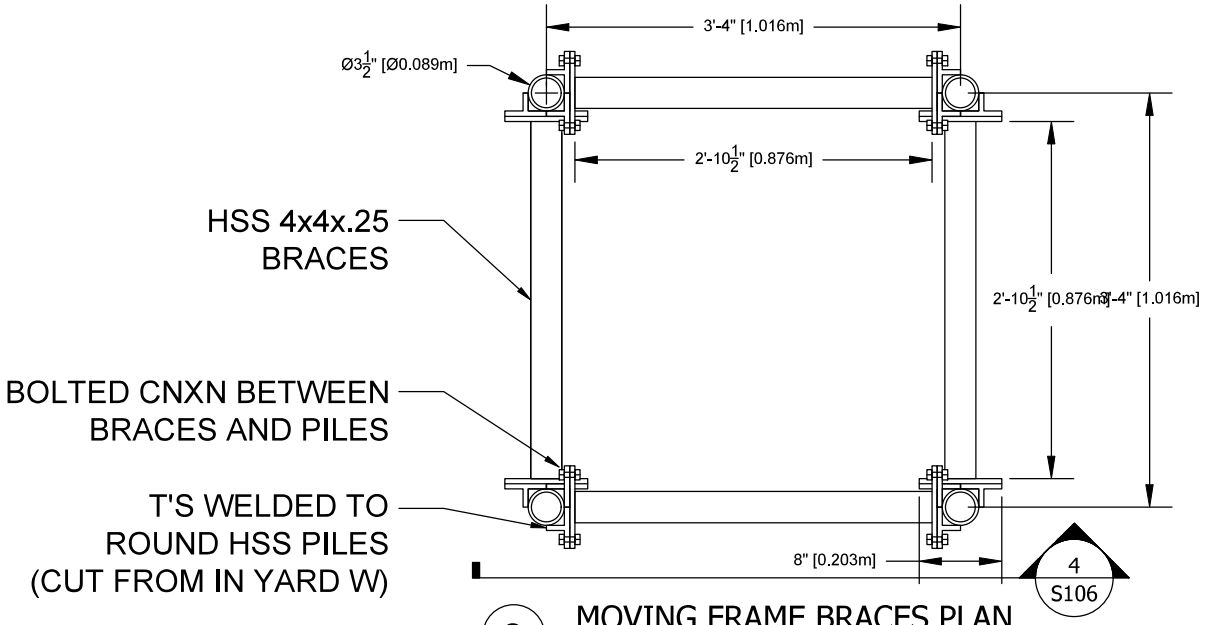

2 MOVING FRAME BRACES PLAN
Scale: 1" = 1'

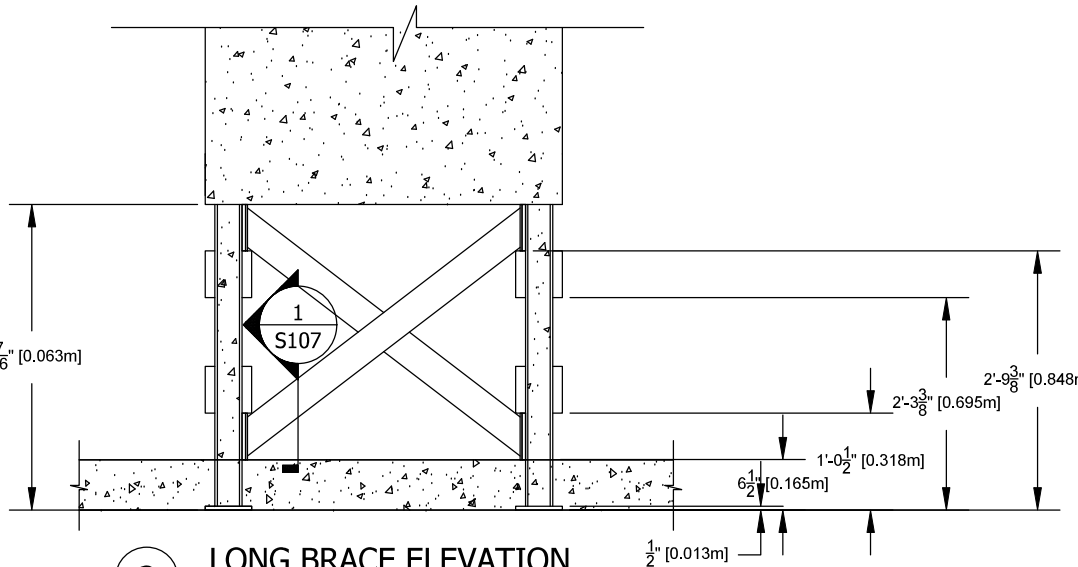

3 LONG BRACE ELEVATION
Scale: 3/4" = 1'

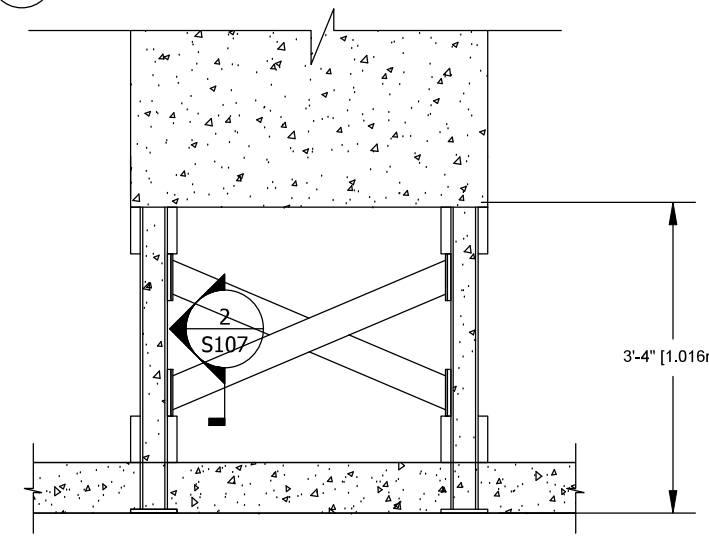

4 SHORT BRACES ELEVATION
Scale: 3/4" = 1'

CIVIL & ENVIRONMENTAL ENGINEERING

General Notes

NOTES:

- USE 2 DOUBLE T'S TO MAKE A SURFACE 8"x6" FOR BOLTING
- USE HSS 3x3x_ FOR BRACES
- ASSUMED T's HAVE ½" FLANGE
- USE ¾" BOLTS AND NUTS FOR BRACE CNXN

No.	Revision/Issue	Date

VERTICAL EVACUATION STRUCTURES

MOVING FRAME DETAILS

Project: NSF VES	Sheet: S106
Date: 6/26/19	
Scale: AS NOTED	

PRODUCED BY AN AUTODESK STUDENT VERSION

PRODUCED BY AN AUTODESK STUDENT VERSION

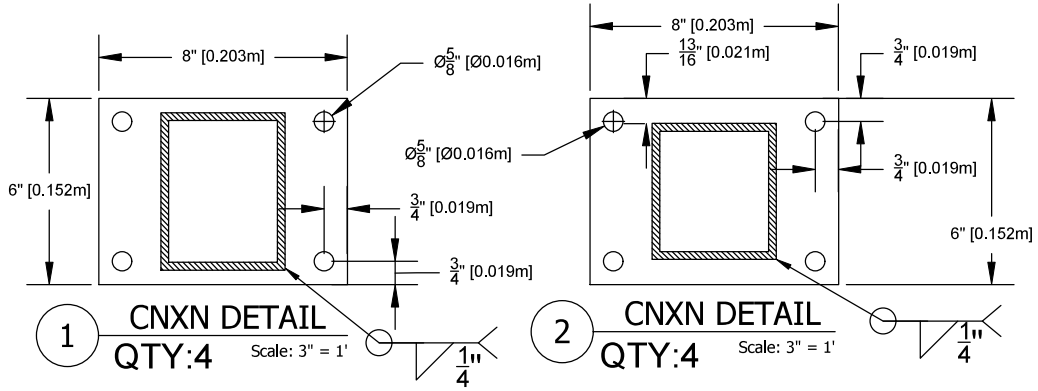

1 CNXN DETAIL QTY:4 Scale: 3" = 1'

2 CNXN DETAIL QTY:4 Scale: 3" = 1'

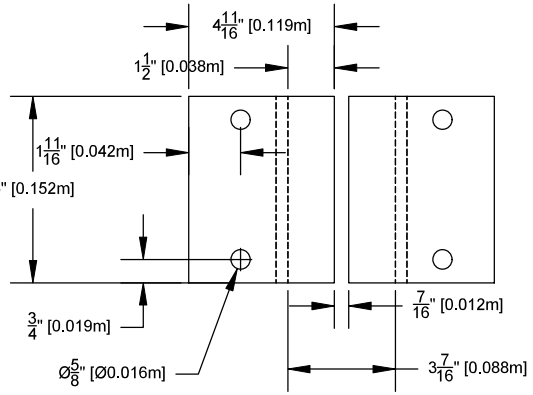

3 PILE CNXN PEICES QTY:8 Scale: 3" = 1'
(16 INDIVIDUAL PIECES)

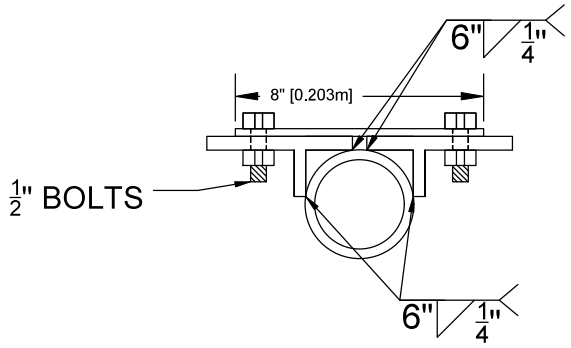

4 PILE CNXN DETAIL Scale: 3" = 1'

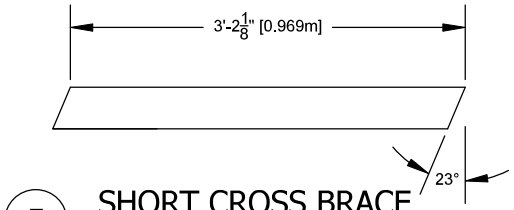

5 SHORT CROSS BRACE Scale: 1" = 1'

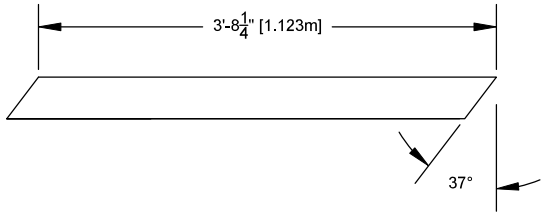

6 LONG CROSS BRACE Scale: 1" = 1'

CIVIL & ENVIRONMENTAL ENGINEERING

General Notes

NOTES:

- USE 2 DOUBLE T'S TO MAKE A SURFACE 8"x6" FOR BOLTING
- USE HSS 4x4x1/4" FOR BRACES
- USE 3/4" BOLTS AND NUTS FOR BRACE CNXN

No.	Revision/Issue	Date

VERTICAL EVACUATION STRUCTURES

MOVING FRAME DETAILS

Project	Sheet
NSF VES	S106
Date: 6/26/19	
Scale: AS NOTED	

PRODUCED BY AN AUTODESK STUDENT VERSION

PRODUCED BY AN AUTODESK STUDENT VERSION

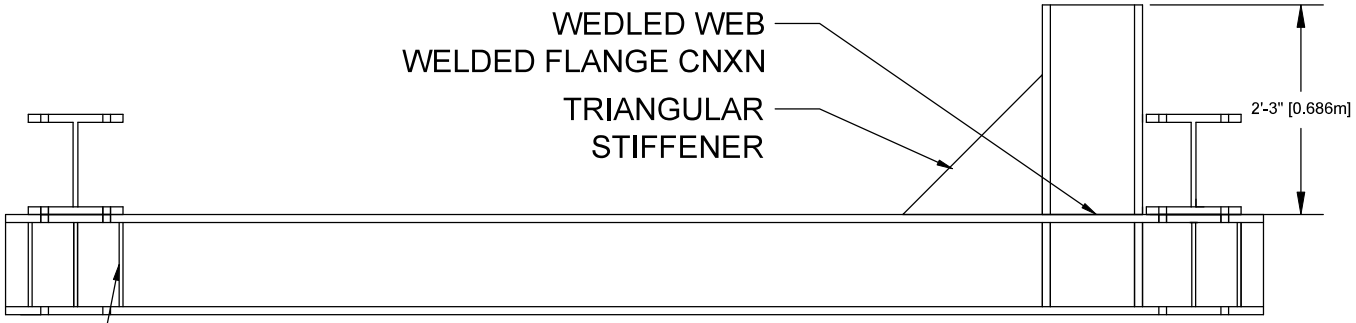

1 FRAME ELEVATION
3/4" = 1'

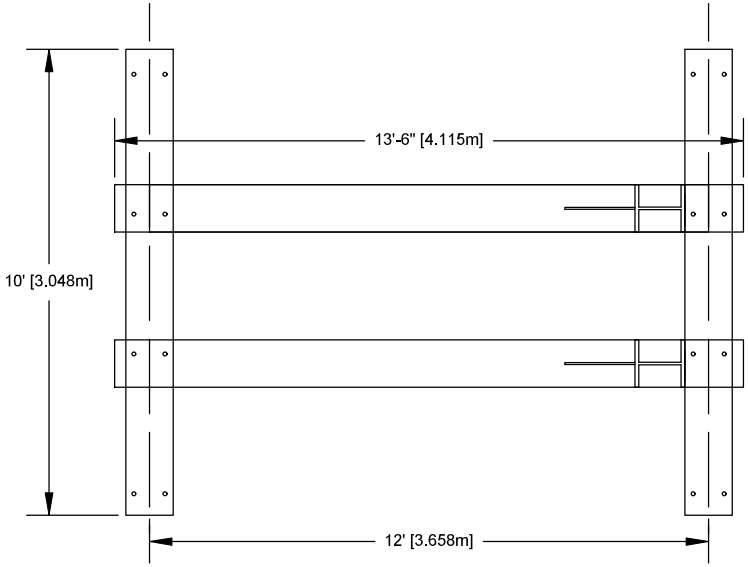

2 FRAME PLAN
3/8" = 1'

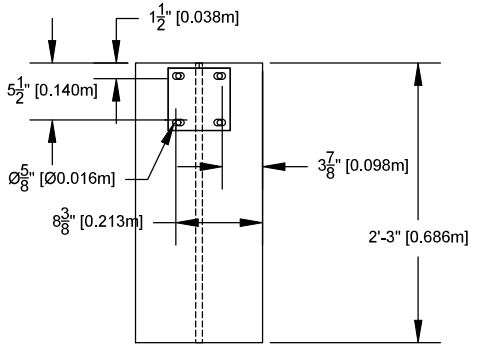

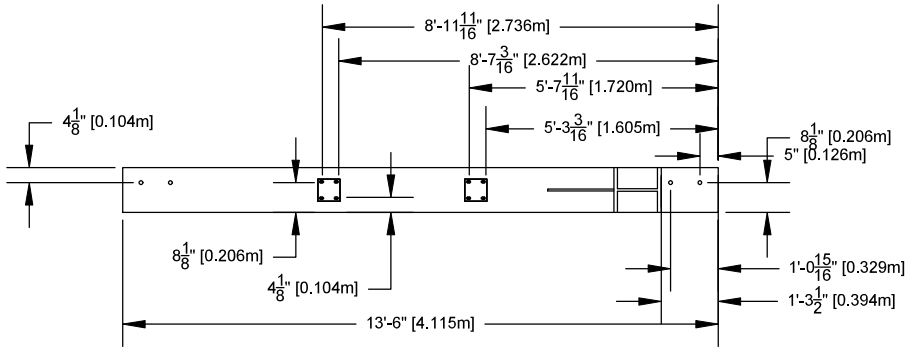

CIVIL & ENVIRONMENTAL ENGINEERING

General Notes

No.	Revision/Issue	Date

VERTICAL EVACUATION STRUCTURES

SUPPORT FRAME DETAILS

Project	Sheet
NSF VES	S107
Date: 6/26/19	
Scale: AS NOTED	

PRODUCED BY AN AUTODESK STUDENT VERSION

PRODUCED BY AN AUTODESK STUDENT VERSION

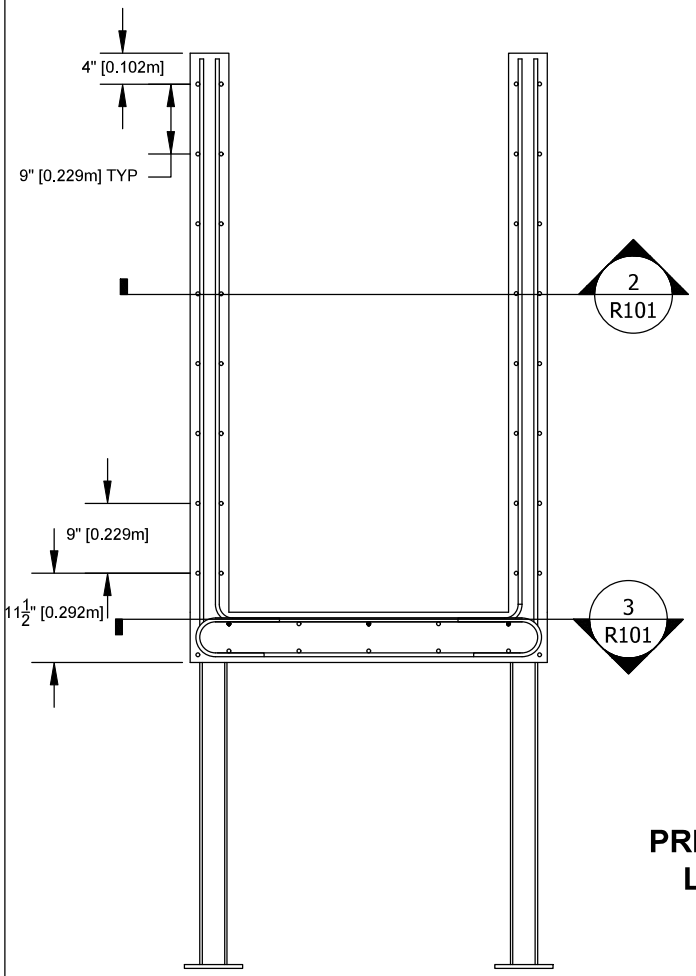

1 SPECIMEN REINFORCEMENT ELEVATION

3/4" = 1'

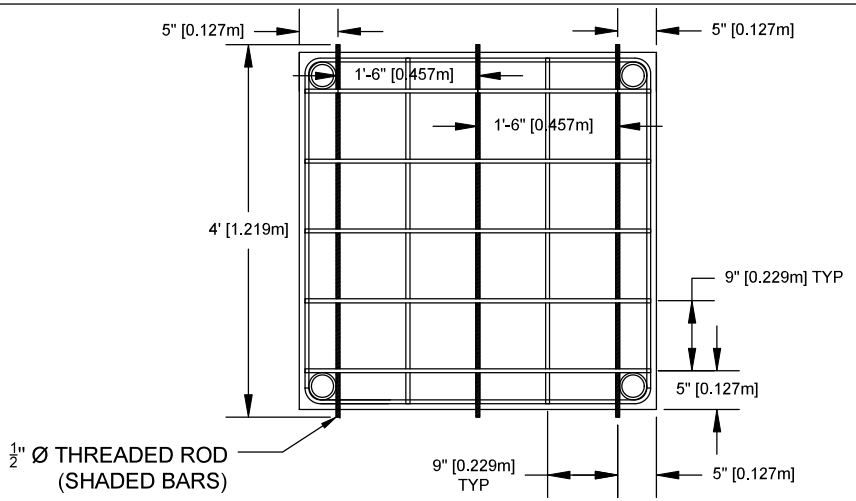

3 SLAB REINFORCEMENT SECTION

Scale: 3/4" = 1'

PRESSURE SENSOR SIDE LAYOUT IS DIFFERENT!

7 ¾" TYP SPACING NOTE EDGE OFFSETS

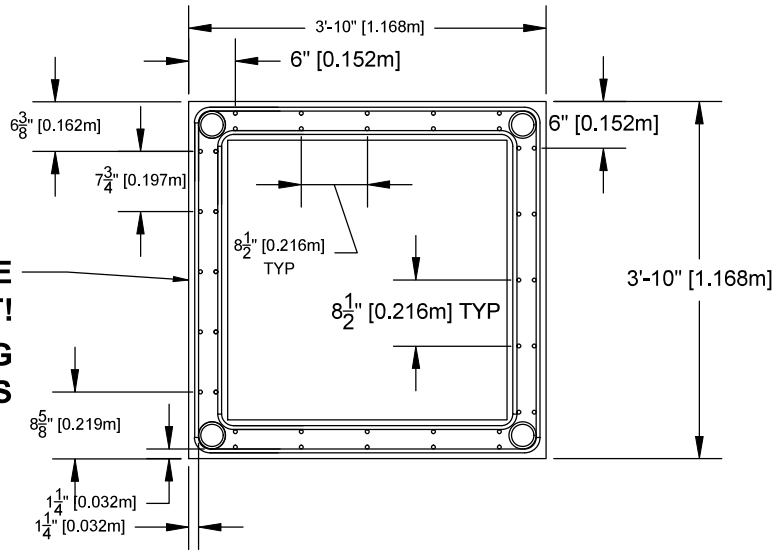

2 WALL REINFORCEMENT SECTION

Scale: 3/4" = 1'

CIVIL & ENVIRONMENTAL ENGINEERING

General Notes

No.	Revision/Issue	Date

VERTICAL EVACUATION STRUCTURES

SPECIMEN REINFORCING

Project	Sheet
NSF VES	R101
Date: 6/26/19	
Scale: AS NOTED	

PRODUCED BY AN AUTODESK STUDENT VERSION

PRODUCED BY AN AUTODESK STUDENT VERSION

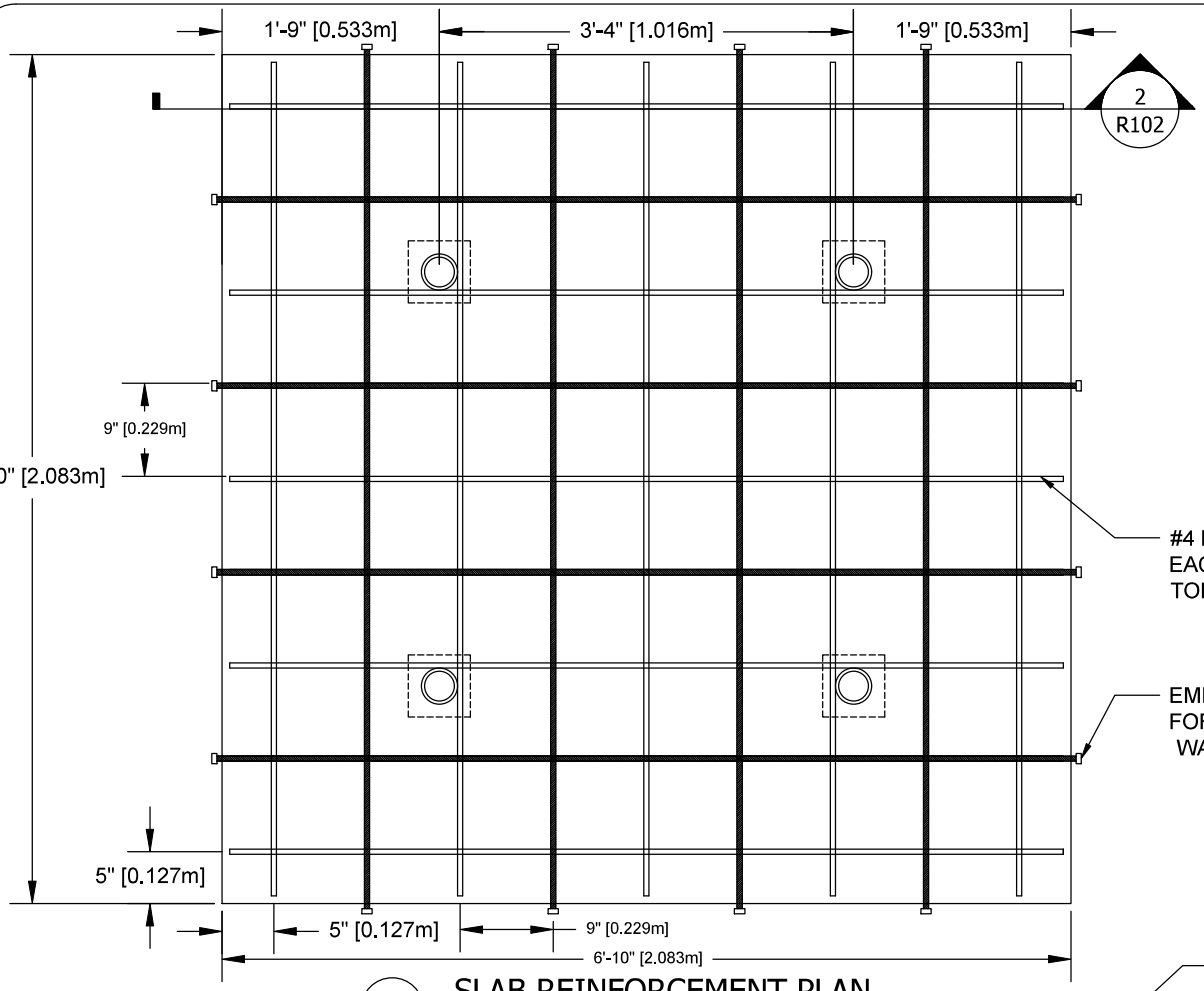

1 SLAB REINFORCEMENT PLAN

1" = 1'

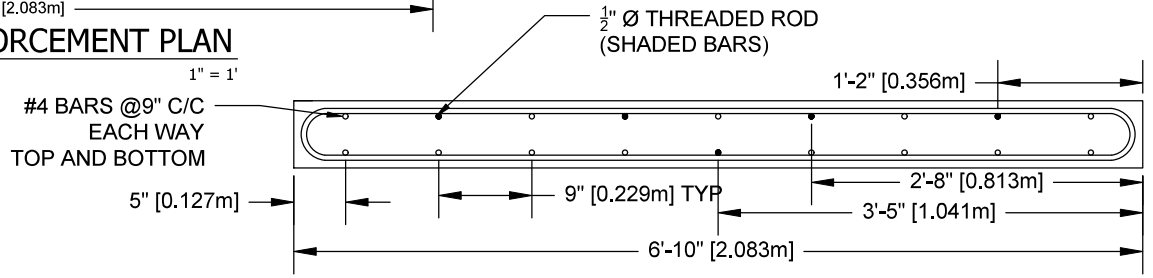

2 SLAB REINFORCEMENT SECTION

Scale: 1" = 1'

CIVIL & ENVIRONMENTAL ENGINEERING

General Notes

No.	Revision/Issue	Date

VERTICAL EVACUATION STRUCTURES

SLAB REINFORCING

Project	Sheet
NSF VES	R102
Date: 6/26/19	
Scale: AS NOTED	

PRODUCED BY AN AUTODESK STUDENT VERSION

PRODUCED BY AN AUTODESK STUDENT VERSION

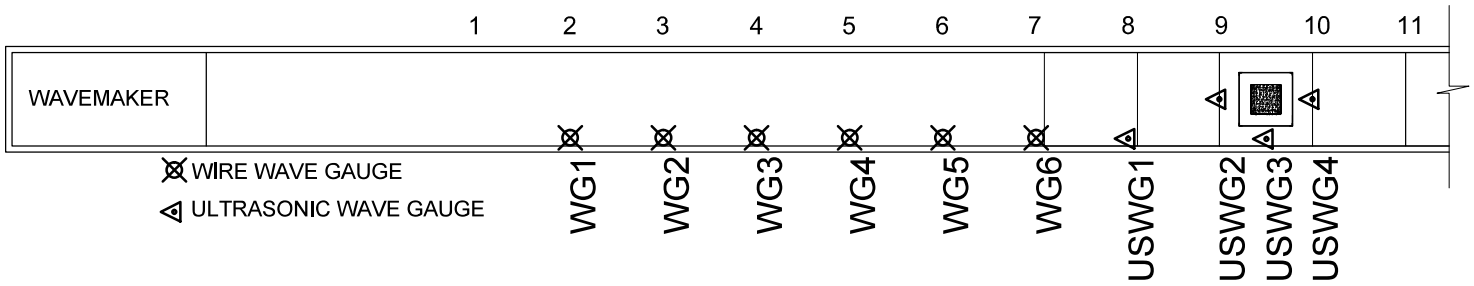

1 WAVE GAUGE LAYOUT PLAN

Scale: N/A

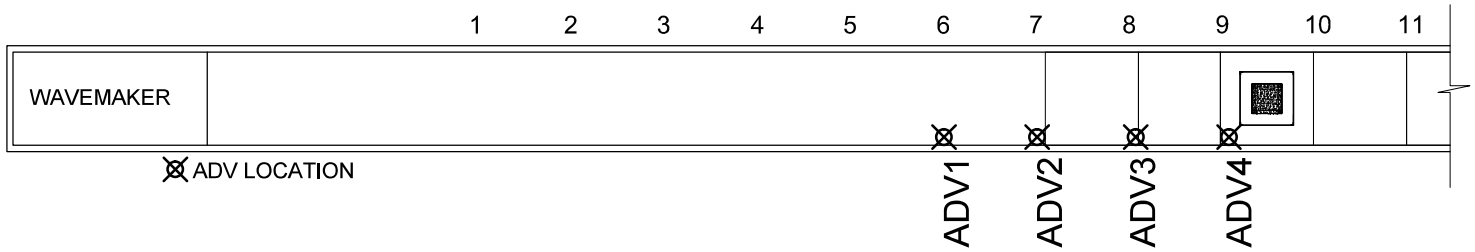

1 ADV LAYOUT PLAN

Scale: N/A

CIVIL & ENVIRONMENTAL ENGINEERING

General Notes

No.	Revision/Issue	Date

VERTICAL EVACUATION STRUCTURES

WAVE GAUGES AND ADV'S

Project: NSF VES	Sheet: I101
Date: 7/4/19	
Scale: AS NOTED	

PRODUCED BY AN AUTODESK STUDENT VERSION

PRODUCED BY AN AUTODESK STUDENT VERSION

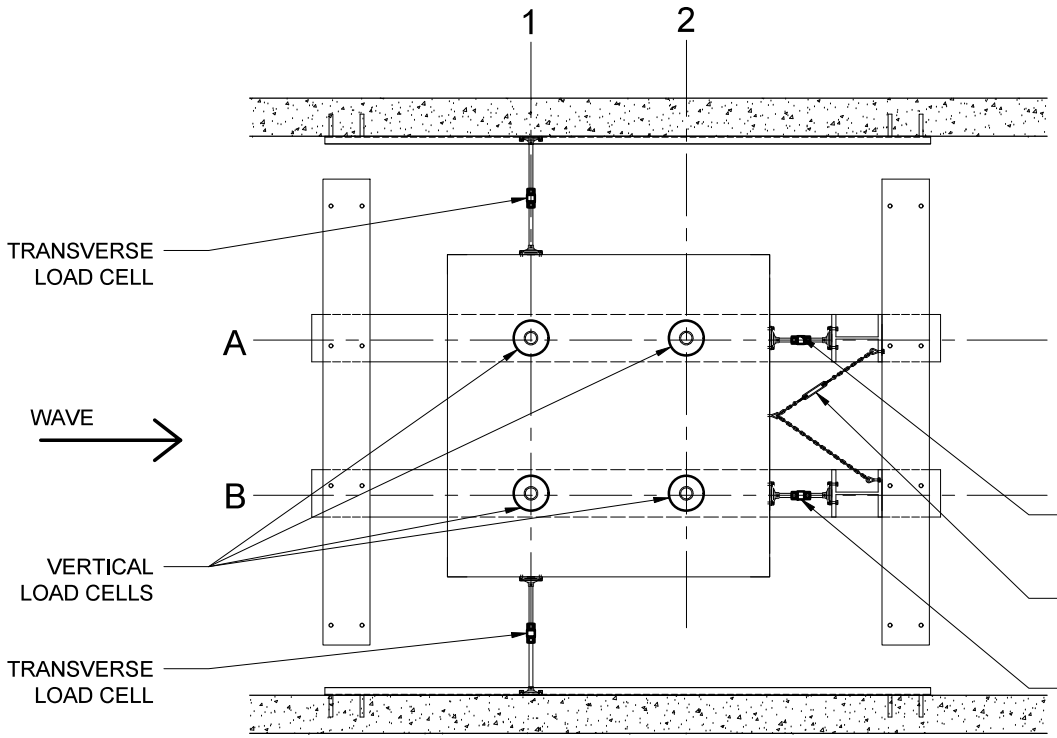

NAMING CONVENTION	
VERTICAL LOAD CELLS	VA1
	VA2
	VB1
	VB2
STREAMWISE LOAD CELLS	SA
	SB
TRANSVERSE LOAD CELLS	TA
	TB

3 LOAD CELL PLAN

Scale: 3/8" = 1'

CIVIL & ENVIRONMENTAL ENGINEERING

General Notes

No.	Revision/Issue	Date

VERTICAL EVACUATION STRUCTURES

LOAD CELL PLAN

Project	Sheet
NSF VES	I102
Date: 7/4/19	
Scale: AS NOTED	

PRODUCED BY AN AUTODESK STUDENT VERSION

PRODUCED BY AN AUTODESK STUDENT VERSION

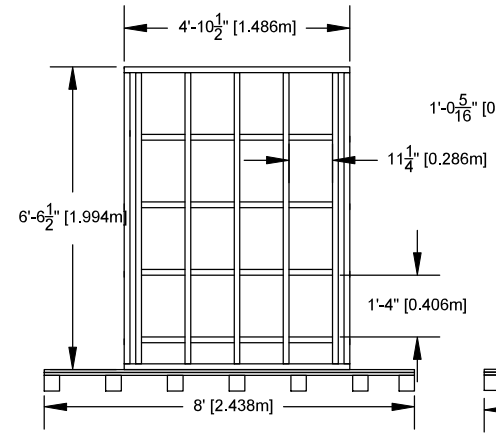

2 LONG OUTSIDE WALL

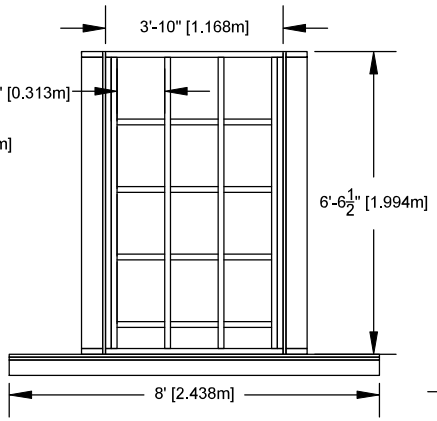

3 SHORT OUTSIDE WALL

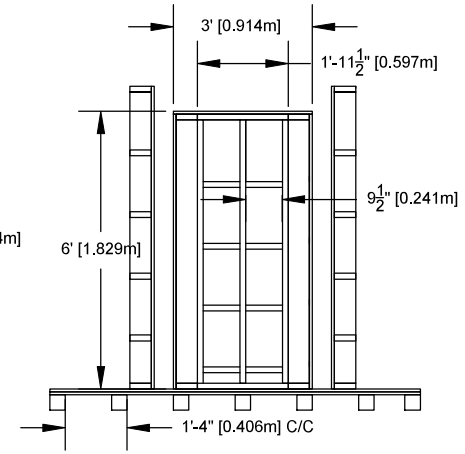

4 SHORT INSIDE WALL

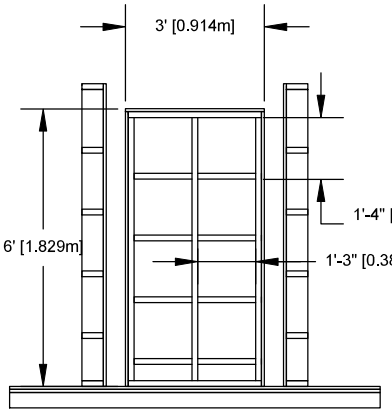

5 LONG INSIDE WALL

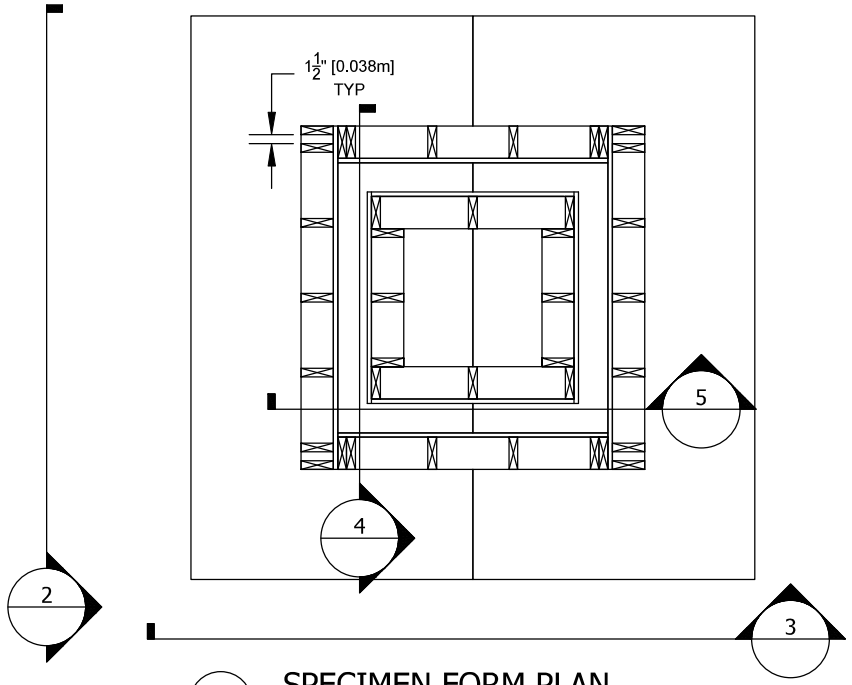

1 SPECIMEN FORM PLAN

CIVIL & ENVIRONMENTAL ENGINEERING

General Notes

No.	Revision/Issue	Date

VERTICAL EVACUATION STRUCTURES

SPECIMEN FORMS

Project	Sheet
NSF VES	F101
Date	
6/26/19	
Scale	
AS NOTED	

PRODUCED BY AN AUTODESK STUDENT VERSION

PRODUCED BY AN AUTODESK STUDENT VERSION

APPENDIX C

SETUP VALIDATION TEST RESULTS

TRANSVERSE LOADING (JACK TIRAL 3):

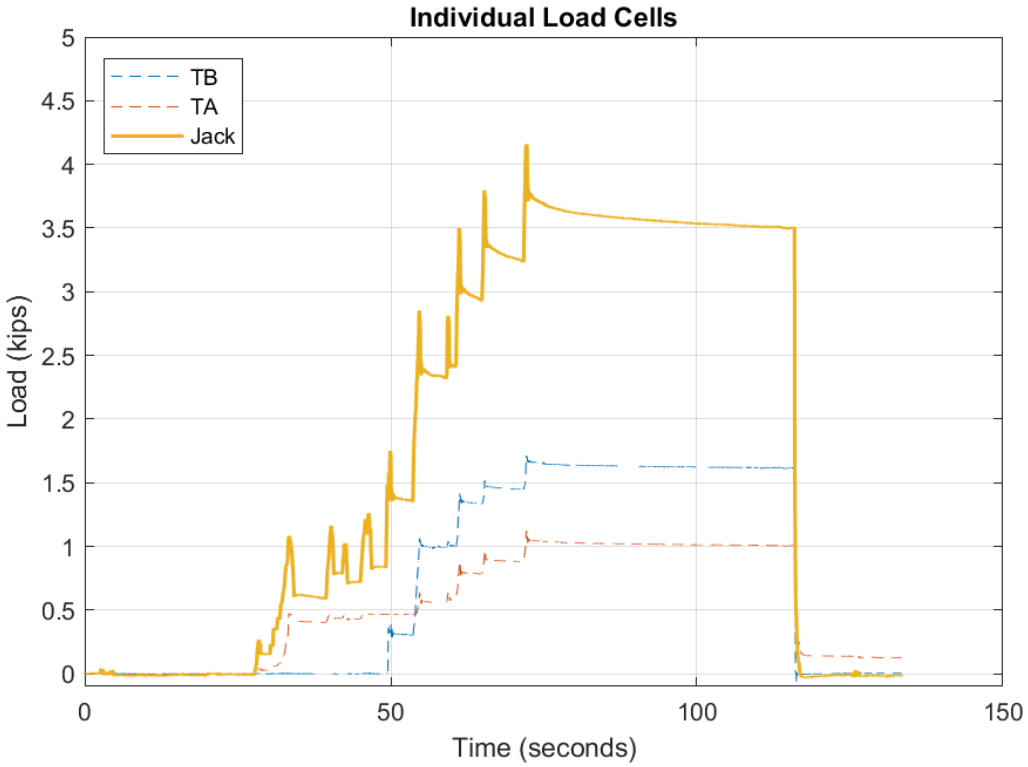

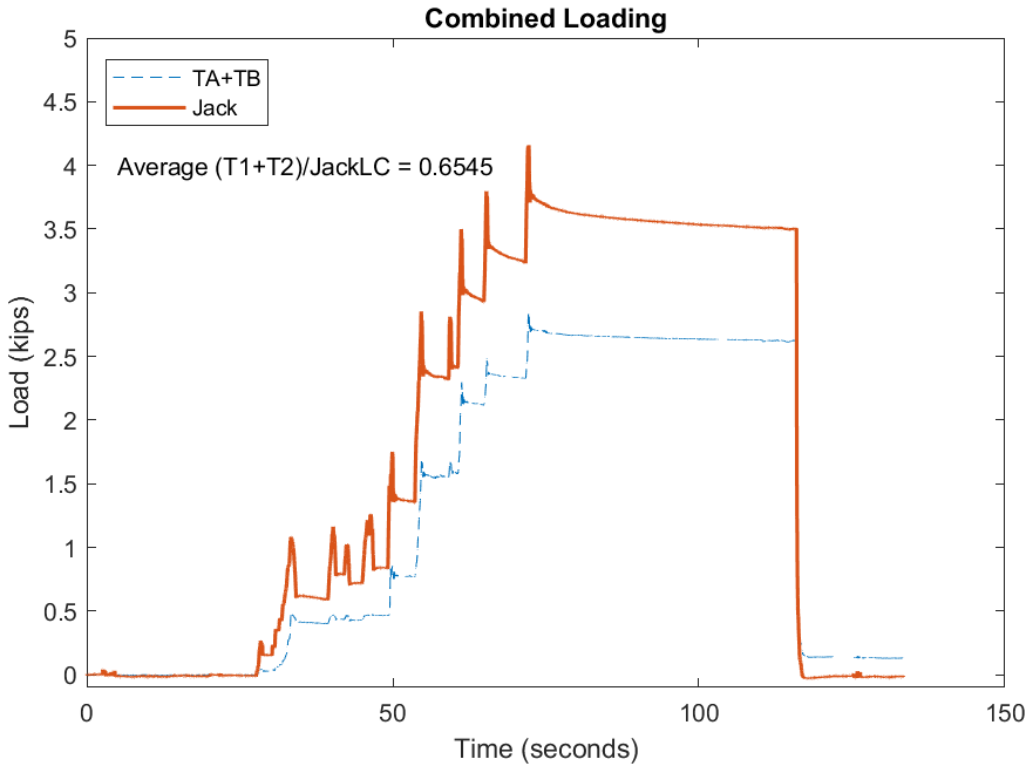
Combined Loading
TA+TB
Jack
Average (T1+T2)/JackLC = 0.6545
Load (kips)
Time (seconds)
0
0.5
1
1.5
2
2.5
3
3.5
4
4.5
5
0
50
100
150

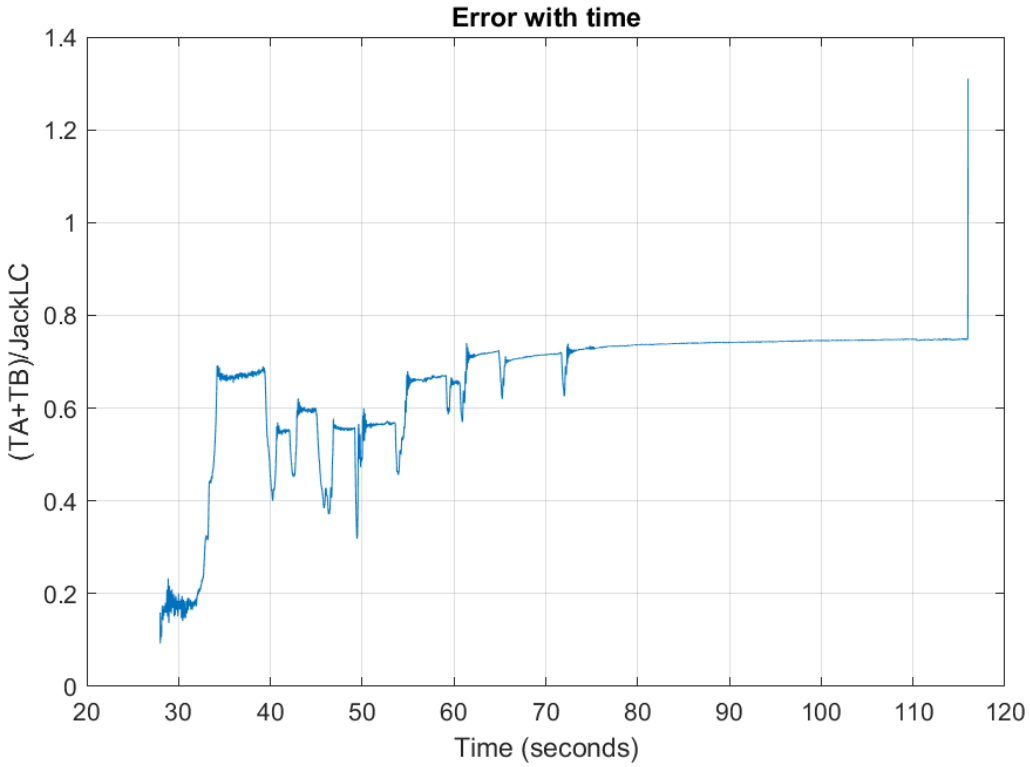
Error with time
(TA+TB)/JackLC
Time (seconds)
0
0.2
0.4
0.6
0.8
1
1.2
1.4
20
30
40
50
60
70
80
90
100
110
120

TRANSVERSE LOADING (JACK TIRAL 5):

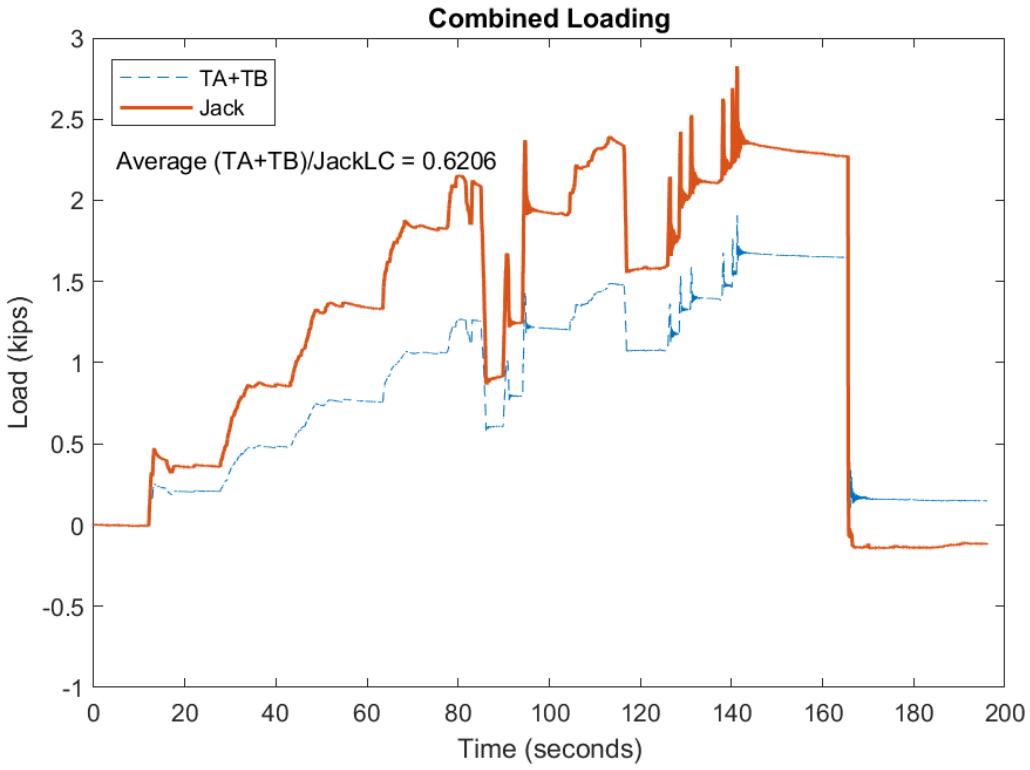

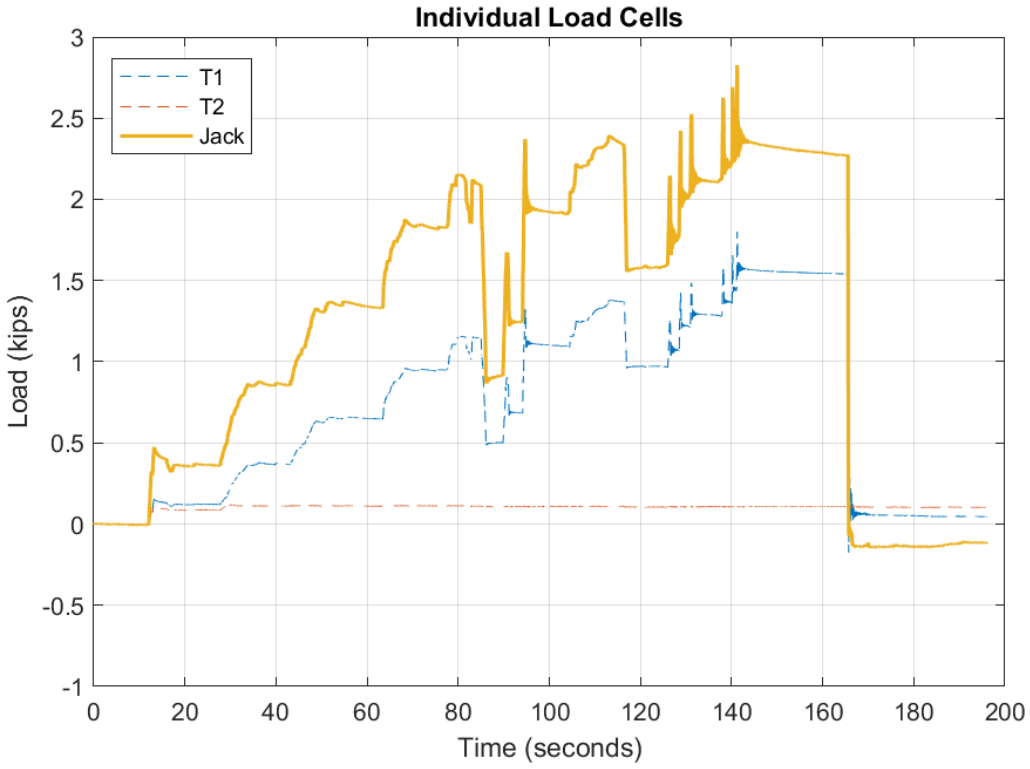

STREAMWISE LOADING: JACK TRIAL 8

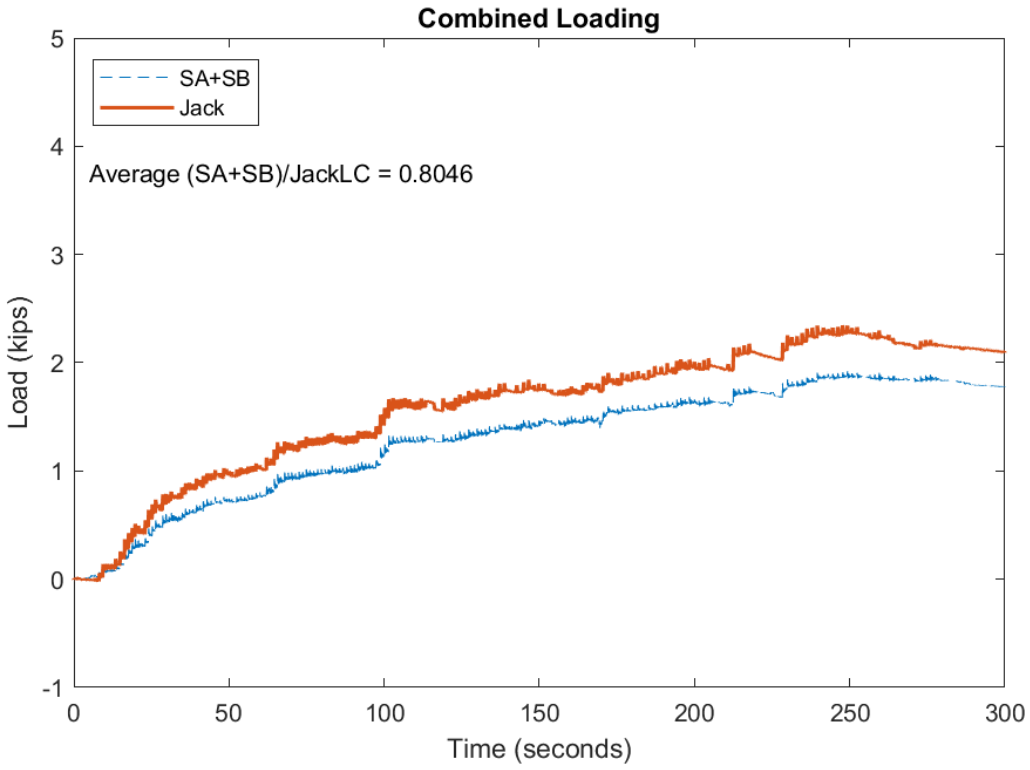

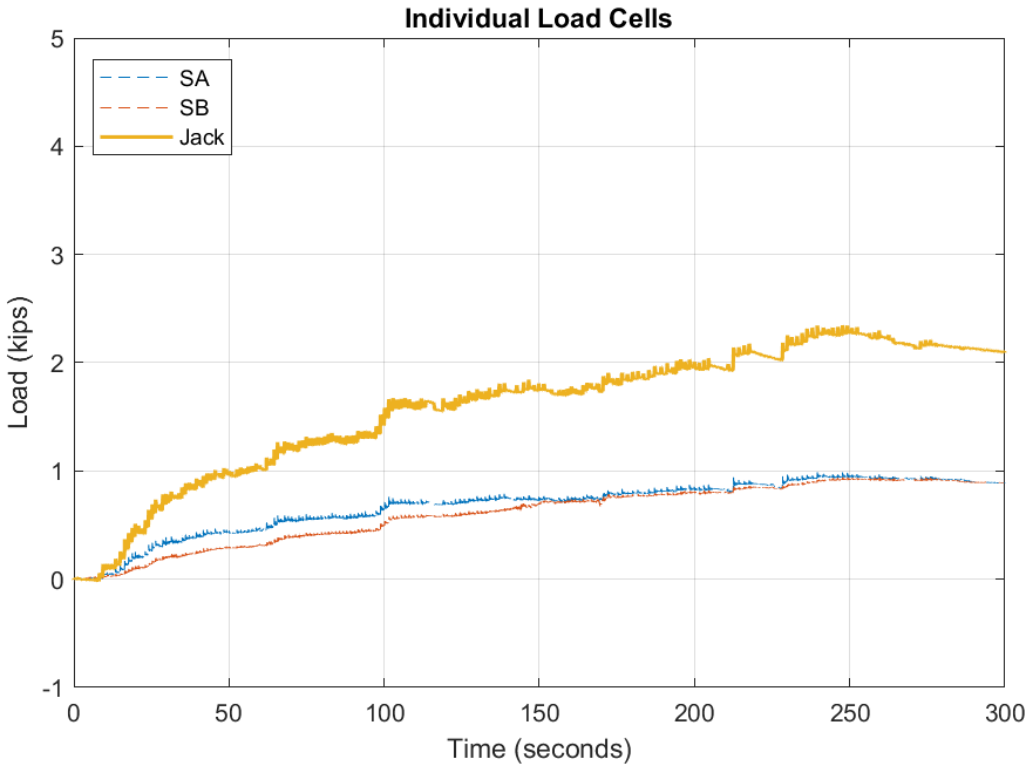

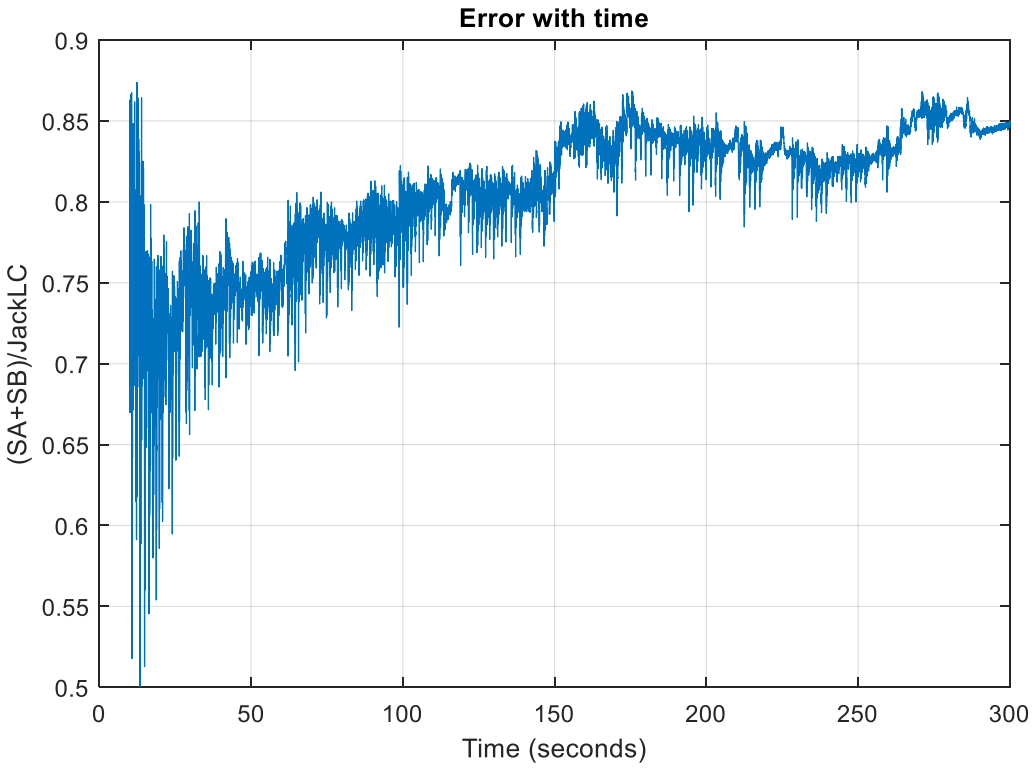

STREAMWISE LOADING: JACK TRIAL 7

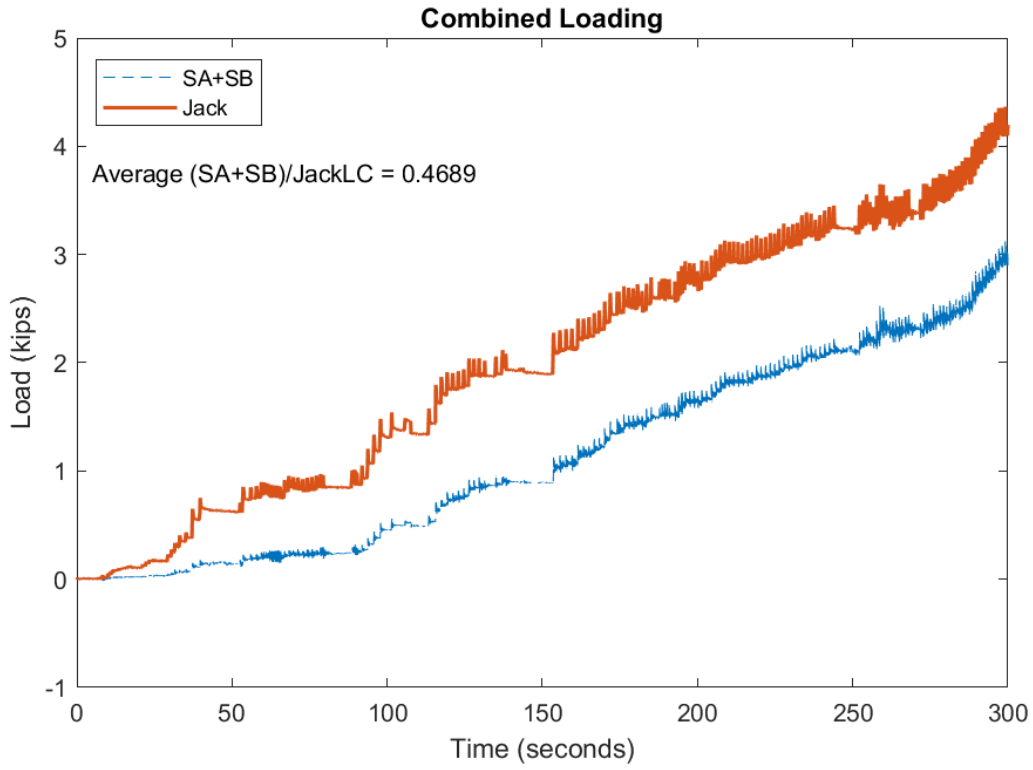

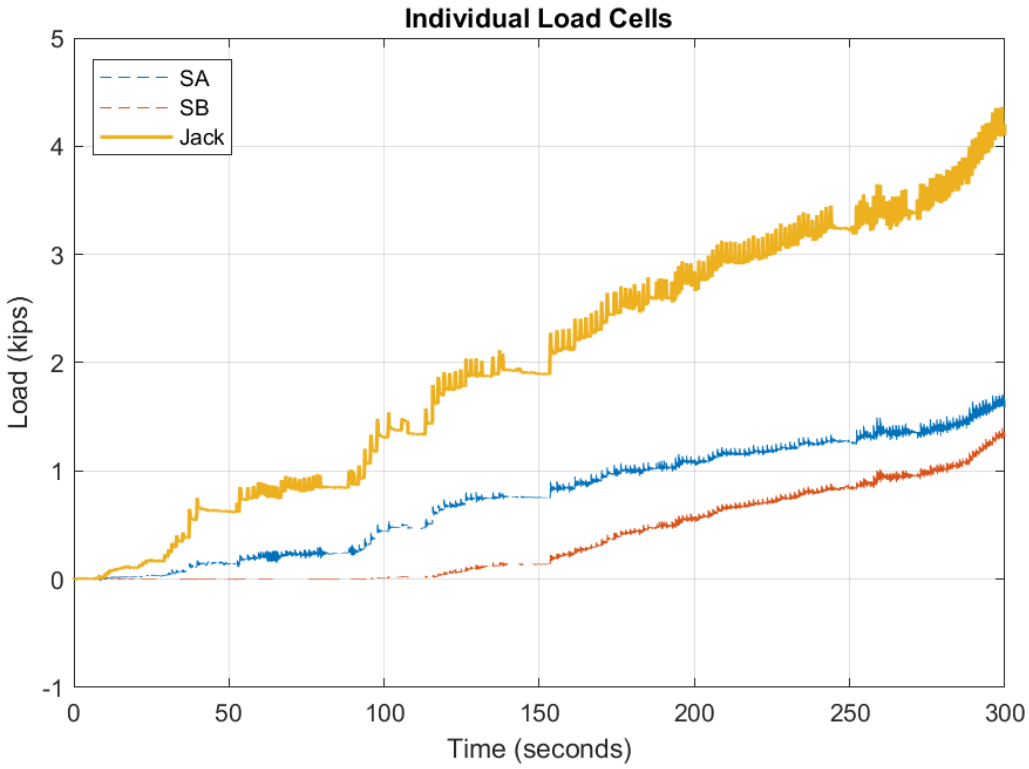
Individual Load Cells
SA
SB
Jack
Load (kips)
Time (seconds)
5
4
3
2
1
0
-1
0
50
100
150
200
250
300